NATIONAL AND KAPODISTRIAN UNIVERSITY OF ATHENS

SCHOOL OF SCIENCES
DEPARTMENT OF INFORMATICS AND TELECOMMUNICATIONS

PROGRAM OF POSTGRADUATE STUDIES

PhD THESIS

Localization and Mobility Management in Heterogeneous Wireless Networks with Network-Assistance

Dionysios G. Xenakis

ATHENS

JULY 2014

European Union
European Social Fund

OPERATIONAL PROGRAMME
EDUCATION AND LIFELONG LEARNING
investing in knowledge society
MINISTRY OF EDUCATION & RELIGIOUS AFFAIRS, CULTURE & SPORTS
MANAGING AUTHORITY

NSRF 2007-2013
programme for development
EUROPEAN SOCIAL FUND

Co- financed by Greece and the European Union

NATIONAL AND KAPODISTRIAN UNIVERSITY OF ATHENS

SCHOOL OF SCIENCES
DEPARTMENT OF INFORMATICS AND TELECOMMUNICATIONS

PROGRAM OF POSTGRADUATE STUDIES

PhD THESIS

Localization and Mobility Management in Heterogeneous Wireless Networks with Network-Assistance

Dionysios G. Xenakis

ATHENS

JULY 2014

European Union
European Social Fund

OPERATIONAL PROGRAMME
EDUCATION AND LIFELONG LEARNING
investing in knowledge society
MINISTRY OF EDUCATION & RELIGIOUS AFFAIRS, CULTURE & SPORTS
MANAGING AUTHORITY

NSRF 2007-2013
programme for development
EUROPEAN SOCIAL FUND

Co- financed by Greece and the European Union

ΕΘΝΙΚΟ ΚΑΙ ΚΑΠΟΔΙΣΤΡΙΑΚΟ ΠΑΝΕΠΙΣΤΗΜΙΟ ΑΘΗΝΩΝ

ΣΧΟΛΗ ΘΕΤΙΚΩΝ ΕΠΙΣΤΗΜΩΝ
ΤΜΗΜΑ ΠΛΗΡΟΦΟΡΙΚΗΣ ΚΑΙ ΤΗΛΕΠΙΚΟΙΝΩΝΙΩΝ

ΠΡΟΓΡΑΜΜΑ ΜΕΤΑΠΤΥΧΙΑΚΩΝ ΣΠΟΥΔΩΝ

ΔΙΔΑΚΤΟΡΙΚΗ ΔΙΑΤΡΙΒΗ

Εντοπισμός θέσης και διαχείριση κινητικότητας σε ετερογενή ασύρματα δίκτυα με υποβοήθηση από το δίκτυο

Διονύσιος Γ. Ξενάκης

ΑΘΗΝΑ

ΙΟΥΛΙΟΣ 2014

Ευρωπαϊκή Ένωση
Ευρωπαϊκό Κοινωνικό Ταμείο

ΕΠΙΧΕΙΡΗΣΙΑΚΟ ΠΡΟΓΡΑΜΜΑ
ΕΚΠΑΙΔΕΥΣΗ ΚΑΙ ΔΙΑ ΒΙΟΥ ΜΑΘΗΣΗ
επένδυση στην κοινωνία της γνώσης
ΥΠΟΥΡΓΕΙΟ ΠΑΙΔΕΙΑΣ & ΘΡΗΣΚΕΥΜΑΤΩΝ, ΠΟΛΙΤΙΣΜΟΥ & ΑΘΛΗΤΙΣΜΟΥ
ΕΙΔΙΚΗ ΥΠΗΡΕΣΙΑ ΔΙΑΧΕΙΡΙΣΗΣ

ΕΣΠΑ 2007-2013
πρόγραμμα για την ανάπτυξη
ΕΥΡΩΠΑΪΚΟ ΚΟΙΝΩΝΙΚΟ ΤΑΜΕΙΟ

Με τη συγχρηματοδότηση της Ελλάδας και της Ευρωπαϊκής Ένωσης

PhD THESIS

Localization and Mobility Management in Heterogeneous Wireless Networks with Network-Assistance

Dionysios G. Xenakis

SUPERVISOR: Lazaros Merakos, Professor UoA

THREE-MEMBER ADVISORY COMMITTEE:

Lazaros Merakos, Professor University of Athens
Ioannis Stavrakakis, Professor University of Athens
Christos Verikoukis, Senior Researcher CTTC, Spain

SEVEN-MEMBER EXAMINATION COMMITTEE

(Signature) (Signature)

Lazaros Merakos,
Professor UoA
(Signature)

Ioannis Stavrakakis,
Professor UoA
(Signature)

Christos Verikoukis,
Senior Researcher CTTC, Spain

(Signature)

Marios Kountouris,
Associate Professor SUPELEC

(Signature)

Athanasia Alonistioti,
Assistant Professor UoA

(Signature)

Eustathios Hadjiefthymiades,
Associate Professor UoA

Christos Xenakis,
Assistant Professor UoP

Examination Date 31/07/2014

ΔΙΔΑΚΤΟΡΙΚΗ ΔΙΑΤΡΙΒΗ

Εντοπισμός θέσης και διαχείριση κινητικότητας σε ετερογενή ασύρματα δίκτυα με υποβοήθηση από το δίκτυο

Διονύσιος Γ. Ξενάκης

ΕΠΙΒΛΕΠΩΝ ΚΑΘΗΓΗΤΗΣ: Λάζαρος Μεράκος, Καθηγητής ΕΚΠΑ

ΤΡΙΜΕΛΗΣ ΕΠΙΤΡΟΠΗ ΠΑΡΑΚΟΛΟΥΘΗΣΗΣ:
Λάζαρος Μεράκος, Καθηγητής ΕΚΠΑ
Ιωάννης Σταυρακάκης, Καθηγητής ΕΚΠΑ
Χρήστος Βερικούκης, Ερευνητής CTTC, Ισπανία

ΕΠΤΑΜΕΛΗΣ ΕΞΕΤΑΣΤΙΚΗ ΕΠΙΤΡΟΠΗ

(Υπογραφή)

Λάζαρος Μεράκος,
Καθηγητής ΕΚΠΑ

(Υπογραφή)

Ιωάννης Σταυρακάκης,
Καθηγητής ΕΚΠΑ

(Υπογραφή)

Χρήστος Βερικούκης,
Ερευνητής CTTC, Ισπανία

(Υπογραφή)

Μάριος Κουντούρης,
Αναπληρωτής Καθηγητής SUPELEC

(Υπογραφή)

Αθανασία Αλωνιστιώτη,
Επίκουρη Καθηγήτρια ΕΚΠΑ

(Υπογραφή)

Ευστάθιος Χατζιευθυμιάδης,
Αναπληρωτής Καθηγητής ΕΚΠΑ

Χρήστος Ξενάκης,
Επίκουρος Καθηγητής Πανεπιστήμιου Πειραιά

Ημερομηνία εξέτασης 31/07/2014

ABSTRACT

Today's heterogeneous wireless network (HWN) is a collection of ubiquitous wireless networking elements (WNEs) that support diverse functional capabilities and networking purposes. In such a heterogeneous networking environment, localization and mobility management will play a key role for the seamless support of emerging applications, such as social networking, massive multiplayer online gaming, device-to-device (D2D) communications, smart metering, first-responder communications, and unsupervised navigation of communication-aware robotic nodes. Most of the existing wireless networking technologies enable the WNEs to assess their current radio status and directly (or indirectly) estimate their relative distance and angle with respect to other WNEs of the same Radio Access Technology (RAT); thus, the integration of such information from the ubiquitous WNEs arises as a natural solution for robustly handling localization between (not necessarily homogeneous) WNEs and mobility management of moving WNEs governed by resource-constrained operation. Under this viewpoint, we investigate the utilization of such spatial information can be used to enhance the performance of localization and mobility management in the today's HWN. In this work we focus and contribute in the following four research areas: i) localization and peer-discovery between non-homogeneous WNEs, ii) network-assisted D2D discovery in cellular networks, iii) energy-efficient handover (HO) decision in the macrocell – femtocell network, and iv) network-assisted vertical handover decision (VHO) for the integrated cellular and WLAN HWN.

In the area of localization and peer-to-peer discovery in HWNs, we derive closed-form expressions for the distance distribution between two heterogeneous WNEs, given partial or full knowledge of the HWN topology. The derived expressions enable us to analyze how different levels of location-awareness affect the performance of localization and peer discovery between (not necessarily homogeneous) WNEs. Optimal strategies for the deployment of WNEs are presented, as means of maximizing the probability of successful discovery between two WNEs of interest, and useful guidelines are drawn for the design of localization and peer discovery in the nowadays HWN.

In the area of D2D discovery in cellular networks, we analyze the performance of network-assisted D2D discovery in random spatial networks and derive useful design guidelines for fine-tuning its performance in cellular systems. Specifically, we derive the distance distribution between two tagged D2D peers conditioned on the core network's knowledge of the cellular network layout. The derived expressions are used to analyze the behavior of the D2D discovery probability with respect to key system parameters, as well as to identify the conditions under which D2D discovery probability is maximized with respect to the base station density. Exact and approximate expressions for the optimal density are also derived, while numerical results provide valuable insights on the key performance tradeoffs inherent to the network-assisted D2D discovery process.

In the area of handover decision for the macrocell – femtocell network, our contribution is three-fold. Firstly, we show that the handover decision can play a key role for handling cross-tier interference in the two-tier macrocell-femtocell network and reducing the energy consumption at the mobile terminals, if standard cellular measurements are to be exploited. Secondly, we propose an energy-efficient handover decision algorithm for the macrocell – femtocell network and discuss all aspects related to its implementation in the Long Term Evolution-Advanced (LTE-A) system of the 3rd Generation Partnership Project (3GPP). We show that compared to other existing algorithms, the proposed algorithm substantially reduces the interference and the energy consumption at the mobile terminals, at the cost of moderate increase in network signaling. Thirdly, we provide a comprehensive discussion on the key research

challenges of mobility management in the presence of femtocells, survey and classify current state-of-the-art HO decision algorithms for femtocells, and provide both qualitative and quantitative comparisons of their performance by using the well-established evaluation methodology of the Small Cell Forum.

In the area of vertical handover decision for heterogeneous wireless networks, we propose an energy-efficient VHO decision algorithm that exploits two major enhancements to the baseline operation of the LTE-A and the IEEE 802.11 systems, including the Access Network Discovery and Selection Function (ANDSF) and the enhanced radio measurement capabilities at the base stations and the IEEE 802.11-2012 conformant access points. To the best of our knowledge, this is the first work to exploit these two exciting new capabilities of the respective 3GPP and IEEE systems, as means of minimizing the power consumption at the multi-mode mobile terminals (MMTs) through energy-efficient vertical handover decision. Extensive system-level simulation results validate the performance of the proposed algorithm, demonstrating its capacity to achieve efficient load balancing between heterogeneous RATs, reduced energy consumption per bit at the mobile terminals and enhanced uplink throughput, at the cost of an increased signaling rate at the ANDSF and the WLAN network.

This doctoral thesis uses both analytical and simulation models to evaluate the performance of the proposed frameworks and algorithms. The mathematical analysis is mainly based in fundamental results in the areas of Probability Theory, Stochastic Processes, and Stochastic Geometry. On the other hand, the simulation-based evaluations are based on the system-level simulation methodology proposed by the Small Cell Forum.

SUBJECT AREA: Mobility Management in Heterogeneous Wireless Networks

KEYWORDS: Localization, Peer-to-peer discovery, Handover, Vertical Handover, Heterogeneous Wireless Networks, Network-assistance, Device-to-Device Discovery, Femtocells, Wireless Local Area Networks

ΠΕΡΙΛΗΨΗ

Το σημερινό ετερογενές δίκτυο ασυρμάτων επικοινωνιών αποτελείται από ένα σύνολο πανταχού-παρόντων ασυρμάτων δικτυακών στοιχείων, τα οποία υποστηρίζουν διαφορετικές τεχνολογικές δυνατότητες και εξυπηρετούν διαφορετικού-τύπου ανάγκες δικτύωσης. Σε ένα τέτοιο ετερογενές δικτυακό περιβάλλον, ο υπολογισμός σχετικής θέσης (localization) και η διαχείριση κινητικότητας (mobility management) θα διαδραματίσουν καθοριστικό ρόλο στην απρόσκοπτη υποστήριξη αναδυόμενων καινοτόμων εφαρμογών, όπως η κοινωνική δικτύωση, τα δικτυακά παιχνίδια με εξαιρετικά μεγάλο αριθμό χρηστών (massive multi-player online gaming), επικοινωνίες συσκευής-με-συσκευή (device-to-device communications), έξυπνων μετρήσεων (smart metering), επικοινωνιών έκτακτης ανάγκης (first responder communications), καθώς και η αυτόνομη πλοήγηση ρομποτικών κόμβων που έχουν δυνατότητα δικτύωσης. Καθώς όλο και περισσότερες ασύρματες δικτυακές τεχνολογίες επιτρέπουν στα ασύρματα δικτυακά στοιχεία τους να αξιολογούν την τρέχουσα κατάσταση του καναλιού επικοινωνίας τους και να εκτιμούν άμεσα (ή έμμεσα) την σχετική τους απόσταση και γωνία ως προς άλλους δικτυακούς κόμβους της ιδίας τεχνολογίας, η αξιοποίηση-ενοποίηση των ανωτέρω πληροφοριών από τα πανταχού-παρόντα ασύρματα δικτυακά στοιχεία, αναδεικνύεται ως η πλέον εφικτή και αποτελεσματική λύση για α) τον υπολογισμό της σχετικής απόστασης μεταξύ δύο (όχι υποχρεωτικά της ίδιας τεχνολογίας) δικτυακών κόμβων ενδιαφέροντος και β) για την διαχείριση κινητικότητας κινητών δικτυακών κόμβων με περιορισμένους πόρους, π.χ. όσους λειτουργούν με μπαταρία. Υπό το πρίσμα της αξιοποίησης των ανωτέρω πληροφοριών για την βελτίωση του υπολογισμού σχετικής θέσης και της διαχείρισης κινητικότητας, στην παρούσα διδακτορική διατριβή επικεντρώνουμε και συμβάλλουμε στις ακόλουθες τέσσερις ερευνητικές περιοχές: i) υπολογισμός σχετικής θέσης και εύρεση σημείου-προς-σημείο (peer-to-peer discovery) μεταξύ ετερογενών ασύρματων δικτυακών στοιχείων, ii) εύρεσης συνδέσεων συσκευής-προς-συσκευή (device-to-device discovery) σε κυψελωτά δίκτυα με υποβοήθηση από το δίκτυο (network-assistance), iii) ενεργειακά-αποδοτικών οριζόντιων μεταπομπών σε δίκτυα μακροκυψελών - φεμτοκυψελών, iv) υποβοηθούμενης από το δίκτυο (network-assisted) κάθετης μεταπομπής σε ενοποιημένα δίκτυα κυψελωτών επικοινωνιών (cellular) και επικοινωνιών τοπικής πρόσβασης (WLAN).

Στην περιοχή υπολογισμού σχετικής θέσης και εύρεσης σημείου-προς-σημείο σε ετερογενή δίκτυα, εξάγουμε αναλυτικές σχέσεις κλειστού τύπου (closed-form expressions) για την κατανομή της σχετικής απόστασης μεταξύ δύο ετερογενών ασυρμάτων δικτυακών στοιχείων, δοσμένης μερικής (ή πλήρους) γνώσης για την γενικότερη τοπολογία του ετερογενούς δικτύου. Η εξαχθείσες σχέσεις μας επιτρέπουν να αναλύσουμε την απόδοση της διαδικασίας υπολογισμού σχετικής θέσης και εύρεσης σημείου-προς-σημείο μεταξύ ασυρμάτων δικτυακών στοιχείων διαφορετικής τεχνολογίας, δοσμένων διαφόρων συνδυασμών πληροφορίας για τις σχετικές θέσεις των ασυρμάτων δικτυακών στοιχείων του ετερογενούς δικτύου. Επιπρόσθετα, εξάγουμε βέλτιστες στρατηγικές για την τοποθέτηση ασυρμάτων δικτυακών στοιχείων στο δίκτυο, με στόχο την μεγιστοποίηση της πιθανότητας επιτυχούς εύρεσης δύο στοιχείων ενδιαφέροντος, και προτείνουμε χρήσιμες κατευθυντήριες γραμμές για τον σχεδιασμό καινοτόμων μηχανισμών υπολογισμού σχετικής θέσης και εύρεσης σημείου-προς-σημείο στο σημερινό ετερογενές δίκτυο. Από όσο γνωρίζουμε, η εργασία αυτή είναι η πρώτη που υιοθετεί το ανωτέρω μοντέλο εντοπισμού σχετικής θέσης και εύρεσης σημείου-προς-σημείο μεταξύ *μη ομογενών* ασύρματων δικτυακών στοιχείων, και αναπτύσσει κατάλληλα μαθηματικά μοντέλα για την ανάλυση της απόδοσης του.

Στην περιοχή εύρεσης συνδέσεων συσκευής-προς-συσκευή σε κυψελωτά δίκτυα με υποβοήθηση από το δίκτυο, αναλύουμε την απόδοση της εύρεσης συνδέσεων

συσκευής-προς-συσκευή σε κυψελωτά δίκτυα με τυχαία κατανομή κόμβων και δυνατότητα υποβοήθησης από το δίκτυο, και εξάγουμε χρήσιμες κατευθυντήριες γραμμές για την βελτίωση της εν λόγω λειτουργίας σε σημερινά κυψελωτά δίκτυα. Πιο συγκεκριμένα, εξάγουμε την κατανομή της σχετικής απόστασης μεταξύ δύο συσκευών ενδιαφέροντος, δοσμένης μερικής ή πλήρους πληροφορίας για την τοπολογία του κυψελωτού δικτύου (από πλευράς δικτύου κορμού). Η εξαχθείσες αναλυτικές εκφράσεις χρησιμοποιούνται για την ανάλυσης της στατιστικής συσχέτισης μεταξύ της πιθανότητας επιτυχούς εύρεσης συνδέσεων συσκευής-προς-συσκευή και των πλέον σημαντικών παραμέτρων συστήματος. Επίσης, η χρήση των εκφράσεων αυτών μας επιτρέπει να αναγνωρίσουμε τις συνθήκες υπό τις οποίες η ανωτέρω πιθανότητα μεγιστοποιείται ως προς την πυκνότητα των κυψελωτών σταθμών. Ακριβής και προσεγγιστικές εκφράσεις παρουσιάζονται για την τιμή της βέλτιστης πυκνότητας κυψελωτών σταθμών, ενώ η χρήση αριθμητικών αποτελεσμάτων μας οδηγεί στην εξαγωγή χρήσιμων συμπερασμάτων για τους αυτογενείς συμβιβασμούς (trade-offs) που διέπουν την απόδοση της εύρεσης συνδέσεων συσκευής-προς-συσκευή σε κυψελωτά δίκτυα με υποβοήθηση από το δίκτυο. Η παρούσα εργασία αποτελεί μία από τις πρώτες εργασίες στην εν λόγω ερευνητική περιοχή.

Στην περιοχή οριζόντιων μεταπομπών σε δίκτυα μακροκυψελών – φεμτοκυψελών, η συμβολή μας ως προς την τρέχουσα βιβλιογραφία εστιάζεται σε τρία σημεία. Πρώτον, η εργασία μας αναδεικνύει ότι η απόφαση μεταπομπής δύναται να διαδραματίσει εξέχων ρόλο για την διαχείριση των παρεμβολών σε δίκτυα μακροκυψελών – φεμτοκυψελών καθώς και για την μείωση της ενεργειακής κατανάλωσης στα κινητά τερματικά, αν αξιοποιηθούν μετρήσεις για την ράδιο-κατάσταση των κυψελωτών σταθμών. Δεύτερον, προτείνουμε έναν ενεργειακά-αποδοτικό αλγόριθμο μεταπομπής για δίκτυα μακροκυψελών – φεμτοκυψελών και εξετάζουμε όλες τις απαιτήσεις εφαρμογής του στο κυψελωτό σύστημα Long Term Evolution-Advanced (LTE-A) που αναπτύχθηκε από την 3rd Generation Partnership Project (3GPP). Εν συγκρίσει με άλλες υπάρχουσες λύσεις, ο προτεινόμενος αλγόριθμος οδηγεί σε μείωση των παρεμβολών και της ενεργειακής κατανάλωσης στα κινητά τερματικά, με κόστος την μέτρια αύξηση του κόστους σηματοδοσίας στο δίκτυο. Τρίτον, αναδεικνύουμε και συζητούμε εκτενώς τις τρέχουσες προκλήσεις για την διαχείριση κινητικότητας σε δίκτυα φεμτοκυψελών, επισκοπούμε και ταξινομούμε υπάρχοντες αλγορίθμους μεταπομπής για φεμτοκυψέλες, και παρέχουμε εκτενείς ποιοτικές και ποσοτικές συγκρίσεις της απόδοσης τους χρησιμοποιώντας την κοινώς αποδεκτή μεθοδολογία προσομοίωσης σε επίπεδο συστήματος του Small Cell Forum.

Στην περιοχή κάθετων μεταπομπών σε ετερογενή ασύρματα δίκτυα, προτείνουμε έναν ενεργειακά-αποδοτικό αλγόριθμο κάθετης μεταπομπής, ο οποίος αξιοποιεί δύο σημαντικές βελτιώσεις που επιτελέστηκαν πρόσφατα στα συστήματα LTE-A (κυψελωτές επικοινωνίες) και IEEE 802.11 (τοπικής ασύρματης πρόσβασης): την Λειτουργία Εύρεσης και Επιλογής Δικτύου Πρόσβασης (Access Network Discovery and Selection Function - ANDSF) και την δυνατότητα εξαγωγής ράδιο-μετρήσεων για την κατάσταση του καναλιού στους κυψελωτούς σταθμούς LTE-A και στα σημεία πρόσβασης που είναι συμβατά με το πρότυπο IEEE 802.11-2012. Από όσο γνωρίζουμε, η παρούσα εργασία είναι η πρώτη που εκμεταλλεύεται τις ανωτέρω δύο βελτιώσεις των συστημάτων LTE-A και IEEE 802.11, με απώτερο στόχο την ελαχιστοποίηση της κατανάλωσης ενέργειας σε κινητά πολλαπλών ράδιο-επαφών (multi-mode mobile terminals – MMTs) διαμέσου της εφαρμογής ενεργειακά-αποδοτικών κάθετων μεταπομπών. Εκτενείς προσομοιώσεις σε επίπεδο συστήματος αναδεικνύουν ότι ο προτεινόμενος αλγόριθμος επιτυγχάνει αποδοτική εξισορρόπηση του φόρτου κίνησης μεταξύ των δύο ετερογενών συστημάτων, οδηγεί σε μειωμένη ενεργειακή κατανάλωση ανά μονάδα δεδομένων (energy per bit) στα κινητά τερματικά, και βελτιώνει σημαντικά την ρυθμαπόδοση στην

ανωφερή ζεύξη (uplink), με κόστος την αύξηση του ρυθμού σηματοδοσίας στην μονάδα ANDSF και στο δίκτυο ασύρματης τοπικής πρόσβασης (Wireless Local Area Network - WLAN).

Η παρούσα διδακτορική διατριβή αποτιμά την απόδοση των προτεινόμενων λύσεων συνδυάζοντας μοντέλα μαθηματικής ανάλυσης και προσομοίωσης σε υπολογιστή. Τα αναπτυχθέντα μαθηματικά μοντέλα βασίζονται κυρίως στην Θεωρία Πιθανοτήτων, Στοχαστικών Διεργασιών, και Στοχαστικής Γεωμετρίας. Αφετέρου, οι αποτιμήσεις που στηρίζονται σε μοντέλα προσομοίωσης βασίζονται στην μεθοδολογία προσομοίωσης σε επίπεδο συστήματος που έχει προταθεί από το Small Cell Forum.

ΘΕΜΑΤΙΚΗ ΠΕΡΙΟΧΗ: Διαχείριση Κινητικότητας σε Ετερογενή Ασύρματα Δίκτυα

ΛΕΞΕΙΣ ΚΛΕΙΔΙΑ: Υπολογισμός σχετικής θέσης, αναζήτηση δικτύου, οριζόντια μεταπομπή, κάθετη μεταπομπή, ετερογενή ασύρματα δίκτυα, υποβοήθηση από το δίκτυο, επικοινωνίες συσκευής-με-συσκευή, φεμτοκυψέλες, δίκτυα ασύρματης τοπικής πρόσβασης

Σε όλους τους καταξιωμένους και άσημους δασκάλους που με δίδαξαν
να εκτιμώ, να δημιουργώ, και να αγωνίζομαι επίμονα για ότι αξίζει.
Στην γυναίκα μου Αναστασία και την κόρη μου Θεοφανία

To all recognized and not-so-recognized tutors that taught me appreciation,
creativity, and persistency in fighting for what it's worth.
To my wife Anastasia and my daughter Theofania

LIST OF PUBLICATIONS / ΛΙΣΤΑ ΔΗΜΟΣΙΕΥΣΕΩΝ

Book Chapters

1) **D. Xenakis**, N. Passas, L. Merakos, and C. Verikoukis, “Energy-Efficient Roaming for Heterogeneous Wireless Networks”, Editors: A. R. Radwan and J. Rodriguez, *Energy Efficient Smart Phones for 5G Networks*, Springer, 2014.
2) **D. Xenakis**, N. Passas, A. Radwan, J. Rodriguez, and C. Verikoukis, "Energy Efficient Mobility Management for the Macrocell - Femtocell LTE-Advanced Network ", appears in "Energy Efficiency - The Innovative Ways for Smart Energy, the Future Towards Modern Utilities", Editor: Moustafa Eissa, InTech Publishers, ISBN: 978-953-51-0800-9, Oct. 2012.
3) D. Tsolkas, **D. Xenakis**, and N. Passas, "Next generation cognitive cellular networks, LTE, WiMAX and wireless broadband access ", appears in "Cognitive Radio and its Application for Next Generation Cellular and Wireless Networks", Editors: Hrishikesh Venkataraman and Gabriel-Miro Muntean, Springer Publishers, ISBN 978-94-007-1826-5, Aug. 2012.
4) D. Tsolkas, **D. Xenakis**, D. Triantafyllopoulou, and N. Passas, "Medium Access Control Layer", to appear in the "Advances on Processing for Multiple Carrier Schemes: OFDM & OFDMA" book, ISBN: 978-1-61470-634-2, Nova Publishers, Editors: N. Zorba, and F. Bader, 2nd quarter 2012.

Peer-reviewed Journals (Accepted)

1) **D. Xenakis**, N. Passas, and L. Merakos, “Multi-Parameter Performance Analysis for Decentralized Cognitive Radio Networks”, *Springer Wireless Networks* (WINET) Journal, vol. 20, issue 4, May 2014.
2) **D. Xenakis**, N. Passas, L. Merakos, and C. Verikoukis, “Mobility Management for Femtocells in LTE-Advanced: Key Aspects and Survey of Handover Decision Algorithms”, *IEEE Communications Surveys and Tutorials*, vol. 16, issue 1, First Quarter 2014.
3) **D. Xenakis**, N. Passas, and C. Verikoukis, “An Energy-Centric Handover Decision Algorithm for the Integrated LTE-Advanced Macrocell - Femtocell Network”, special issue on Wireless Green Communications and Networking, *Elsevier Computer Communications*, vol. 35, issue 14, August 2012.
4) **D. Xenakis**, D. Tsolkas, N. Passas, N. Alonistioti, and L. Merakos, “Dynamic Resource Allocation in Adaptive Wireless OFDMA Systems”, *Wiley Wireless Communications and Mobile Computing (WCMC) Journal*, vol. 12, iss. 11, pages 985–998, 10 Aug 2012.

Peer-reviewed Conferences (Accepted)

1) R. Shrivastava, S. Costanzo, K. Samdanis, D. Grace, **D. Xenakis**, N. Passas, L. Merakos, “Elastic RAN for Efficient Resource Management in LTE/LTE-A FDD/TDD HetNets” *IEEE CloudNet 2014*, Luxembourg, Oct 2014.
2) **D. Xenakis**, N. Passas, L. Merakos, and C. Verikoukis, “ARCHON: An ANDSF-Assisted Energy-Efficient Vertical Handover Decision Algorithm for the Heterogeneous IEEE 802.11/LTE-Advanced Network”, IEEE International Conference on Communications (IEEE ICC) 2014 , Sydney, Australia, June 2014.

3) S. Costanzo, **D. Xenakis**, N. Passas, and L. Merakos, “OpeNB: A framework for Virtualizing Base Stations in LTE-Advanced Networks”, IEEE International Conference on Communications (IEEE ICC) 2014, Sydney, Australia, June 2014.

4) **D. Xenakis**, N. Passas, L. Merakos, and C. Verikoukis, “Energy-Efficient and Interference-Aware Handover Decision for the LTE-Advanced Femtocell Network”, IEEE International Conference on Communications (IEEE ICC) 2013, Budapest, Hungary, June 2013.

5) **D. Xenakis**, N. Passas, and C. Verikoukis, “A Novel Handover Decision Policy for Reducing Power Transmissions in the two-tier LTE-Advanced network”, IEEE International Conference on Communications (IEEE ICC) 2012, Ottawa, Canada, June 2012.

6) **D. Xenakis**, N. Passas, L. Di Gregorio, and C. Verikoukis, “A Context-Aware Vertical Handover Framework Towards Energy-Efficiency”, The 73rd IEEE Vehicular Technology Conference (IEEE VTC), Budapest, Hungary, May 2011.

7) D. Tsolkas, **D. Xenakis**, N. Passas, and L. Merakos, “Opportunistic Spectrum Access over Mobile WiMAX Networks”, The 15th IEEE International Workshop on Computer-Aided Modeling Analysis and Design of Communication Links and Networks (IEEE CAMAD 2010), Miami, USA, December 2010.

8) D. Xenakis, D. Tsolkas, N. Passas, and L. Merakos, “Dynamic resource allocation in adaptive wireless multiuser multicarrier systems”, European Wireless 2010, Lucca, Italy, April 2010.

9) D. Xenakis, D. Tsolkas, N. Passas, and L. Merakos, “A Dynamic Subchannel Allocation Algorithm for IEEE 802.16e Networks”, IEEE International Symposium on Wireless Pervasive Computing (IEEE ISWPC) 2008, Santorini, Greece, May 2008.

Deliverables in European Projects

1) J. Kibiłda, J. Watral, R. Piesiewicz, T. Moreira, A. Gomes, **D. Xenakis**, M. Raspopoulos, A. Radwan, J. Rodriguez, and J. Cardoso, “Energy efficient Vertical Handover algorithms: Final Specification”, Deliverable 6.3 in ICT- 248577 C2POWER, January 2013.

2) M. Raspopoulos, E. Charalambous, S. Stavrou, J. Kibiłda, R. Piesiewicz, **D. Xenakis**, C. Verikoukis, T. Moreira, A. Gomes, A. Radwan, J. Rodriguez, “C2POWER Mobility Platform for Vertical Handover Provision and description of the modules provided to WP7”, Deliverable 6.2 in ICT-248577 C2POWER, June 2012.

3) A. Gomes, E. Sá, P. Neves, J. Rodriguez, A. Radwan, P. Marques, M. Albano, M. Raspopoulos, S. Stavrou, E. Charalambous, R. Fedrizzi, S. Kandeepan, D. Noguet, L. Dussopt, P. Trapps, J. Kibilda, M. Filo, R. Piesiewicz, Q. Zhang, K. Moessner, H. Gromat, C. Gruet, H. Mokrani**, D. Xenakis**, “Scenarios, System architecture definition and performance metrics”, Deliverable 2.2 in ICT-248577 C2POWER, Oct. 2010.

Lectures and Seminars in International Conferences / Projects

1) **D. Xenakis**, "Mobility Management for Multi-tier Cellular Networks: Research Challenges and Modeling Issues", 1st FP7 MITN-CROSSFIRE Seminar, 5 July 2013, SUPELEC, Paris - France.

2) **D. Xenakis**, "Mobility Management for Femtocells in LTE-Advanced: Key Aspects and Research Challenges", Advanced Networking Class, Spring Semester 2012 - 2014.

3) **D. Xenakis**, "Component and System Level Energy Saving for Femtocells in Future Mobile Heterogeneous Networks", Advanced Networking Class, Spring Semester 2012 - 2014.

4) **D. Xenakis**, C. Verikoukis, "Context-Aware Handover Decision for the LTE-Advanced Network of Small Cells", Cognitive Platform Day 2013, OTE Academy, Athens – Greece, 21 June 2013.

5) **D. Xenakis**, N. Passas, L. Merakos, and C. Verikoukis, "Mobility Management for Femtocells in LTE-Advanced: Key Aspects, Survey of Handover Decision Algorithms and Context-Aware Algorithmic Design", FP7 ICT-Acropolis (NoE) Winter School, 15 Feb 2013, CTTC, Barcelona - Spain.

6) **D. Xenakis**, M. Huetwohl, N. Passas, T. Moreira, A. Gomes, A. Radwan, J.Rodriguez, and Ch. Verikoukis, "Energy-efficient Business Models and Mobility Management for the LTE-Advanced Femtocell Network", Femto Forum, Networks Group, Wroclaw, Sept. 2012.

7) **D. Xenakis**, C. Verikoukis, "Energy-Efficient Mobility Management for the Integrated Macrocell-Femtocell LTE-Advanced Network", Femtocell Winter School, February 6-10, 2012, Barcelona, Spain.

Peer-reviewed Journals (Under Revision)

1) **D. Xenakis**, M. Kountouris, L. Merakos, N. Passas, and C. Verikoukis, “Performance Analysis of Network-Assisted D2D Discovery in Random Spatial Networks”, *submitted to IEEE Transactions on Wireless Communications*, May 2014.

2) **D. Xenakis**, N. Passas, L. Merakos, and C. Verikoukis, “Handover Decision for Small Cells: Algorithms, Lessons Learned and Simulation Study”, May 2014.

3) **D. Xenakis**, N. Passas, L. Merakos, and C. Verikoukis, “Advanced Mobility Management for Reduced Interference and Energy Consumption in the Two-tier LTE-Advanced Network”, *Elsevier Computer Networks*, *first revision*, May 2014.

Peer-reviewed Journals (Under Preparation)

1) **D. Xenakis**, “Localization and Peer Discovery using Spatial Information from the Heterogeneous Wireless Network”, 2014.

2) **D. Xenakis**, N. Passas, L. Merakos, and C. Verikoukis, “ANDSF-Assisted Vertical Handover Decision for the Heterogeneous IEEE 802.11/LTE-Advanced Network”, under preparation, 2014.

3) S. Costanzo, **D. Xenakis**, N. Passas, and L. Merakos “Shifting network virtualization to the access network: A methodological framework for the LTE-Advanced system”, under preparation, 2014.

ΣΥΝΟΠΤΙΚΗ ΠΑΡΟΥΣΙΑΣΗ ΤΗΣ ΔΙΔΑΚΤΟΡΙΚΗΣ ΔΙΑΤΡΙΒΗΣ (GREEK SYNOPSIS)

Τα τελευταία χρόνια έχουν εγκατασταθεί παγκοσμίως ασύρματα σημεία σύνδεσης ετερογενών τεχνολογικών δυνατοτήτων και χαρακτηριστικών, κάθε ένα από τα οποία έχει βελτιστοποιηθεί για την εξυπηρέτηση αναγκών διαφορετικού σκοπού και ετερογενών απαιτήσεων επικοινωνίας. Πιο συγκεκριμένα, έχουν εγκατασταθεί σταθμοί βάσης για ασύρματες κυψελωτές επικοινωνίες μεγάλης εμβέλειας, γνωστοί και ως μάκρο-κυψέλες (macrocells), σταθμοί βάσης για ασύρματες κυψελωτές επικοινωνίες μικρής και πολύ μικρής εμβέλειας, περιλαμβανομένων μικρό-κυψελών (microcells), πίκο-κυψελών (picocells), και φέμτο-κυψελών (femtocells), σημεία σύνδεσης για τοπική πρόσβαση σε μη αδειοδοτημένο φάσμα, για παράδειγμα σημεία πρόσβασης για ασύρματη τοπική πρόσβαση IEEE 802.11 (Wireless Local Area Networks – WLAN), αισθητήρες χαμηλής ισχύος ειδικού σκοπού, για παράδειγμα ZigBee sensors για μετρήσεις και επικοινωνία σε Έξυπνα Ηλεκτρικά Δίκτυα (Smart Grid), καθώς και μία ευρεία γκάμα λοιπών σημείων σύνδεσης που υποστηρίζουν διάφορους τύπους τεχνολογιών ασύρματης πρόσβασης. Άξιο αναφοράς είναι και το γεγονός ότι ως σημεία σύνδεσης με το ασύρματο κυψελωτό δίκτυο μπορούν να λογίζονται πλέον (υπό προϋποθέσεις) και τα τερματικά χρηστών που βρίσκονται εντός εμβέλειας (επικοινωνίες Συσκευής-με-Συσκευή – Device-to-Device Communications). Από τα ανωτέρω, γίνεται αντιληπτό ότι η διαχείριση κινητικότητας σε ετερογενή ασύρματα δίκτυα επικοινωνιών εγείρει προκλήσεις σε πολλά επίπεδα και φάσεις της υλοποίησης της σε πραγματικά συστήματα.

Αναπόσπαστο κομμάτι της διαχείρισης κινητικότητας αποτελούν η αναζήτηση των ετερογενών σημείων σύνδεσης εντός εμβέλειας του χρήστη και η επιλογή του πλέον κατάλληλου για μεταπομπή του χρήστη σε αυτό, σύμφωνα με τις δυνατότητες και τις απαιτήσεις επικοινωνίας του εκάστωτε χρήστη. Επιπρόσθετο βήμα για την βέλτιστη διαχείριση κινητικότητας των χρηστών σε ετερογενή δίκτυα επικοινωνιών αποτελεί και η διαδικασία εντοπισμού της σχετικής θέσης του χρήστη ως προς κάποιο σημείο ενδιαφέροντος, γνωστή και ως *localization*. Μέσω της διαδικασίας αυτής μπορούν να βελτιστοποιηθούν οι διάφορες παράμετροι επικοινωνίας του χρήστη με το ετερογενές δίκτυο καθώς και να υποστηριχθούν διάφορες καινοτόμες υπηρεσίες με βάση την θέση της κινητής συσκευής του χρήστη. Σε κάθε περίπτωση, καθότι οι σύγχρονες κινητές συσκευές υποστηρίζουν ένα μεγάλο εύρος διεπαφών τεχνολογιών ασύρματης πρόσβασης, η κοινή χρήση των διεπαφών είτε για τον εντοπισμό θέσης είτε για την αναζήτηση και μεταπομπή του χρήστη σε κάποιο σημείο σύνδεσης, μειώνει δραματικά το χρόνο ζωής της μπαταρίας. Συνεπώς, η ελαχιστοποίηση της κατανάλωσης ενέργειας στο κινητό σε συνδυασμό με την απρόσκοπτη διαχείριση κινητικότητας και τον εντοπισμό των κινητών χρηστών σε ένα ετερογενές ασύρματο δίκτυο επικοινωνιών αποτελεί σημαντική πρόκληση.

Υπό την ανωτέρω σκοπιά, η παρούσα διδακτορική διατριβή στοχεύει στην αξιοποίηση υπαρχουσών πληροφοριών σχετικής θέσης ή κατάστασης λειτουργίας των διαφόρων σημείων σύνδεσης στο ετερογενές ασύρματο δίκτυο επικοινωνιών με στόχο την βελτίωση της ποιότητα υπηρεσίας και την ελαχιστοποίηση της κατανάλωσης ενέργειας των κινητών συσκευών δια της εφαρμογής πιο εξελιγμένων μηχανισμών εντοπισμού θέσης, αναζήτησης ετερογενών σημείων σύνδεσης, και μεταπομπής στο πλέον κατάλληλο σημείο σύνδεσης του δικτύου. Ως κατάλληλο σημείο σύνδεσης η διατριβή ορίζει το σημείο σύνδεσης που ελαχιστοποιεί την κατανάλωση του κινητού τερματικού διατηρώντας παράλληλα ένα συγκεκριμένο μέσο ρυθμό σήματος προς παρεμβολές και θόρυβο (Signal to Interference plus Noise Ratio – SINR), ο οποίος προσαρμόζεται με βάση τις ανάγκες επικοινωνίας του εκάστωτε χρήστη.

Ως προς αυτή την κατεύθυνση, η παρούσα διδακτορική διατριβή περιλαμβάνει/προτείνει τα κάτωθι: α) ένα αναλυτικό μοντέλο για την ανάλυση της απόδοσης εντοπισμού σχετικής θέσης (localization) και εντοπισμού κόμβων-στόχων (peer discovery) σε ετερογενή ασύρματα δίκτυα επικοινωνιών, δοσμένων διαφόρων συνδυασμών πληροφορίας ως προς την σχετική απόσταση και γωνία μεταξύ μέρους των σημείων σύνδεσης του δικτύου, β) ένα αναλυτικό μοντέλο για την ανάλυση της απόδοσης της διαδικασίας αναζήτησης συσκευών-στόχων για την εγκαθίδρυση συνδέσεων συσκευής-προς-συσκευή με την βοήθεια του δικτύου κυψελωτών επικοινωνιών (network-assisted Device-to-Device discovery), γ) αλγορίθμους οριζόντιας μεταπομπής (handover) σε ετερογενή δίκτυα μάκρο-κυψελών – φέμτο-κυψελών που ελαχιστοποιεί την ισχύ εκπομπής των κινητών συσκευών διατηρώντας ένα προκαθορισμένο μέσο στόχο SINR, δ) έναν αλγόριθμο κάθετης μεταπομπής (vertical handover) χρηστών σε ετερογενή δίκτυα κυψελωτών σταθμών βάσης και σημείων ασύρματης τοπικής πρόσβασης (WLAN) που ελαχιστοποιεί την συνολική κατανάλωση επικοινωνίας των κινητών συσκευών διατηρώντας παράλληλα ένα προκαθορισμένο μέσο στόχο SINR, και ε) μία εκτενή βιβλιογραφική επισκόπηση, ταξινόμηση, ποιοτική και ποσοτική ανάλυση της απόδοσης υπαρχουσών αλγορίθμων μεταπομπής σε ετερογενή δίκτυα μάκρο-κυψελών και μικρών κυψελών.

Κοινό σημείο αναφοράς όλων των προτεινόμενων αναλυτικών μοντέλων και αλγορίθμων βελτιστοποίησης είναι η αξιοποίηση πληροφορίας θέσης ή ραδιο-κατάστασης των στοιχείων του δικτύου, από τα γειτονικά σημεία σύνδεσης του ετερογενούς ασύρματου δικτύου επικοινωνιών. Κάποιες παράμετροι της ραδιο-κατάστασης των στοιχείων του δικτύου που λαμβάνονται υπόψη είναι ως η ισχύς εκπομπής, το επίπεδο παρεμβολών, και η λαμβανόμενη ισχύ σήματος στον δέκτη. Βάση για την ανάπτυξη των αναλυτικών μοντέλων αποτελέσαν η Θεωρία Πιθανοτήτων, η Θεωρία Στοχαστικών Διεργασιών και η Στοχαστική Γεωμετρία, ενώ η απόδοση των προτεινόμενων αλγορίθμων αποτιμήθηκε αξιοποιώντας την κοινώς αποδεκτή και ευρέως διαδομένη μεθοδολογία αξιολόγησης με προσομοίωση σε επίπεδο συστήματος (system-level simulations) του Small Cell Forum. Η δομή της διδακτορικής διατριβής έχει ως ακολούθως.

Στο πρώτο κεφάλαιο της διδακτορικής διατριβής, περιγράφεται την τρέχουσα κατάσταση στο πεδίο των ασυρμάτων δικτύων επικοινωνιών και συνοψίζονται οι τελευταίες μεταβολές στην τρέχουσα αρχιτεκτονική τους. Στην συνέχεια, τίθενται οι βασικοί προβληματισμοί που αφορούν στη μελέτη και την εξέλιξη των πεδίων αυτών με έμφαση στα διαχείρισης κινητικότητας, εντοπισμού και ενέργειας στα κινητά τερματικά, οριοθετώντας το πλαίσιο εντός του οποίου κινείται η θεματολογία της διδακτορική διατριβής. Στο κεφάλαιο αυτό αναφέρονται επίσης οι ιδιαιτερότητες των σύγχρονων περιβαλλόντων ασύρματων δικτύων επικοινωνιών, στα οποία παρατηρείται αλληλοεπικάλυψη πολλών διαφορετικών τεχνολογιών πρόσβασης σε μια γεωγραφική περιοχή, ενώ παράλληλα αναδεικνύονται οι προκλήσεις και οι ευκαιρίες που προκύπτουν από την συνύπαρξη των υπαρχουσών συστημάτων ασύρματης πρόσβασης στον χώρο. Παράλληλα, δίνεται μια σύντομη περιγραφή των βασικών λειτουργιών σημαντικών συστημάτων ασύρματης πρόσβασης, μεταξύ των οποίων τα συστήματα 3rd Generation Partnership Project for the Long term Evolution – Advanced system (3GPP LTE-Advanced) και IEEE 802.11-2012, με απώτερο στόχο την ανάδειξη των λειτουργικών χαρακτηριστικών που τους επιτρέπει την υποστήριξη πιο αποδοτικών και εξελιγμένων μηχανισμών εντοπισμού θέσης, αναζήτησης κόμβων-στόχων, καθώς και μεταπομπής βάση συγκεκριμένων κριτηρίων απόφασης. Επίσης, παρέχεται μία διεξοδική συζήτηση για τα κύρια χαρακτηριστικά και τις προκλήσεις διαχείρισης κινητικότητας σε δίκτυα φέμτο-κυψελών, δίνοντας έμφαση στις φάσεις α) αναγνώρισης κυψελών, β) διαχείρισης πρόσβασης, γ) αναζήτησης κυψέλης, δ)

επιλογής/επανεπιλογής κυψέλης, ε) απόφασης μεταπομπής, και στ) εκτέλεσης μεταπομπής. Σημαντικό κομμάτι του πρώτου κεφαλαίου αποτελεί η αποτύπωση της τρέχουσας βιβλιογραφίας σε κάθε επιμέρους περιοχή ενδιαφέροντος και η σύνοψη των σημαντικότερων αποτελεσμάτων που προέκυψαν από την έρευνα ανά περιοχή.

Στο δεύτερο κεφάλαιο, αναλύουμε με μεγαλύτερη λεπτομέρεια το πρόβλημα εντοπισμού θέσης και αναζήτησης κόμβων-στόχων αξιοποιώντας ράδιο-μετρήσεις από το ετερογενές ασύρματο δίκτυο επικοινωνιών και παρουσιάζει εκτενώς την τρέχουσα βιβλιογραφία που σχετίζεται με το εν λόγω θέμα. Στην συνέχεια περιγράφουμε το μοντέλο του συστήματος υπό εξέταση, καθώς και το μοντέλο συλλογής της πληροφορίας σχετικής απόστασης και γωνίας μεταξύ των μέρους κόμβων του δικτύου. Το κύριο μέρος του κεφαλαίου αυτού είναι οι αναλυτικές σχέσεις, μαζί με τις αποδείξεις τους, ως προς την κατανομή πιθανότητας της σχετικής απόστασης μεταξύ του κόμβου πηγής (source peer) και του κόμβου στόχου (target) στο ετερογενές ασύρματο δίκτυο. Βασιζόμενοι στις σχέσεις αυτές, ο μελετούμε την μονοτονία της κατανομής πιθανότητας ως προς διάφορες παραμέτρους συστήματος, και παρουσιάζει αναλυτικές σχέσεις για παραμέτρους συστήματος που μεγιστοποιούν την πιθανότητα εύρεσης του σημείου στόχου. Το κεφάλαιο ολοκληρώνεται με την επαλήθευση των αποτελεσμάτων και την εξαγωγή χρήσιμων σχεδιαστικών αρχών για την διαδικασία εντοπισμού / αναζήτησης συγκεκριμένων σημείων στόχων σε ετερογενή ασύρματα δίκτυα επικοινωνιών.

Στο τρίτο κεφάλαιο αναλύεται το πρόβλημα της αναζήτησης συσκευών-στόχων σε κυψελωτά συστήματα επικοινωνιών τυχαίας τοπολογίας, με την αξιοποίηση πληροφοριών θέσης στην πλευρά του δικτύου. Ακολουθώντας την ίδια δομή με το προηγούμενο κεφάλαιο, στην συνέχεια περιγράφουμε το μοντέλο του συστήματος υπό θεώρηση και παρουσιάζουμε αναλυτικές σχέσεις, μαζί με τις αποδείξεις τους, ως προς την κατανομή πιθανότητας της σχετικής απόστασης μεταξύ του κόμβου πηγής (source peer) και του κόμβου στόχου (target) στο ετερογενές ασύρματο δίκτυο. Βασιζόμενοι στις σχέσεις αυτές, στην συνέχεια μελετούμε την μονοτονία της κατανομής πιθανότητας ως προς διάφορες παραμέτρους συστήματος, και παρουσιάζουμε αναλυτικές σχέσεις για την πυκνότητα του κυψελωτού δικτύου που μεγιστοποιεί την πιθανότητα εύρεσης μίας συσκευής στόχου. Οι αρχές αυτές επιβεβαιώνονται στο τέλος του κεφαλαίου με την αποτύπωση των αναλυτικών αποτελεσμάτων, ενώ παράλληλα εξάγονται επιπρόσθετες σχεδιαστικές επιλογές για την βελτιστοποίηση της αναζήτησης συσκευών-στόχων σε κυψελωτά συστήματα επικοινωνιών με υποβοήθηση από το δίκτυο.

Στο τέταρτο κεφάλαιο, παρουσιάζεται η σχετική βιβλιογραφία και ο προτεινόμενος αλγόριθμος οριζόντιας μεταπομπής σε κυψελωτά δίκτυα μάκρο-κυψελών – φέμτο-κυψελών που θέτει ως στόχο την αναγνώριση και σύνδεση με το σταθμό βάσης που ελαχιστοποιεί την κατανάλωση του κινητού τερματικού διατηρώντας παράλληλα ένα συγκεκριμένο μέσο ρυθμό σήματος προς παρεμβολές και θόρυβο ο οποίος προσαρμόζεται με βάση τις ανάγκες επικοινωνίας του χρήστη. Μέρους του κεφαλαίου αυτού αποτελούν η περιγραφή του μοντέλου συστήματος, το σύνολο των πληροφοριών που αξιοποιούνται από τον προτεινόμενο αλγόριθμο, καθώς μία νέα πολιτική οριζόντιας μεταπομπής η οποία, βασιζόμενη σε μετρήσεις των σταθμών βάσης, αναγνωρίζει τον σταθμό βάσης που ελαχιστοποιεί την απαιτούμενη εκπομπή ισχύος στο κινητό τερματικό του χρήστη δοσμένου ενός κατωφλίου ποιότητας σήματος που ικανοποιεί την ποιότητα υπηρεσίας των συνδέσεων του εν λόγω χρήστη. Στην συνέχεια, παρουσιάζουμε αποτελέσματα προσομοίωσης σε επίπεδο συστήματος, τα οποία αναδεικνύουν την υπεροχή της προτεινόμενης πολιτικής ως προς άλλες υπάρχουσες λύσεις. Η προτεινόμενη πολιτική οριζόντιας μεταπομπής ενσωματώνεται σε έναν ολοκληρωμένο αλγόριθμο οριζόντιας μεταπομπής, ο οποίος πέρα από τον υπολογισμό της απαιτούμενης εκπομπής ισχύος στο κινητό τερματικό του χρήστη λαμβάνει υπόψη την διαθεσιμότητα των πόρων και τα δικαιώματα πρόσβασης του χρήστη στις

υποψήφιες κυψέλες προς μεταπομπή. Το κεφάλαιο ολοκληρώνεται με την παρουσίαση εκτενών προσομοιώσεων σε επίπεδο συστήματος για την απόδοση του προτεινόμενου αλγορίθμου από πλευράς ρυθμαπόδοσης, ενεργειακής αποδοτικότητας, παρεμβολών στην ανωφερή και στην κατωφερή ζεύξη, αξιοποίησης των φέμτο-κυψελών, και άλλων συναφών μετρικών, χρησιμοποιώντας την μεθοδολογία αξιολόγησης του Small Cell Forum. Η απόδοση του προτεινόμενου αλγορίθμου οριζόντιας μεταπομπής συγκρίνεται με τους πλέον πρόσφατους αλγορίθμους οριζόντιας μεταπομπής για κυψελωτά δίκτυα μάκρο-κυψελών – φέμτο-κυψελών.

Στο πέμπτο κεφάλαιο, παρουσιάζεται προτεινόμενος αλγόριθμος κάθετης μεταπομπής σε ετερογενή δίκτυα 3GPP LTE-Advanced και IEEE 802.11-2012, που θέτει ως στόχο την σύνδεση με το σταθμό βάσης που ελαχιστοποιεί την κατανάλωση του κινητού τερματικού διατηρώντας παράλληλα μία συγκεκριμένη ποιότητα σήματος στην ανωφερή ζεύξη. Μεταξύ άλλων, το κεφάλαιο περιλαμβάνει την περιγραφή του μοντέλου συστήματος, το σύνολο των πληροφοριών που αξιοποιούνται από τον προτεινόμενο αλγόριθμο, καθώς και τον προτεινόμενος αλγόριθμος κάθετης μεταπομπής. Το κεφάλαιο ολοκληρώνεται με την παρουσίαση εκτενών προσομοιώσεων σε επίπεδο συστήματος για την απόδοση του προτεινόμενου αλγορίθμου από πλευράς ρυθμαπόδοσης, ενεργειακής αποδοτικότητας, παρεμβολών στην ανωφερή και στην κατωφερή ζεύξη, αποφόρτισης του κυψελωτού δικτύου, και άλλων συναφών μετρικών. Η απόδοση του προτεινόμενου αλγορίθμου οριζόντιας μεταπομπής συγκρίνεται με δύο βασικούς αλγορίθμους κάθετης μεταπομπής, που δίνουν προτεραιότητα στο ένα ή στο άλλο δίκτυο.

Στο έκτο κεφάλαιο, η διδακτορική διατριβή παρουσιάζει μία εκτενή βιβλιογραφική επισκόπηση, ταξινόμηση, ποιοτική και ποσοτική ανάλυση απόδοσης υπαρχουσών αλγορίθμων μεταπομπής σε ετερογενή δίκτυα μάκρο-κυψελών και μικρών κυψελών. γίνεται μια λεπτομερής αναφορά των ανωτέρω φάσεων στο δίκτυο 3GPP LTE-Advanced για την καλύτερη κατανόηση των ανοιχτών προβλημάτων σε πραγματικά συστήματα. Βασιζόμενοι στην συζήτηση για την φάση απόφασης μεταπομπής, στην συνέχεια συνοψίζονται και ταξινομούνται οι πιο σημαντικοί αλγόριθμοι απόφασης μεταπομπής για δίκτυα φεμτοκυψελών, ενώ παρουσιάζονται εκτενώς τρεις αλγόριθμοι από κάθε αναγνωρισθείσα κλάση αλγορίθμων απόφασης μεταπομπής. Το κεφάλαιο περιλαμβάνει ποιοτική και ποσοτική ανάλυση των υπαρχουσών λύσεων, συμπεριλαμβανομένων και των προτεινόμενων, ενώ τα αποτελέσματα των ανωτέρω συγκρίσεων αξιοποιούνται για την εξαγωγή χρήσιμων αρχών για τον μελλοντικό σχεδιασμό αλγορίθμων οριζόντιας μεταπομπής για δίκτυα μακροκυψελών – φεμτοκυψελών.

Η διδακτορική διατριβή ολοκληρώνεται στο έβδομο κεφάλαιο, στο οποίο αποτυπώνονται τα ζητήματα που αντιμετωπίστηκαν, συνοψίζεται η ερευνητική συνεισφορά της διατριβής, και αναδεικνύεται η καινοτομία των προταθέντων λύσεων. Για κάθε επιμέρους περιοχή, επισημαίνονται οι μελλοντικές επεκτάσεις των λύσεων που προτάθηκαν. Μεταξύ άλλων, η συμβολή της παρούσας διδακτορικής διατριβής στις τέσσερις βασικές περιοχές που επικέντρωσε, μπορεί να συνοψιστεί ως ακολούθως.

Στην περιοχή υπολογισμού σχετικής θέσης και εύρεσης σημείου-προς-σημείο σε ετερογενή δίκτυα, εξάγουμε αναλυτικές σχέσεις κλειστού τύπου (closed-form expressions) για την κατανομή της σχετικής απόστασης μεταξύ δύο ετερογενών ασυρμάτων δικτυακών στοιχείων, δοσμένης μερικής (ή πλήρους) γνώσης για την γενικότερη τοπολογία του ετερογενούς δικτύου. Η εξαχθείσες σχέσεις μας επιτρέπουν να αναλύσουμε την απόδοση της διαδικασίας υπολογισμού σχετικής θέσης και εύρεσης σημείου-προς-σημείο μεταξύ ασυρμάτων δικτυακών στοιχείων διαφορετικής τεχνολογίας, δοσμένων διαφόρων συνδυασμών πληροφορίας για τις σχετικές θέσεις των ασυρμάτων δικτυακών στοιχείων του ετερογενούς δικτύου. Επιπρόσθετα, εξάγουμε

βέλτιστες στρατηγικές για την τοποθέτηση ασυρμάτων δικτυακών στοιχείων στο δίκτυο, με στόχο την μεγιστοποίηση της πιθανότητας επιτυχούς εύρεσης δύο στοιχείων ενδιαφέροντος, και προτείνουμε χρήσιμες κατευθυντήριες γραμμές για τον σχεδιασμό καινοτόμων μηχανισμών υπολογισμού σχετικής θέσης και εύρεσης σημείου-προς-σημείο στο σημερινό ετερογενές δίκτυο. Από όσο γνωρίζουμε, η εργασία αυτή είναι η πρώτη που υιοθετεί το ανωτέρω μοντέλο εντοπισμού σχετικής θέσης και εύρεσης σημείου-προς-σημείο μεταξύ *μη ομογενών* ασύρματων δικτυακών στοιχείων, και αναπτύσσει κατάλληλα μαθηματικά μοντέλα για την ανάλυση της απόδοσης του.

Στην περιοχή εύρεσης συνδέσεων συσκευής-προς-συσκευή σε κυψελωτά δίκτυα με υποβοήθηση από το δίκτυο, αναλύουμε την απόδοση της εύρεσης συνδέσεων συσκευής-προς-συσκευή σε κυψελωτά δίκτυα με τυχαία κατανομή κόμβων και δυνατότητα υποβοήθησης από το δίκτυο, και εξάγουμε χρήσιμες κατευθυντήριες γραμμές για την βελτίωση της εν λόγω λειτουργίας σε σημερινά κυψελωτά δίκτυα. Πιο συγκεκριμένα, εξάγουμε την κατανομή της σχετικής απόστασης μεταξύ δύο συσκευών ενδιαφέροντος, δοσμένης μερικής ή πλήρους πληροφορίας για την τοπολογία του κυψελωτού δικτύου (από πλευράς δικτύου κορμού). Η εξαχθείσες αναλυτικές εκφράσεις χρησιμοποιούνται για την ανάλυσης της στατιστικής συσχέτισης μεταξύ της πιθανότητας επιτυχούς εύρεσης συνδέσεων συσκευής-προς-συσκευή και των πλέον σημαντικών παραμέτρων συστήματος. Επίσης, η χρήση των εκφράσεων αυτών μας επιτρέπει να αναγνωρίσουμε τις συνθήκες υπό τις οποίες η ανωτέρω πιθανότητα μεγιστοποιείται ως προς την πυκνότητα των κυψελωτών σταθμών. Ακριβής και προσεγγιστικές εκφράσεις παρουσιάζονται για την τιμή της βέλτιστης πυκνότητας κυψελωτών σταθμών, ενώ η χρήση αριθμητικών αποτελεσμάτων μας οδηγεί στην εξαγωγή χρήσιμων συμπερασμάτων για τους αυτογενείς συμβιβασμούς (trade-offs) που διέπουν την απόδοση της εύρεσης συνδέσεων συσκευής-προς-συσκευή σε κυψελωτά δίκτυα με υποβοήθηση από το δίκτυο. Η παρούσα εργασία αποτελεί μία από τις πρώτες εργασίες στην εν λόγω ερευνητική περιοχή.

Στην περιοχή οριζόντιων μεταπομπών σε δίκτυα μακροκυψελών – φεμτοκυψελών, η συμβολή μας ως προς την τρέχουσα βιβλιογραφία εστιάζεται σε τρία σημεία. Πρώτον, η εργασία μας αναδεικνύει ότι η απόφαση μεταπομπής δύναται να διαδραματίσει εξέχων ρόλο για την διαχείριση των παρεμβολών σε δίκτυα μακροκυψελών – φεμτοκυψελών καθώς και για την μείωση της ενεργειακής κατανάλωσης στα κινητά τερματικά, αν αξιοποιηθούν μετρήσεις για την ράδιο-κατάσταση των κυψελωτών σταθμών. Δεύτερον, προτείνουμε έναν ενεργειακά-αποδοτικό αλγόριθμο μεταπομπής για δίκτυα μακροκυψελών – φεμτοκυψελών και εξετάζουμε όλες τις απαιτήσεις εφαρμογής του στο κυψελωτό σύστημα Long Term Evolution-Advanced (LTE-A) που αναπτύχθηκε από την 3rd Generation Partnership Project (3GPP). Εν συγκρίσει με άλλες υπάρχουσες λύσεις, ο προτεινόμενος αλγόριθμος οδηγεί σε μείωση των παρεμβολών και της ενεργειακής κατανάλωσης στα κινητά τερματικά, με κόστος την μέτρια αύξηση του κόστους σηματοδοσίας στο δίκτυο. Τρίτον, αναδεικνύουμε και συζητούμε εκτενώς τις τρέχουσες προκλήσεις για την διαχείριση κινητικότητας σε δίκτυα φεμτοκυψελών, επισκοπούμε και ταξινομούμε υπάρχοντες αλγορίθμους μεταπομπής για φεμτοκυψέλες, και παρέχουμε εκτενείς ποιοτικές και ποσοτικές συγκρίσεις της απόδοσης τους χρησιμοποιώντας την κοινώς αποδεκτή μεθοδολογία προσομοίωσης σε επίπεδο συστήματος του Small Cell Forum.

Στην περιοχή κάθετων μεταπομπών σε ετερογενή ασύρματα δίκτυα, προτείνουμε έναν ενεργειακά-αποδοτικό αλγόριθμο κάθετης μεταπομπής, ο οποίος αξιοποιεί δύο σημαντικές βελτιώσεις που επιτελέστηκαν πρόσφατα στα συστήματα LTE-A (κυψελωτές επικοινωνίες) και IEEE 802.11 (τοπικής ασύρματης πρόσβασης): την Λειτουργία Εύρεσης και Επιλογής Δικτύου Πρόσβασης (Access Network Discovery and Selection Function - ANDSF) και την δυνατότητα εξαγωγής ράδιο-μετρήσεων για την κατάσταση

του καναλιού στους κυψελωτούς σταθμούς LTE-A και στα σημεία πρόσβασης που είναι συμβατά με το πρότυπο IEEE 802.11-2012. Από όσο γνωρίζουμε, η παρούσα εργασία είναι η πρώτη που εκμεταλλεύεται τις ανωτέρω δύο βελτιώσεις των συστημάτων LTE-A και IEEE 802.11, με απώτερο στόχο την ελαχιστοποίηση της κατανάλωσης ενέργειας σε κινητά πολλαπλών ράδιο-επαφών (multi-mode mobile terminals – MMTs) διαμέσου της εφαρμογής ενεργειακά-αποδοτικών κάθετων μεταπομπών. Εκτενείς προσομοιώσεις σε επίπεδο συστήματος αναδεικνύουν ότι ο προτεινόμενος αλγόριθμος επιτυγχάνει αποδοτική εξισορρόπηση του φόρτου κίνησης μεταξύ των δύο ετερογενών συστημάτων, οδηγεί σε μειωμένη ενεργειακή κατανάλωση ανά μονάδα δεδομένων (energy per bit) στα κινητά τερματικά, και βελτιώνει σημαντικά την ρυθμαπόδοση στην ανωφερή ζεύξη (uplink), με κόστος την αύξηση του ρυθμού σηματοδοσίας στην μονάδα ANDSF και στο δίκτυο ασύρματης τοπικής πρόσβασης (Wireless Local Area Network - WLAN).

TABLE OF CONTENTS

LIST OF FIGURES

LIST OF TABLES

PREFACE

This PhD thesis has been pursued at the Department of Informatics and Telecommunications at the National and Kapodistrian University of Athens, Greece, and co-financed by the Heracleitus II research program. All of these years I was lucky to be tutored by recognized researchers and everyday-life heroes that inspired my work and provided me with a clear focus in my life. Among others, I was very lucky be supervised by Professor Lazaros Merakos, who has always been supportive to me from my early research steps during my BSc and MSc theses, providing me constructive feedback in my research activity all of these years. On the other hand, the contribution and advise of Dr. Nikos Passas has been invaluable to my research perspective and everyday life, since apart from keeping my motivation clear and providing me with a creative, firm, yet competitive working environment, he has also been an irreplaceable fellow traveler and supporter of all my activities till now. During my PhD thesis I was also very lucky to collaborate with Dr. Christos Verikoukis, which has taught me how to identify and follow recent trends in wireless networking, gave me several opportunities for actively participating in state-of-the-art research efforts, and most importantly, taught me how to work with clear focus and persistency in the areas that suit my personal charismas and capacity as a researcher. Besides, in that field, my collaboration with Professor Marios Kountouris has been of paramount importance. Marios has selflessly provided me useful guidelines on the optimization of the proposed stochastic models, which are now integral part of my PhD Thesis.

Apart from having an invaluable 'net' of research fellows and tutors, my inclination for research would have never been expressed if I didn't have the undivided support and sincere contribution of my family. This personal 'safe-net' has been initially expressed by my parents and me close-environment, and subsequently expressed in terms of unconditional love and altruistic support from my own family. My wife Anastasia and daughter Theofania have taught me everyday-life lessons that will accompany me for the remainder of my existence: prioritize your needs and address them in descending order (it works great!), be persistent and methodical with your personal goals, and never give up your fight, this is a fight for us all. Their faith has been the cornerstone of handling all kind of difficulties in this PhD thesis till now.

For the aforementioned reasons, I would like to acknowledge these diverse contributions of all the aforementioned persons and thank them from the bottom of my heart. Last but not least, I would also like to thank all the organizations and projects that funded my research efforts.

This research has been co-financed by the European Union (European Social Fund – ESF) and Greek national funds through the Operational Program "Education and Lifelong Learning" of the National Strategic Reference Framework (NSRF) - Research Funding Program: Heracleitus II. Investing in knowledge society through the European Social Fund.

European Union
European Social Fund

MINISTRY OF EDUCATION & RELIGIOUS AFFAIRS, CULTURE & SPORTS
MANAGING AUTHORITY

Co- financed by Greece and the European Union

ΠΡΟΛΟΓΟΣ

Η παρούσα διδακτορική διατριβή έγινε στο Τμήμα Πληροφορικής και Τηλεπικοινωνιών του Εθνικού και Καποδιστριακού Πανεπιστημίου Αθηνών, ενώ χρηματοδοτήθηκε από το πρόγραμμα Ηράκλειτος ΙΙ. Όλα αυτά τα χρόνια είχα την ευτυχία να διδαχθώ από καταξιωμένους ερευνητές και καθημερινούς ήρωες, οι οποίοι ενέπνευσαν την δουλειά μου και μου παρείχαν καθαρό κίνητρο στην ζωή μου. Μεταξύ άλλων, ήμουν ιδιαιτέρως τυχερός να με επιβλέπει ο καθηγητής Λάζαρος Μεράκος, ο οποίος με στήριζε από τις πρώτες μου ερευνητικές προσπάθειες στην πτυχιακή και διπλωματική μου εργασία, παρέχοντας μου εποικοδομητικά σχόλια για την ερευνητική μου δραστηριότητα με στωικότητα. Αφετέρου, η συνεισφορά και οι συμβουλές του Δρ. Νίκου Πασσά ήταν μεγίστης σημασίας για την ερευνητική μου αντίληψη και την καθημερινότητα μου, καθώς πέρα από την διατήρηση του ερευνητικού μου κινήτρου και την εξασφάλιση ενός δημιουργικού, σταθερού, αλλά ανταγωνιστικού εργασιακού περιβάλλοντος, ο Νίκος είναι αναντικατάστατος συνοδοιπόρος και υποστηρικτής όλων των δραστηριοτήτων μου μέχρι τώρα. Κατά την διάρκεια της διδακτορικής μου διατριβής, είχα την τύχη να συνεργαστώ με τον κ. Χρήστο Βερικούκη από το CTTC, ο οποίος με έμαθε να αναγνωρίζω και να παρακολουθώ τις τρέχουσες ερευνητικές τάσεις στην περιοχή, μου παρείχε σημαντικές ευκαιρίες για ενεργή μου συμμετοχή σε τρέχουσες ερευνητικές διεργασίες, και κυρίως, μου δίδαξε να δουλεύω συγκεντρωμένα και με επιμονή στις ερευνητικές περιοχές που ταιριάζουν στα προσωπικά μου χαρακτηριστικά ως ερευνητής. Άλλωστε, στο συγκεκριμένο πεδίο, η συνεργασία μου με τον καθηγητή Μάριο Κουντούρη από το SUPELEC ήταν εξέχουσας σημασίας. Ο Μάριος μου παρείχε ανιδιοτελώς σημαντικές κατευθυντήριες γραμμές και υποδείξεις για το κομμάτι της βελτιστοποίησης των προτεινόμενων στοχαστικών μοντέλων τα οποία είναι πλέον αναπόσπαστο κομμάτι της διατριβής μου.

Πέραν του πολύτιμου δικτύου από ερευνητικούς συνεργάτες και καθηγητές, η κλίση μου για την έρευνα δεν θα μπορούσε ποτέ να εκφραστεί αν δεν είχα την αμέριστη συμπαράσταση και ειλικρινή στήριξη της οικογένειας μου. Αυτό το προσωπικό ‘δίχτυ ασφαλείας’ στήθηκε αρχικώς από τους γονείς μου και το κοντινό μου περιβάλλον, και στην συνέχεια εξεφράσθην, σε όρους ανιδιοτελούς αγάπης και υποστήριξης, από την δική μου οικογένεια. Η γυναίκα μου Αναστασία και η κόρη μου Θεοφανία, με δίδαξαν μαθήματα που θα με ακολουθούν σε όλη μου την ζωή: ιεράρχησε τις ανάγκες σου και αντιμετώπισε τες σε φθίνουσα σειρά (δουλεύει!), να είσαι επίμονος και μεθοδικός με τους προσωπικούς σου στόχους, και ποτέ μην παρατάς την μάχη, είναι μια μάχη όλων μας. Η πίστη τους αποτέλεσε τον ακρογωνιαίο λίθο στην αντιμετώπιση όλων των δυσκολιών της διατριβής μου μέχρι τώρα. Για όλους τους ανωτέρω λόγους, ευχαριστώ τους ανωτέρω ανθρώπους από τα βάθη της καρδιάς μου. Τέλος, ευχαριστώ θερμά τους οργανισμούς χρηματοδότησαν την ερευνητική μου προσπάθεια.

Η παρούσα έρευνα έχει συγχρηματοδοτηθεί από την Ευρωπαϊκή Ένωση (Ευρωπαϊκό Κοινωνικό Ταμείο - ΕΚΤ) και από εθνικούς πόρους μέσω του Επιχειρησιακού Προγράμματος «Εκπαίδευση και Δια Βίου Μάθηση» του Εθνικού Στρατηγικού Πλαισίου Αναφοράς (ΕΣΠΑ) – Ερευνητικό Χρηματοδοτούμενο Έργο: Ηράκλειτος ΙΙ. Επένδυση στην κοινωνία της γνώσης μέσω του Ευρωπαϊκού Κοινωνικού Ταμείου.

Ευρωπαϊκή Ένωση
Ευρωπαϊκό Κοινωνικό Ταμείο

ΕΠΙΧΕΙΡΗΣΙΑΚΟ ΠΡΟΓΡΑΜΜΑ
ΕΚΠΑΙΔΕΥΣΗ ΚΑΙ ΔΙΑ ΒΙΟΥ ΜΑΘΗΣΗ
επένδυση στην κοινωνία της γνώσης
ΥΠΟΥΡΓΕΙΟ ΠΑΙΔΕΙΑΣ & ΘΡΗΣΚΕΥΜΑΤΩΝ, ΠΟΛΙΤΙΣΜΟΥ & ΑΘΛΗΤΙΣΜΟΥ
ΕΙΔΙΚΗ ΥΠΗΡΕΣΙΑ ΔΙΑΧΕΙΡΙΣΗΣ

ΕΣΠΑ 2007-2013
πρόγραμμα για την ανάπτυξη
ΕΥΡΩΠΑΪΚΟ ΚΟΙΝΩΝΙΚΟ ΤΑΜΕΙΟ

Με τη συγχρηματοδότηση της Ελλάδας και της Ευρωπαϊκής Ένωσης

1. INTRODUCTION

Over the past few years, wireless networks have transformed from a set of single-tier operator-deployed circuit-switched systems, designed to support voice-centric services in wide geographical regions, to a set of multi-tier networking clusters of user-installed IP-based wireless networking elements (WNEs), designed to support heterogeneous communication capabilities and diverse networking requirements. The nowadays heterogeneous wireless network (HWN) is composed by tower-mounted cellular base stations (BSs) providing wide area coverage (a.k.a. macrocells), user-deployed low-power and small-sized base stations that boost the area spectral efficiency of the licensed spectrum [1] (e.g. femtocells), wireless local area network (WLAN) stations that enable high-data rate connections to the Internet over the unlicensed spectrum [2], as well as other low-cost low-power and battery-operated sensors that monitor, measure, and commute localized changes in nearby sink nodes [3][4] (e.g. energy monitoring in the smart grid). In such a heterogeneous wireless networking environment, the mobile terminals (or the WNEs) are required to *discover* the set of nearby WNEs that they can access and, if needed, to seamlessly transfer their ongoing services by *associating with* the one(s) that meet their particular communication requirements. Even though different terms are used among the different systems for the *discovery*, e.g. *network discovery* in IEEE-based systems or *cell search* in 3GPP-systems, and the *association* phase, e.g. *handover* for intra-system mobility in cellular systems and *vertical handover* for inter-system mobility between heterogeneous systems, the *discovery* and *association* phases are integral part of the *mobility management* (MM) process of all the existing wireless networking technologies.

Since the nowadays mobile terminals are equipped with numerous radio access interfaces, that enable them to access the Internet via multiple Radio Access Technologies (RATs), mobility management is a challenging issue for safeguarding the robustness of the nowadays HWN. Firstly, the support of multiple radio interfaces asks for increased complexity and battery consumption at the mobile terminal, due to the substantially increased number of (not necessarily homogeneous) WNEs that should be discovered and evaluated with respect to their ability to support the service requirements of the mobile terminal. Secondly, the recent surge of interest for the direct exchange of localized traffic between nearby devices without network involvement, a.k.a. peer-to-peer (P2P) communications, questions the scalability of the predominant user-assisted network-controlled mobility management model that is currently adopted by the vast majority of cellular networks. Social networking applications, massive multiplayer online gaming, device-to-device (D2D) communications, smart metering, first-responder communications, and unsupervised navigation of communication-aware robotic nodes, are only some of the emerging applications that motivate this disruptive communication paradigm [4][5][6]. Thirdly, the nowadays HWN is characterized by the unplanned deployment of densely overlapping (in coverage) WNEs that serve diverse communication purposes over the same spectrum. This feature not only dictates the employment of semi-autonomous terminal-based discovery, but also transforms the nowadays HWN to a stochastic system dominated by the spatial dependencies of the heterogeneous WNEs.

Aiming to improve the mobility, interference, and energy management at the WNEs, more and more wireless networking technologies incorporate a suite of

measurement capabilities to their baseline operation. Such measurements enable the fixed (or moving) WNEs to assess the status of the ambient radio environment, e.g. interference level in a specific spectrum band, and directly (or indirectly) estimate their physical distance and angle with respect to other WNEs of the same RAT. The incorporation of knowledge on the radio status or the spatial dependencies between the WNEs, arises as the natural solution for effectively handling the unplanned and overlapping deployment of WNEs upon mobility management. The integration of such spatial information can also be the cornerstone for more accurate localization between WNEs that do not necessarily support the same RAT, i.e. heterogeneous WNEs. Besides, localization, which refers to the process by which a WNE estimates its physical distance (or connectivity) to another WNE, is currently considered as a vital component in the future 5G network where the estimation of proximity between the myriads of WNEs can be a limiting performance factor [7].

Under this viewpoint, in this doctoral thesis we investigate how knowledge of the radio status or the spatial distribution of the WNEs can be used to enhance the performance of localization, discovery, and association in the nowadays HWN. Besides, the exploitation of such spatial information is the common denominator for all algorithms and analytical models developed in this work. The remainder of this section is organized as follows. In section 1.1, we start with an illustrative example that motivates the utilization of radio/positioning measurements from the heterogeneous WNEs as means of improving the performance of localization, discovery, and association in the nowadays HWN. In section 1.2, we briefly summarize the key aspects of existing wireless networking technologies and overview the recent trends for heterogeneous wireless networking that are relevant to our work. Finally, in section 1.3 we summarize related works and our key contributions in the areas of localization and peer-discovery in HWN (section 1.3.1), device-to-device discovery in cellular network (section 1.3.2), energy-efficient handover decision in the macrocell – femtocell network (section 1.3.3), and energy-efficient vertical handover decision in the cellular/Wi-Fi network (section 1.3.4).

1.1 Motivating Example and Research Areas

In Figure 1 we depict an instance of the nowadays HWN, which is composed by long-range cellular BSs, e.g. macrocells, numerous small-sized stations that operate in the licensed spectrum, e.g. picocells or femtocells, WLAN access points that operate in the unlicensed spectrum, e.g. Wi-Fi hotspots, dual-mode cellular/Wi-Fi hotspots (fourth generation (4G) hotspots), low-power sensors, e.g. ZigBee sensors, localized traffic aggregators/sink nodes, e.g. dual-mode Wi-Fi/ZigBee smart meters, D2D-enabled cellular devices, and communication-enabled robotic nodes, e.g. dual-mode Wi-Fi/cellular robots.

To better comprehend the key research areas of this work, consider the scenario where the dual-mode robot (source peer) seeks to discover a malfunctioning ZigBee sensor (target peer) to replace it. The dual-mode robot is assumed to host active connections to the Internet. Firstly, the communication-enabled robot is required to (continuously re-)assess its physical distance to the malfunctioning ZigBee sensor by employing localization, i.e. estimate the distance Z_1. Secondly, as the robot moves towards the malfunctioning ZigBee sensor, at some point it will have to choose between associating with Femto 1 (femtocell) or BS 2 (macrocell), which refers to the scenario of intra-system mobility in the macrocell-femtocell network, i.e. *horizontal handover*. In the sequel, the robot will have to

choose between associating with Femto 2 (femtocell), Wi-Fi 2 (WLAN access point), BS 2 (macrocell) or BS 1 (macrocell), which refers to the scenario of inter-system mobility between heterogeneous RATs, i.e. *vertical handover*. Since the robot is a battery-operated device, its ongoing services should be seamlessly transferred to the WNE that not only guarantees a prescribed Quality of Service (QoS) target, but also requires the minimum energy consumption overhead for communications, i.e. need for *energy-efficient* horizontal or vertical handovers. Finally, assuming that the ZigBee sensor (Sensor 1) is located in a difficult to access area, the dual-mode robot is required to discover a local D2D-enabled device (User 1) that will be responsible for remotely navigating the robot by exploiting visual signal from its on-board camera (localized real-time video traffic).

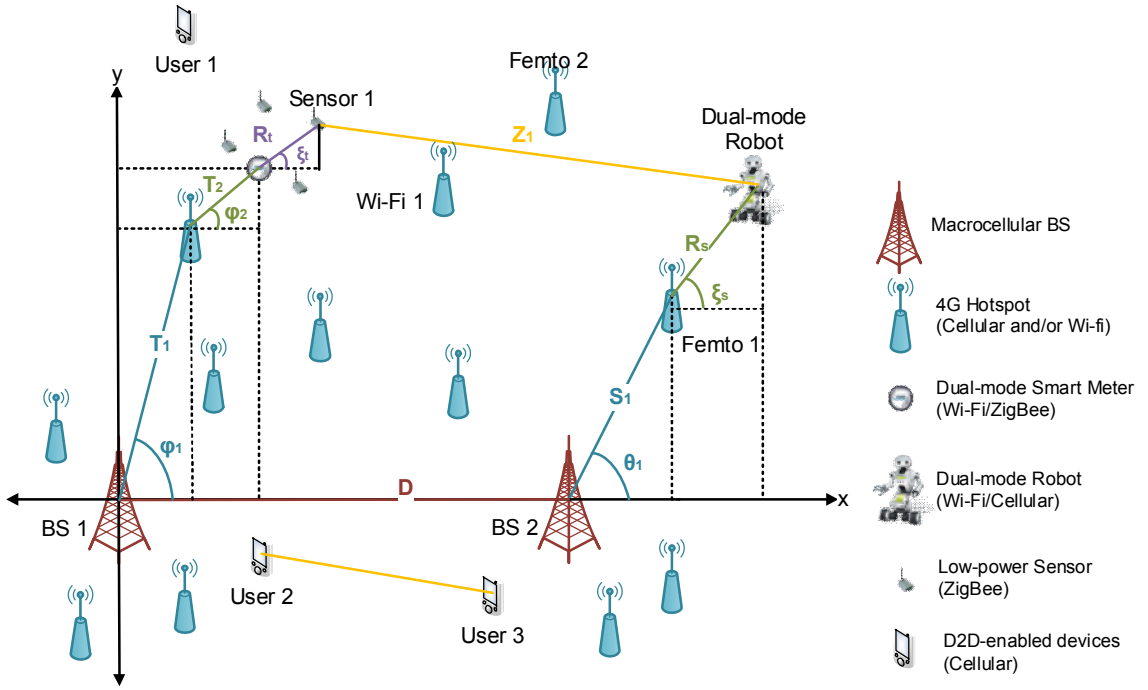

Figure 1: Motivating example for localization and mobility management in wireless heterogeneous networks using network-assistance

Aiming to cover the first challenge, which refers to the localization between not necessarily homogeneous WNEs over large geographical areas, e.g. the robot and the ZigBee sensor, in this work we analyze how partial or full knowledge on the spatial dependencies between the nodes, e.g. relative distances and angles with respect to a reference direction, affect the localization precision and the peer discovery accuracy in the nowadays multi-tier clustered HWN. On the other hand, aiming to cover the challenge of energy-efficient horizontal handover in the macrocell – femtocell network, we propose an energy-efficient handover algorithm that exploits standard measurements on the radio status of nearby base stations (femtocells or macrocells) to identify the one that minimizes the transmit power at the mobile terminal given a prescribed mean Signal to Interference plus Noise Ratio (SINR) target (QoS indicator). To address the challenging issue of energy-efficient network selection between cellular and WLAN WNEs, we propose an energy-efficient vertical handover algorithm that utilizes standard measurements on the radio status of nearby base stations or WLAN access points, in order to identify the point of attachment (PoA) that minimizes the power consumption at the mobile terminal given a prescribed mean SINR (QoS indicator). Finally, we also analyze how different combinations of location

information on the cellular network layout can be used to enhance the performance of network-assisted D2D discovery. We note that even though we use the example in Figure 1 to allow a more easy understanding of the research areas addressed in this work, the proposed analytical models and algorithms apply to more generic scenarios and deployment layouts. More details on the proposed analytical or algorithmic frameworks are provided in the subsequent sections.

1.2 Key Technologies and Recent Trends for Heterogeneous Wireless Networking

In this section, we briefly overview the key features of the existing wireless technologies and the recent trends for heterogeneous wireless networking that are relevant to our work. It is not in our intentions to provide a comprehensive survey of the respective technologies, yet we choose to emphasize on their key aspects that are related with our work. In section 1.2.1 we briefly overview the key features of the Long Term Evolution – Advanced (LTE-A) system of the 3rd Generation Partnership Project (3GPP), present the standard measurement capabilities at the cellular base stations and the mobile terminals, and discuss the 3GPP Access Network Discovery Function (ANDSF) that enables smooth inter-networking and mobility management between 3GPP and non-3GPP networks. In section 1.2.2, we introduce the key features of the IEEE 802.11-2012 Standard and focus on the measurement capabilities available for the IEEE 802.11-2012 conformant stations (STAs). In section 1.2.3, we overview the key features of the femtocell technology, emphasize on the open issues for mobility management, and summarize how these issues are resolved in the LTE-A system. This section concludes with a brief discussion on the key aspects of D2D communications (section 1.2.4).

1.2.1 The LTE-Advanced system

1.2.1.1 Key Features

The LTE-A system is the technological advancement of the 3GPP LTE system [8], and typically refers to its recent Releases (Rel.) 10/11/12. LTE-A incorporates a plethora of technical improvements to the LTE Rel. 8/9 system, including carrier aggregation, advanced multi-antenna techniques, relaying, and enhanced support for heterogeneous deployments (including femtocells), aiming to fulfill and even surpass the International Mobile Telecommunications (IMT)-Advanced requirements set by the International Telecommunication Union (ITU) [8][9].

In LTE-A, a transmission to/from a mobile terminal can utilize up to five component carriers with carrier aggregation, i.e., a deployment bandwidth of up to 100MHz, where each component carrier uses the LTE Rel. 8 structure for backwards compatibility. Advanced spatial multiplexing is also provided, using up to eight-layer Multiple Input Multiple Output (MIMO) for the downlink (DL) and four-layer MIMO for the uplink (UL). Combined with carrier aggregation, the use of MIMO can lead to a peak data rate of 1Gbps and 0.5Gbps for the DL and UL directions, respectively [10]. To further improve spectral efficiency, LTE-A enables enhanced single-cell multi-user MIMO support, while to lower the interference at mobile terminals located close to multiple cells, the standard provisions for coordinated multipoint (CoMP) transmissions. A wide range of heterogeneous deployments are supported in LTE-A, mainly including picocells, femtocells and

relays, with the aim to extend network coverage, increase system capacity and lower transmit power.

Current literature includes various surveys and studies on the key aspects of the LTE-A system and the technical challenges for femtocell support. The key differences between the LTE-A and LTE Release 8/9 systems, along with a short discussion on the technical improvements in LTE-A, are discussed in [9] and [10]. The main challenges and the impact of using carrier aggregation in LTE-A are thoroughly investigated in [11], while the application of MIMO and relaying in IMT-Advanced standards are discussed in [12] and [13], respectively. With the emphasis given to the LTE system, various interference coordination and cancellation techniques are overviewed in [14], while focusing on the LTE-A system with multi-hop relaying, the performance of semi-static interference coordination schemes for radio resource allocation and power control is demonstrated in [15]. In the following, we discuss the key entities of the LTE-A network architecture.

1.2.1.2 LTE-A Network Architecture

The LTE-A network architecture is composed by the Evolved Packet Core (EPC) and the Evolved Universal Terrestrial Radio Access Network (E-UTRAN). The main logical entities in the EPC are the Mobility Management Entity, the Serving Gateway (S-GW), and the Packet Data Network Gateway (P-GW). On the other hand, the E-UTRAN consists of multiple evolved NodeBs (eNBs), which are essentially the point of attachment of the mobile terminals with the LTE-A network. The mobile devices in LTE-A are typically referred to as User Equipments (UEs). The eNBs are interconnected with each other by means of the X2 interface. The eNBs are also connected by means of the S1 interface to the EPC, more specifically to the MME by means of the S1-MME interface and to the S-GW by means of the S1-U interface. The S1 interface supports a many-to-many relation between MMEs / S-GWs and eNBs. Figure 2 depicts the LTE-A network architecture.

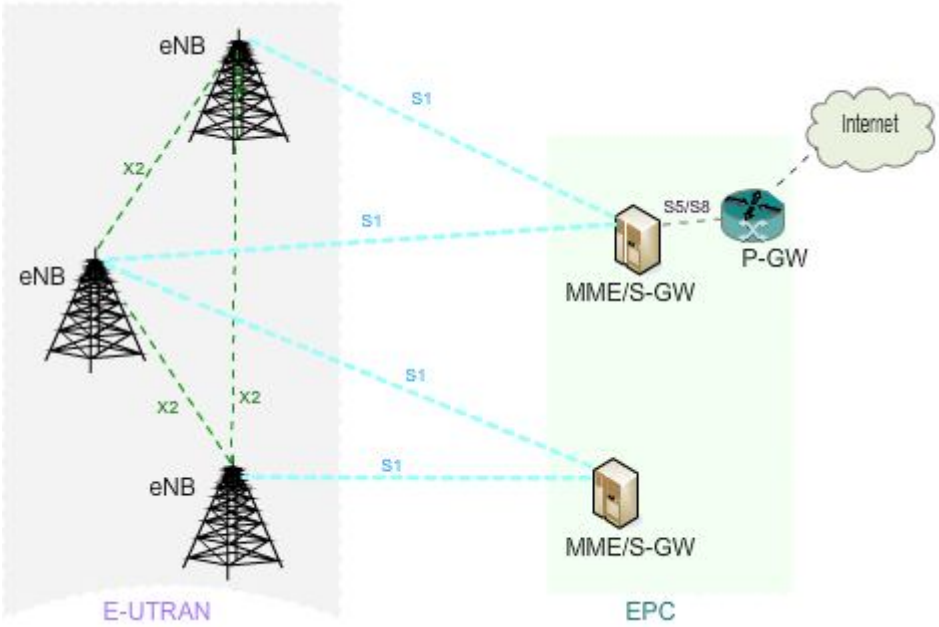

Figure 2: LTE-A network architecture

The PDN Gateway (P-GW) hosts the functions of per-user based packet filtering (e.g. deep packet inspection), lawful interception of packets, IP address allocations for the UEs, UL and DL transport level packet marking, UL and DL

service level charging, gating and rate enforcement. The S-GW hosts the functions of lawful interception, charging, accounting, packet routing and forwarding, as well as mobility anchoring for intra and inter-3GPP MM. The MME implements the functions of core network signaling for MM between 3GPP access networks, idle state mobility handling (e.g., paging), tracking area list management, roaming, bearer control, security and authentication. In practical deployments, the MME and the S-GW are typically merged within the same physical entity. On the other hand, the eNBs provide user and control plane protocol terminations towards the UE, and support the functions of radio resource management, admission control, scheduling and transmission of paging / broadcast messages, measurement configuration for mobility and scheduling, as well as routing of user plane data towards the S-GW.

1.2.1.3 Radio Measurement Capabilities

To resourcefully facilitate mobility and radio resource management, 3GPP has incorporated a suite of standard measurement capabilities for the LTE Rel. 9 conformant base stations and UEs [16]. These measurements can also be performed by LTE-A conformant base stations and UEs. Among others, LTE-A base stations are capable of measuring the timing difference (TD) and angle of arrival (AoA) with respect to other eNBs or UEs, measure the transmit power on the DL reference signal (RS), a.k.a. DL RS Tx measurement, and assess the received interference power at the radio site, a.k.a. RIP measurement. In addition, LTE-A conformant UEs can measure the overall received signal strength (RSS) in symbols with reference signals , a.k.a. RSSI measurement, evaluate the received signal power from a target eNB, a.k.a. RSRP measurement, or even evalute the received signal quality from a target eNB, a.k.a. RSRQ measurement. In Table 1, we summarize some of the measurements capabilities that enable LTE-A conformant base stations and UEs to assess their radio status.

Table 1: Measurement Capabilities [16]

Measurement	Definition	Performed by
Reference signal received power (RSRP)	The linear average over the power contributions (in [W]) of the resource elements that carry cell-specific reference signals within the considered measurement frequency bandwidth. For RSRP determination the cell-specific reference signals R0 shall be used while if the UE may use R1 in addition to R0 if it is reliably detected. The reference point for the RSRP shall be the antenna connector of the UE.	UE
E-UTRA Carrier Received Signal Strength Indicator (RSSI)	The linear average of the total received power (in [W]) observed only in OFDM symbols containing reference symbols for antenna port 0, over $R_{c,DL}$ number of RBs by the UE from all sources, including co-channel serving and non-serving cells, adjacent channel interference, thermal noise etc. RSSI is not reported as a stand-alone measurement rather it is utilized for deriving RSRQ.	UE

Reference Signal Received Quality (RSRQ)	The ratio $R_{c,DL}$×RSRP/(E-UTRA carrier RSSI) where $R_{c,DL}$ is the number of RB's of the E-UTRA carrier RSSI measurement bandwidth. The measurements in the numerator and denominator shall be made over the same set of RBs. The reference point for the RSRQ shall be the antenna connector of the UE.	UE
Downlink Reference Signal Transmitted Power (DL RS Tx)	The linear average over the power contributions (in [W]) of the resource elements that carry cell-specific reference signals which are transmitted by a tagged cell within its operating system bandwidth. For DL RS TX power determination the cell-specific reference signals R0 and if available R1 can be used. The reference point for the DL RS TX power measurement shall be the TX antenna connector.	eNB
Received Interference Power (RIP)	The uplink received interference power, including thermal noise, within one physical RB's bandwidth of N_{SC}^{RB} resource elements. The reported value shall contain a set of Received Interference Powers for all the uplink physical RBs. The reference point for the measurement shall be the RX antenna connector.	eNB

1.2.1.4 Access to the 3GPP EPC via non-3GPP access networks

The smooth integration of 3GPP cellular systems and IEEE-based WLANs has always been challenging [17]. Aiming to realize the so-called heterogeneous networking paradigm, 3GPP provided several functional enhancements to the EPC of the LTE-A system, such as the deployment of the ANDSF module [18][19]. The ANDSF can assist multi-mode mobile terminals (MMTs), i.e., devices that are equipped with both 3GPP and non-3GPP radio interfaces, to discover and select an appropriate point of attachment (PoA) in the heterogeneous network, i.e., either a 3GPP cell or a WLAN access point (AP). The ANDSF contains data management and control functionality necessary to provide access network discovery and selection assistance data to the UEs, in line with the mobile operators' policies. The ANDSF responds to the UE requests for access network discovery information (pull mode), while it is able to initiate data transfer to the UE (push mode) based on network triggers or as a result of previous communication with the UE. Three types of information are provided by the ANDSF: the inter-system mobility policy, the access network discovery information and the inter-system routing policy.

The inter-system mobility policy is a set of operator-defined rules and preferences that affect the inter-system mobility decisions taken by the UE. The UE uses the inter-system mobility policy when it can route IP traffic only over a single radio access interface, at a given time, in order to a) decide when inter-system mobility is allowed or restricted, and b) to select the most preferable access technology type or access network that should be used to access the EPC.

The access network discovery information may include the access technology type (e.g. WLAN, Worldwide Interoperability for Microwave Access (WiMAX)), the radio access network identifier (e.g. the SSID of a WLAN), other technology specific information, e.g. one or more carrier frequencies, as well as validity

conditions, i.e. conditions indicating when the provided access network discovery information is valid (e.g. a location). The UE may retain and use the access network discovery information provided by the ANDSF until new/updated information is retrieved.

The Inter-System Routing Policy is utilized to route IP traffic simultaneously over multiple radio access interfaces i.e., simultaneous utilization of different RANs. This information is utilized for deciding whether a RAN is restricted for a specific IP traffic flow and in general, for selecting the most preferable RANs to route IP traffic that matches specific criteria (e.g. all traffic to a specific PoA, or all traffic belonging to a specific IP flow, or all traffic of a specific application, etc).

The roaming architecture for the ANDSF module is depicted in Figure 1, where H-ANDSF stands for the Home-ANDSF module and V-ANDSF for the Visiting-ANDSF module while on UE roaming. Note that the ANDSF services are provided to the UE via the S14 interface [18]. A more detailed analysis regarding the ANDSF functionality can be found in [18] [19] [20].

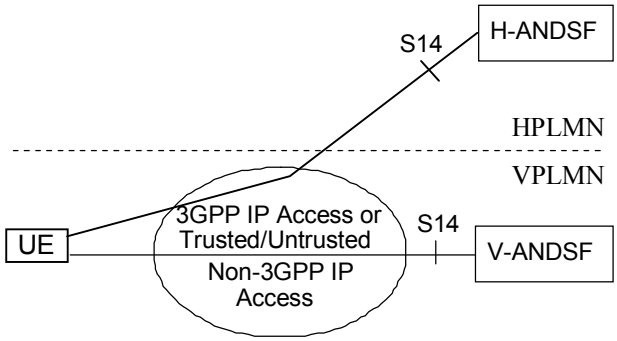

Figure 3: Roaming Architecture for Access Network Discovery Support Functions [18]

Even though 3GPP specifies the baseline functionality of the ANDSF, it also enables the operators to deploy their own (implementation-dependent) inter-system mobility policies. On the other hand, the use of this policy depends on the implementation of the multi-mode mobile terminals (MMTs), given that both the discovery and the association processes are performed at the MMT.

1.2.2 The IEEE 802.11-2012 system: Overview and Measurement Capabilities

The baseline version of the standard, i.e., the IEEE 802.11-2007 Standard [21], has been recently updated to its current version, i.e., the IEEE 802.11-2012 Standard [2], to include a series of amendments developed over the past few years, e.g., IEEE 802.11k IEEE 802.11n. The IEEE 802.11-2012 release includes technical corrections and clarifications to the baseline IEEE 802.11 Standard, as well as enhancements to the existing medium access control (MAC) and physical layer (PHY) functions, e.g., support for higher transmission/reception rates, use of power control, and radio measurement capabilities. One of the key differences between IEEE 802.11-2007 and IEEE 802.11-2012, is the so-called radio resource measurement (RRM) service. The RRM service includes measurements that extend the functionality, reliability, and maintainability of WLANs by specifying the baseline measurement capabilities of IEEE 802.11-2012

conformant equipment across different vendors. The measurement data are commuted to upper layers of the communications stack [22].

An IEEE 802.11-2012-conformant STA can perform local measurements, request a measurement from another STA, or be requested by another STA to make one or more standard measurements and return the respective measurement outcome. The radio measurement data is made available to the STA management and upper protocol layers, where it can be used for a wide range of applications, such as radio resource and mobility management. Both the measurement requests and reports are conveyed through IEEE 802.11 management frames. Some of the most important measurement capabilities in IEEE 802.11-2012 are as follows: beacon, frame, channel load, noise histogram, STA Statistics, location configuration information, neighbor report, link measurement, and transmit stream/category measurement. A measurement pause mechanism (request-only type mechanism) and a measurement pilot (report-only mechanism) are also provisioned in the Standard. In Table 2, we summarize some of the STA measurement capabilities in the IEEE 802.11-2012 Standard that are relevant to our work. Note that the IEEE 802.11-2012 Standard does not differentiate the IEEE 802.11-2012 conformant mobile terminals and access points, and considers them both as STAs.

Table 2: IEEE 802.11-2012 measurement capabilities [2]

Measurement	Definition
Received Channel Power Indicator (RCPI)	An indication of the total channel power (signal, noise, and interference) of a received IEEE 802.11 frame, transmitted from STA s to STA s', measured on the channel and at the antenna connector used to receive the frame at STA s'. The RCPI value can be translated in dBm according to the respective formula in [2].
Average Noise Power Indicator (ANPI)	A MAC indication of the average noise plus interference power measured by STA s, when the channel is idle as defined by three simultaneous conditions: 1) the Virtual CS mechanism indicates idle channel, 2) the STA s is not transmitting a frame, and 3) the STA s is not receiving a frame. The ANPI value can be translated in dBm according to the respective formula in [2].
Received Signal to Noise Indicator (RSNI)	An indication of the signal to noise plus interference ratio of a received IEEE 802.11 frame, transmitted from STA s to STA s'. RSNI is defined by the ratio of the received signal power (RCPI-ANPI) to the noise plus interference power (ANPI) as measured on the channel and at the antenna connector used to receive the frame.
Max Transmit Power (MTP)	The Max Transmit Power field is a 2's complement signed integer and is 1 octet in length, providing an upper limit, in units of dBm, on the transmit power as measured at the output of the antenna connector to be used by STA s on the current channel. The maximum tolerance for the value reported in Max Transmit Power field shall be 5 dB. The value of the Max Transmit Power field shall be less than or equal to the Max Regulatory Power value for the current channel.
Transmit Power Used	The Transmit Power Used field is a 2's complement signed integer and is 1 octet in length. It shall be less than or equal to the Max Transmit Power and indicates the actual power used as measured at

(TPU)	the output of the antenna connector, in units of dBm, by STA s when transmitting the frame containing the Transmit Power Used field. The Transmit Power Used value is determined any time prior to sending the frame in which it is contained and has a tolerance of ±5 dB.

1.2.3 Femtocells: Key features, Mobility Management Challenges, and Integration in the LTE-Advanced System

One of the most challenging issues in the nowadays mobile communications is the smooth integration of small-sized cells into the predominant macro-cellular network layout [23]. Small cells are short-range, low-power and low-cost cellular access points that support fewer users compared to macrocells, embody the functionality of a regular base station and operate in the mobile operator's licensed spectrum. Small cells are considered a promising solution for improving cellular coverage, enhancing system capacity and supporting the plethora of emerging home/enterprise applications. Various small cell technologies have been deployed over the past few years, mainly including femtocells, picocells, and microcells, with broadly increasing radii from femtocells to microcells. Microcells and picocells are operator-managed, whereas femtocells are typically installed and managed by the consumer in an unplanned manner [24]. Different from microcells and picocells, femtocells utilize the end-user's broadband backhaul to reach the mobile operator network (Figure 4). To cope with the comparably denser yet unplanned network layout, femtocells feature edge-based intelligence which spans over the implementation of enhanced self-x capabilities, such as self-configuration, self-optimization and self-healing, as well as advanced radio resource, interference, security, and mobility management. Other small cell technologies progressively incorporate femtocell features as well, aiming to enhance the user experience and reduce the mobile operator's maintenance and administration overhead.

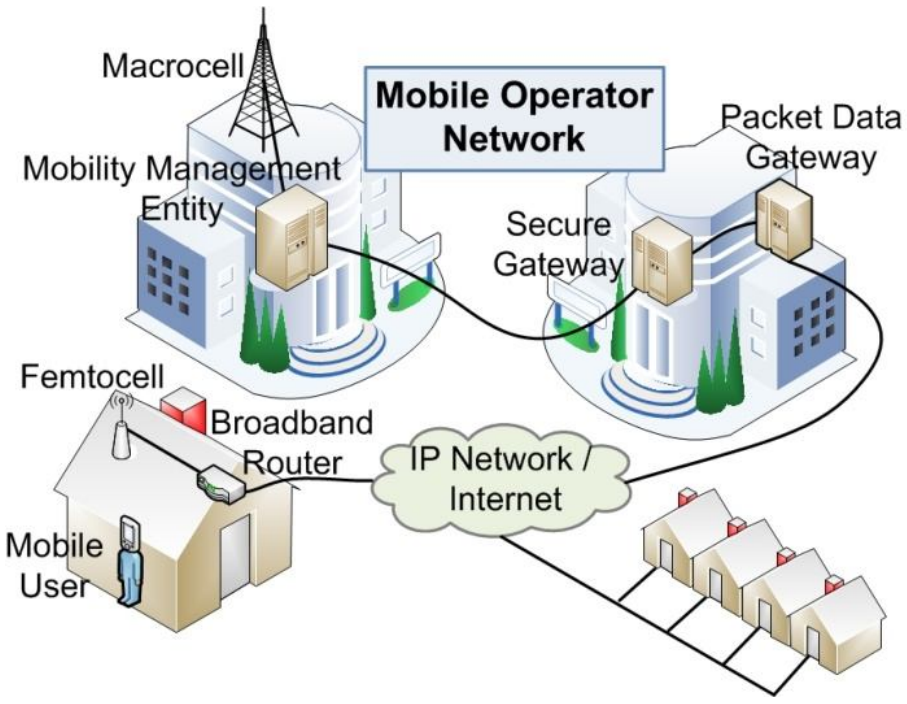

Figure 4: Femtocell deployment example

Support of femtocells necessitates the deployment of more complicated MM procedures to cope with a) the dense network layout, b) the short cell radii, c) the employment access control, and d) the unplanned deployment. The dense network layout and the short cell radii augment the negative impact of user mobility, enlarge the number of candidate cells during the HO decision phase and increase the HO probability even for low speed users. On the other hand, the use of access control may severely degrade the SINR performance for the macrocell and femtocell tiers under certain interference scenarios, e.g., when a nearby operating user is not a member of a closed access femtocell in proximity [25]. Apart from increasing the interference at the cell sites, the unplanned deployment of femtocells complicates the MM procedure in many aspects as well, e.g., the serving cell is unable to provide a complete neighbor cell list to the mobile UEs.

This section discusses the key aspects and research challenges of MM support in the presence of femtocells and overviews the respective procedures followed in the LTE-A system. The discussion focuses on the phases of a) cell identification, b) access control, c) cell search, d) cell selection/reselection, e) HO decision, and f) HO execution, which are thoroughly investigated in the context of femtocell support and the LTE-A system. The remainder of this section is organized as follows. Section 1.2.3.1 discusses the key features of the LTE-A system and overviews the network architectural enhancements required to support femtocells. Sections 1.2.3.2 and 1.2.3.3 investigate the technical challenges of the cell identification and access control procedures, respectively, while section 1.2.3.4 discusses the key aspects of cell search in the presence of femtocells. Sections 1.2.3.5, 1.2.3.6, and 1.2.3.7, provide a comprehensive discussion on the research challenges for supporting femtocells in terms of cell selection/reselection, HO decision, and HO execution, respectively.

1.2.3.1 Support of Femtocells in LTE-Advanced

Support of femtocells necessitates the deployment of certain network architectural and procedural enhancements in the LTE-A network architecture system. Figure 5 depicts the overall E-UTRAN architecture in the presence of femtocells [26]. In the context of LTE-A, a macrocell station is referred to as eNB and a femtocell station as Home eNB (HeNB).

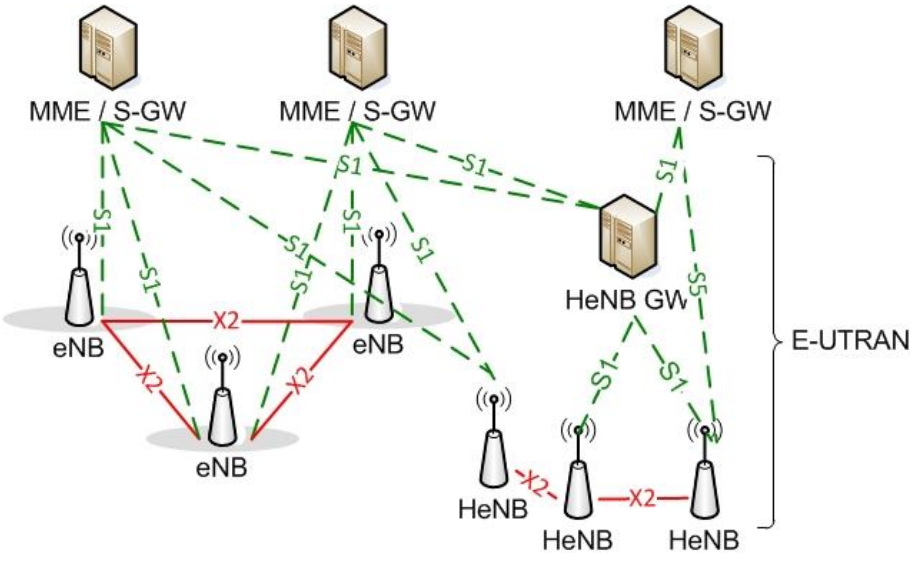

Figure 5: Support of femtocells in the E-UTRAN architecture [26]

According to LTE-A, the functions supported by the HeNBs are the same as those supported by the eNBs, while the same implies for the procedures run

between the HeNBs and the EPC. The HeNB GW acts as a concentrator for the control plane to support a large number of HeNBs in a scalable manner. The deployment of HeNB GW is optional; however, if present, it appears to the HeNBs as an MME and to the EPC as an eNB.

The eNBs interconnect with each other through the X2 interface [27][28], while they also connect to the EPC through the S1 interface [29][30]. The same implies for the connection between the HeNBs and the EPC whereas, different from LTE-Advanced Rel. 8/9, the LTE-A standard supports direct connectivity between the HeNBs through the X2 interface. The X2 interface between the HeNBs is supported independent of whether any of the involved HeNBs is connected to a HeNB GW. However, X2-based HO between HeNBs is allowed only if no access control at the MME is needed, i.e., either when the HO is performed between closed/hybrid access HeNBs with the same Closed Subscribers Group (CSG) ID, or when the target HeNB supports open access. Even though the X2 interface is supported both between eNBs and between HeNBs, the LTE-A standard does not support direct X2-based connectivity between eNBs and HeNBs. This design option mainly follows from the increased complexity required in terms of infrastructure and signaling overhead [31]. Table 3 summarizes part of the technical specifications (TSs) that relate to the MM support of femtocells in the LTE-A system.

Table 3: TSs related to the MM support of femtocells in LTE-A

Technical Specification	Title	Release Date	Relation to MM support for femtocells
3GPP TS 36.211 V10.4.0	Physical Channels and Modulation	Dec. 2011	Describes the procedures followed to generate and demodulate the Reference Signals used for MM support in LTE-A
3GPP TS 36.214 V10.1.0	Physical layer; Measurements	Mar. 2011	Describes standard UE and the E-UTRAN signal quality measurements that can be used for enhancing MM support in LTE-A
3GPP TS 36.300 V10.7.0	E-UTRAN; Overall description	Mar. 2012	Describes the network architectural and procedural E-UTRAN enhancements to support femtocells. It also includes the MM procedures followed in the presence of femtocells.
3GPP TS 36.331 V10.5.0	Radio Resource Control (RRC); Protocol specification	Mar. 2012	Describes the structure and the information elements broadcasted within the various system information blocks. The procedures followed for SI are also described.
3GPP TS 36.410 V10.2.0	S1 general aspects and principles	Sept. 2011	Describes general aspects of the S1 interface, and defines the S1 interface protocol functions
3GPP TS 36.413 V10.5.0	S1 Application Protocol (S1AP)	Mar. 2012	Describes the S1 interface procedures used to support various LTE-A functions, including MM
3GPP TS 36.420 V10.2.0	X2 general aspects and principles	Sept. 2011	Describes general aspects of the X2 interface, and defines the X2 interface protocol functions
3GPP TS 36.423 V10.5.0	X2 application protocol (X2AP)	Mar. 2012	Describes the X2 interface procedures used to support various LTE-A functions, including MM

1.2.3.2 Cell Identification

The cell identification procedure involves the mechanisms and identifiers used to distinguish femtocells from macrocells and/or other femtocells. Although the additional overhead required to broadcast unique cell identifiers over the network seems negligible, it can be quite high in the long-term given that a) the cell identification information should be transmitted in a frequent and periodic basis to ensure its systematic acquisition by the network nodes, and b) existing standards sophisticatedly scramble this information within the broadcast channels to lower the radio resource overhead required to transmit it [32]. To this end, cellular systems typically use a limited number of PCIs over the network to enable the identification of cells in a local scale.

Taking into account the limited range of PCI values and the large number of small-sized cells within the macrocell coverage, a dense PCI reuse is expected in the presence of femtocells [33]. This dense reuse of PCIs makes infeasible for the network entities to uniquely identify the target cells based only on the measurement reports provided by the mobile terminals, i.e., the signal measurement list may include measurements for different cells with the same PCI. Moreover, the unplanned deployment of femtocells hinders the centralized assignment of PCI values in an optimized manner, and dictates the employment of distributed PCI selection algorithms at the femtocells. An intelligently-enhanced PCI selection algorithm can improve the distribution of PCIs in a local scale; however, the limited range of PCI values can still result in the PCI confusion problem.

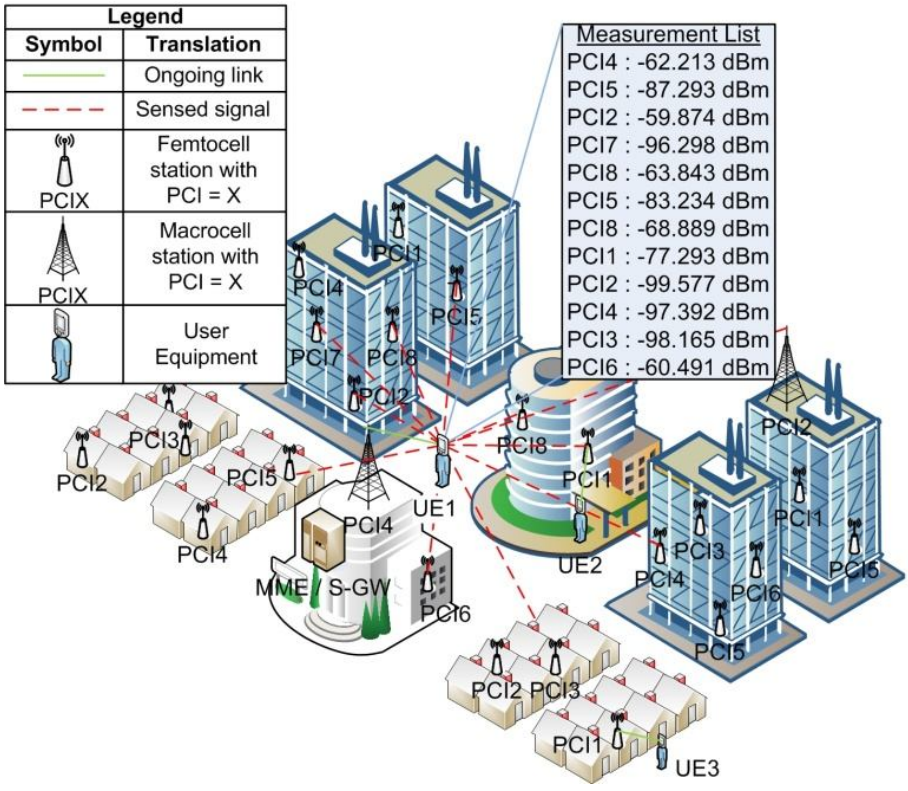

Figure 6: PCI confusion problem in the presence of femtocells

Assuming a PCI range of 8 values, i.e., PCI1 to PCI8, Figure 6 illustrates an instance of the PCI confusion problem in the presence of femtocells. UE1 reports to its current serving macrocell with PCI4 the list of measurements, which contains more than one cells with the same PCI, e.g., there exist a macrocell and

a femtocell with PCI2. As a consequence, the serving cell is unable to identify which one of the cells with PCI2 it should handover the UE1.

Based on the discussion above, the cell identification phase comprises two key research challenges: a) how to minimize the negative impact of the PCI reuse by using distributed PCI selection algorithms, and b) what procedures can guarantee the unique identification of nearby cells from a system engineering perspective. Referring to the first challenge, current literature includes various algorithms for PCI selection [34]-[40]. However, further work is required to support intelligently-enhanced and distributed PCI selection for femtocells, e.g., use of cognitive and cooperative approaches. Referring to the second challenge, some solutions to the problem include the use of a) hierarchical cell structuring, b) separate public land mobile network (PLMN) identities (ID), c) carrier reservation, d) Physical Cell Identifier (PCI) reservation, and e) upper-layer approaches. Hierarchical cell structuring allows the network operators to categorize the cells into different layers and assign them with different priorities. The separate PLMN ID approach uses a different PLMN identity for each cell tier, e.g., one for the macrocell tier, one for the femtocell tier, and so on. The carrier and PCI reservation approaches reserve a particular set of carrier frequencies or PCIs per tier, which is commuted to the network nodes within broadcast messages. Finally, the upper-layer approaches include the acquisition of the unique cell global identifiers (CGI) which, however, are typically signaled in a less frequent basis.

Let us now focus on the femtocell identification procedure in the LTE-A system. The LTE-A system uses a total of 504 PCI values, which are assigned to the eNBs based on either centralized or distributed assignment algorithms [26]. In more detail, the LTE-A system provisions for a PCI selection framework based on self-configuration. The operation, administration, and maintenance (OAM) system signals to the (H)eNB a specific PCI value (centralized approach), or a list of PCI values to select (distributed approach). In the distributed approach, the (H)eNB may avoid using PCIs which have been reported by the UEs, or by neighbor (H)eNBs over the X2 interface, or acquired through other implementation dependent methods. Note that although the LTE-A standard provides some recommendations on how the PCI selection can be performed, the implementation of distributed PCI selection algorithms is an open issue.

Referring to the PCI confusion problem, LTE-A resolves it by configuring the UEs to acquire the unique E-UTRAN cell global identifier (ECGI) of the target cells, i.e., a layer-2 approach. However, the ECGIs are acquired on specific occasions only, e.g., on demand by the serving cell, owing to the increased delay required (up to 80ms). To further enhance the cell identification procedure, the LTE-A system can reserve a range of PCI values or carrier frequencies for femtocell use only and broadcast this information within the system information block (SIB) messages. Note that the reserved PCI range applies only to the frequency of the PLMN where the UE received this information and is valid for a maximum of 24 hours within the entire PLMN.

1.2.3.3 Access Control

Access control is of key importance in femtocell deployments, given that femtocells utilize the consumer's broadband backhaul and support up to a few users. Current literature identifies three femtocell access modes: closed, open and hybrid [33][41]. In the closed access mode only a limited group of users is allowed to camp on and utilize the femtocell station, in order to guarantee the exclusive utilization of the radio resources for subscribed-use only. Under certain

interference scenarios, however, the closeness of this mode may severely degrade the SINR performance for both subscribed and non-subscribed users due to cross-tier interference [25]. The latter effect is mitigated in the open access mode, where all users are allowed to utilize the femtocell station. Nevertheless, the short cell radii in combination with the openness of this mode dictate the use of more sophisticated MM to anticipate with the increased HO occurrence rate and the enlarged HO execution signaling overhead. Given that femtocells support up to a few users, sustaining an acceptable HO failure probability is also challenging in the open access mode. Hybrid access integrates the benefits of both the closed and open access modes. Even though it enables the support of non-subscribed users, it simultaneously provides prioritized access to subscribed users. However, advanced HO decision, admission control and scheduling algorithms are required for this mode, to efficiently support non-subscribed access while sustaining an acceptable QoE for the subscribed users.

Under the viewpoint of MM, access control complicates the support of femtocells in three aspects. Firstly, the UEs should be aware of the femtocells they can access and secondly, the femtocell stations should enable nearby users to identify the access type they support. Both these steps are required a) to avoid initiating a HO towards not accessible femtocells and b) to minimize the energy consumption and delay required for identifying them. Thirdly, a trusted network entity should validate the membership status of the mobile terminals prior to accessing the femtocell stations. This entity should be located to the access or the core network, while the access control procedure should be performed in a secure and backwards compatible manner.

In the context of the LTE-A system, a UE is considered part of a CSG either if it is permitted to utilize a particular set of closed access femtocells, referred to as CSG cells, or if it receives prioritized service on a particular set of hybrid access femtocells, referred to as hybrid cells. To enable the identification of the access type and the CSG they support, the HeNBs broadcast the CSG indicator and the CSG identity (CSG ID), respectively. The CSG indicator is set to ‘true’ for CSG cells and to ‘false’ for hybrid cells. On the other hand, the CSG ID information is broadcast by every E-UTRAN cell in a fixed schedule within the SIB type 1 [32]. Even though hybrid cells are accessible as CSG cells to the subscribed UEs, they appear as normal cells to all other UEs. Besides, the UEs are aware of the CSG cells they can access by maintaining a CSG whitelist. The MME is responsible for performing UE access control prior to accessing the CSG cells, based on stored CSG subscription data for the UEs. As a result, the HO execution signaling always passes through the MME and the S1 interface, unless an X2-based HO execution is taking place.

1.2.3.4 Cell Search

Cell search is the procedure by which the UE acquires time and frequency synchronization with a nearby cell in order to identify it and measure its signal quality. The measurement phase is an integral part of inter-cell mobility and is performed on pilot or reference signals broadcast by the cells in a predefined time - frequency basis. Cell search is typically triggered by events related to the signal quality of the serving and neighbor cells, e.g., the signal strength of the serving cell falls below a prescribed threshold, while it is performed during idle downlink (DL) / uplink (UL) periods provided either by DRX or packet scheduling, i.e., gap assisted measurements. Even though a longer search period enhances the measuring accuracy and increases the number of identified cells, it also disrupts the service continuity and increases the energy consumption at the UEs.

In large-scale deployments of femtocells, cell search is challenging in many aspects. The received signal strength from nearby femtocells can be subject to fast variations owed to the low transmit power. To this end, the cell search triggering process should be reassessed in order to avoid frequent yet unnecessary measurement derivation. On the other hand, even though the network typically provides a neighbor cell list (NCL) to assist the cell search at the UEs, inbound mobility to femtocells is unlikely to be assisted with such information. This follows from the fact that a) the use of femtocells is subject to access control, i.e., the NCL should be adapted according to the UE subscriptions, b) femtocells are installed and managed by the consumers in a random manner, i.e., the owners can install/uninstall, switch on/off the femtocell station, or change the supported access method, and c) a limited number of neighbor cells can be signaled within the NCL, e.g., up to 32 [26]. As a consequence, support of femtocells dictates migration from network-controlled to UE-based autonomous cell search procedures, which can be founded on the use of cooperative and cognitive radio strategies. Similar approaches can be used to construct a complete NCL at the macrocell and the femtocell stations as well, to further shorten the duration and enhance the accuracy of the cell search procedure, e.g., neighbor cells can share their NCLs.

More sophisticated DRX and packet scheduling strategies are also required to support femtocell search, while keeping the energy consumption, QoS maintenance and Quality of Experience (QoE) degradation overheads at acceptable levels. Current literature includes various approaches for NCL tracking [42]-[46] and DRX [47]-[49] under the viewpoint of femtocells. However, further work is required to meet the femtocell-specific performance trade-offs mentioned above. Little light has also been shed on the issue of UE-based autonomous cell search in the presence of femtocells.

Let us now focus on the cell search procedure for femtocells in the LTE-A system. E-UTRAN cell search is based on following the primary and secondary synchronization signals in the DL direction, which are transmitted over the central 72 sub-carriers of the first and sixth subframe in each frame [26]. Two basic signal quality measurements are supported at the UEs: the RSRP and the RSRQ [16]. Both these measurements are performed on the DL reference signals transmitted by every E-UTRAN cell in a predefined time-frequency basis [50]. Different cell search approaches apply in LTE-A, depending on whether the UE is in the connected or the idle state.

When the UE is in the connected state, the E-UTRAN cell search procedure is based on configuration provided by the network. Both event-triggered and periodical measurement reporting criteria are supported in LTE-A, while blacklists can also be used to prevent the UE from measuring specific neighbor cells. The serving LTE-A cell is not required to provide the UEs with neighbor cell information, however, it should at least indicate the carrier frequency of the inter-frequency neighbor cells. A NCL can also be provided to handle specific cases of inter-cell mobility and commute to the UEs cell-specific parameters related to the cell search and measurement phase, e.g., cell-specific offset [26]. Cell search for CSG and hybrid cells in the connected state is different from the (normal) E-UTRAN cell search procedure in one aspect: the use of proximity estimation. Proximity estimation was originally introduced in LTE-Advanced Rel. 9. According to it, the serving cell configures the UE to provide an indication of proximity whenever it determines, based on autonomous search procedures, that it is near an accessible CSG or hybrid cell. Upon receiving an indication of proximity, the

serving cell may configure the UE to perform signal quality measurements and acquire the system information of the new cell.

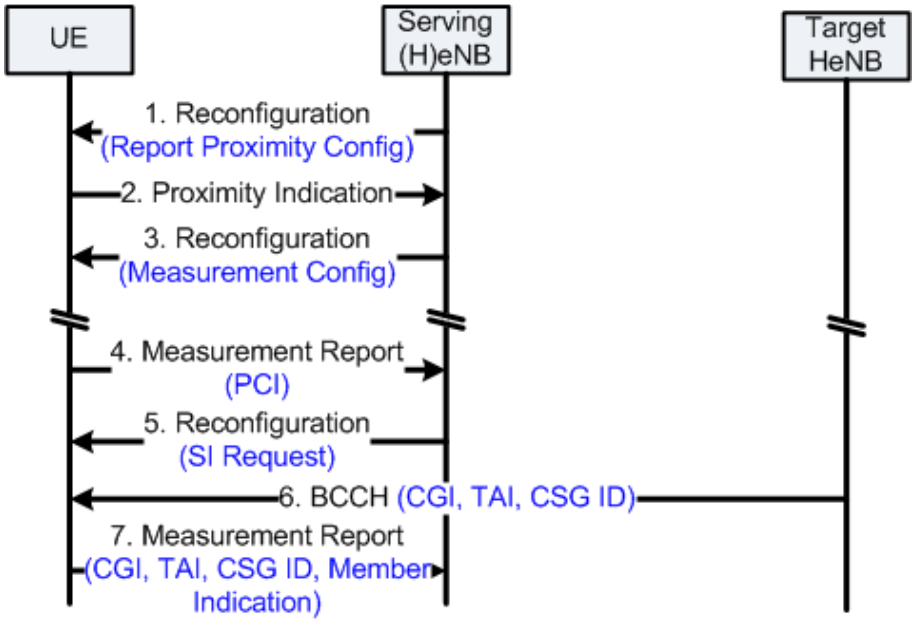

Figure 7: Cell search and measurement signaling in LTE-A

The cell search and measurement procedure for femtocells in LTE-A is illustrated in Figure 7. First, the serving cell configures the UE with proximity indication control (step 1). Using autonomous search procedures, the UE identifies the presence of a nearby femtocell and reports it back to the serving cell (step 2). Accordingly, the serving cell reconfigures the UE to measure and report the signal quality of the target HeNB (steps 3 and 4, respectively). In step 5, the serving cell reconfigures the UE to acquire the system information (SI) of the target HeNB by overhearing the broadcast control channel (BCCH) (step 6). The cell search procedure is concluded in step 7, where the UE reports the acquired SI to the serving cell. Note that steps 4 – 6 are used for cell identification.

When the UE is in the idle state, cell search for CSG cells is based on a UE autonomous search function which determines itself when/where to search without being assisted with network information about frequencies dedicated to CSG cells. To assist the search function on mixed carriers, i.e., carriers used by both eNBs and HeNBs, all CSG cells on mixed carriers broadcast a range of PCI values reserved for CSG use only. This information can optionally be broadcast by non-CSG cells as well, while it is valid for a maximum of 24 hours and only to the frequency of the PLMN received. Manual selection of CSG cells is also supported in LTE-A, while the autonomous search function for CSG cells can be disabled if the CSG whitelist of the UE is empty. Note that in specific occasions, the serving cell can provide the UE with a NCL that includes CSG cells, e.g., when the network aims to trigger a CSG cell search at the UE. Cell search for hybrid cells in the idle state follows the normal E-UTRAN cell search procedure, where the serving cell relies on the UE to detect neighbor cells and indicates only the carrier frequencies of inter-frequency neighbor cells. Note that the implementation of the autonomous search function and the use of the PCI split information are left open by the LTE-A standard.

1.2.3.5 Cell Selection/Reselection

Cell selection refers to the attachment procedure where the UE is idle and not camped on a cell, e.g., during the UE switch-on phase or upon losing network

coverage. On the other hand, cell reselection refers to the inter-cell mobility procedure where the UE is idle and is already camped on a cell. To employ cell selection, the UE searches all the frequency bands of the cellular system, identifies the cells operating in each carrier frequency and follows a random access procedure to camp on the most suitable cell. Note that stored or cache information can be utilized to shorten the cell selection phase. Apart from using the signal quality as the primary criterion, other criteria or restrictions may also apply, e.g., use of blacklists including specific cells or tracking areas. On the other hand, cell reselection is based on measuring the signal quality of nearby cells and using a) cell ranking criteria, b) frequency priorities provided by the network, or c) other UE-specific optimization criteria. The cell reselection procedure can be assisted by the network with a NCL, while it can also be optimized by using stored or cache information at the UE [46].

Two major research challenges relate to the performance of cell selection/reselection in the presence of femtocells: a) the optimized formation of tracking areas (TA), and b) the use of femtocell-specific cell selection/reselection strategies.

Referring to the first challenge, it is known that the cellular network keeps track of idle UEs by using TAs, i.e., a group of neighbor cells. TAs are used to notify the UE in case of an incoming voice call or data packet connection, e.g., via paging the UE. Even though the use of large TAs reduces the cell selection/reselection signaling and energy consumption overheads at the UE side (i.e., less frequent TA update), it also increases the signaling, energy consumption, and radio resource overhead at the network side (i.e., more cells are required to broadcast the paging messages for the tagged UE). Attaining an acceptable performance trade-off between these two points is even more challenging in the presence of femtocells, where the cellular network consists of randomly and non-uniformly deployed stations of small size.

Referring to the second challenge, cell selection/reselection is typically based on cell ranking or absolute frequency priorities. However, the support of femtocells dictates the use of more sophisticated cell selection/reselection strategies to offload the macrocell tier by increasing the utilization of the femtocell infrastructure. These strategies should anticipate the signaling and delay overhead for cell selection/reselection, and be adapted to the femtocell-specific features, e.g., access control and fast variation of the wireless medium. Stored or cache information can also be used to speed up the cell selection/reselection procedure and efficiently handle the enlarged number of candidate cells.

In LTE-A, cell selection for hybrid cells consists of searching the E-UTRA frequency bands, identifying the strongest cell for each carrier frequency and reading the SI to acquire the respective PLMN identities. Based on this operation, the UE identifies a cell that a) satisfies the cell selection criteria, b) has a PLMN identity belonging to the allowed PLMN identities of the UE, c) is not included in a blacklist, and d) does not belong to a forbidden TA. If it is not possible to identify such a cell, the UE camps on a cell that satisfies the first two conditions. Apart from the procedure described above, cell selection for CSG cells can be additionally based on the UE autonomous search function and the CSG whitelist of the UE.

Cell reselection in LTE-A can be summarized as follows. For intra-frequency cell reselection the UE uses cell ranking, whereas for inter-frequency reselection the UE relies on absolute frequency priorities broadcast in the system information,

i.e., the UE camps on the highest priority frequency available. LTE-A enables the use of layer-specific parameters for inter-frequency neighbor cells, e.g., layer-specific offset [26]. Cell-specific reselection parameters can also be used when a NCL is provided by the serving cell, e.g., cell-specific offset. The cell reselection parameters apply for all the UEs in a cell, except if other configurations are in effect, e.g., use of speed-dependent reselection parameters. As in cell selection, cell reselection for CSG cells is based on the UE autonomous search function and the CSG whitelist of the UE. A NCL with CSG cells can also be signaled to the UE in order to handle specific cases of inter-cell mobility. Manual cell selection/reselection to CSG or hybrid cells is also supported in LTE-A.

1.2.3.6 Handover Decision

Cell HO consists of all the decision and signaling procedures required to seamlessly transfer the ongoing connections of a tagged UE from its current serving cell to another cell. The decision part of a cell HO is referred to as the HO decision phase, while the signaling part as the HO execution phase. In prominent cellular networks, the HO decision phase is performed at the serving cell and is based on signal quality measurements provided by the UE, i.e., UE-assisted network-controlled HO [51]. The HO decision phase is typically used to offload highly congested macrocells and improve the received signal quality at the mobile UEs.

The impact of the HO decision phase is even more prominent in the presence of femtocells, owing to the short-range nature of communications, the denser network layout and the fast varying radio environment. To this end, apart from the received signal strength at the UEs, the HO decision phase should also account for a) the divergent interference levels at the cell sites, b) the uneven power transmissions on the RS of the macrocell and femtocell stations, and c) the increased sensitiveness on user mobility. The HO decision can also be used to improve the energy-efficiency of the network nodes and handle the interference in a macroscopic level, i.e., without using power control, radio resource or interference management.

Current literature includes various HO decision algorithms for the two-tier macrocell-femtocell network [52]-[71]. The vast majority of existing algorithms prioritize femtocell over macrocell access based on signal strength [52]-[56], [70], UE speed [58]-[61], or traffic-type criteria [58] [60]. In most of the cases, the impact of the HO algorithms on the energy consumption, interference, system capacity and network signaling is not investigated. On the other hand, the vast majority of existing HO decision algorithms focus on the inter-tier HO decision scenario and assume the strongest cell (SC) algorithm for the intra-tier HOs, i.e., for macrocell-to-macrocell and femtocell-to-femtocell HOs. However, the SC algorithm does not account for the actual transmit power on the RS of the candidate cells, nor the interference level at the cell sites [66]. Another weak aspect of existing approaches is the assumption of simple network layouts to attain analytical tractability, e.g., single-macrocell single-femtocell [52]-[54].

Femtocell-specific HO decision making poses a series of research challenges. The triggering of the HO decision phase should be carefully reassessed in the context of femtocells and the use of other IMT-Advanced features should also be considered prior to HO decision making, e.g., use of multi-antenna techniques or carrier aggregation. Instead of using the received signal strength as the primary criterion, the HO decision phase for femtocells should also account for the actual Radio Frequency (RF) interference and RS power transmissions at the cell sites

in order to sustain an acceptable SINR performance at the UEs. Attaining a good performance trade-off between exploiting the femtocell utilization opportunities and sustaining a low HO probability is another critical issue. The joint optimization of the interference and energy consumption performance at the network nodes should be integrated within the HO decision phase as well. On the other hand, more sophisticated analytical models are required to validate the performance of the proposed algorithms in terms of SINR performance, interference, energy consumption and throughput. Attaining backwards compatibility with the standard cellular operation should also be investigated during the design of HO decision algorithms.

1.2.3.7 Handover Execution

HO execution consists of all the necessary signaling procedures for performing inter-cell mobility when the UE is in the connected state. In the presence of femtocells, increased signaling and delay overheads are required for HO execution provided that a) femtocells connect to the core network through the user's broadband backhaul, and b) the signaling load passes through additional network entities, e.g., access control entity or femtocell gateway (GW). More complicated signaling procedures are also required to integrate the femtocell-specific processes into the HO execution phase, e.g., autonomous search, PCI resolution, and access control. The same implies when the deployed HO decision algorithm utilizes an enriched set of parameters that account for the target cells' status[60][62][71]. Current literature includes various studies for improving the wired and cellular backhaul under the viewpoint of femtocells [72]-[76]. The deployment of femtocell GWs is a widely accepted solution for enhancing the HO execution in a scalable and backwards-compatible manner [23][26].

In the following, we summarize the feasible HO execution scenarios in the presence of femtocells and overview the signaling procedures for deploying them in LTE-A. Depending on a) the type of the serving cell, b) the type of the target cell, and c) the need for using access control. Table 4 summarizes the HO execution scenarios in the two-tier macrocell-femtocell LTE-A network and indicates the interface under use. Note that access control does not apply to the HO execution scenarios 1 and 2 (the target cell is an eNB) and that in the HO scenario 3 the serving cell can be either an eNB, or a HeNB. The HO execution scenarios 1 and 2 do not require any procedural enhancements for the LTE-A system, given that regular E-UTRAN procedures can be used for handing over to an eNB. In contrast, inbound mobility to femtocells (i.e., the HO execution scenarios 3, 4, and 5), necessitates the use of proximity estimation, the resolution of the PCI confusion problem and the employment of access control (scenario 3).

Table 4: HO execution scenarios in the two-tier macrocell-femtocell LTE-A network

HO Scenario	Serving Cell	Target Cell	Access Control	HO Type	HO Execution Interface
1	eNB	eNB	Does not apply	Regular E-UTRAN	X2
2	HeNB	eNB	Does not apply	Outbound from HeNB	S1
3	(H)eNB	HeNB	Yes	Inbound to HeNB	S1
4	eNB	HeNB	No	Inbound to HeNB	S1
5	HeNB	HeNB	No	Inbound to HeNB	X2 / S1

Figure 8 depicts the most complicated HO execution signaling procedure for inbound mobility to a HeNB, i.e., the HO execution scenario 3. The cell search and measurement phase is performed in steps 1 – 7, which implement the

proximity indication control (steps 1 – 2), the signal quality measurement request/report (step 3 – 4), and the cell identification (steps 5 – 7) phases. Based on the HO decision outcome in step 8, the serving (H)eNB includes the ECGI and the CSG ID of the target HeNB in a HO request message sent to the MME (step 9). If the target HeNB is a hybrid cell, the access mode is also included in the message. The MME validates the UE membership status on the target HeNB in step 10, and if no access control restrictions apply, a HO request message is forwarded to the target HeNB (steps 11 – 12) including the reported CSG ID. The target HeNB verifies that the reported CSG ID matches the broadcast CSG ID and allocates an appropriate set of resources for the tagged UE (step 13). Depending on the supported access type and the UE membership status, priority-based radio resource allocation can be employed in step 13. The HO execution procedure is concluded in steps 14 – 17, where the target HeNB acknowledges the HO request to the MME (steps 14 – 15), the MME sends a HO command message to the serving (H)eNB (step 16), and the serving (H)eNB notifies the UE to initiate its transition to the target HeNB (step 17).

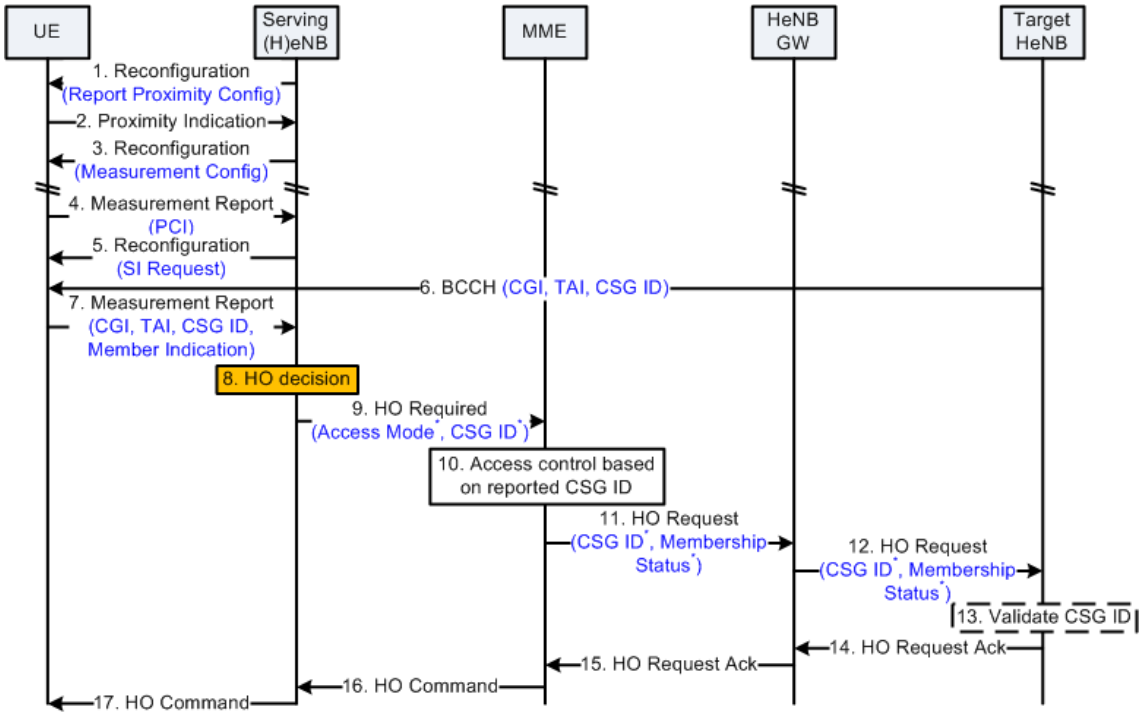

Figure 8: HO execution signaling procedure for inbound mobility to a HeNB

Note that the signaling procedure for supporting the HO execution scenario 4 is similar to the one followed in Figure 8, with the difference that the step of MME-based access control is omitted (step 10). The same implies for the HO execution scenario 5, where in addition, the X2 interface can be used to exchange the HO request/commands between the serving and the target HeNB in order to reduce the required signaling and delay overheads.

1.2.4 Key aspects of Device-to-Device Communications: A Brief Overview

D2D communications have recently drawn significant attention owing to the unprecedented demand for direct exchange of localized traffic between nearby cellular devices. Even though the support of D2D communications has been primarily motivated by applications such as social networking and public safety communications [5], the direct exchange of localized traffic can also be used to offload the cellular access network, as well as to establish bidirectional links for

carrying out localized measurement/control data in the Smart Grid [4]. Among others, D2D communications are expected to reduce the transmit power for wireless communications and reduce the communication delay, i.e. neighbor devices can directly exchange localized traffic without network involvement. Moreover, D2D communications are envisaged to play a key role in cellular traffic offloading, by increasing the cellular capacity and enabling more sophisticated load balancing. Another key advantage of D2D communications is their capability to increase the area spectral efficiency of the licensed spectrum and extend the cell coverage area. Finally, D2D communications are also expected to launch the design of innovative location-based services.

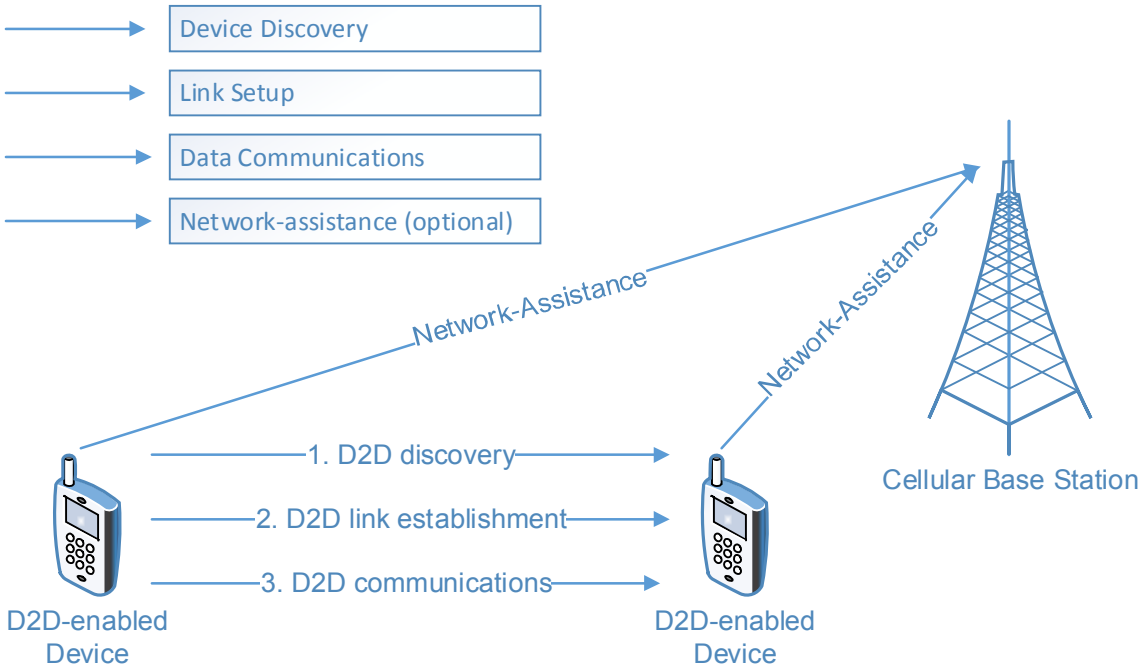

Figure 9: Device-to-Device Communications Procedure

The D2D communication procedure consists of three main phases: D2D discovery, D2D link establishment, and D2D communications. D2D discovery involves the process by which a D2D-enabled user detects other D2D-enabled devices in its vicinity. D2D link establishment is the process by which the two D2D-enabled devices setup a direct radio link in order to directly exchange data. Finally, D2D communications include the maintenance and utilization of the established link to directly exchange data between the D2D-enabled users without routing packets through the cellular access network. D2D discovery and communications are within the scope of the LTE Release 12 system [8], a.k.a. LTE-A. 3GPP focuses on two types of D2D discovery: direct and network-assisted D2D discovery. The direct discovery is solely based on the capabilities of the D2D-enabled devices to autonomously discover, or indicate their presence to, other D2D-enabled devices without network involvement. On the contrary, network-assisted discovery, often referred to as EPC-level discovery, relies on the core network's capability to determine the proximity of the D2D-enabled devices. Both methods have their own advantages and unique challenges. On the one hand, direct D2D discovery can be deployed even when the D2D-enabled devices are outside the network coverage, whereas network-assisted discovery enables network operators to better handle the energy, signaling, and interference burden occurred by D2D discovery.

A key advantage of network-assisted discovery is its potential for more accurate estimation of the proximity between D2D-enabled devices by exploiting existing knowledge of the cellular network layout. Besides, the EPC is at least aware of the BS with which the cellular devices associate with, also coined as the associated BS [77][78]. This knowledge combined with additional information on the spatial relation between the respective associated BSs, such as the inter-site distance or the relative position of the D2D peers with respect to their associated BSs, e.g. distance and angle, can be the cornerstone for more accurate D2D discovery at the EPC. This type of D2D discovery is within the scope of our work.

1.3 Related Works and Key Contributions

1.3.1 Localization and Peer-Discovery in Heterogeneous Wireless Networks

Localization poses several challenges that span from mitigating (or exploiting) prominent effects of the wireless medium [6], [79]-[81]to employing multi-user detection (MUD) [82] and cooperation [83][84] for more accurate localization. The impact of non line-of-sight propagation on localization is discussed in [79], where the authors propose regression algorithms that robustly identify and mitigate it in ultra wide-band (UWB) networks. The authors in [6], demonstrate how the spatial predictability of wireless channels can be exploited, to jointly optimize the communication and motion plan of robots over predefined trajectories. The challenging issue of early detection in the UWB sensor network is discussed in [80], while a tree-based solution is presented in [81] to mitigate asymmetric links in sensor networks. Low-complexity MUD techniques for cellular systems are presented in [82], while the performance of cooperative RF-based localization between homogeneous WNEs is assessed in [83]. The interplay between accuracy and communication delay upon cooperative localization is analyzed in [84], where the authors conclude that standard cooperation may result in the worst possible accuracy/delay trade-off. Our work is complementary to the ones in [6],[79]-[84] since we focus on how to integrate the localization outcome from heterogeneous WNEs so as to enable localization and peer discovery between distant and not necessarily homogeneous WNEs.

The Poisson point process (PPP) has been recently shown to be as accurate as the grid model and a good fit for modeling the locations of small-sized stations in multi-tier cellular networks with independent tiers [1]. Besides, the PPP model has been used to derive near-optimal strategies for random peer discovery in homogeneous networks [85] and quantify its performance under the joint impact of channel fading and random node distribution [86]. In parallel, a considerable amount of works identify that the locations of short-range WNEs are not completely random, e.g. sensors [87], femtocells [88], or more generic WNEs [89][90], and typically form clusters around other WNEs of increased radii, e.g. macrocells. Different from [1],[87]-[90] in this paper we propose a M-tier HWN model that accounts both for the tiered structure of generic HWNs and the spatial dependencies between heterogeneous WNEs, e.g. clustering. Moreover, different from [85][86], we focus on location-aware peer discovery between not necessarily homogeneous WNEs and analyze how partial (or full) knowledge of the HWN layout affects its performance.

The key contributions of our work (section 2) can be summarized as follows:

- We derive closed-form expressions for the conditional probability density function (pdf) and complementary cumulative distribution function (ccdf) of the relative distance between two heterogeneous WNEs, given partial (or full) knowledge of the spatial relations between their upper-tier parent WNEs.
- The derived pdf expressions describe the statistical behavior of localization between distant and not necessarily homogeneous WNEs. To the best of our knowledge, this is the first work to consider this disruptive localization paradigm and analyze its performance.
- We analyze the performance of location-aware peer discovery between heterogeneous WNEs given partial (or full) knowledge of the spatial relations between their upper-tier WNEs. To the best of our knowledge, this is the first work to address this challenging issue.
- We analyze the impact of the key system parameters on the performance of location-aware peer discovery and derive optimal strategies for the placement of upper-tier WNEs as means of maximizing the peer discovery probability between two heterogeneous WNEs of interest.
- We provide valuable insights for the design of location-aware peer discovery in the nowadays HWN. We show that a denser tier-1 layout may deteriorate the performance of location-aware peer discovery. Also, we show that the accuracy of AoA measurements in low-tier WNEs can be relaxed without significantly affecting the performance of peer discovery.

1.3.2 Device-to-Device Discovery in Cellular Networks

The research on D2D discovery and communications is currently in its infancy. Most of the related literature to our work deals with the analysis and optimization of D2D communications. The authors in [91] analyze the performance of a distributed multi-hop spectrum access protocol for D2D communications, focusing on the impact of D2D communications on the macrocell network and the power savings attained due to the employment of single or multi-hop D2D routes. A bio-inspired algorithm for direct D2D discovery and synchronization is proposed in [92], based on the formation of acyclic graphs in the D2D network and the deployment of the firefly algorithm. Simulation results demonstrate that compared to existing schemes, the proposed algorithm requires less time to achieve network synchronization and reduced number of messages for direct D2D discovery.

PPPs, which have been extensively used for the analysis of multi-tier cellular networks [1], [93]-[96], are increasingly used to model and analyze the performance of D2D communications. In [97], the authors analyze the performance of two fundamental spectrum sharing schemes and provide design guidelines for D2D communications in the uplink of cellular networks. The D2D proximity is based on the physical distance between the D2D peers. The work in [98] considers D2D communications in Poisson networks with time/frequency hopping to randomize interference and analytical expressions for the SINR and throughput, as well as optimal strategies for time/frequency hopping are derived. The authors in [99] investigate how mobility and network assistance affect the performance of multicast D2D transmissions in Poisson networks. Optimal network assistance strategies are discussed towards minimizing the retransmission times of multicast messages given certain constraints. The challenging issue of power control is addressed in [100], in which the authors focus on a single macrocell BS with circular coverage where the locations of the

D2D transmitters are PPP distributed. Assuming that the distance between a D2D pair is fixed, the authors propose a centralized power control algorithm that maximizes the SINR of the standard cellular link while satisfying the individual target SINR of the D2D links. The performance of distributed on-off power control is also analyzed and optimal D2D transmission policies are discussed.

To the best of our knowledge, our work (section 3) is the first to analytically address the challenging issue of network-assisted D2D discovery in random spatial networks. Our key contributions can be summarized as follows:

- We derive closed-form expressions for the conditional pdf and ccdf of the distance between two D2D peers, given various combinations of location information parameters including at least the distance or the neighboring degree between their associated BSs. The derived expressions can be readily used to analyze problems that involve the relative distance between two D2D peers, such as interference analysis or hybrid automatic repeat request (HARQ) [5].
- We analyze the performance of network-assisted D2D discovery given the most prominent combinations of location information parameters. Our analysis readily quantifies how different levels of location knowledge affect the D2D discovery probability. The derived expressions can also be used to analyze the performance of cluster-based D2D discovery in the absence of network coverage or serve as an upper performance bound for SINR-based D2D discovery.
- We examine the behavior of the D2D discovery probability with respect to key system parameters, with the emphasis given on the BS density. We identify conditions under which the D2D discovery is optimized and provide analytical expressions for computing the optimal BS density.
- We provide useful design guidelines for network-assisted D2D discovery. We show that above a certain BS density, the D2D discovery probability $\mathcal{A}_{\mathcal{J}}$ is primarily affected by the inter-site distance and that, under certain conditions, denser network layouts reduce the D2D discovery probability. We also show that in medium to high density networks the D2D discovery probability may increase with the neighboring degree between their associated BSs.

1.3.3 Handover Decision in the Macrocell – Femtocell Network

Current literature includes various approaches for handling interference in femtocell networks [15] [15] [55] [101]-[107]. A wide range of interference coordination and cancellation techniques are summarized in [14], with the emphasis given to the LTE system. To mitigate cross-tier interference in the two-tier network, advanced radio resource allocation and power control schemes are proposed in [55] [101]-[103]. Focusing on the LTE-A system with multi-hop relaying, the performance of semi-static interference coordination schemes for radio resource allocation and power control, in both the frequency and time domain, is demonstrated in [15]. The achievable SINR performance of the macrocell tier is investigated in [104], with respect to the number of femtocells deployed in the two-tier network. A utility-based SINR adaptation algorithm is subsequently proposed for the femtocell nodes, aiming to mitigate the interference caused to the macrocell tier in a distributed manner. Two interference mitigation strategies are proposed in [105], which suppress the cross-tier interference to the macrocell tier by adjusting the maximum transmit power at the femtocell users. Based on decentralized Q-learning and knowledge

dissemination among the femtocell stations, a self-optimization approach is described in [106], which is shown to sustain an improved macrocell capacity and SINR performance compared to an independent learning approach. An orthogonal random beamforming-based strategy is proposed in [107], aiming to reduce the cross-tier interference in the two-tier network, increase the spatial opportunity of the femtocell nodes, and mitigate the degradation to the macrocell capacity. Analytical and numerical results illustrate that combined with opportunistic channel selection and distributed power control, the proposed strategy sustains the macrocell throughput and reduces the mean transmit power at the femtocell nodes. Different from the approaches above, our work (section 4) describes a novel interference mitigation approach based on the employment of interference-aware HO decision making.

Current literature also includes various algorithms and studies for the HO decision phase in the two-tier network [55] [58] [59] [61] [62] [70] [109]. Two different sets of speed and RSS-based HO decision rules are proposed in [61], to minimize the HO probability in the two-tier network. The proposed rules are shown to increase the user-perceived throughput in high speed UEs, and reduce the HO probability compared to a soft HO decision approach. The authors in [58] propose two different HO decision strategies depending on the traffic type of the user. For non real-time traffic, a SC-based HO decision strategy is proposed, while for real-time traffic, the proposed strategy consists of executing an outband femtocell HO only when the minimum required RSS for service continuity is reached. Although the employment of these strategies is shown to reduce the number of HOs in the system, the impact of the consequential RF interference on the user-perceived throughput is not investigated. An adaptive HO Hysteresis Margin (HHM) approach is presented in [70], where the HHM value is adapted according to the estimated path loss between the UE and the target cell. It is shown that even though a large HHM lowers the number of unnecessary HOs, it simultaneously degrades the throughput performance. Aiming to sustain a low outage probability for the LTE-A users, the authors in [108] propose a fractional soft HO decision algorithm, which takes into account the user traffic type and uses the feature of carrier aggregation. Even though theoretical and simulation results illustrate low outage probability, the performance of the proposed algorithm in terms of energy consumption and interference at the LTE-A nodes is not discussed. To mitigate cross-tier interference and reduce the number of HOs in the network, the work in [55] is based on the concept of intra-cell HOs which, however, is closer to radio resource management rather than HO decision making. The proposal in [62] allows for an inbound HO to femtocells depending on the traffic type and the current user mobility status. A variant of this algorithm is presented in [59], with the addition of a simple analysis regarding the required signaling overhead based on the work in [109]. Founded on simulation results, the work in [110] concludes that more efficient interference coordination and HO execution procedures can be employed, if the communication between the macrocell and the femtocell tiers is performed through the X2, rather than the S1 interface.

To summarize, current HO decision algorithms emphasize on reducing the number of HOs in the two-tier network mainly based on user mobility and traffic type criteria. In most of the cases, the impact of the proposed algorithms on the UE energy consumption, the RF interference, and the network signaling load, is not investigated. On the other hand, existing approaches mainly focus on the inter-tier HO decision scenario, and assume the employment of the SC algorithm for the intra-tier HO scenario, i.e., eNB-to-eNB and HeNB-to-HeNB HOs (Figure

10). The SC HO decision algorithm, however, does not take into account the actual transmit power on the reference signals of the candidate cells, neither it takes into account the RF interference at the cell sites, which are both expected to diverge from site to site in the LTE-A network, owing to the unplanned deployment and the self-optimization mechanisms. As a result, the employment of the interference-agnostic SC algorithm is expected to degrade the SINR performance, compromise seamless connectivity, increase the outage probability and enlarge the HO signaling.

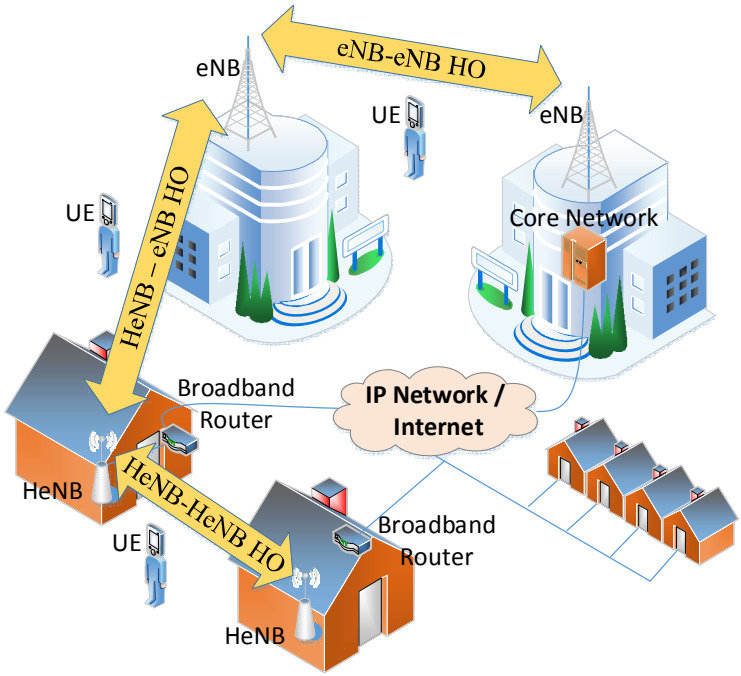

Figure 10: Two-tier LTE-A network and type of HOs

In our work, we jointly consider the impact of interference, energy consumption, and user mobility during the HO decision phase in the two-tier LTE-A network. A strong innovation of our work is the exchange and utilization of standard LTE-A measurements to accurately estimate the mean UE transmit power on a per candidate cell basis, given a prescribed mean SINR target. The exclusion of candidate LTE-A cells which can compromise wireless connectivity, and the incorporation of the user's prescribed SINR target during the mean UE transmit power estimation, are two more important features of the proposed algorithm towards sustained wireless connectivity, enhanced QoS support, and reduced outage probability. Finally, the comprehensive description of the network signaling procedure required for employing the proposed algorithm, guarantees backwards compatibility with LTE-A and provides insights for advanced interference and mobility management in the two-tier network.

1.3.4 Energy-Efficient Vertical Handover Decision in the Cellular / Wi-Fi network

Current literature includes a noteworthy amount of algorithms for horizontal and vertical handover decision for heterogeneous networks [78] [111] [112]. However, only a few works utilize the ANDSF functionality for efficient network discovery and seamless mobility at the MMT. In addition, even though the utilization of standard LTE-A measurements for handover has been proposed in [66][71][113], the joint utilization of the enhanced radio measurement capabilities of the LTE-A

and the IEEE 802.11-2012 systems is an unexplored research area [114]. Even though 3GPP specifies the baseline functionality of the ANDSF, it also enables the operators to deploy their own (implementation-dependent) inter-system mobility policy. On the other hand, the use of this policy depends on the MMT implementation, given that both the RAT selection and the PoA association are performed at the MMT (VHO). The VHO decision plays a key role in the supported QoS and the power consumption at the MMT, given that different RATs use different radio capabilities and result in varying power consumption per interface state [115].

In this work, we propose an Andsf-assisted eneRgy-effiCient vertical Handover decisiON (ARCHON) algorithm for the heterogeneous IEEE 802.11-2012 / LTE-A network. The proposed algorithm, referred to as ARCHON, enables a MMT to select the network PoA that minimizes its average overall power consumption and guarantees a mean SINR target for its ongoing connections. ARCHON is based on a) a backwards-compatible methodology for estimating the average overall MMT power consumption on a per candidate PoA basis, b) an energy-efficient inter-system mobility policy that translates the estimation methodology at the ANDSF to simple energy-efficient decision thresholds for the MMT, and c) a novel intra-system mobility policy that allows the MMT to select the least power consuming PoA in the heterogeneous network.

1.3.5 Mobility Management in the LTE-Advanced Network with Femtocells

Even though MM support and HO decision are of critical importance in the two-tier macrocell-femtocell LTE-A network, current literature lacks of surveys and comparative studies engaged with the matter. The report in [116] provides a brief discussion on the key aspects of MM support for femtocells in LTE-Advanced Rel. 8, whereas the support of femtocells in the IMT-Advanced amendment of the WiMAX system, i.e., the IEEE 802.16m standard, is discussed in [117]. The HO procedure in the LTE-A and IEEE 802.16m systems is overviewed in [118]. The technical aspects and research challenges of the HO procedure in mobile WiMAX, i.e., the IEEE 802.16e amendment, are investigated in [119], with the emphasis given in the medium access control (MAC), network, and cross-layer related issues. Under the viewpoint of 60GHz based wireless systems, the survey in [120] overviews the HO procedure for various RATs and discusses the suitability of existing horizontal and vertical HO decision algorithms. The survey in [121] provides a comprehensive overview of existing MM architectures in heterogeneous wireless networks and discusses the key design challenges for vertical MM. A novel architecture for seamless mobility is subsequently proposed, founded on the concept of context-awareness. A wide range of context-aware functionalities for mobile and wireless networking are surveyed in [122], and a classification of current state-of-the-art proposals per functionality is also provided. The authors in [111] survey, classify and compare existing VHO decision strategies, and propose their own approach for VHD algorithm for next generation heterogeneous wireless networks. In a more recent study in [112], the authors survey and classify VHO algorithms for the 4G heterogeneous wireless network and provide a detailed comparison with regards to their performance.

Different from [9]-[15], [23]-[25], [118], [119], [121], and [122] in our work we discuss the open issues for MM support in the presence of femtocells and overview the key aspects of MM in the LTE-A system. On the other hand, different from [111],[112], and [120], we survey current state-of-the-art HO decision algorithms for the two-tier macrocell-femtocell network and overview

their key features, main advantages and disadvantages under the viewpoint of the LTE-A system. We also evaluate the performance of the most prominent current state-of-the-art algorithms by providing both qualitative and quantitative comparisons. The quantitative comparisons are based on the system-level evaluation methodology proposed by the Small Cell Forum [123].

2. LOCALIZATION AND PEER DISCOVERY USING SPATIAL INFORMATION FROM THE HETEROGENEOUS WIRELESS NETWORK

The nowadays heterogeneous wireless network is a collection of ubiquitous wireless networking elements (WNEs) that support diverse functional capabilities and networking purposes. In such a heterogeneous networking environment, localization and peer discovery will play a key role for the seamless support of emerging applications that span from the direct exchange of localized traffic between homogeneous WNEs (peer-to-peer communications) to the unsupervised navigation of robotic nodes using spatial information from the ubiquitous HWN infrastructure. The spatial distribution of WNEs is neither completely random nor subject to regularly planned installation [90]. Instead, most of the WNEs are typically clustered around a specific point of interest, e.g. a collection of ZigBee sensors around a dual-mode Wi-Fi/ZigBee sink node or a set of access points inside a building. This spatial property is increasingly identified to characterize most of the current state-of-the-art networking systems and play a key role to their statistical behavior [87]-[90]. Even though the clustered installation of WNEs is prominent in the nowadays HWN, the relative distances and angles between the WNEs still govern the performance of almost all functions necessary to its fundamental operation, e.g. WNE discovery, association, and power control. To this direction, most of the existing wireless networking technologies enable the direct (or indirect) estimation of the distances and angles between their WNEs, the integration of such spatial information is a natural solution for robustly handling the unprecedented demand for localization and peer discovery between the myriads of WNEs.

In light of the above discussion, in this section we propose a fairly general M-tier model of networking clusters that captures the spatial dependencies between the WNEs of the nowadays HWN. Each tier of the proposed HWN model, consists of WNEs that serve similar communication purposes and support the same RAT. WNEs belonging to the M-th tier, coined as tier-M WNEs, are assumed to be clustered around (some of) the WNEs belonging to the $(M-1)$-th tier, coined as tier-$(M-1)$ parent WNEs. Similarly, the tier-$(M-1)$ WNEs are clustered around (some of) the WNEs of the $M-2$-th tier, and so on. Under this hierarchical clustering model, we analyze the performance of localization and peer discovery between two tagged (and not necessarily homogeneous) WNEs. We show that given knowledge of the HWN layout, the peer discovery probability of the two WNEs is given by the respective (conditional) complementary cumulative distribution function (ccdf) of their relative distance. Accordingly, we derive closed-form expressions on the distance distribution between them, given partial (or full) knowledge of the relative distances and angles of their parent WNEs. The derived expressions enable us to derive optimal strategies for the deployment of higher-tier WNEs, as means of maximizing the peer discovery probability between the two WNEs. Numerical results conclude our work, providing valuable insights for the design of localization and peer discovery in HWNs.

The remainder of this section is organized as follows. In section 2.1, we present the proposed *M*-tier model and discuss our location information model. In section 2.2, we derive closed-form expressions for the conditional pdf and ccdf of the relative distance between two heterogeneous WNEs given different levels of knowledge for the HWN topology. In section 2.3, we present optimal strategies for the deployment of upper-tier WNEs, while in section 2.4 we investigate the impact

of the system parameters on the performance of location-aware peer discovery, drawing useful guidelines for its design in the nowadays HWN. Section 2.5 summarizes our key contributions and includes our conclusions.

2.1 System Model

2.1.1 System Description

We consider a fairly general HWN of M tiers, where each tier consists of WNEs that serve similar communication purposes and support the same RAT. We consider that the first tier, coined as tier-1, is composed by medium to long range WNEs, e.g. macrocells, which are spatially distributed according to a homogeneous PPP Φ_1 with intensity λ in the Euclidean plane. Without assuming a specific RAT for tier-*m* WNEs with $m \geq 2$, we consider that tier-*m* WNEs are clustered around *some of* the existing tier-*(m-1)* WNEs. We emphasize on around *some of* and *not all* tier-$(m-1)$ WNEs, since in practical deployments we do not expect a tier-m cluster to be present around every tier-$(m-1)$ WNE. Let Φ_m denote the complete Point Process (PP) of tier-m WNEs, i.e. the union of all tier-m clusters. Given that a tier-*m* cluster is present around the tier-*(m-1)* WNE $v_i \in \Phi_{(m-1)}$, we assume it to be in the form $N_{v_i}^m = N_i^m + v_i$, where the point sets N_i^m are identically independently distributed (i.i.d) and independent of the parent PP Φ_{m-1}. All tier-m clusters are modeled by the Thomas cluster process as follows [90]: a) the number of points in each tier-m cluster is Poisson distributed with mean $\bar{c}_m$, and b) the WNEs in a tier-m cluster are scattered independently according to a symmetric normal distribution around the parent tier-$(m-1)$ WNE with variance σ_{m}^2.

We now turn our attention to two tagged WNEs of interest, coined as *source* and *target* peers. We consider that the source peer associates with a tier-m_s WNE, coined as the *associated WNE of the source peer*, and that the target peer associates with a tier-m_t WNE, coined as the *associated WNE of the target peer*. The associated WNEs of the two peers can belong to different tiers in the HWN. Accordingly, the two peers do not necessarily support the same RAT. We assume that the source and the target peers are located around their associated WNEs according to a symmetric normal distribution with variances σ_s^2 and σ_t^2, respectively. The locations of the two peers are assumed to be mutually independent and independent of the locations of other WNEs.

Assumption 2.1. *Let (x_u, y_u) and (x_v, y_v) denote the Cartesian coordinates of a tier-m WNE $u \in N_v^m$ and its parent tier-(m-1) WNE $v \in \Phi_{m-1}$, respectively. The x and y components of the relative distance between the tier-m WNE u and its parent tier-(m-1) WNE v, i.e. the random variables $x_m = x_u - x_v$ and $y_m = y_u - y_v$, are independent.*

Assumption 2.1 states that the knowledge of the relative x-axis distance between a WNE and its parent WNE does not provide any information on the relative distance in the y-axis. We consider the same assumption to hold for the x and y components of the relative distance between the source/target peers and their associated WNEs. Lemma 2.1 readily follows from Assumption 2.1.

Lemma 2.1. *The x and y components of the relative distance between a tier-m WNE u and its parent tier-(m-1) WNE v, i.e. the random variables $x_m = x_u - x_v$ and $y_m = y_u - y_v$, are independent and normally distributed with variance σ_m^2.*

Proof. Can be readily proved by using Assumption 1 and the methodology in [124].

□

If not fixed and known, the distance D between a tier-1 WNE and its k-th nearest tier-1 WNE in Φ_1 follows a generalized Gamma distribution (k will be termed as their neighboring degree).

Lemma 2.2. *The pdf $f_D(d)$ of the distance D between a tier-1 WNE and its k-th nearest neighbor in Φ_1 is given by*

$$f_D(d) = \frac{2(\pi\lambda)^k}{\Gamma[k]} d^{2k-1} e^{-\pi\lambda d^2}, \qquad (2.1)$$

where $\Gamma[k]$ is the Gamma function.

Proof. The proof is derived in [96].

□

2.1.2 Location Information Model

Since we are interested on analyzing how different levels of location-awareness affect the performance of localization and peer discovery in HWNs, to the remainder of this work we consider the presence of a location information server (LIS) that has fundamental knowledge of the HWN layout. We consider that the two peers can acquire such knowledge on demand to the LIS by using higher-layer services over the common IP layer. We also consider that part of the WNEs in the HWN, if not all, can push/pull positioning measurements to the LIS over the common IP layer. The LIS is assumed to be aware of basic system parameters, such as the tier-1 intensity λ and the deployment variances σ_m^2 $(m > 1)$, σ_s^2 and σ_t^2. Besides, these parameters can be estimated by overhearing the pilot signals broadcast throughout the HWN or by accounting for the typical range supported by different RATs, e.g. femtocells cover up to a few meters and UWB sensors up to a few centimeters.

In the sequel, we assume that the LIS is aware of the clustering relations between the WNEs, and thus capable of identifying the sequence of parent WNEs for both peers (up to tier-1). For brevity, we refer to the tier-m WNE in the sequence of parent WNEs for the source peer as the *tier-m parent of the source peer* ($m < m_s$), and use a similar terminology for the parents of the target peer ($m < m_t$). In practical scenarios, the sequence of parent WNEs (up to tier-1) can be identified either by exploiting knowledge from the installation phase, e.g., the locations of cellular BSs can be known, or by performing measurements on the TD, ToA, RSS, or RF power level, of higher-tier WNEs [2][3][16][79]. For example, a dual-mode cellular / Wi-fi hotspot can measure the RSS from all nearby macrocells and set the one with the strongest signal as its parent. On the other hand, a sensor node can identify the nearest multi-RAT sink node by measuring the RF power level, or counting the number of hops to, all nearby sink nodes [3].

Table 5: Location Information Parameters (Spatial Information)

Parameter	Notation	Comments
Inter-site distance between the tier-1 parent WNEs of the peers	D	Can be estimated by performing TD or RSRP measurements between the tier-1 parent WNEs of the two peers [16].

Neighboring degree between the tier-1 parent WNEs of the peers	k	Can be estimated in a similar manner with D (lower accuracy is required).
Distance between the source peer and its associated WNE	R_s	Can be estimated by performing TD [16], Time of Arrival (ToA) [76], RSS[2][16], or RF power level [3], either at the source peer or its associated WNE.
Angle between the source peer and its associated WNE	ξ_s	Can be estimated by performing AoA measurements [16] or by employing other indirect estimation methodologies depending on the RAT, e.g. [125]-[126].
Distance between the target peer and its associated WNE	R_t	Can be estimated in a similar manner with R_s.
Angle between the target peer and its associated WNE	ξ_t	Can be estimated in a similar manner with ξ_s.
Distance between the tier-*m* and the tier-*(m-1)* parent WNEs of the source peer	S_{m-1}	Can be estimated by performing TD [16], ToA [76], RSS[2][16], or RF power level [3], either at the tier-*m* parent WNE or at the tier-*(m-1)* parent WNE, depending on the RAT.
Angle between the tier-*m* and the tier-*(m-1)* parent WNEs of the source peer	θ_{m-1}	Can be estimated in a similar manner with ξ_s, depending on the RAT. It is assumed to be measured with respect to the reference direction from the tier-1 parent of the source peer to the tier-1 parent of the target peer (Figure 11).
Distance between the tier-*m* and the tier-*(m-1)* parent WNEs of the target peer	T_{m-1}	Can be estimated in a similar manner with S_{m-1}.
Angle between the tier-*m* and the tier-*(m-1)* parent WNEs of the target peer	ϕ_{m-1}	Can be estimated in a similar manner with ξ_s, depending on the RAT. It is assumed to be measured with respect to the reference direction from the tier-1 parent of the source peer to the tier-1 parent of the target peer (Figure 11).

Aiming to capture the different levels of location-awareness that the LIS can provide to the peers, we consider it capable of utilizing spatial information on the relative distance and angle between two tagged WNEs of interest. In Table 5, we list the spatial information considered in this paper and provide insights on how they can be estimated in existing systems. Note that we do not assume that the LIS has full knowledge of these measurements. Instead, we investigate how certain combinations of them affect the performance of localization and peer discovery in HWNs. The combined distance and angle measurements with

respect to a target WNE, can be viewed as the *relative polar coordinates* of the measuring WNE with respect to the target WNE.

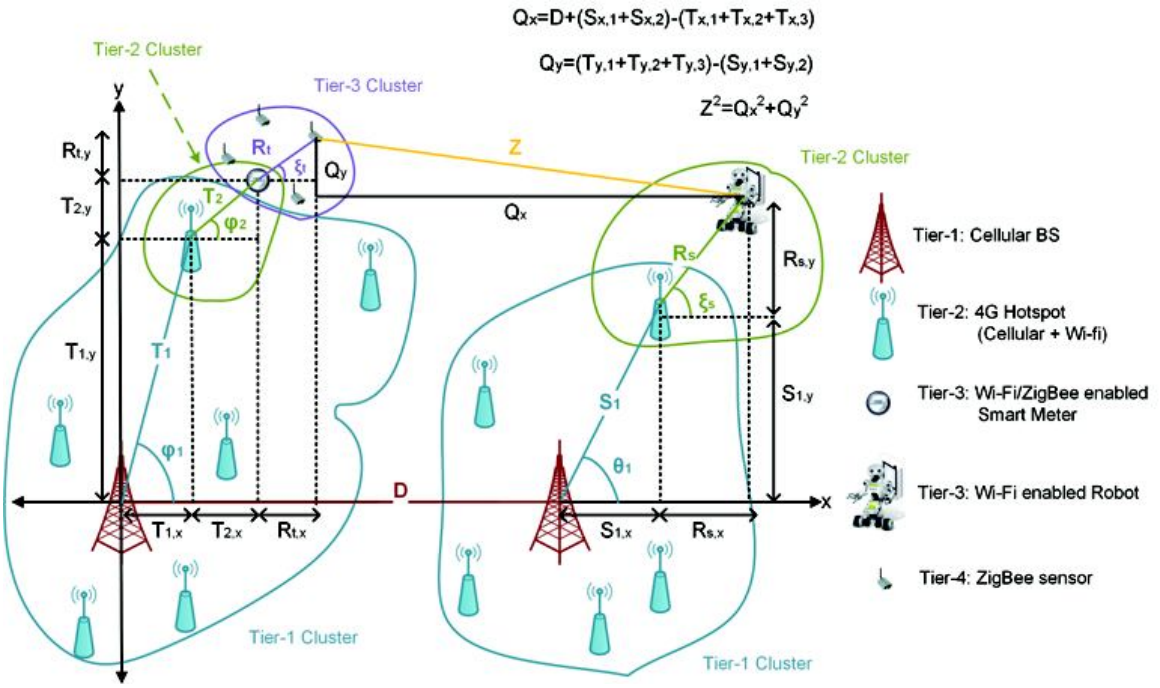

Figure 11: Localization and (location-aware) peer discovery using spatial information from heterogeneous WNEs

In the sequel, we denote by $\mathcal{L}_s$ and $\mathcal{L}_t$ the set of parent WNEs of the source and the target peer, respectively, for which the LIS has knowledge of their relative polar coordinates with respect to their upper-tier parent WNEs. The remainder set of parent WNEs are denoted by $\bar{\mathcal{L}}_s$ and $\bar{\mathcal{L}}_t$, respectively. Figure 11 depicts all parameters and random variables (RVs) involved in our analysis.

2.1.3 Performance Metrics

The performance of localization and peer discovery is tightly coupled with the definition of proximity between the two peers. Aiming to cover both *range-based* and *connectivity-based* approaches [83], we define the peer discovery probability as follows:

$$\mathcal{A}_{\mathcal{J}} \triangleq P[cZ^{-a} \geq Z_{th}|\mathcal{J}], \qquad (2.2)$$

where $\mathcal{J}$ denotes the available knowledge of the HWN topology, c is a scaling factor, a is a decay exponent, Z is the distance between the two peers, and Z_{th} is a fixed threshold that guarantees proximity between the two peers. Assuming that c refers to the transmit power at the source peer (in Watts), a to the path loss exponent, and Z_{th} the receiver sensitivity at the target peer (in Watts), (2.2) models the connectivity-based approach. In the contrary, for $c = 1$ and $a = -1$, (2.2) reduces to the *range-based* approach where Z_{th} refers to the distance threshold (in meters). By rearranging (2.2), it can be readily shown that the peer discovery probability is given by the ccdf of the distance Z at the point $\left(\frac{c}{Z_{th}}\right)^{\frac{1}{a}}$, conditioned on the available knowledge $\mathcal{J}$.

2.2 Distance Distributions and Localization in Multi-user Clustered HWNs

In Section 2.2.1, we derive closed-form expressions for the pdf and ccdf of the distance Z between two tagged WNEs, given knowledge of at least the inter-site distance D and partial (or full) knowledge of the relative polar coordinates of the source/target peers (with respect to their associated WNEs), or the relative polar coordinates of *some* of their parent WNEs (with respect to their upper-tier parent WNEs). In section 2.2.2, we generalize the derived expressions to the case where, instead of the distance D, the LIS has knowledge of the neighboring degree k between the tier-1 parents of the peers. These expressions are useful when the tier-1 WNEs are unable to accurately estimate their relative distance, e.g. due to indoor deployment. Notably, the pdf of the relative distance Z between two tagged WNEs can also be viewed as the statistical behavior of localization between them, given (the respective) knowledge of the HWN layout.

2.2.1 Distance distribution between two WNEs given the distance D

Theorem 2.1. *The conditional pdf $f_{Z|D}(z)$ of the distance Z between the source and the target WNEs in a multi-tier clustered random HWN, given a) the distance D between their tier-1 parent WNEs and b) the relative polar coordinates of their parent WNEs in $\mathcal{L}_s$ and $\mathcal{L}_t$, is given by*

$$f_{Z|D}(z) = \frac{z}{\sigma^2} e^{-\frac{\eta_x^2+\eta_y^2+z^2}{2\sigma^2}} I_0\left[\frac{z\sqrt{\eta_x^2+\eta_y^2}}{\sigma^2}\right], \quad (2.3)$$

where $I_0[x]$ is the modified Bessel function and the parameters η_x, η_y, and σ are given by:

$$\eta_x = D + \sum_{j\in\mathcal{L}_s} S_j \cos\phi_j - \sum_{i\in\mathcal{L}_t} T_i \cos\theta_i, \quad (2.4)$$

$$\eta_y = \sum_{i\in\mathcal{L}_t} T_i \sin\theta_i - \sum_{j\in\mathcal{L}_s} S_j \sin\phi_j, \quad (2.5)$$

$$\sigma^2 = \sum_{j\in\bar{\mathcal{L}}_s} \sigma_j^2 + \sigma_s^2 + \sum_{i\in\bar{\mathcal{L}}_t} \sigma_i^2 + \sigma_t^2. \quad (2.6)$$

The corresponding ccdf $\bar{F}_{Z|D}(z)$ is given by

$$\bar{F}_{Z|D}(z) = Q_1\left[\frac{\sqrt{\eta_x^2+\eta_y^2}}{\sigma}, \frac{z}{\sigma}\right], \quad (2.7)$$

where $Q_M[a,b]$ is the Marcum-Q function. If the relative polar coordinates (R_s, ξ_s) of the source peer are also given, (2.3) and (2.7) are in effect for the η_x, η_y, and σ parameters in (2.29)-(2.31). Instead, if the relative polar coordinates (R_t, ξ_t) of the target peer are given, (2.3) and (2.7) are in effect for the parameters in (2.32)-(2.34). Finally, if both the relative polar coordinates (R_s, ξ_s) and (R_t, ξ_t) are given, (2.3) and (2.7) are in effect for the parameters in (2.35)-(2.37).

Proof. See Appendix I.A.

□

The ccdf result in Theorem 2.1 can be used to analytically evaluate the peer discovery probability between two WNEs (2.2), given any combination of spatial information that includes the inter-site distance D. The requirement of knowing the distance D can be easily met in real-life HWN, where the locations of tier-1 WNEs typically remain fixed over time. Noticeably, the results in Theorem 2.1 not only allow heterogeneous WNEs to handle the uncertainty on their proximity, but

also enable them to employ different levels of location-awareness by adapting the peer discovery accuracy (or localization error) with respect to the available spatial information. Since different communication radii are met among the different WNEs of a HWN, more accurate estimates on the relative polar coordinates of low-tier WNEs will be critical only for applications requiring high localization precision or peer discovery accuracy, e.g. when a physical/visual contact is required. Obviously, when the tier-1 parent WNE is common for the two tagged WNEs, Theorem 2.1 is in effect for $D = 0$. In Corollary 2.1, we demonstrate how two tagged WNEs can evaluate their distance Z when the LIS has full knowledge of the involved WNEs.

Corollary 2.1. *The distance Z between the source and the target WNEs in a multi-tier clustered random HWN, given a) the distance D between their tier-1 parent WNEs, b) the relative polar coordinates (S_j, ϕ_j) of all parent WNEs of the source peer ($1 < j \leq m_s$), c) the relative polar coordinates (T_i, θ_i) of all parent WNEs of the target peer ($1 < i \leq m_t$), d) the relative polar coordinates (R_s, ξ_s) of the source peer, and e) the relative polar coordinates (R_t, ξ_t) of the target peer, is given by $Z = \sqrt{(D + Z_x)^2 + Z_y^2}$ where the parameters Z_x and Z_y are given by:*

$$Z_x = \sum_{j=1}^{m_s} S_j \cos\phi_j + R_s \cos\xi_s - \sum_{i=1}^{m_t} T_i \cos\theta_i - R_t \cos\xi_t, \tag{2.8}$$

$$Z_y = \sum_{i=1}^{m_t} T_i \sin\theta_i + R_t \sin\xi_t - \sum_{j=1}^{m_s} S_j \cos\phi_j - R_s \sin\xi_s. \tag{2.9}$$

Proof. The proof is derived by plugging (2.18), (2.19), $R_{s,x} = R_s \cos\xi_s$, $R_{s,y} = R_s \sin\xi_s$, $R_{t,x} = R_t \cos\xi_t$ and $R_{t,y} = R_t \sin\xi_t$ in (2.17) (see Appendix I.A).

□

2.2.2 Distance distribution between two WNEs given the neighboring degree k

Remark 2.1 *The probability distribution of the distance Z, given the neighboring degree k between the tier-1 parent WNEs of the two peers, is given by integrating the results in Theorem 2.1 with respect to the distance $D \geq 0$. The pdf of the distance D is given in (2.1).*

Note that the distance D is part of the η_x parameters for all the scenarios in Theorem 2.1. Unfortunatelly, the integration of the Modified Bessel function in (2.3) or the Marcum-Q function in (2.7) with respect to the pdf in (2.1), cannot be expressed in closed-form, owing to the presence of square roots, powers, and special functions of the integration parameter D. Hence, Remark 2.1 can only be used to numerically evaluate the pdf $f_{Z|k}(z)$ and the ccdf $\bar{F}_{Z|k}(z)$. Interestingly, there exists a special case where the pdf $f_{Z|k}(z)$ and the ccdf $\bar{F}_{Z|k}(z)$ are derived in closed-form.

Theorem 2.2. *The conditional pdf $f_{Z|k}(z)$ of the distance Z between the source and the target WNEs in a multi-tier clustered random HWN, given only the neighboring degree k between the tier-1 parent WNEs of the two peers, i.e. $L_s = \emptyset$ and $L_t = \emptyset$, is given by*

$$f_{Z|k}(z) = \frac{1}{\sigma^2}\left(\frac{\varepsilon_{k-1}-1}{\varepsilon_{k-1}}\right)^k z e^{-\frac{\pi\lambda z^2}{\varepsilon_{k-1}}} L_{k-1}\left[-\frac{\pi\lambda z^2}{(\varepsilon_{k-1}-1)\varepsilon_{k-1}}\right], \tag{2.10}$$

where $L_n[x]$ is the Laguerre polynomial and $\varepsilon_{k-1} = 2\pi\lambda\sigma^2 + 1$. The ccdf $\bar{F}_{Z|k}(z)$ is given by

$$\bar{F}_{Z|k}(z) = \frac{e^{-\frac{\pi\lambda z^2}{\varepsilon_{k-1}}}}{\varepsilon_{k-1}} \sum_{n=0}^{k-1} \varepsilon_n \left(\frac{\varepsilon_{k-1}-1}{\varepsilon_{k-1}}\right)^n L_n\left[-\frac{\pi\lambda z^2}{(\varepsilon_{k-1}-1)(\varepsilon_{k-1})}\right], \quad (2.11)$$

where $\varepsilon_n = 1$ *for all* $n < k-1$.

Proof. See Appendix I.B.

□

When the LIS has knowledge of the neighboring degree k and all parameters listed in Corollary 2.1 (except from D), the distance Z is function of a single RV: the distance D. For brevity, we denote the respective pdf and ccdf by $f_{Z|k,full}(z)$ and $\bar{F}_{Z|k,full}(z)$, respectively.

Theorem 2.3. *The conditional pdf* $f_{Z|k,full}(z)$ *of the distance* Z *between the source and the target WNEs in a multi-tier clustered random HWN, given a) the neighboring degree* k *between their tier-1 parent WNEs, b) the relative polar coordinates* (S_j, ϕ_j) *of all parent WNEs of the source peer (*$1 < j \leq m_s$*), c) the relative polar coordinates* (T_i, θ_i) *of all parent WNEs of the target peer (*$1 < i \leq m_t$*), d) the relative polar coordinates* (R_s, ξ_s) *of the source peer, and e) the relative polar coordinates* (R_t, ξ_t) *of the target peer, is given by*

$$f_{Z|k,full}(z) = \begin{cases} 0, & z \leq |Z_y| \\ \frac{2(\pi\lambda)^k}{\Gamma[k]} \frac{z}{\sqrt{z^2 - Z_y^2}} \left(d_1^{2k-1} e^{-\pi\lambda d_1^2} U[d_1] + d_2^{2k-1} e^{-\pi\lambda d_2^2} U[d_2]\right), & z > |Z_y| \end{cases} \quad (2.12)$$

where $U[x]$ *is the unit step function,* $d_1 = -Z_x - \sqrt{z^2 - Z_y^2}$, $d_2 = -Z_x + \sqrt{z^2 - Z_y^2}$, *and the parameters* Z_x *and* Z_y *are given by (2.8) and (2.9), respectively.*

The ccdf $\bar{F}_{Z|k,full}(z)$ *is given by*

$$\bar{F}_{Z|k,full}(z) = \begin{cases} 0, & z \leq |Z_y| \\ \frac{(\Gamma[k] - \Gamma[k, \pi\lambda d_1^2]) U[d_1] + \Gamma[k, \pi\lambda d_2^2]}{\Gamma[k]}, & , \ z > |Z_y| \end{cases} \quad (2.12)$$

where $\Gamma[k, x]$ *is the upper partial Gamma Function*.

Proof. See Appendix I.C.

□

2.3 Optimal Network Deployment for Location-Aware Peer Discovery

Recall that the relative locations of low-tier WNEs follow a symmetric normal distribution around their upper-tier parent WNEs with variance σ_m^2 $(1 < m \leq M)$. The parameter σ_m^2 can be physically interpreted in many ways, including a) the uncertainty (or localization error) on the locations of low-tier WNEs around their parent WNEs, b) the (squared) communication range of upper-tier WNEs that are parents to lower-tier WNEs, and c) the accuracy loss due to the deployment of parent WNEs in the specific location. Besides, the strategic deployment of WNEs can play a key role in meeting emerging purpose-driven targets. A motivating example could be the optimized deployment of sink nodes in industrial environments with numerous metering sensors, as means of minimizing the number of multi-hop transmissions between sensors. Another interesting applications is the strategic placement of rapidly deployable cells or low-power sensors, for more accurate localization of communication-enabled targets under

emergency situations. The strategic deployment of WNEs is also critical for jointly optimizing the communication and navigation processes of robotic nodes [6].

In the sequel, we draw useful guidelines on how to optimize the deployment variance(s) of a single (or multiple) tier(s) over certain geographical regions of interest, e.g. in regions where two tagged WNEs carry out their main activity. We model the aggregated impact of the deployment variances in multiple HWN tiers by decomposing the parameter σ^2 into $\sigma^2 = \sigma_o^2 + \sigma_n^2$, where σ_o^2 denotes the sum of variances from the tiers that are subject to optimization, and σ_n^2 the sum of the remainder variances that constitute σ^2. Obviously, σ_o^2 may refer to a single tier.

Theorem 2.4. *Let* $\zeta = \sqrt{\eta_x^2 + \eta_y^2}\left(\frac{c}{Z_{th}}\right)^{-\frac{1}{a}}$ *and* $\sigma^2 = \sigma_o^2 + \sigma_n^2$*, where the parameters* η_x*,* η_y*, and* σ^2 *are adapted according to Theorem 2.1. For* $\zeta < 1$*, the peer discovery probability* $\mathcal{A}_D$ *decreases with* σ_o^2*. For* $\zeta > 1$*, the probability* $\mathcal{A}_D$ *attains an optimal operation point (maximum) if the sum of the variance(s) of interest, i.e. the* σ_o^2 *parameter, satisfies the condition:*

$$I_0\left[\frac{\eta_x^2+\eta_y^2}{\zeta(\sigma_n^2+\sigma_o^2)}\right] = \zeta I_1\left[\frac{\eta_x^2+\eta_y^2}{\zeta(\sigma_n^2+\sigma_o^2)}\right]. \quad (2.14)$$

The optimal variance, denoted by σ_o^{2*}*, can be approximated by*

$$\sigma_o^{2*} \approx \frac{8(\zeta-1)(\eta_x^2+\eta_y^2)}{\zeta(3\zeta+1)} - \sigma^2. \quad (2.15)$$

Proof. See Appendix D.

□

Theorem 2.4 can be interpreted as follows. As the sum of variances of interest (σ_o^2) decreases, the distance Z between the two peers tends to be statistically closer to the known distance that separates the two peers, i.e. the distance $\sqrt{\eta_x^2 + \eta_y^2}$, which in turn, for $\zeta < 1$, is lower than the maximum range for successful peer discovery i.e. the parameter $\left(\frac{c}{Z_{th}}\right)^{-\frac{1}{a}}$. On the other hand, when $\zeta > 1$, the minimum (known) distance between the two peers is greater than the maximum range for successful peer discovery. Thus, a higher uncertainty on the locations of the peers and their parent WNEs, part of which are included in σ_o^2, increases the probability that the two peers are within proximity (up to a certain point: the σ_o^{2*} parameter). Unfortunatelly, the derivation of similar results on the monotonicity of $\mathcal{A}_k$ with respect to σ_o^2 is cumbersome, since (2.11) involves powers, exponentials, and special functions of the parameter σ^2. We now turn our attention to the impact of the tier-1 intensity λ on the peer discovery probability $\mathcal{A}_{k,full}$. Notably, we show that when the LIS has knowledge of all parameters in Theorem 2.3, there exists an optimal tier-1 deployment strategy that maximizes the performance of location-aware peer discovery.

Theorem 2.5. *The peer discovery probability* $\mathcal{A}_{k,full}$*: (a) is equal to 1 for* $z \leq |Z_y|$*, (b) is equal to 0 for* $z > |Z_y|$ *and* $d_2 \leq 0$*, (c) increases with* λ *for* $z > |Z_y|$*,* $d_2 > 0$*, and (d) exhibits an optimal operation point for* $z > |Z_y|$*,* $d_2 > 0$*,* $d_1 > 0$*, if the tier-1 intensity is given by*

$$\lambda^* = \frac{k\ln\frac{d_1^2}{d_2^2}}{\pi\left(d_1^2-d_2^2\right)}. \quad (2.16)$$

Proof. Properties (a) and (b) follow from (2.13). Property (c) follows from the fact that the derivative of $\mathcal{A}_{k,full} = 1 - \frac{\Gamma[k,\pi\lambda d_2^2]}{\Gamma[k]}$ with respect to λ, is always positive. Property (d) follows by differentiating $\mathcal{A}_{k,full} = \frac{\Gamma[k,\pi\lambda d_1^2] - \Gamma[k,\pi\lambda d_2^2]}{\Gamma[k]}$ with respect to λ and solving $\frac{\partial \mathcal{A}_{k,full}}{\partial \lambda} = 0$.

□

2.4 Numerical Results and Design Guidelines

In this section, we analyze the impact of the key system parameters on the peer discovery probability given partial (or full) knowledge of the HWN topology. By using the expressions presented before, we identify how different levels of location-awareness affect the performance of peer discovery and derive useful guidelines for its design in the nowadays HWN. When relevant, we consider the multi-tier HWN layout illustrated in Figure 11.

2.4.1 On the Impact of the Deployment Variance σ and the Tier-1 Intensity λ

In this section, we identify optimal strategies for the deployment of tier-1 and low-tier WNEs, and examine how partial knowledge of the HWN topology, or inaccurate positioning measurements, affect the performance of peer discovery. In Figure 12, we plot the impact of the standard deviation σ_0 on the peer discovery probability $\mathcal{A}_D$ (location information for at least the distance D). The σ_0 parameter is a measure of the uncertainty on the locations of WNEs/peers (around their parent WNEs), for which the LIS has no knowledge of their relative polar coordinates.

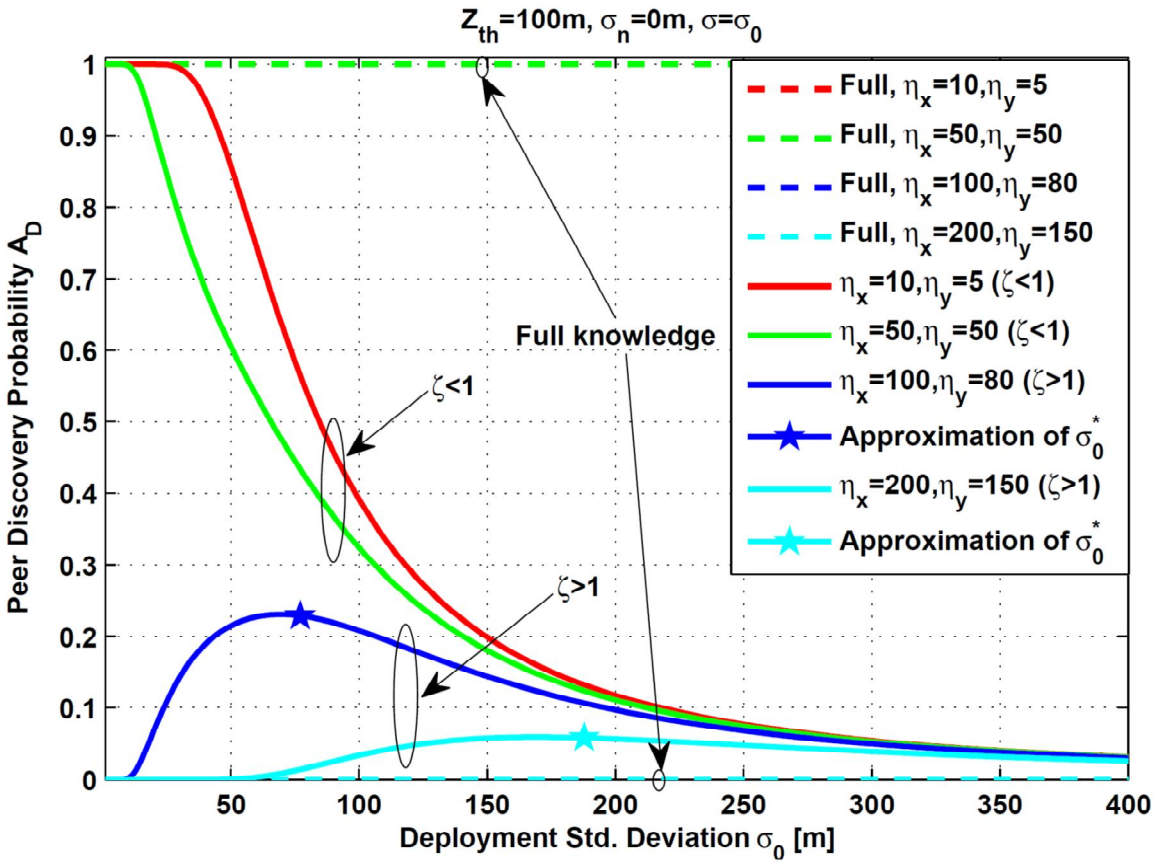

Figure 12: Peer Discovery Probability given D vs. Deployment Std. deviation σ.

As expected, if the LIS has full knowledge on the coordinates of the peers and their parent WNEs, the peer discovery is either successful or not. Given $Z_{th} = 100m$, $c = 1$, and $a = -1$, i.e. range-based discovery, the peer discovery is successful ($\mathcal{A}_D = 1$) if the x-axis and y-axis components of the relative distance between the two peers, i.e. the η_x and η_y parameters, satisfy the condition $\eta_x^2 + \eta_y^2 \leq Z_{th}^2$, e.g. ($\eta_x = 10m, \eta_y = 5m$) and ($\eta_x = 50m, \eta_y = 50m$). Interestingly, when the LIS has partial (or inaccurate) knowledge of the parent WNEs/peers coordinates, the statistical behavior of $\mathcal{A}_D$ alters with respect to σ_0 depending on the ratio of a) the known distance between the two peers $\sqrt{\eta_x^2 + \eta_y^2}$, and b) the peer discovery threshold Z_{th}.

The aforementioned ratio corresponds to ζ in Theorem 2.4 (range-based discovery). For ($\eta_x = 10m, \eta_y = 5m$) and ($\eta_x = 50m, \eta_y = 50m$), which both result in $\zeta < 1$, the probability $\mathcal{A}_D$ decreases with σ_0. This behavior is in line with Theorem 2.4 and follows from the fact that a higher σ_0 prolongs the tail of the distance distribution between i) the WNEs/peers with unknown relative polar coordinates and ii) their parent WNEs. Notably, σ_0 dominates the η_x and η_y parameters above a certain point, i.e. for $\sigma_0 > 200m$, $\mathcal{A}_D$ is roughly the same for all η_x and η_y values. On the other hand, for ($\eta_x = 100m, \eta_y = 80m$) and ($\eta_x = 200m, \eta_y = 150m$), which both result in $\zeta > 1$, the performance of peer discovery improves with σ_0 up to a certain point. This behavior is due to the fact that for $\zeta > 1$, a small uncertainty on the coordinates of WNEs/peers with unknown locations, statistically reduces the 'gap' between the known distance separating the two peers and the Z_{th} threshold. Notably, the optimal σ_0^* is well approximated by the square root of (2.15) (highlighted with a star). The results in Figure 12

highlight that the employment of more accurate positioning measurements is more meaningful when $\zeta < 1$, and that the deployment of additional low-tier WNEs should be carefully handled when $\zeta > 1$. These two design guidelines can be the basis for a) optimizing the frequency/accuracy of positioning at the WNEs so as to pertain the signaling/processing overhead at low levels and b) the strategic deployment of additional low tier WNEs to maximize the performance of location-aware peer discovery.

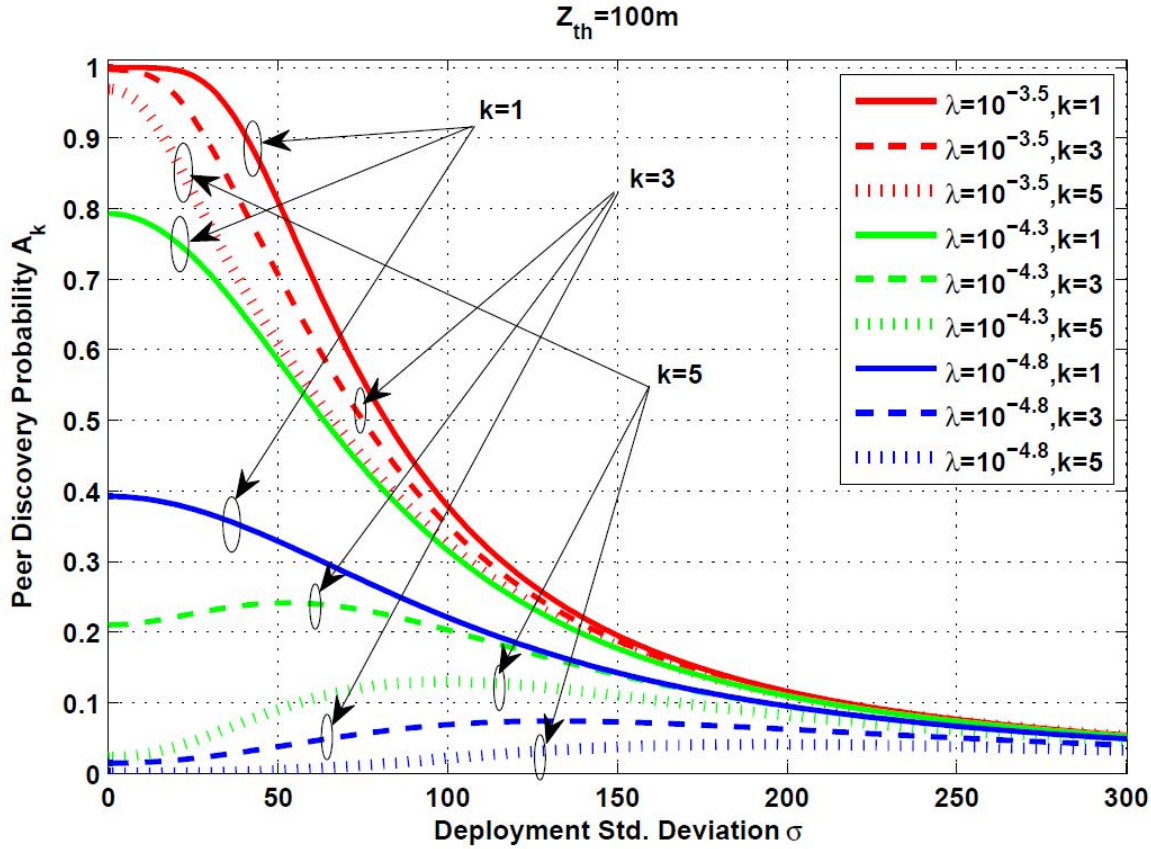

Figure 13: Peer Discovery Probability given k vs. Deployment Std. deviation σ.

In Figure 13, we plot the effect of σ on the peer discovery probability $\mathcal{A}_k$ (information for only the neighboring degree k). As expected, the probability $\mathcal{A}_k$ decreases with k. However, the impact of higher k is less evident when the WNEs are densely deployed, e.g. for $\lambda = 10^{-3.5}$ (one tier-1 WNE per $50m^2$), and becomes prominent in higher tier-1 intensities, e.g. for $\lambda = 10^{-4.8}$ (one tier-1 WNE per $250m^2$). Once again, σ is shown to dominate the performance of $\mathcal{A}_k$. Notably, Figure 13 reveals the existence of optimal deployment strategies for the low-tier WNEs, even when the LIS is only aware of k, e.g. observe $k = 3{,}5$ for $\lambda = 10^{-4.3}, 10^{-4.8}$. Besides, Figure 13 highlights that even fundamental parameters on the HWN layout, such as the neighboring degree k, carry enough information to infer about the outcome of peer discovery and optimize its performance in the nowadays HWN.

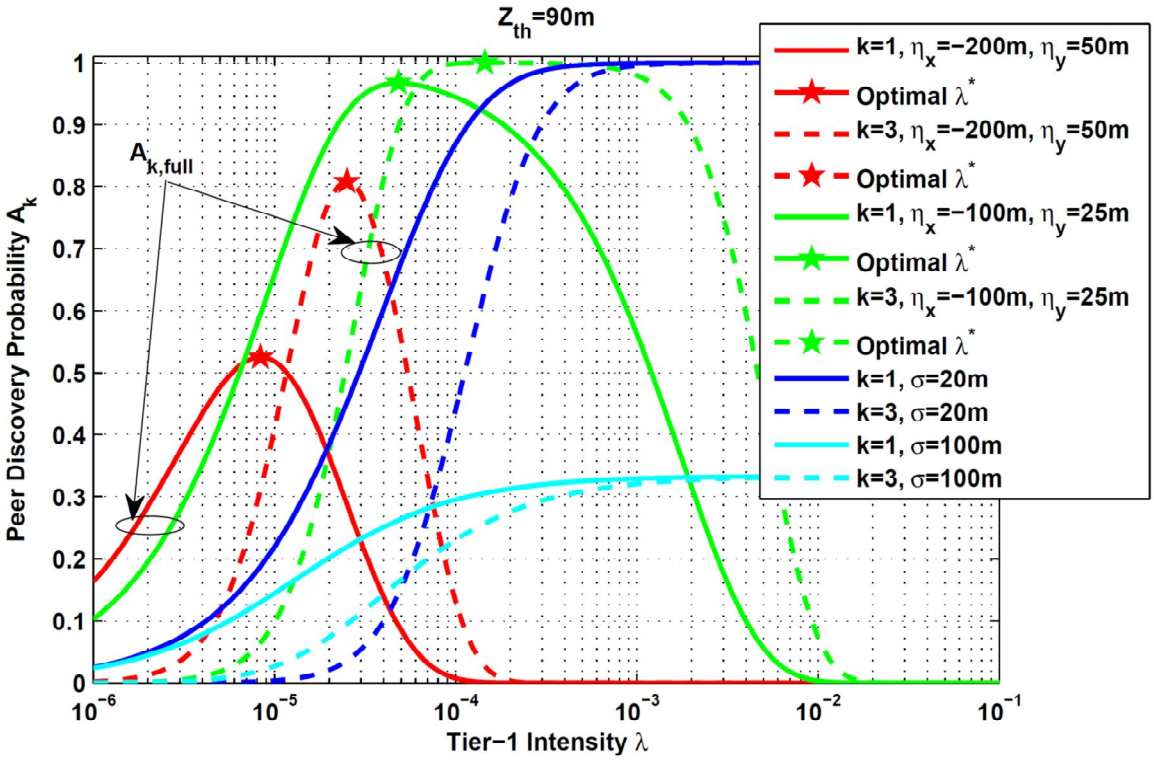

Figure 14: Peer Discovery Probability given k vs. Tier-1 intensity λ

Let us now examine the impact of the tier-1 intensity on the peer discovery probability $\mathcal{A}_k$ (Figure 14). When the LIS has knowledge of only the neighboring degree k, the probability $\mathcal{A}_k$ increases with λ and decreases with k (blue and cyan plots). This behavior is in line with intuition, since a higher λ statistically reduces the distance between the tier-1 WNEs and a higher k increases it. However, the performance gains following from the densification of tier-1 are limited by the uncertainty on the parent WNE locations (modeled by σ). For example, when the discovery threshold is lower than the aggregate std. deviation σ, e.g. $Z_{th} = 90m < \sigma = 100m$, an increase of the tier-1 intensity λ by two orders of magnitude leaves the performance of peer discovery roughly unaffected (Figure 14), e.g. for $\sigma = 100m$ and $\lambda = 10^{-3} \rightarrow 10^{-1}$. On the other hand, when the LIS is aware of k and has full knowledge on the relative polar coordinates of the peers and their parent WNEs ($m > 1$), there exists an optimal tier-1 intensity λ^* that maximizes $\mathcal{A}_k$. This behavior is in line with Theorem 2.5 and, notably, the optimal λ^* is computed by (2.16) (highlighted with a star). When the tier-1 parent WNEs of the two peers are distant neighbors, e.g., $k = 3$, the optimal λ^* shifts to higher values that statistically reduce the distance between the tier-1 WNEs. In addition, the performance gains following from the densification of tier-1 are shown to be lower when the η_x and η_y components are high (green vs. red plots). Hence, if not subject to optimization, the deployment of additional tier-1 WNEs may deteriorate (rather than improve) the performance of peer discovery when the LIS is aware of k (instead of D).

2.4.2 On the Impact of Transmit Power

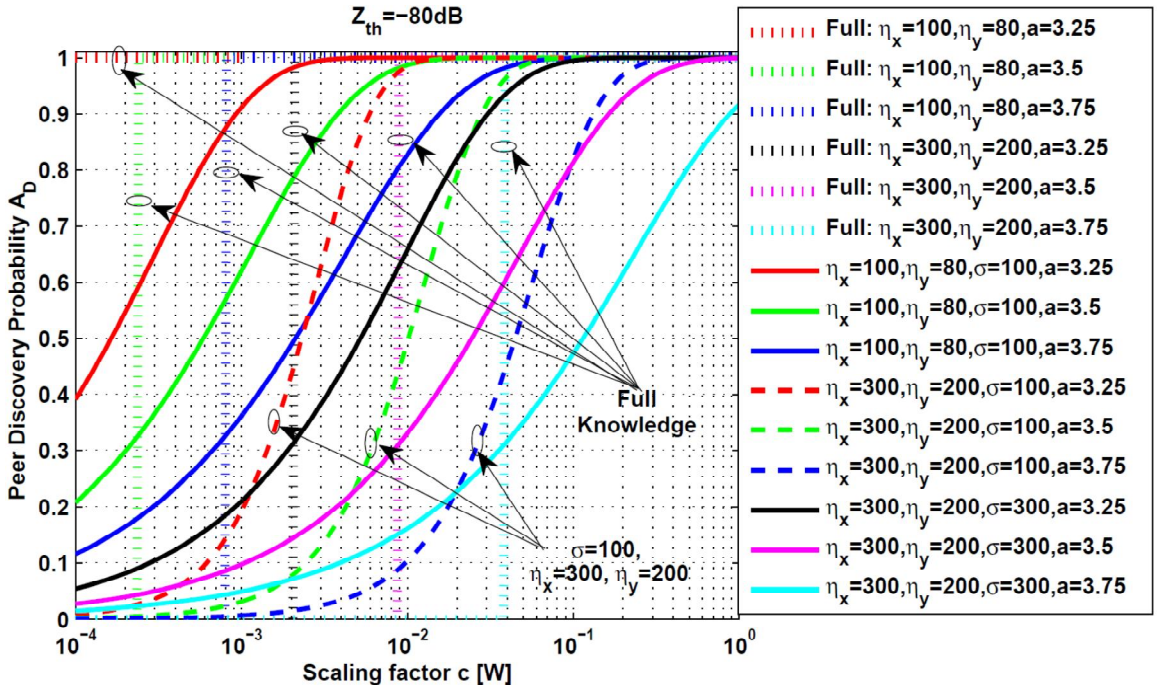

Figure 15: Peer Discovery Probability given D vs. Scaling factor c [W]

We now turn our attention to the impact of the scaling factor c (connectivity-based discovery). The peer discovery treshold (receiver sensitivity) is set to $Z_{th} = -80$dB. Given location information for at least the distance D, the peer discovery probability a) increases with the transmit power c, b) is inversely proportional to the path loss exponent a, and c) decreases with the relative distance components $|\eta_x|$ and $|\eta_y|$ (Figure 15). When the LIS has full knowledge on the relative coordinates of the peers and their parent WNEs (dotted lines), the transmit power c for successful peer discovery can be readily estimated by using Corollary 2.1 (dotted lines). On the other hand, when the LIS has partial knowledge of the WNEs/peers coordinates (solid and dashed lines), an increase of the distance components η_x and η_y is shown to be more preferrable, in terms of transmit power requirements, compared to a similar increase to the uncertainty on the WNEs/peers locations (modeled by σ). This relation can be easily observed by comparing the red solid, red dashed, and black solid lines. Thus, when the transmit power is a limiting performance factor at the source peer, the utilization of measurements (to lower the uncertainty on the WNEs locations) can play a key role in reducing the power transmissions/consumption required for peer discovery. An instantiation of such an approach, is the employment of measurements from the tier-1 and tier-2 parent WNEs of the ZigBee sensor (target peer) in Figure 11, as means of reducing the transmit power for peer discovery at the battery-operated robot (source peer).

2.4.3 On the Impact of Angles between the WNEs

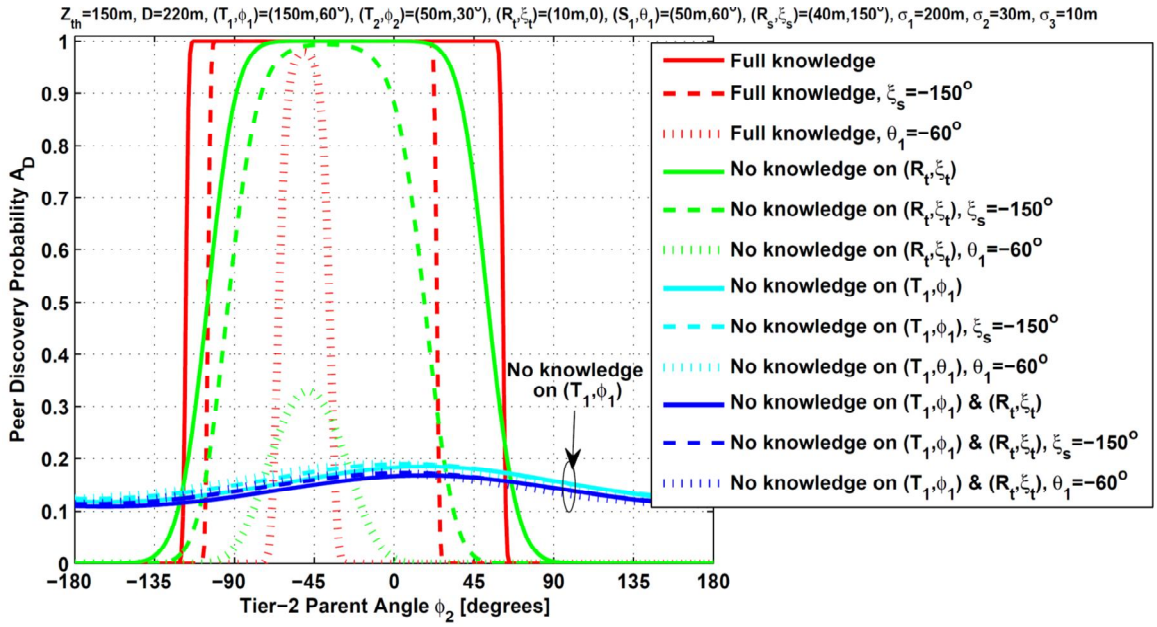

Figure 16:Peer Discovery Probability given D vs. Tier-2 Parent Angle ϕ_2 [degrees]

The employment of accurate AoA measurements increases the complexity and processing requirements for the radio transceiver. Under this viewpoint, in Figure 16 we investigate the impact of the ϕ_2 angle between the tier-3 and the tier-2 parents of the target peer on the probability $\mathcal{A}_D$. As expected, when the LIS has full knowledge on the locations of the peers and their parent WNEs, the peer discovery can be either successful or not. Notably, there exists a ϕ_2 interval within which the peer discovery remains roughly unaffected. This interval is shown to be expanded, shifted, or compressed, in relation with the remainder parameters governing the HWN topology. For example, if the angle ξ_t between the target peer and its parent tier-3 WNE is equal to -150^o (instead of 150^o), then the ϕ_2 interval for successful peer discovery is compressed and shifted to the left (red dashed line in Figure 16). This effect is due the fact that for $\theta_2 = -150^o$ the two peers are separated by a higher distance (Figure 11). Even more evident is the compression of the ϕ_2 interval when the angle between the tier-1 and tier-2 parent WNEs of the source peer is set to $\theta_1 = -60^o$ instead of ($\theta_1 = 60^o$) (red dotted line), since the distance between them is even higher. Such an effect is also expected in the nowadays HWN, where the distance between WNEs in higher tiers is (on the average) higher compared to the one between lower-tier WNEs.

Interestingly, a similar interval exists when the LIS is not aware of the relative coordinates of the target peer (green lines). Notice that the lack of such information prolongs the tail of the respective ϕ_2 interval with full knowledge towards both directions. When the LIS has no knowledge of the coordinates (T_1, θ_1) of the tier-2 parent WNE, the probability $\mathcal{A}_D$ is shown to remain roughly unaffected by the values of ϕ_2 (blue and cyan lines). This relation indicates that the benefits from performing accurate measurements on the angles between low-tier WNEs is marginal when the relative coordinates of high-tier parent WNEs are not known to the LIS.

From the discussion above, we identify two important design guidelines. Firstly, the accurate estimation of the angle between low-tier WNEs and their parent

WNEs is necessary only when the LIS is required to fine-tune its estimation on the peer discovery outcome. Secondly, depending on the available spatial information, the low-tier WNEs can relax the accuracy of their AoA measurements without significantly deteriorating the performance of peer discovery. The range of this relaxation (error tolerance) can be estimated by using the results of this work.

2.5 Key Contributions and Conclusions

More and more WNEs are capable of estimating their distance and angle to other nearby WNEs of the same technology. Integrating such spatial information from the ubiquitous WNEs of different RATs, is a key enabler for fine-grained localization and effective peer discovery between the myriads of WNEs. The key contributions of our work can be summarized as follows. Firstly, we have derived closed-form expressions for the conditional pdf and ccdf of the distance Z between two heterogeneous WNEs, given partial (or full) knowledge of the spatial relations between their upper-tier parent WNEs. Secondly, the derived pdf expressions describe the statistical behavior of localization between distant and not necessarily homogeneous WNEs. To the best of our knowledge, this is the first work to consider this disruptive localization paradigm and analyze its performance. Thirdly, we have analyzed the performance of location-aware peer discovery between heterogeneous WNEs given partial (or full) knowledge of the spatial relations between their upper-tier WNEs. To the best of our knowledge, this is the first work to address this challenging issue. Fourthly, we have analyzed the impact of the key system parameters on the performance of location-aware peer discovery and derived optimal strategies for the placement of upper-tier WNEs as means of maximizing the peer discovery probability between two heterogeneous WNEs of interest. Fifthly, we have identified conditions under which the strategic installation of WNEs, or the use of positioning measurements from additional WNEs, enhances the performance of location-aware peer discovery. Approximate and exact expressions have been presented to compute the deployment std. deviation of low-tiers or the tier-1 intensity that maximize the performance of location-aware peer discovery. Finally, we have provided valuable insights for the design of location-aware peer discovery in the nowadays HWN. Among others, we have shown that even fundamental parameters on the HWN layout carry enough information for estimating the outcome of peer discovery and fine-tuning its performance. Finally, we have showed that depending on the availability of spatial information, low-tier WNEs can relax the accuracy of their angle measurements while pertaining a desired peer discovery probability target.

3. NETWORK-ASSISTED D2D DISCOVERY IN RANDOM SPATIAL CELLULAR NETWORKS

Device-to-Device (D2D) discovery is the inextricable prelude for the direct exchange of localized traffic between cellular users in proximity (D2D communications). The D2D discovery process can be based on either autonomous actions taken by D2D-enabled devices (direct D2D discovery), or core network functionalities to estimate proximity between D2D-enabled peers (network-assisted D2D discovery). A key advantage of the latter is its potential to exploit fundamental knowledge on the cellular network layout towards better handling with the energy, signaling, and interference burden for D2D discovery. In this paper, we analyze the performance of network-assisted D2D discovery in random spatial networks and derive useful design guidelines for fine-tuning its performance. Specifically, we derive the distance distribution between two D2D peers conditioned on the core network's knowledge on the cellular network layout, assuming that the base stations are distributed according to a Poisson point process. The derived expressions are used for analyzing the behavior of the D2D discovery probability with respect to key system parameters, as well as for identifying conditions under which D2D discovery probability is maximized with respect to the BS density. Exact and approximate expressions for the optimal BS density are also derived. Numerical results validate the accuracy of our findings and provide valuable insights on the performance tradeoffs inherent to network-assisted D2D discovery.

The remainder of this paper is organized as follows. In section 3.1, we present our system model and assumptions, while in section 3.2 we derive analytical expressions for the conditional pdf and ccdf of the distance between two D2D peers given certain combinations of location information parameters. In section 3.3, we investigate how the BS density affects the D2D discovery probability and derive analytical expressions for computing the optimal BS density (when relevant). The impact of the key system parameters on the D2D discovery performance is assessed in Section 3.4, where we additionally provide useful design guidelines for network-assisted D2D discovery. Section 3.5 concludes our work.

3.1 System Model

3.1.1 Performance Metrics

Since, the performance of D2D discovery is tightly coupled with the definition of proximity between D2D peers [127], in this work we consider that two D2D-enabled devices are in proximity whenever the *long-term averaged* received signal power from the D2D source is greater than or equal to the receiver sensitivity at the D2D target. We choose to follow this definition for two main reasons. Firstly, the D2D discovery process is most likely to be based on the long-term average and not the *instantaneous* received power at the D2D target, i.e. small-scale fading is averaged out. Secondly, this notion of proximity is closer to the one used between the user equipments and the cellular BSs during cell search [93]. Assuming that the path loss is inversely proportional to the distance between the D2D peers and governed by a path loss exponent a, the D2D discovery probability is defined as

$$\mathcal{A}_{\mathcal{J}} \triangleq P[P_t Z^{-a} \geq P_r | \mathcal{J}], \qquad (3.1)$$

where $\mathcal{J}$ denotes the available knowledge on the cellular network layout (at the EPC), P_t the transmit power at the D2D source, P_r the receiver sensitivity at the D2D target, and Z the distance between the D2D peers. The receiver sensitivity is typically fixed and depends on the system parameters that specify the reference measurement channel [128], e.g. duplexing mode and bandwidth. By rearranging (3.1), it can be easily shown that the D2D discovery probability corresponds to the cdf of the distance Z at the point $\left(\frac{P_t}{P_r}\right)^{\frac{1}{a}}$, conditioned on the available knowledge $\mathcal{J}$ at the EPC.

3.1.2 System Description

We consider a D2D-enabled cellular network, where the locations of all cellular BSs, including both macrocells and small cells, are distributed according to a homogeneous PPP Φ_B with intensity λ_B in the Euclidean plane. Without assuming a specific distribution for the users, we consider that a) the Point Process Φ_U describing the user locations is stationary and isotropic, and b) the x and y coordinates of a tagged user are independent of those of other users in Φ_U. We consider that all users associate with the nearest BS in Φ_B [94] and focus on the network-assisted D2D discovery process between a tagged user, referred to as *D2D source*, and a (specific) target D2D-enabled user, referred to as *D2D target*. We further focus on the scenario where the network is capable of identifying the associated BS of the D2D peers, and utilize UE and BS positioning measurements to enhance the performance of D2D discovery.

Table 6: Cellular-based Location Information Parameters

Parameter	Notation	Estimation methodology
Distance between the D2D source and its associated BS	R_s	By using Timing Advance measurements at the respective BS (standard capability in LTE/LTE-A [16]).
Angle between the D2D source and its associated BS	θ_s	By performing AoA measurements at the associated BS of the D2D source with respect to the reference direction from the associated BS of the D2D source to the associated BS of the D2D target. AoA is a standard measurement capability in LTE/LTE-A [16].
Distance between the D2D target and its associated BS	R_t	In a similar manner with the estimation of R_s.
Angle between the D2D target and its associated BS	θ_t	By exploiting AoA measurements at the associated BS of the D2D target, similarly to the estimation of θ_s.
Neighboring degree between the associated BS of the D2D source and the associated BS of the	k	By utilizing knowledge from the network planning phase or by performing Timing Advance measurements for the associated BS of the D2D target. This estimation can also be based on the RSRP from the associated BS of the D2D target [16].

D2D target		
Inter-site distance between the associated BS of the D2D source and the associated BS of the D2D target	D_k	By using a similar methodology with the estimation of k. However, comparably higher accuracy is required.

Table 6 lists the measurements considered in this paper and highlights how they can be performed in LTE/LTE-Advanced. Note that we do not assume that all of these measurements are available to the EPC. Instead, we investigate how certain combinations of these measurements (location information parameters) can enhance the network-assisted D2D discovery process at the EPC. Figure 17 depicts all parameters and random variables involved in our analysis. The following lemma states that, if not fixed and known at the EPC, the distance D_k between a random point in the system and its k-th nearest (neighboring) BS in Φ_B follows a generalized Gamma distribution.

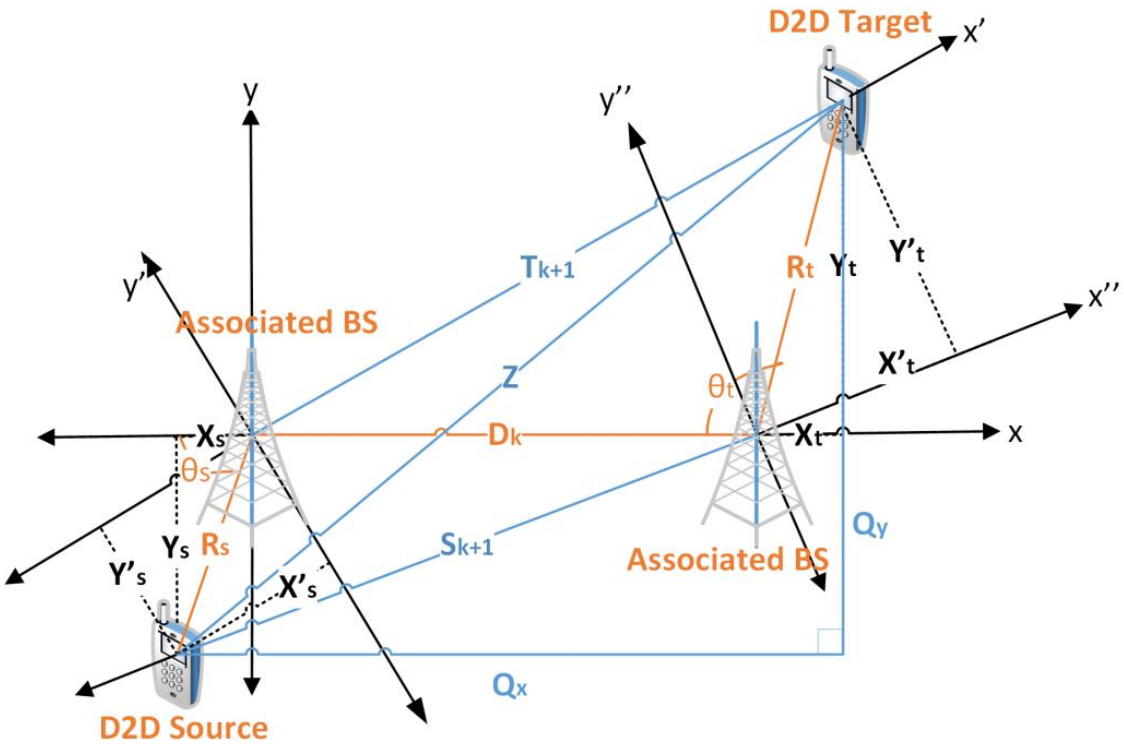

Figure 17: System model parameters and related Random Variables

Lemma 3.1. *The pdf $f_{D_k}(d)$ of the distance D_k between a random point in the system and the k-th neighboring BS in the PPP Φ_B is given by*

$$f_{D_k}(d) = \frac{2(\pi\lambda_B)^k}{\Gamma[k]} d^{2k-1} e^{-\pi\lambda_B d^2}, \quad (3.2)$$

where $\Gamma[k]$ is the Gamma function.

Proof. The proof is derived by using Slivnyak's theorem and the result in [96].

□

Lemma 3.1 provides the pdf of the inter-site distance D_k between a tagged BS and its k-th neighbor. However, for $k = 1$, it also provides the pdf of the distances

R_s and R_t: Rayleigh-distributed RVs with parameter $b^2 = \frac{1}{2\pi\lambda_B}$. If not fixed and known at the EPC, in a similar manner with [129], we assume that the angles θ_s and θ_t satisfy the following property:

Assumption 3.1. *The angle θ_s between the D2D source and its associated BS as well as the angle θ_t between the D2D target and its associated BS are uniform circular in the interval $(-\pi, \pi]$ and independent of the distances R_s and R_t, respectively.*

Assumption 3.1 states that the D2D peers are uniformly distributed around their associated BS, having no bias on residing towards a specific direction, or adapting the distance to their associated BS depending on their angle to other BSs. The D2D discovery probability can be computed by the ccdf of the distance Z conditioned on the available location information parameters $\mathcal{J}$.

Lemma 2.2. *Given knowledge on the location information parameters in $\mathcal{J}$, the D2D discovery success probability is given by the complement of the corresponding conditional ccdf of the distance Z, denoted by $\bar{F}_{Z|\mathcal{J}}$, at point $\left(\frac{P_t}{P_r}\right)^{\frac{1}{a}}$, i.e.*

$$\mathcal{A}_{\mathcal{J}} = 1 - \bar{F}_{Z|\mathcal{J}}\left(\left(\frac{P_t}{P_r}\right)^{\frac{1}{a}}\right). \qquad (3.3)$$

Proof. The proof easily follows by rearranging (3.1).

□

In the following, we consider that the transmit power P_t at the D2D source and the receiver sensitivity P_r at the D2D target are fixed and known to the EPC. Note that the single-tier PPP model is in line with multi-tier cellular network models that use individual and independent PPPs to model each tier [1][93][95], since the superposition of independent PPPs is again a PPP of intensity the sum of each tier intensity [130]. We adopt this model since we are interested in the performance of network-assisted D2D discovery and not in the performance of a specific cellular tier.

3.2 Distance Distributions in D2D-Enabled Networks with Location-Assistance

3.2.1 Statistical distance between two D2D peers given the distance D

In this section, we derive closed-form expressions for the pdf and the ccdf of the distance Z, given four distinct combinations of location information parameters: a) knowledge of only the inter-site distance D_k, b) knowledge of D_k and the relative position of the D2D target with respect to its associated BS in polar coordinates, i.e. $[R_t, \theta_t]$, c) knowledge of D_k and the relative position of the D2D source with respect to its associated BS in polar coordinates, i.e. $[R_s, \theta_s]$, and d) knowledge of all the aforementioned parameters. The last combination allows a direct computation of Z. Given knowledge on the parameters in $\mathcal{J}$, we denote the corresponding conditional pdf and ccdf of the distance Z by $\mathrm{f}_{Z|\mathcal{J}}$ and $\bar{F}_{Z|\mathcal{J}}$, respectively.

Theorem 3.1. *The conditional pdf $f_{Z|D_k}(z)$ of the distance Z between two D2D peers, given that the associated BS of the D2D source and the associated BS of the D2D target are separated by a distance $D_k = D$, is given by*

$$f_{Z|D_k}(z) = \pi\lambda_B z e^{-\frac{\pi\lambda_B}{2}(z^2+D^2)} I_0[\pi\lambda_B zD], \quad (3.4)$$

where $I_0[x]$ is the modified Bessel function of the first kind and zero-th order. The corresponding ccdf $\bar{F}_{Z|D_k}(z)$ is given by

$$\bar{F}_{Z|D_k}(z) = Q_1\left[\sqrt{\pi\lambda_B}D, \sqrt{\pi\lambda_B}z\right], \quad (3.5)$$

where $Q_M[a,b]$ is the Marcum-Q function.

Proof. See Appendix II.A.

□

Theorem 3.1 provides an analytical tool for handling the uncertainty on the distance between two D2D peers, given location information that typically remains fixed over time: the inter-site distance D_k. In the next theorem, we derive closed-form expressions for the conditional pdf and ccdf of the distance Z given additional knowledge on the relative position of the D2D target.

Theorem 3.2. *The conditional pdf $f_{Z|D_k,R_t,\theta_t}(z)$ of the distance Z between two D2D peers, given that a) the associated BS of the D2D source and the associated BS of the D2D target are separated by a distance $D_k = D$, and b) the relative position of the D2D target with respect to its associated BS equals to $[R_t = T, \theta_t = \rho]$ in polar coordinates, is given by*

$$f_{Z|D_k,R_t,\theta_t}(z) = 2\pi\lambda_B z e^{-\pi\lambda_B(z^2+D^2+T^2-2DT\cos(\pi-\rho))} I_0\left[2\pi\lambda_B z\sqrt{D^2+T^2-2DT\cos(\pi-\rho)}\right]. \quad (3.6)$$

The corresponding ccdf $\bar{F}_{Z|D_k,R_t,\theta_t}(z)$ is given by

$$\bar{F}_{Z|D_k,R_t,\theta_t}(z) = Q_1\left[\sqrt{2\pi\lambda_B(D^2+T^2-2DT\cos(\pi-\rho))}, z\sqrt{2\pi\lambda_B}\right]. \quad (3.7)$$

Proof. See Appendix II.B.

□

The expressions in Theorem 3.2 further reduce the uncertainty on the distance between the D2D peers by incorporating additional knowledge on the relative position of the D2D target with respect to its associated BS. However, in contrast with the acquisition and caching of the D_k parameter, the relative position of the D2D target is expected to vary over time, requiring monitoring measurements by the associated BS. In Corollary 3.1, we present the conditional pdf and ccdf of the distance Z in the scenario where, instead of the relative position of the D2D target, the EPC is aware of the relative position of the D2D source.

Corollary 3.1. *The conditional pdf $f_{Z|D_k,R_s,\theta_s}(z)$ and ccdf $\bar{F}_{Z|D_k,R_s,\theta_s}(z)$ of the distance Z between two D2D peers, given that a) the associated BS of the D2D source and the associated BS of the D2D target are separated by a distance $D_k = D$, and b) the relative position of the D2D source with respect to its associated BS equals to $[R_s = S, \theta_s = \varphi]$ in polar coordinates, are given by (3.6) and (3.7), respectively, for $T = S$ and $\rho = \pi - \varphi$.*

Proof. Corollary 3.1 is proved by working in the Cartesian plane $x''y''$ centered at the position of the associated BS of the D2D source with positive x-axis the direction from the associated BS of the D2D source to the associated BS of the D2D target. The distance Z is given by

$$Z = \sqrt{(X'_t + S_{k+1})^2 + {Y'_t}^2}, \quad (3.8)$$

where X'_t and Y'_t are independent normal RVs with zero mean and equal variance $b^2 = \frac{1}{2\pi\lambda_B}$. Note that S_{k+1} is given by the law of cosines as $S_{k+1} = \sqrt{D^2 + S^2 - 2DS\cos\varphi}$ and is a fixed parameter. The remainder of the proof is similar to the one in Theorem 3.2.

In the following, we present a formula for directly estimating the distance Z when the EPC is aware of all the aforementioned parameters $\{D_k, R_t, \theta_t, R_s, \theta_s\}$.

□

Proposition 3.1. *The distance Z between two D2D peers, given that a) the associated BSs of the two D2D peers is $D_k = D$, b) the relative position of the D2D target with respect to its associated BS equals to $[R_t = T, \theta_t = \rho]$, and c) the relative position of the D2D source with respect to its associated BS equals to $[R_s = S, \theta_s = \varphi]$, is given by*

$$Z = \sqrt{(D + T\cos\rho - S\cos\varphi)^2 + (T\sin\rho - S\sin\varphi)^2}. \quad (3.9)$$

Proof. The proof is derived by substituting $D_k = D$, $X_t = T\cos(\rho)$, $Y_t = T\sin(\rho)$, $X_s = S\cos\varphi$ and $Y_s = S\sin\varphi$ in (3.23) (see Appendix II.A).

□

3.2.2 Statistical distance between two D2D peers given the neighboring degree k

Let us now focus on the scenarios where instead of the inter-site distance D_k, the EPC is aware of the neighboring degree k between the associated BSs of the D2D peers. Such a scenario may happen when the BSs face difficulties on (accurately) estimating the distance between them, e.g. in indoor deployment. We point out that the scenario where the D2D peers are associated with the same BS, i.e. $k = 0$, is modeled by substituting $D_k = 0$ in the expressions of the previous subsection.

Theorem 3.3. *The conditional pdf $f_{Z|k}(z)$ of the distance Z between two D2D peers, given that the associated BS of the D2D source is the n-th neighbor of the associated BS of the D2D target, i.e. $k = n$, is given by*

$$f_{Z|k}(z) = \pi\lambda_B \left(\frac{2}{3}\right)^n z e^{-\frac{\pi\lambda_B z^2}{3}} L_{n-1}\left[-\frac{\pi\lambda_B z^2}{6}\right], \quad (3.10)$$

where $L_n[x]$ is the Laguerre polynomial. The respective ccdf $\bar{F}_{Z|k}(z)$ is given by

$$\bar{F}_{Z|k}(z) = \frac{1}{3} e^{-\frac{\pi\lambda_B z^2}{3}} \sum_{m=0}^{n-1} \varepsilon_m \left(\frac{2}{3}\right)^m L_m\left[-\frac{\pi\lambda_B z^2}{6}\right], \quad (3.11)$$

where $\varepsilon_m = 1$ $\forall m < n-1$ and $\varepsilon_{n-1} = 3$.

Proof. See Appendix II.C.

□

Remark 3.1 *Noticeably, Theorem 3.3 extends the results in Theorem 3.1 by providing closed-form expressions for the conditional pdf and the ccdf of the distance Z given information for only on the neighboring degree k. This is achieved due to the fact that the arguments of the Bessel and the Marcum-Q functions in Theorem 3.1 are in a simple form. However, this is not the case for Theorem 3.2 and Corollary 3.1, where the respective arguments involve square*

roots and powers of the distance parameter D_k.This property complicates the derivation of closed-form extensions and enables numerical evaluations only.

Corollary 3.2. *The conditional pdf $f_{Z|k,R_t,\theta_t}(z)$ of the distance Z between two D2D peers, given that a) the associated BS of the D2D source is the n-th neighbor of the associated BS of the D2D target, i.e. $k=n$, and b) the relative position of the D2D target with respect to its associated BS equals to $[R_t=T,\theta_t=\rho]$ in polar coordinates, is given by*

$$f_{Z|k,R_t,\theta_t}(z)=\frac{2(\pi\lambda_B)^n}{\Gamma[n]}\int_0^\infty f_{Z|x,R_t,\theta_t}(z)x^{2n-1}e^{-\pi\lambda_B x^2}\mathrm{d}x, \quad (3.12)$$

where the conditional pdf $f_{Z|x,R_t,\theta_t}(z)$ is given in (3.6) for $D_k=x$. The corresponding ccdf $\bar{F}_{Z|k,R_t,\theta_t}(z)$ is given by

$$\bar{F}_{Z|k,R_t,\theta_t}(z)=\frac{2(\pi\lambda_B)^n}{\Gamma[n]}\int_0^\infty \bar{F}_{Z|x,R_t,\theta_t}(z)x^{2n-1}e^{-\pi\lambda_B x^2}\mathrm{d}x, \quad (3.13)$$

where the conditional ccdf $\bar{F}_{Z|x,R_t,\theta_t}(z)$ is given in (3.7) for $D_k=x$.

Proof. The proof follows from the law of total probability, expression (3.2), and Theorem 3.2.

□

Corollary 3.3. *The conditional pdf $f_{Z|k,R_t,\theta_t}(z)$ and ccdf $\bar{F}_{Z|k,R_s,\theta_s}(z)$ of the distance Z between two D2D peers, given that a) the associated BS of the D2D source is the n-th neighbor of the associated BS of the D2D target, i.e. $k=n$, and b) the relative position of the D2D source with respect to its associated BS equals to $[R_s=S,\theta_s=\varphi]$ in polar coordinates, are given by (3.12) and (3.13), respectively, for $T=S$ and $\rho=\pi-\varphi$.*

Proof. The proof follows easily from the law of total probability, expression (3.2), Corollaries 3.1 and 3.2.

□

Let us now focus on the scenario where the EPC is aware of the neighboring degree k and the relative positions of the D2D peers with respect to their associated BSs. Different from Proposition 3.1, the knowledge of k leaves uncertainty on the distance D_k between the associated BSs of the D2D peers. Interestingly, the respective conditional pdf and ccdf of the distance Z can be derived in closed-form.

Theorem 3.4. *The conditional pdf $f_{Z|k,R_t,\theta_t,R_s,\theta_s}(z)$ of the distance Z between two D2D peers, given that a) the associated BS of the D2D source is the n-th neighbor of the associated BS of the D2D target, i.e. $k=n$, b) the relative position of the D2D source with respect to its associated BS equals to $[R_s=S,\theta_s=\varphi]$, and c) the relative position of the D2D target with respect to its associated BS equals to $[R_t=T,\theta_t=\rho]$, is given by*

$$f_{Z|k,R_t,\theta_t,R_s,\theta_s}(z)=\begin{cases}0, & z\le|Q_y|\\ \frac{2(\pi\lambda_B)^n}{\Gamma[n]}\frac{z}{\sqrt{z^2-Q_y^2}}\sum_{m=1}^{2}\frac{\left(-Q_x+q_m\sqrt{z^2-Q_y^2}\right)^{2n-1}U\left[-Q_x+q_m\sqrt{z^2-Q_y^2}\right]}{e^{\pi\lambda_B\left(-Q_x+q_m\sqrt{z^2-Q_y^2}\right)^2}}, & z>|Q_y|\end{cases} \quad (3.15)$$

, where $U[x]$ is the unit step function, $Q_x=-Tcos\rho-Scos\varphi$, $Q_y=Tsin\rho-Ssin\varphi$ and

$$q_m = \begin{cases} 1, & \mathrm{m} = 1 \\ -1, & m = 2 \end{cases} \quad (3.14)$$

The corresponding ccdf $\bar{F}_{Z|k,R_t,\theta_t,R_s,\theta_s}(z)$ *is given by*

$$\bar{F}_{Z|k,R_t,\theta_t,R_s,\theta_s}(z) = \begin{cases} 0 & z \le |Q_y| \\ \frac{(\Gamma[n]-\Gamma[n,\pi\lambda_B d_1^2])U[\mathrm{d}_1]+\Gamma[n,\pi\lambda_B d_2^2]}{\Gamma[n]} & z > |Q_y|, d_2 > 0 \\ 1 & z > |Q_y|, d_2 \le 0 \end{cases} \quad (3.16)$$

, where $\Gamma[n,x]$ is the upper incomplete Gamma Function, $d_1 = -Q_x - \sqrt{z^2 - Q_y^2}$, and $d_2 = -Q_x + \sqrt{z^2 - Q_y^2}$.

Proof. See Appendix II.D.

□

3.3 Optimal Network Deployment for Network-Assisted D2D Discovery

In this section, we provide guidelines for optimal network deployment as a means to optimize the probability of successful network-assisted D2D discovery. Specifically, we turn our attention to the impact of the BS density λ_B on the D2D discovery probability $\mathcal{A}_\mathcal{J}$, which is of high practical interest since network densification is currently considered as a very promising way to increase the network spectral efficiency. To this direction, we examine the monotonicity of the D2D discovery probability $\mathcal{A}_\mathcal{J}$ with respect to λ_B, given the location information parameters discussed in the previous section, and provide analytical expressions for the optimal BS density. Since $\mathcal{A}_\mathcal{J}$ is given by the cdf of the distance Z at $\left(\frac{P_t}{P_r}\right)^{\frac{1}{a}}$ (3.1), by definition, it follows that $\mathcal{A}_\mathcal{J}$ is a) proportional to the transmit power P_t and b) inversely proportional to the receiver sensitivity P_r and the path loss exponent a. We consider that the monotonicity of $\mathcal{A}_\mathcal{J}$ with respect to the parameters D_k and k can be examined in a similar manner with the one below.

Theorem 3.5. *Let* $q = D\left(\frac{P_t}{P_r}\right)^{-\frac{1}{a}}$*, where* D *is the value of inter-site distance* D_k *between the associated BSs of the two D2D peers. Given the distance* D*, the D2D discovery probability* $\mathcal{A}_{D_k}$ *increases with* λ_B *for* $q < 1$*. However, for* $q > 1$ *there exists an optimal BS density* λ_B^* *that maximizes the D2D discovery probability and satisfies the following property:*

$$I_0\left[\frac{\pi\lambda_B^* D^2}{q}\right] - qI_1\left[\frac{\pi\lambda_B^* D^2}{q}\right] = 0. \quad (3.17)$$

The optimal BS density can be analytically approximated as

$$\lambda_B^* \approx \frac{q(1+3q+\sqrt{39q^2-6q-17})}{16\pi D^2(q-1)}. \quad (3.18)$$

Proof. See Appendix II.E.

□

The parameter $\left(\frac{P_t}{P_r}\right)^{\frac{1}{a}}$ corresponds to the maximum distance for successful D2D discovery between the D2D peers. On the other hand, the distance between a user and the associated BS is inversely proportional to λ_B since, by definition, it is Rayleigh distributed with parameter $\frac{1}{2\pi\lambda_B}$. Therefore, as the BS density increases, the distance Z between the D2D peers tends to reach the inter-site distance D_k between their associated BSs, i.e. a higher λ_B reduces uncertainty on the user position around the associated BS. Based on these observations, Theorem 3.5 can be interpreted as follows: as λ_B increases, the distance Z between the D2D peers tends to be statistically closer to the inter-site distance D_k, which for $q < 1$ is by definition lower than the maximum range for successful D2D discovery, i.e. $D_k < \left(\frac{P_t}{P_r}\right)^{\frac{1}{a}}$. However, for $q > 1$, the inter-site distance D_k is greater than the maximum D2D discovery range and, above a certain BS density, the distance Z tends to be statistically greater than the D2D discovery range.

Interestingly, Theorem 3.5 can be extended to the scenario where, apart from the inter-site distance D_k, the EPC is additionally aware of the relative positions of the D2D pairs with respect to their associated BS. This can be shown by noticing that the ccdf results in Theorem 3.2 are in a similar form with the ones in Theorem 3.1. In more detail, if the EPC is aware of the relative position of the D2D source, Theorem 3.5 applies for $q = \sqrt{D^2 + S^2 - 2DS\cos\varphi}\left(\frac{P_t}{P_r}\right)^{-\frac{1}{a}}$. On the other hand, if the EPC is aware of the relative position of the D2D target, Theorem 3.5 applies for $q = \sqrt{D^2 + T^2 - 2DT\cos(\pi - \rho)}\left(\frac{P_t}{P_r}\right)^{-\frac{1}{a}}$. The proof is omitted. We now focus on the scenarios where, instead of the distance D_k, the EPC is aware of the neighboring degree k.

Theorem 3.6. *When the EPC is aware of the neighboring degree $k = n$, the (conditional) D2D discovery probability $\mathcal{A}_k$ increases with λ_B.*

Proof. By using Theorem 3.3 and (3.1), the D2D discovery probability $\mathcal{A}_k$ is given by

$$\mathcal{A}_k = 1 - \frac{1}{3}e^{-\frac{\pi\lambda_B z^2}{3}}\sum_{m=0}^{n-1}\varepsilon_m\left(\frac{2}{3}\right)^m L_m\left[-\frac{\pi\lambda_B z^2}{6}\right], \quad (3.19)$$

where $\varepsilon_m = 1, \forall m < n-1$ and $\varepsilon_{n-1} = 3$. By differentiating with respect to λ_B we get:

$$\frac{\partial\mathcal{A}_k}{\partial\lambda_B} = \pi z^2 e^{-\frac{\pi\lambda_B z^2}{3}}\sum_{m=0}^{n-1}\varepsilon_m\frac{2^{m-1}}{3^{m+2}}\left(2L_m\left[-\frac{\pi\lambda_B z^2}{6}\right] - L_{m-1}^1\left[-\frac{\pi\lambda_B z^2}{6}\right]\right), \quad (3.20)$$

where $L_m^1[x] = (m+1)\sum_{v=0}^{m}\frac{(-m)_k z^k}{(k+1)!k!}$ corresponds to the generalized Laguerre polynomial of the first order. Now, since all parameters in (3.20) are positive real numbers and by definition $L_{m-1}^1[x] < L_m[x]$ for $x < 0$, it follows that $\frac{\partial\mathcal{A}_k}{\partial\lambda_B} > 0$, which completes the proof.

□

Different from Theorem 3.5, Theorem 3.6 shows that a higher BS density will always improve the performance of network-assisted D2D discovery if the EPC is aware of the neighboring degree k. This mainly follows from the fact that the inter-site distance D_k is not a fixed parameter as in Theorem 3.5, yet, it is inversely proportional to the BS density λ_B (3.2).

Theorem 3.7. *Let d_1 and d_2 denote the (fixed) parameters defined in Theorem 3.4. Given that a) the associated BS of the D2D source is the n-th neighbor of the associated BS of the D2D target, i.e. $k = n$, b) the relative position of the D2D source with respect to its associated BS equals to $[R_s = S, \theta_s = \varphi]$ in polar coordinates, and c) the relative position of the D2D target with respect to its associated BS equals to $[R_t = T, \theta_t = \rho]$ in polar coordinates, the D2D discovery probability $\mathcal{A}_{k,R_t,\theta_t,R_s,\theta_s}$ satisfies the following properties with respect to λ_B:*

1. For $z \leq |Q_y|$, $\mathcal{A}_{k,R_t,\theta_t,R_s,\theta_s}$ is fixed and equal to 1.

2. For $z > |Q_y|$ and $d_2 \leq 0$, $\mathcal{A}_{k,R_t,\theta_t,R_s,\theta_s}$ is fixed and equal to 0.

3. For $z > |Q_y|$, $d_2 > 0$, and $d_1 \leq 0$, $\mathcal{A}_{k,R_t,\theta_t,R_s,\theta_s}$ increases with λ_B.

4. For $z > |Q_y|$, $d_2 > 0$, and $d_1 > 0$, there exists an optimal BS density λ_B^* that maximizes the D2D discovery probability $\mathcal{A}_{k,R_t,\theta_t,R_s,\theta_s}$ and is given by

$$\lambda_B^* = \frac{n \ln \frac{d_1^2}{d_2^2}}{\pi (d_1^2 - d_2^2)}. \quad (3.21)$$

Proof. Properties 1 and 2 follow from (3.16). On the other hand, by combining (3.16) and (3.1) for $z > |Q_y|$, $d_2 > 0$, and $d_1 \leq 0$, we get that $\mathcal{A}_{k,R_t,\theta_t,R_s,\theta_s} = 1 - \frac{\Gamma[n, \pi \lambda_B d_2^2]}{\Gamma[n]}$. By differentiating with respect to λ_B, it can be readily shown that $\frac{\partial \mathcal{A}_{k,R_t,\theta_t,R_s,\theta_s}}{\partial \lambda_B} > 0$.

On the other hand, when $z > |Q_y|$, $d_2 > 0$, and $d_1 > 0$, the D2D discovery probability is given as $\mathcal{A}_{k,R_t,\theta_t,R_s,\theta_s} = \frac{\Gamma[n, \pi \lambda_B d_1^2] - \Gamma[n, \pi \lambda_B d_2^2]}{\Gamma[n]}$ (Eqs. (3.1) (3.16)). By differentiating with respect to λ_B we get:

$$\frac{\partial \mathcal{A}_{k,R_t,\theta_t,R_s,\theta_s}}{\partial \lambda_B} = (\pi \lambda_B)^n \frac{d_2^{2n} e^{-\pi \lambda_B d_2^2} - d_1^{2n} e^{-\pi \lambda_B d_1^2}}{\lambda_B \Gamma[n]}. \quad (3.22)$$

Now, solving $\frac{\partial \mathcal{A}_{k,R_t,\theta_t,R_s,\theta_s}}{\partial \lambda_B} = 0$ with respect to λ_B yields (3.21).

□

3.4 Numerical Results and Design Guidelines

In this section, we provide numerical results in order to study the impact of the key system parameters on the D2D discovery probability and derive useful guidelines for the design of network-assisted D2D discovery. The receiver sensitivity is set to $P_r = -93.5$ dBm, which is typical for the LTE-Advanced system with Frequency Division Duplexing (FDD) and bandwidth equal to (or greater than) 5 MHz.

3.4.1 Effect of BS Density

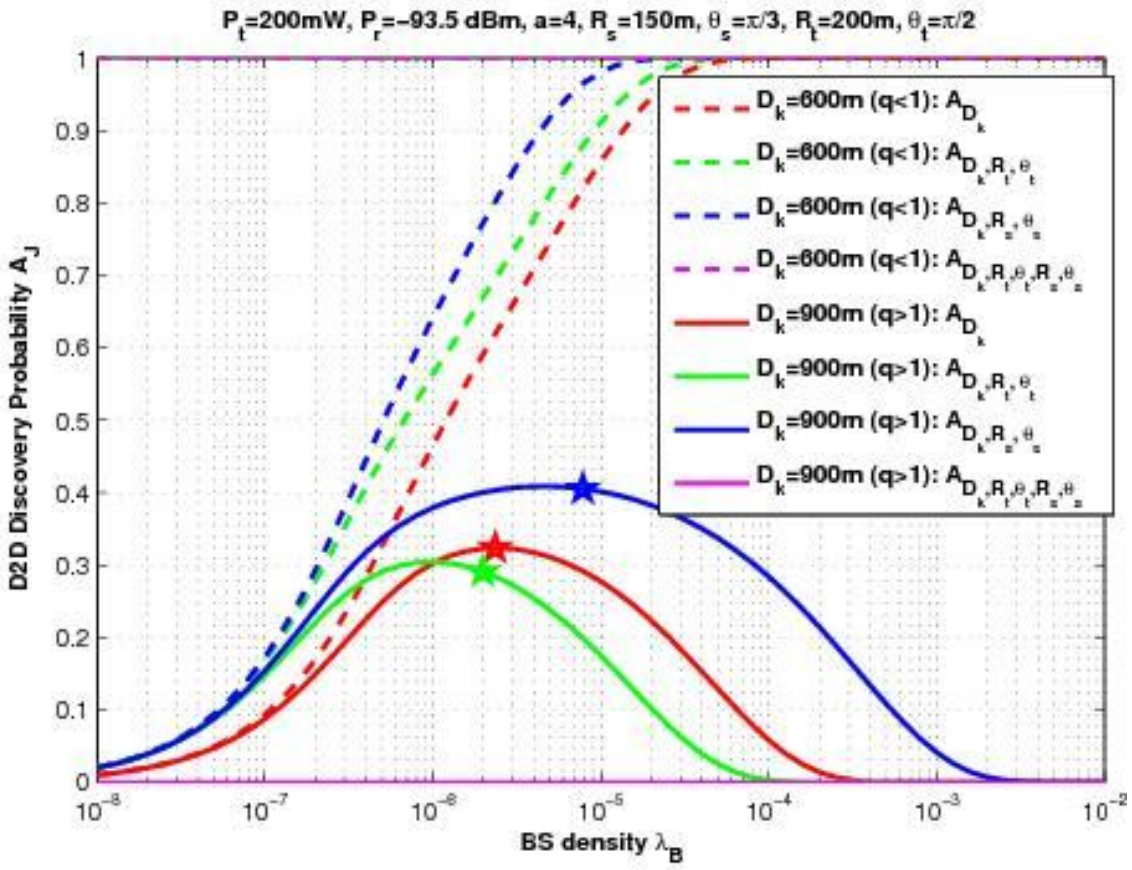

Figure 18: D2D Discovery Probability given D_k vs. BS density

Figure 18 depicts the impact of the BS density λ_B on the D2D discovery probability given location information that includes at least the inter-site distance D_k. We focus on two inter-site distances $D_k = 600$ m and $D_k = 900$ m which, in combination with the parameters shown in Fig. 2, result in D2D discovery success ($\mathcal{A}_{D_k,R_t,\theta_t,R_s,\theta_s} = 1$) and failure ($\mathcal{A}_{D_k,R_t,\theta_t,R_s,\theta_s} = 0$), respectively. When the EPC is aware of only the inter-site distance $D_k = D$, the D2D discovery probability $\mathcal{A}_{D_k}$ increases with λ_B for $D_k = 600$ m, since $q < 1$ (as shown in Theorem 3.5). On the other hand, for $D_k = 900$ m, which corresponds to $q > 1$, there exists an optimal BS density that maximizes the D2D discovery probability and is well approximated by (3.18) (highlighted with the red star). Similar properties are shown when the EPC has additional knowledge on the relative positions of the D2D target or the D2D source, i.e. $\mathcal{A}_{D_k,R_t,\theta_t}$ and $\mathcal{A}_{D_k,R_s,\theta_s}$, respectively. The approximations on the optimal BS density for $\mathcal{A}_{D_k,R_t,\theta_t}$ and $\mathcal{A}_{D_k,R_s,\theta_s}$, indicated by the blue and green star, respectively, are also shown to be close to the λ_B parameter that maximizes the respective D2D discovery probabilities. Recall that the approximation accuracy can be increased by using more terms from (3.62) and (3.63).

The results in Figure 18 indicate that conditioned on knowledge of the relative position of the D2D source, or the D2D target, the statistical behavior of the D2D discovery probability and the optimal λ_B^* significantly alters compared to $\mathcal{A}_{D_k}$, especially when $q > 1$ (the ratio of the Marcum-Q arguments in the ccdf results is higher than one). This follows from the fact that, if not known at the EPC, the locations of the D2D peers are considered to follow a symmetric normal

distribution around their associated BS, i.e. Rayleigh-distributed distance combined with uniformly distributed angle. However, when a D2D peer is located in between the two associated BSs, and its location is known to the EPC, the probability of successful D2D discovery increases. This relation can be easily verified in Fig. 2, by comparing the results for $\mathcal{A}_{D_k,R_s,\theta_s}$ and $\mathcal{A}_{D_k}$ and taking into account that $R_s = 200$ m and $\theta_s = \pi/3$ (Figure 17).

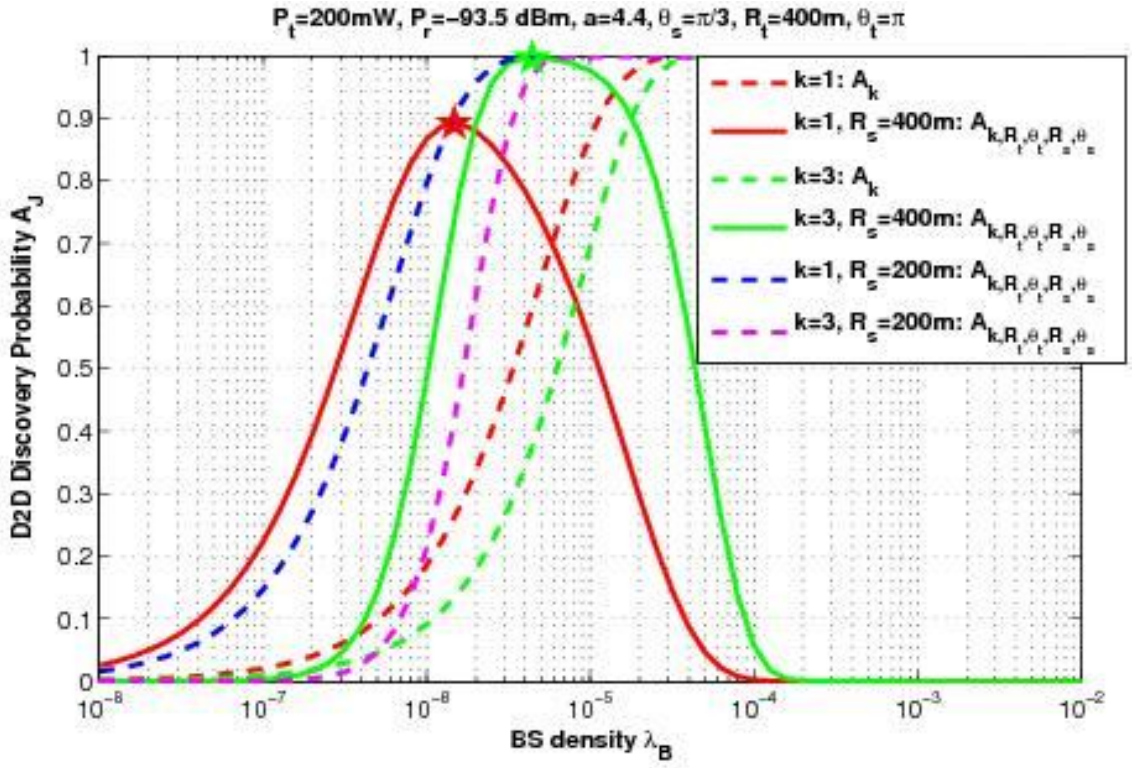

Figure 19: D2D Discovery Probability given k vs. BS density

In Figure 19, we plot the impact of λ_B on the D2D discovery probability, given knowledge of only the neighboring degree k, or the neighboring degree k and the relative positions of the D2D peers. As provided by Theorem 3.6, the D2D discovery probability A_k always increases with λ_B, while given additional knowledge on the relative position of the D2D peers the corresponding D2D probability $\mathcal{A}_{k,R_t,\theta_t,R_s,\theta_s}$ is also increasing with respect to λ_B for $R_s = 200$ m. However, for $R_s = 400$ m the probability $\mathcal{A}_{k,R_t,\theta_t,R_s,\theta_s}$ is maximized for a BS density that can be computed by (3.21) (highlighted with a star). These results are in line with Theorem 3.7 since the parameters $R_s = 200$ m and $R_s = 400$ m, in combination with the system parameters in Figure 19, correspond to $d_1 < 0$ and $d_1 > 0$, respectively.

We now explore how the neighboring degree k affects the D2D discovery probability. As expected, a higher k reduces the D2D discovery probability given knowledge only on k, i.e. $A_{k=1} > A_{k=3}$. The same applies when the relative position of the D2D peers is known to the EPC and $R_s = 200$ m (magenta dashed), which corresponds to $d_1 < 0$, i.e. $\mathcal{A}_{k=1,R_t,\theta_t,R_s,\theta_s} > \mathcal{A}_{k=3,R_t,\theta_t,R_s,\theta_s}$. However, this is not in effect for $R_s = 400$ m ($d_1 > 0$) in medium to very high BS densities ($\lambda_B > 10^{-5}$), where the D2D probability for $k = 3$ (green continuous) is shown to be higher compared to the one for the same parameters and $k = 1$ (red continuous). This follows from the fact that given k, a higher λ_B increases the statistical distance D_k between the associated BSs of the D2D peers which,

combined with the given positions of the D2D peers, shifts the peak of the D2D discovery probability to higher BS densities.

3.4.2 Effect of Inter-site Distance

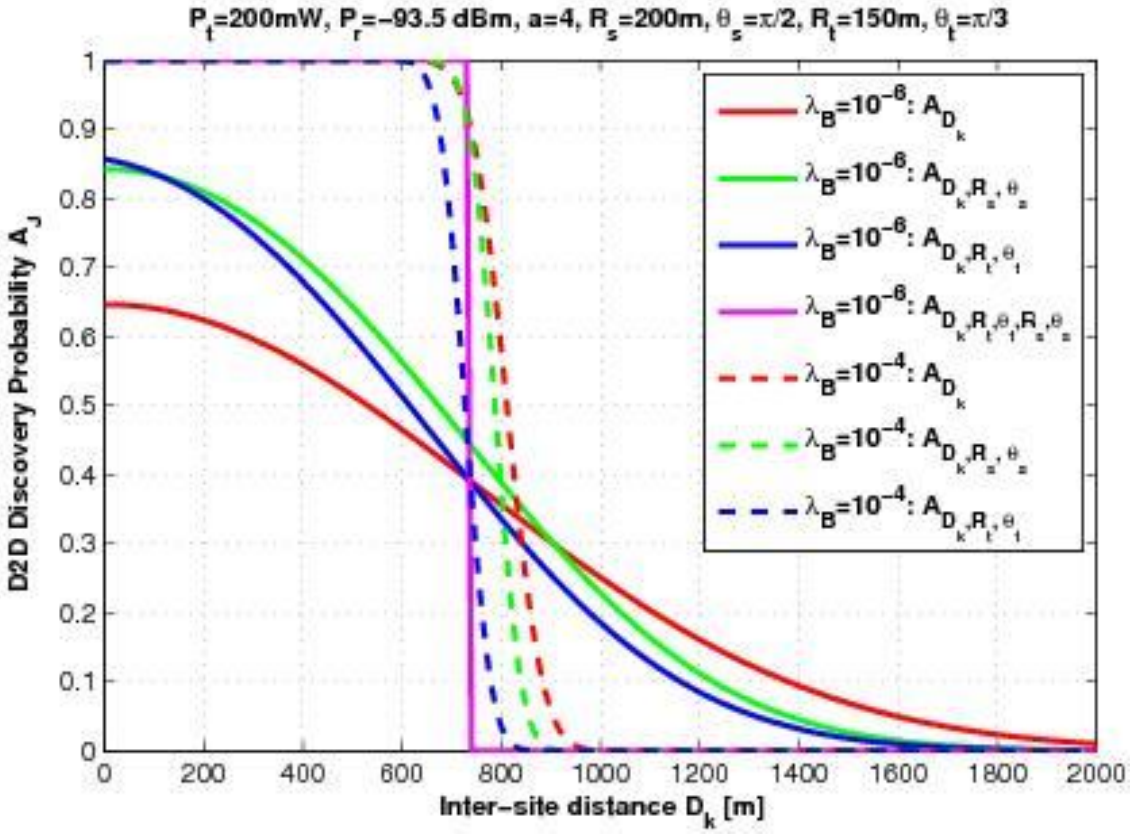

Figure 20: D2D Discovery Probability given D_k vs. Inter-site distance D_k

We now examine the impact of the inter-site distance D_k on the D2D discovery probability given knowledge of at least the distance D_k (Figure 20). Firstly, we observe that given the same set of location parameters, a higher BS density prolongs the tail of the D2D discovery probability, owing to the increased uncertainty on the D2D source and/or D2D target positions around their associated BS. This is also expected if we consider that for the given set of system parameters, the maximum range for successful D2D discovery is equal to $\left(\frac{P_t}{P_r}\right)^{\frac{1}{a}} = 813.3$ m, whereas the average distance between a user and its associated BS is equal to 157m and 1570m for $\lambda_B = 10^{-4}$ and $\lambda_B = 10^{-6}$, respectively, i.e. expected value of the Rayleigh distribution with parameter $\frac{1}{\sqrt{2\pi\lambda_B}}$. Hence, above a certain BS density, the performance of D2D discovery is primarily affected by the inter-site distance D_k and not the relative positions of the D2D peers, which can be approximated by the position of their associated BSs. This approach can reduce the overhead required for user positioning while leaving the D2D discovery probability unaffected.

For $\lambda_B = 10^{-4}$, we observe that the D2D discovery probability $\mathcal{A}_{D_k}$ is higher compared to the one given additional knowledge on $[R_t, \theta_t]$, i.e. $\mathcal{A}_{D_k,R_t,\theta_t}$. This can be explained as follows: conditioned on $[R_t = 200m, \theta_t = \pi/3]$ (Figure 17), the distance Z between the D2D peers is statistically higher compared to the scenario with no knowledge on $[R_t, \theta_t]$ (Figure 17), where the position of the D2D

target is considered to follow a symmetrical normal distribution around its associated BS $\left(\sigma^2 = \frac{1}{2\pi\lambda_B}\right)$. This effect is more prominent for $\lambda_B = 10^{-4}$, where the uncertainty on position of the D2D source is significantly reduced compared to the one for $\lambda_B = 10^{-6}$. Similar arguments can be used to compare $\mathcal{A}_{D_k}$ and $\mathcal{A}_{D_k,R_s,\theta_s}$.

3.4.3 Effect of Transmit Power

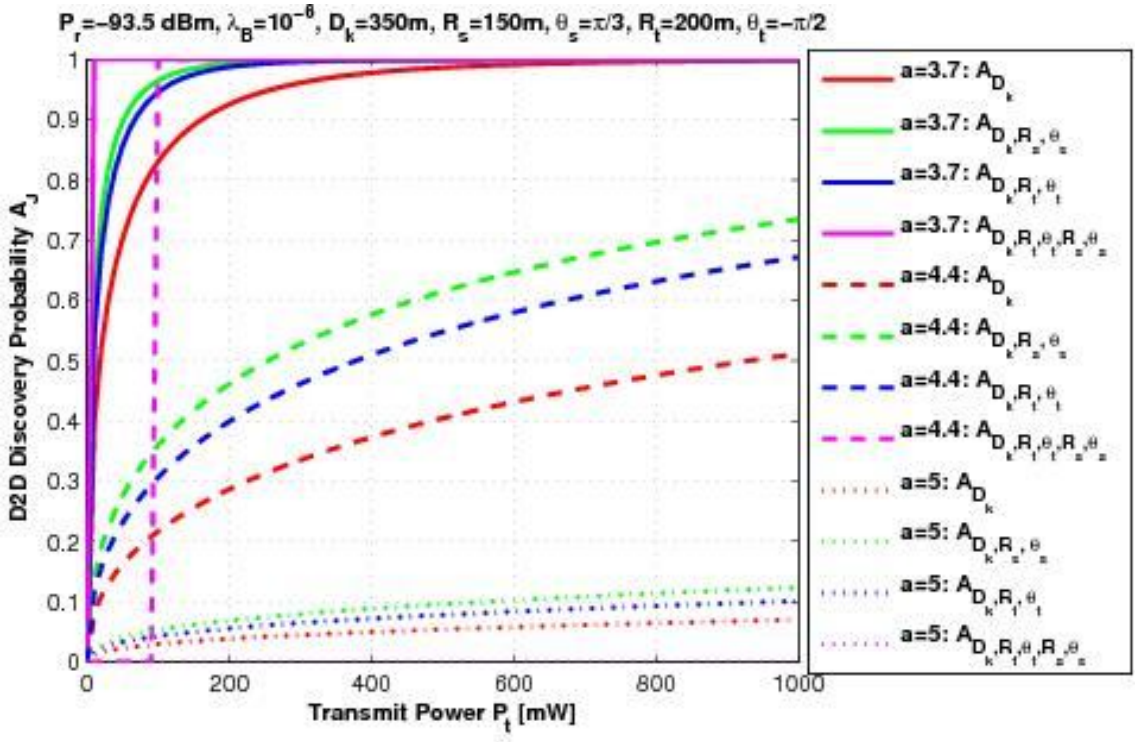

Figure 21: D2D Discovery Probability given D_k vs. Transmit power P_t

D2D discovery will be performed under unfavorable channel conditions, due to the lower height of the transmitter-receiver pair, the increased number of obstacles between the D2D peers, and the low transmit power required to avoid interference with other cellular connections. Under this viewpoint, in Figure 21 we plot the impact of the transmit power P_t on the D2D discovery probability under high path loss exponents and given information for at least the inter-site distance D_k. As expected, the D2D discovery probability increases with P_t under all combinations of location information. However, the (positive) impact of increasing P_t on the D2D discovery probability strongly depends on the path loss exponent governing the D2D channel. For example, for $a = 3.7$, we observe that $P_t = 200$ mW suffices to attain a D2D discovery probability higher than 90% for all combinations of location information parameters. On the other hand, for $a = 4.4$, the D2D discovery probability can be greatly improved with a slight increase in the transmit power whereas, for $a = 5$, it remains roughly unaffected. Note that, for the given set of parameters, additional knowledge on $[R_s, \theta_s]$ and/or $[R_t, \theta_t]$ significantly alters the statistical behavior of the D2D discovery probability, especially for $a = 4.4$.

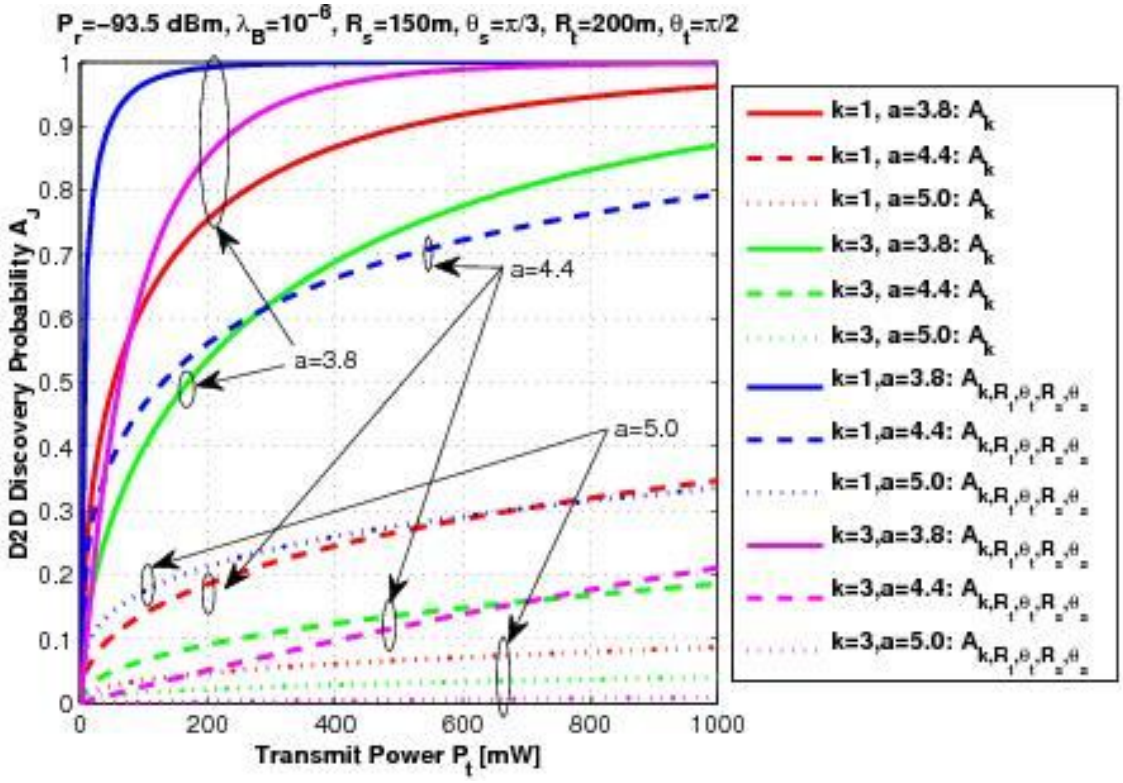

Figure 22: D2D Discovery Probability given k vs. Transmit Power P_t

In Figure 22, we depict the relation between P_t and the D2D discovery probability given at least the neighboring degree k. As expected, a higher k reduces the D2D discovery probability, due to the statistical increase on the inter-site distance D_k. By comparing the impact of P_t on $\mathcal{A}_{k,R_t,\theta_t,R_s,\theta_s}$ and $\mathcal{A}_k$ for $k = 1$, it can also be seen that the knowledge on $[R_s, \theta_s]$ and $[R_t, \theta_t]$ greatly alters the statistical behavior of the D2D discovery probability with respect to P_t. However, differently from the results in Figure 21, this applies for all path loss exponents under scope. This property weakens for higher neighboring degrees ($k = 3$).

To summarize, when the EPC is aware of the neighboring degree k instead of the distance D_k, additional knowledge on the relative positions of the D2D peers may significantly improve the accuracy of network-assisted D2D discovery, especially for low k. On the other hand, the employment of network-assisted D2D discovery can significantly reduce unnecessary transmissions of D2D discovery signals that increase the network interference and deplete the battery at the mobile terminals. To this direction, the presented results can be used to assist the D2D source upon selecting an appropriate transmit power for a prescribed D2D discovery probability target, by exploiting fundamental location information at the EPC.

3.4.4 Effect of the Angle of the D2D target

In Figure 23, we plot the statistical behavior of the D2D discovery probability with respect to θ_t (Figure 17), for all combinations that include θ_t. Obviously, the statistical behavior of the remainder D2D discovery probabilities remains unchanged with respect to θ_t. Given full knowledge on the network layout, we observe that the D2D discovery can be either successful or not. However, depending on the fixed parameters, there exists a θ_t interval within which the D2D discovery is always successful, i.e. $A_{D_k,R_t,\theta_t,R_s,\theta_s} = 1$. Moreover, we observe that the probability $\mathcal{A}_{D_k,R_t,\theta_t,R_s,\theta_s}$ for $\theta_s = \pi/3$ is a mirror function of $\mathcal{A}_{D_k,R_t,\theta_t,R_s,\theta_s}$ for

$\theta_s = -\pi/3$ with respect to 180^o, which corresponds to the direction towards the associated BS of the D2D source. For the given parameters in Figure 23, an increase to the distance R_s symmetrically expands the θ_t interval where $\mathcal{A}_{D_k,R_t,\theta_t,R_s,\theta_s} = 1$ towards both directions. This result follows from the given θ_s under scope, since for $\theta_s = \pi/3$ a higher distance R_s reduces the distance Z between the D2D peers.

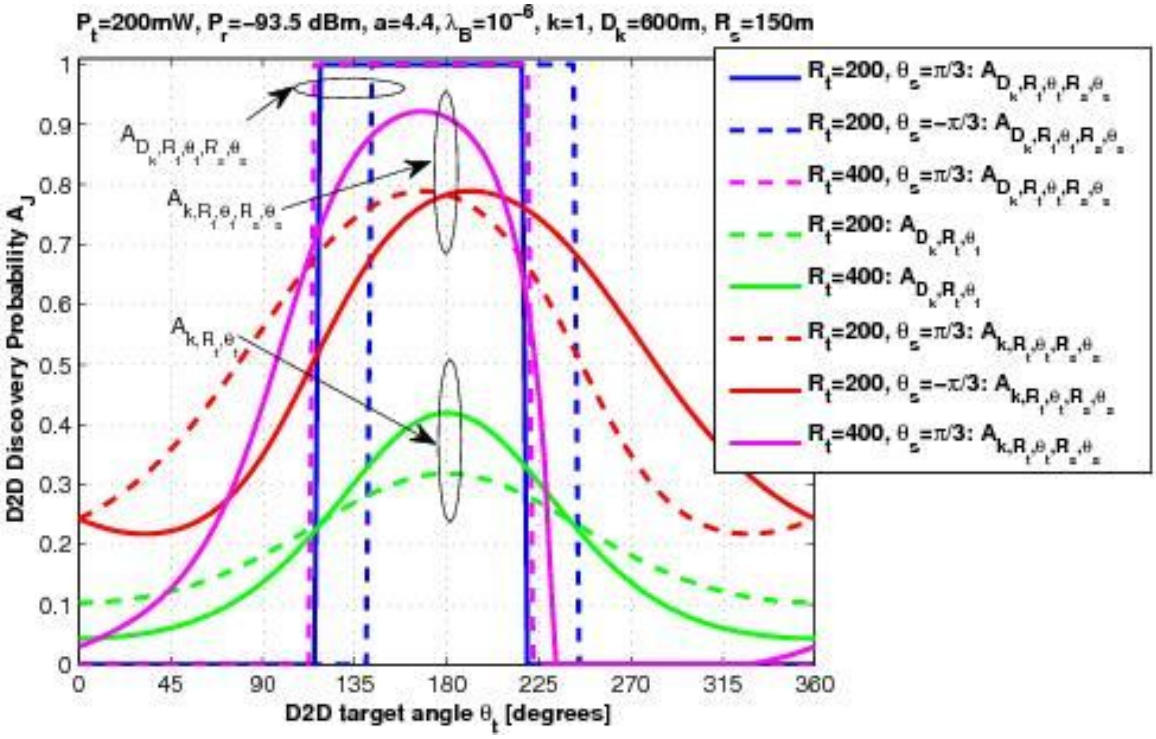

Figure 23: D2D Discovery Probability vs. D2D target angle θ_t

When the EPC is aware of only the parameters $\{D_k, R_t, \theta_t\}$, the corresponding D2D discovery probability is higher for all angles θ_t that reside closer to the associated BS of the D2D source (green line), i.e. 180^o. On the other hand, an increase to the distance R_t enlarges the D2D discovery probability for θ_t towards the same direction and reduces it for the ones residing towards the opposite one (green dashed line). Both these results are expected if we consider that in the absence of knowledge of $[R_s, \theta_s]$, the D2D source is considered to follow a symmetric normal distribution around its associated BS.

Similar to $\mathcal{A}_{D_k,R_t,\theta_t,R_s,\theta_s}$, the D2D discovery probability $\mathcal{A}_{k,R_t,\theta_t,R_s,\theta_s}$ for $R_s = \pi/3$ is mirrored for $R_s = -\pi/3$, with respect to the direction towards the associated BS of the D2D source (180^o). However, in contrast with $\mathcal{A}_{D_k,R_t,\theta_t,R_s,\theta_s}$, an increase to the distance R_t 'stretches' the probability $\mathcal{A}_{k,R_t,\theta_t,R_s,\theta_s}$ towards the direction of the D2D source in a non-symmetric manner. This behavior follows from the knowledge of the EPC on the relative position of the D2D source and the fact that the R_t is now higher ($R_t = 400$ m). The combination of these conditions creates bias on the D2D discovery probability towards specific coordinates for the D2D target.

It follows that the knowledge on the relative positions of the D2D peers majorly impacts the D2D discovery performance, especially in sparse to medium network deployments where the uncertainty on the relative positions of the users (around their associated BSs) is high. The results in Figure 23 also indicate that, under certain conditions, the estimation accuracy for the angles θ_t and θ_s can be relaxed without affecting the performance of network-assisted D2D discovery.

Such an approach could significantly reduce the overheads required for accurately measuring the AoA of the D2D peers at the associated BSs.

3.5 Key Contributions and Conclusions

In this paper, we have analyzed the statistical behavior of the distance between two D2D peers conditioned on existing knowledge for the cellular network deployment. The ccdf expressions were used to analyze the performance of network-assisted D2D discovery and provide useful insights on how different levels of location awareness affect its performance. We also have examined how unplanned cellular network densification affects the performance of network-assisted D2D discovery and provided analytical expressions for the optimal BS density that maximizes the D2D discovery probability. Accordingly, we investigated the key performance tradeoffs inherent to the network-assisted D2D discovery and provided useful guidelines for its design in random spatial networks. Among others, the present results can be used to select the transmit power at the D2D source for a given D2D discovery probability target, reduce unnecessary D2D discovery signals, identify the optimal BS density for network-assisted D2D discovery, and relax the accuracy of user positioning while leaving the D2D discovery probability unaffected.To the best of our knowledge, this is was first work to analytically address the challenging issue of network-assisted D2D discovery in random spatial networks.

Our key contributions can be summarized as follows:

- We have derived closed-form expressions for the conditional pdf and ccdf of the distance Z between two D2D peers, given various combinations of location information parameters including at least the distance D_k or the neighboring degree k. The derived expressions can be readily used to analyze problems that involve the distance Z between two D2D peers, such as interference analysis or hybrid automatic repeat request [5].
- We have analyzed the performance of network-assisted D2D discovery given the most prominent combinations of location information parameters. Our analysis readily quantifies how different levels of location knowledge affect the D2D discovery probability. The derived expressions can also be used to analyze the performance of cluster-based D2D discovery in the absence of network coverage or serve as an upper performance bound for SINR-based D2D discovery.
- We have examined the behavior of the D2D discovery probability with respect to key system parameters, with the emphasis given on the BS density. We have identified conditions under which the D2D discovery is optimized and provide analytical expressions for computing the optimal BS density.
- We have provided useful design guidelines for network-assisted D2D discovery. We have shown that above a certain BS density, the D2D discovery probability $\mathcal{A}_J$ is primarily affected by the inter-site distance D_k and that, under certain conditions, denser network layouts reduce the D2D discovery probability. We also have shown that in medium to high density networks the probability $\mathcal{A}_J$ may increase with k.

4. NETWORK-ASSISTED ENERGY-EFFICIENT HANDOVER FOR MACROCELL-FEMTOCELL NETWORKS

Femtocells are attracting a fast increasing interest nowadays, as a promising solution to improve indoor coverage, enhance system capacity, and lower transmit power. Technical challenges still remain, however, mainly including interference, security and mobility management, intercepting wide deployment and adoption from mobile operators and end users. This section describes a novel handover decision policy for the two-tier LTE-Advanced network, towards reducing power transmissions at the mobile terminal side. The proposed policy is LTE-Advanced backward-compatible, as it can be employed by suitably adapting the handover hysteresis margin with respect to a prescribed SINR target and standard LTE-Advanced measurements. Simulation results reveal that compared to the widely-adopted strongest cell policy, the proposed policy can greatly reduce the power consumption at the LTE-Advanced mobile terminals, and lower the interference network-wide. The proposed policy is integrated in a novel handover decision algorithm for the macrocell – femtocell network, which additionally accounts for the access rights of the user at the target femtocells as well as the resource availability at the candidate base stations. Two different signaling procedures are also proposed to implement the proposed algorithm in the LTE-A system, while extensive system-level simulation results demonstrate its performance.

The remainder of this section is organized as follows. In section 4.1, we present our system model and discuss the strongest-cell handover decision policy. In section 4.2, we describe the proposed energy-efficient handover decision policy while in section 4.3 we include system-level simulation results to assess its performance. In section 4.4, we present the proposed energy-efficient handover decision algorithm and in section 4.5 we investigate how it can be implemented, in terms of signaling, in the LTE-A system. In section 4.6, we provide extensive system-level simulation results on its performance by using the evaluation methodology of the Small Cell Forum. Finally, in section 4.7 we draw our conclusions and summarize our key contributions.

4.1 System Model

4.1.1 System Description

We consider a LTE-A network, operating in the band set $\boldsymbol{N} \coloneqq \{1, \dots, N\}$. Let $\boldsymbol{R_n} \coloneqq \{1, \dots, R_n\}$ denote the set of Resource Blocks (RB) in band $n \in \boldsymbol{N}$, $\boldsymbol{C_n}$ the set of cells operating in band n, including both eNBs and HeNBs, and $\boldsymbol{U_n}$ the set of active users connected to a cell in $\boldsymbol{C_n}$. For a tagged user u, let $\overline{\gamma}^{u}_{target}$ denote the prescribed mean SINR target for attaining the required QoS, $RSRP^{u}_{min}$ the minimum required RSRP value for sustaining wireless connectivity with the network, and $\boldsymbol{L_u} \subseteq \bigcup_{n \in \boldsymbol{N}} \boldsymbol{C_n}$ the set of candidate and accessible LTE-A cells identified during the network discovery phase. Given two network nodes x and y, which can be either LTE-A cells or UEs, let $\overline{P}^{T}_{x}$ denote the transmit power of node x, $\left(\overline{\sigma}^{T}_{x}\right)^2$ the noise power in node x, and $\overline{h}^{T}_{x \to y}$ the channel gain between nodes x and y, all averaged within the operating bandwidth of the respective nodes over the time interval T. Accordingly, the mean UL SINR between user $u \in \boldsymbol{U_n}$ and cell $s \in \boldsymbol{C_n}$ for the time interval T is given as follows:

$$\overline{\gamma}_{u\to s}^{T} = \frac{\overline{P}_{u}^{T}\cdot\overline{h}_{u\to s}^{T}}{\sum_{c\in \boldsymbol{C_n}-\{s\}}\overline{P}_{c}^{T}\cdot\overline{h}_{c\to s}^{T}+\sum_{u'\in \boldsymbol{U_n}-\{u\}}\overline{P}_{u'}^{T}\cdot\overline{h}_{u'\to s}^{T}+\left(\overline{\sigma}_{s}^{T}\right)^{2}} \quad (4.1)$$

where the numerator corresponds to the receive signal strength for user u in the serving cell s, the first and the second terms of the denominator to the interference caused by cells and users operating in-band, respectively, and the third term to the noise power at cell s. By using (4.1) and taking into account the requirement for sustaining the prescribed mean SINR target $\overline{\gamma}_{target}^{u}$, the mean UE transmit power of user u for a candidate cell $c \in \boldsymbol{L_u}$ can be estimated as follows:

$$\overline{P}_{u\to c}^{T} = \frac{\overline{\gamma}_{target}^{u}\cdot\left(\sum_{c'\in \boldsymbol{C_n}-\{c\}}\overline{P}_{c'}^{T}\cdot\overline{h}_{c'\to c}^{T}+\sum_{u'\in \boldsymbol{U_n}-\{u\}}\overline{P}_{u'}^{T}\cdot\overline{h}_{u'\to c}^{T}+\left(\overline{\sigma}_{c}^{T}\right)^{2}\right)}{\overline{h}_{u\to c}^{T}} \quad (4.2)$$

Note that the positive impact of handing over to cell $c \in \boldsymbol{L_u}$, in terms of lower interference, is incorporated in (4.2) by omitting the interference caused to cell c by the ongoing user connection with the current serving cell s, i.e., $\overline{P}_{u}^{T}\cdot\overline{h}_{u\to s}^{T}$. Eq. (4.2) can also be used to estimate the mean UE power consumption of the tagged user u in cell c, owing to transmit power.

Table 7: Signal quality measurements for the LTE-A system [16]

Measurement	**Measured by**	**Notation**
Reference Signal Received Power (RSRP)	UE	$RSRP_{c\to u}^{T}$
E-UTRAN Carrier Received Signal Strength Indicator (RSSI)	UE	$RSSI_{c\to u}^{T}$
Reference Signal Received Quality (RSRQ)	UE	$RSRQ_{c\to u}^{T}$
Downlink Reference Signal Transmitted Power (DL RS Tx)	E-UTRAN	$P_{c,RS}^{T}$
Received Interference Power (RIP) over the RB set $\boldsymbol{R_n}$	E-UTRAN	$\overline{I}_{c}^{T}$

The LTE-A standard describes a wide set of signal quality measurements for the LTE-A access network and the UEs in [16], which can be utilized to accurately estimate the mean UL SINR in (4.1) and the mean UE transmit power in Eq. (4.2). The LTE-A measurements used in this paper, along with the respective notation for a tagged user u, cell c, and time interval T, are summarized in Table I. Note that the RIP measurement in Table I, denoted by $\overline{I}_{c}^{T}$, corresponds to the linear average of the RIP measurements performed over the utilized RB of cell c. To the remainder of this paper, it is assumed that for all the UEs connected to it, each serving cell has a consistent list of candidate cells and signal quality measurements describing their status. Even though the acquisition of these measurements is described in section 4.5, the network discovery phase is outside the scope of this paper.

4.1.2 Strongest Cell Handover Decision Algorithm

In the context of LTE-A, the SC HO decision algorithm consists of handing over to the candidate cell with the highest RSRP status, which also exceeds over the RSRP status of the serving cell plus a policy-defined HHM for a time period namely the Time To Trigger (TTT) [51]. The HHM is typically introduced to

mitigate frequency-related propagation divergences, and the negative impact of the ping-pong effect. Based on the system model description in Section 3.1, the SC HO decision algorithm can be summarized as follows:

$$\arg\max_{c\in \boldsymbol{L_u}} RSRP^{TTT}_{c\to u,(dB)} \coloneqq \left\{c \middle| RSRP^{TTT}_{c\to u,(dB)} > RSRP^{TTT}_{s\to u,(dB)} + HHM_{c,(dB)}\right\} \quad (4.3)$$

where $HHM_{c,(dB)}$ corresponds to the HHM for cell $c \in \boldsymbol{L_u}$, and $X_{(dB)}$ to the value of X in decibels (dB). Taking into account the definition of the RSRP measurement [16], it follows that:

$$RSRP^{TTT}_{c\to u} = P^{TTT}_{c,RS} \cdot \overline{h}^{TTT}_{c\to u} \quad (4.4)$$

By substituting (4.4) to (4.3), it can be shown that the SC algorithm facilitates mobility towards candidate cells with higher RS transmit power, and/or improved channel gain. However, in order for the SC algorithm to improve the channel gain for the tagged LTE-A link (4.4), comparable RS transmit powers should be radiated among the candidate cells. However, this is not in effect in the two-tier LTE-A network provided that a) eNBs typically radiate higher RS transmit power compared to HeNBs, and b) femtocell self-optimization can result in different RS transmit powers between the HeNBs. In addition, the SC algorithm does not necessarily improve the SINR performance ((4.1) and (4.2)) given that divergent interference levels are expected at the LTE-A cell sites owing to the unplanned deployment. The SC algorithm's unawareness on the actual RS transmit power and the interference level at the cell sites, is also expected to increase the UE transmit power, which in turn rises the interference level network-wide and exhausts the UE battery lifetime. The value of the HHM parameter is another open issue for the SC algorithm.

4.2 The Proposed Handover Decision Policy

In this section we propose the UE Transmit Power Reduction (UTPR) policy in the following, which relies on handing over to the cell with the minimum required UE transmit power, while maintaining the mean SINR target.

The following analysis is pursued to derive the HHM required for minimizing the UE power transmissions, based on the available set of standard LTE-Advanced measurements in Table 13. It is assumed that user u receives service from cell s, which has consistent LTE-Advanced measurements describing the status of every candidate cell $c \in \boldsymbol{L_u}$ for user u, for the time interval $T = TTT$. Using (4.4) under the assumption of a symmetric channel gain, the following estimation can be made:

$$\overline{h}^{T}_{u\to c} \cong \overline{h}^{T}_{c\to u} = \frac{RSRP^{T}_{c\to u}}{P^{T}_{c,RS}} \quad (4.5)$$

By the RIP measurement definition in [16], it follows that:

$$\overline{I}^{T}_{c} = \left(\sum_{c'\in \boldsymbol{C_n}-\{c\}} \overline{P}^{T}_{c'} \cdot \overline{h}^{T}_{c'\to c} + \sum_{u'\in \boldsymbol{U_n}} \overline{P}^{T}_{u'} \cdot \overline{h}^{T}_{u'\to c} + \left(\overline{\sigma}^{T}_{c}\right)^2\right) \quad (4.6)$$

Using (4.3), (4.5), and (4.6), it can be shown that the UE power transmission on the serving cell s is given by (4.7).

$$\overline{P}^{T}_{u} \triangleq \overline{P}^{T}_{u\to s} = \frac{\overline{\gamma}^{u}_{target} \cdot P^{T}_{s,RS} \cdot \overline{I}^{T}_{s}}{RSRP^{T}_{s\to u}} \quad (4.7)$$

Following a similar approach, the UE transmit power on the candidate cell c can be estimated as follows:

$$\overline{P}_{u\to c}^{T} = \frac{\overline{\gamma}_{target}^{u}\cdot P_{c,RS}^{T}\cdot\left(\overline{I}_{c}^{T}-\overline{P}_{u}^{T}\cdot\overline{h}_{u\to c}^{T}\right)}{RSRP_{c\to u}^{T}} \quad (4.8)$$

where the term $\overline{P}_{u}^{T}\cdot\overline{h}_{u\to c}^{T}$ is introduced to include the positive impact of handing over to cell $c \in \boldsymbol{L_u}$, if cells c and s operate in the same LTE-Advanced band (if not, it is omitted), i.e, if $c,s \in \boldsymbol{C_n}$. Accordingly, handing over to the candidate cell c, is expected to result in reduced UE transmit power compared to the one used in the current serving cell s, if the following are in effect:

$$\overline{P}_{u\to s}^{T} > \overline{P}_{u\to c}^{T} \quad (4.9)$$

$$\frac{\overline{\gamma}_{target}^{u}\cdot P_{s,RS}^{T}\cdot\overline{I}_{s}^{T}}{RSRP_{s\to u}^{T}} > \frac{\overline{\gamma}_{target}^{u}\cdot P_{c,RS}^{T}\cdot\left(\overline{I}_{c}^{T}-\overline{P}_{u}^{T}\cdot\overline{h}_{u\to c}^{T}\right)}{RSRP_{c\to u}^{T}} \quad (4.10)$$

$$RSRP_{c\to u}^{T} > RSRP_{s\to u}^{T}\cdot\frac{P_{c,RS}^{T}\cdot\left(\overline{I}_{c}^{T}-\overline{P}_{u}^{T}\cdot\overline{h}_{u\to c}^{T}\right)}{P_{s,RS}^{T}\cdot\overline{I}_{s}^{T}} \quad (4.11)$$

where (4.10) is derived by using (4.7), and (4.8), and (4.11) by rearranging (4.10). Note that the parameter $\overline{P}_{u}^{T}$ is given by (4.7). By taking the respective parameter values in dB, (4.11) can be rearranged as follows:

$$RSRP_{c\to u,(dB)}^{TTT} > RSRP_{s\to u,(dB)}^{TTT} + HHM_{c,(dB)}^{UTPR} \quad (4.12)$$

where the parameter $HHM_{c,(dB)}^{UTPR}$ is given by (4.13).

$$HHM_{c,(dB)}^{UTPR} = \begin{cases} 10\log\frac{P_{c,RS}^{TTT}\cdot\left(\overline{I}_{c}^{TTT}-\overline{P}_{u}^{TTT}\cdot\overline{h}_{u\to c}^{TTT}\right)}{P_{s,RS}^{TTT}\cdot\overline{I}_{s}^{TTT}} & c,s \in \boldsymbol{C_n} \\ 10\log\frac{P_{c,RS}^{TTT}\cdot\overline{I}_{c}^{TTT}}{P_{s,RS}^{TTT}\cdot\overline{I}_{s}^{TTT}} & otherwise \end{cases} \quad (4.13)$$

It can be seen that (4.12) can be utilized as a HO decision criterion for minimizing the UE power transmissions in the two-tier LTE-Advanced network. To achieve this, (4.13) can be incorporated in the standard LTE-Advanced HO procedure, as an adaptive HHM. Given that a HHM for mitigating the side-effects of user mobility is still required, the $HHM_{c,(dB)}^{UTPR}$ parameter should be incorporated as an additional HHM in the strongest cell HO decision policy. Taking this into account, the proposed UTPR HO decision policy can be described as follows:

$$\arg\max_{c\in\boldsymbol{L_u}} RSRP_{c\to u,(dB)}^{TTT} \coloneqq \left\{c \mid RSRP_{c\to u,(dB)}^{TTT} > RSRP_{s\to u,(dB)}^{TTT} + HHM_{c,(dB)} + HHM_{c,(dB)}^{UTPR}\right\} \quad (4.14)$$

Summarizing, the proposed UTPR policy is based on standard LTE-Advanced measurements, while it is employed by introducing an adaptive HHM to the standard LTE-Advanced HO procedure. The employment of the UTPR policy does not require any enhancements for the LTE-Advanced UEs. An enhanced network signaling procedure is necessitated, however, to convey the E-UTRAN measurements amongst the cells. This signaling procedure can be based on directly exchanging the required measurement information through the standard X2 – interface [26]. Alternatively, a core network entity can be deployed for gathering, maintaining, and disseminating the required E-UTRAN measurements on demand. This CN entity can also control the E-UTRAN measurement signaling load, i.e., LTE-Advanced measurement requests and reports, depending on the current CN load, the LTE-Advanced cells' status, and other network-related parameters.

4.3 Numerical Results

This section includes selected numerical results to evaluate the performance of the proposed HO decision policy in the two-tier LTE-Advanced network. The simulation scenario is based on the evaluation methodology described in [123], while the proposed UTPR policy is compared against the strongest cell HO decision policy, referred to as SC policy in the following.

4.3.1 Simulation Model and Parameters

A conventional hexagonal LTE-Advanced network is considered, including a main LTE-Advanced cluster composed of 7 LTE-Advanced cells, where each LTE-Advanced cell consists of 3 hexagonal sectors. The wrap-around technique is used to extend the LTE-Advanced network, by copying the main LTE-Advanced cluster symmetrically on each of the 6 sides. A set of blocks of apartments, referred to as *femtoblocks*, are uniformly dropped within the main LTE-Advanced cluster according to the parameter d_{FB}, which indicates the femtoblock deployment density within the main LTE-Advanced cluster, i.e., the percentage of the main LTE-Advanced cluster area covered with femtoblocks. Each femtoblock is modeled according to the dual stripe model for dense urban environments in [123]. According to it, each femtoblock consists of two stripes of apartments separated by a 10 m wide street, while each stripe has two rows of $A = 5$ apartments of size 10×10 m. For a tagged femtoblock, femtocells are deployed with a femtocell deployment ratio parameter r_{fc}, which indicates the percentage of apartments with a femtocell [113]. Each femtocell initially serves one associated user, while in general, it can serve up to 4 users. Femtocells and femtocell users are uniformly dropped inside the apartments. Each LTE-Advanced user is member of up to one CSG, where the CSG ID per user and femtocell is uniformly picked from the set $\{1, 2, 3\}$. Each LTE-Advanced sector initially serves ten macrocell users, which are uniformly distributed within it. The user mobility model consists of two parameters: the user speed v_t and the user direction φ_t [71], which are updated by:

$$v_t = N(\bar{v}, s_u) \text{ and } \varphi_t = N\left(\varphi_{t-1}, 2\pi - \varphi_{t-1} \tan\left(\frac{\sqrt{v_t}}{2}\right) \Delta t\right) \quad (4.15)$$

where $\bar{v}$ indicates the mean user speed, s_u the speed standard deviation, Δt the time between two updates of the model, and $N(a, b)$ the Gaussian distribution [51]. Unless differently stated, it is assumed that $\bar{v} = 3$ km/h and $s_u = 1$ km/h.

The macrocell stations operate in a LTE-Advanced band centered at 2 GHz, utilizing a 5MHz bandwidth. The macrocell inter-site distance is set to 500m. The operating band for each femtocell is uniformly picked from a band set including the macrocell operating band and the two adjacent frequency bands of 5MHz bandwidth. The minimum required SINR per UE is set to $\overline{\gamma}_t^u = 3$ dB, while the communications are carried out in full buffer [123]. The shadowing standard deviation for the macrocell and femtocell stations are 8 and 4 dB, respectively, and the noise figures are set to 5 and 8 dB in that order. The macrocell downlink RS power transmissions are normally distributed with a mean of 23 dBm and standard deviation 3dB, while the femtocell downlink RS power transmissions are uniformly distributed within the [0,10] dBm interval. The UE power class is set to 23 dBm, and the maximum transmit power for the macrocell and femtocell stations are set to 43 and 10 dBm, respectively. The path loss is described by the models for the dual stripe layout [123], while the frequency-selective fading is

Rayleigh distributed [51]. Finally, the overall simulation time is set to 1000 sec with a simulation unit of $\Delta t = 1$ sec.

4.3.2 System-level Simulation Results

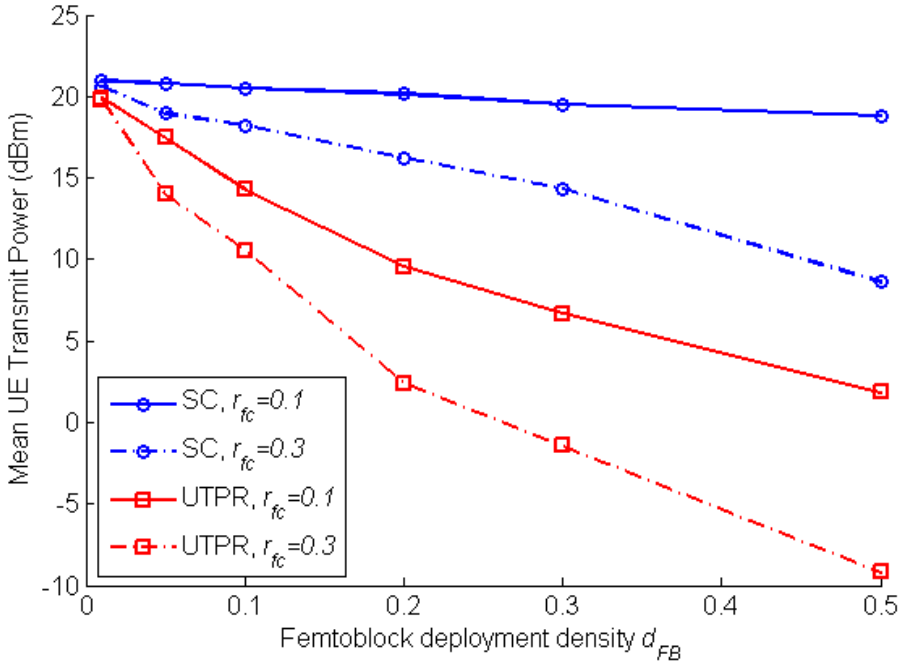

Figure 24:Mean UE transmit power versus the femtoblock deployment density

Figure 24 depicts the performance of the SC and UTPR policies in terms of mean UE transmit power. As expected, an increased femtoblock deployment density d_{FB} results in lower UE transmit power for both policies. However, a higher femtocell deployment density r_{fc} is required for the SC policy to lower the UE transmit power. On the contrary, the UTPR policy results in comparably lower UE transmit power, even for low r_{fc}, especially when a higher femtoblock deployment density characterizes the network layout. This improvement originates from the incorporation of the actual downlink RS and received interference power at the cell sites, while it varies from 1 to 20 dB, depending on the femtoblock and the femtocell deployment density. Given that the transmit power is the main UE power consumption contributor, this improvement corresponds to an equally reduced UE power consumption, too.

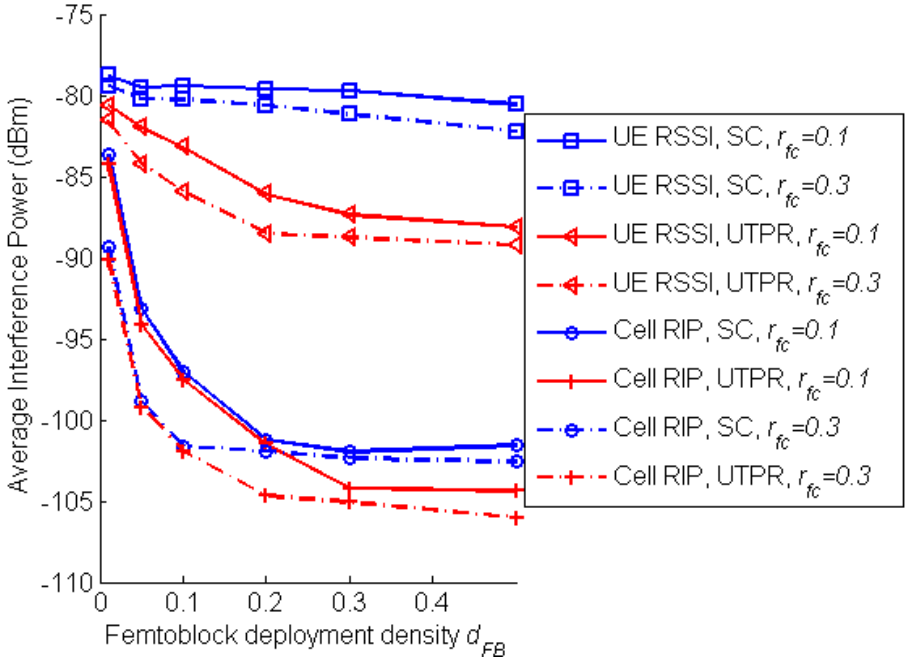

Figure 25: Average interference power at the UE and the LTE-Advanced cell sites, versus the femtoblock deployment density

Figure 25 illustrates that the proposed UTPR policy greatly lowers the Received Interference Power as well, both in terms of RSSI at the UEs (up to 8 dB) and RIP at the LTE-Advanced cell sites (up to 3 dB). This positive impact originates from the proposed policy's tendency in handing over to cells with lower RIP, leading to reduced number of UE interferers in congested bands and lower UE transmit power per band network-wide.

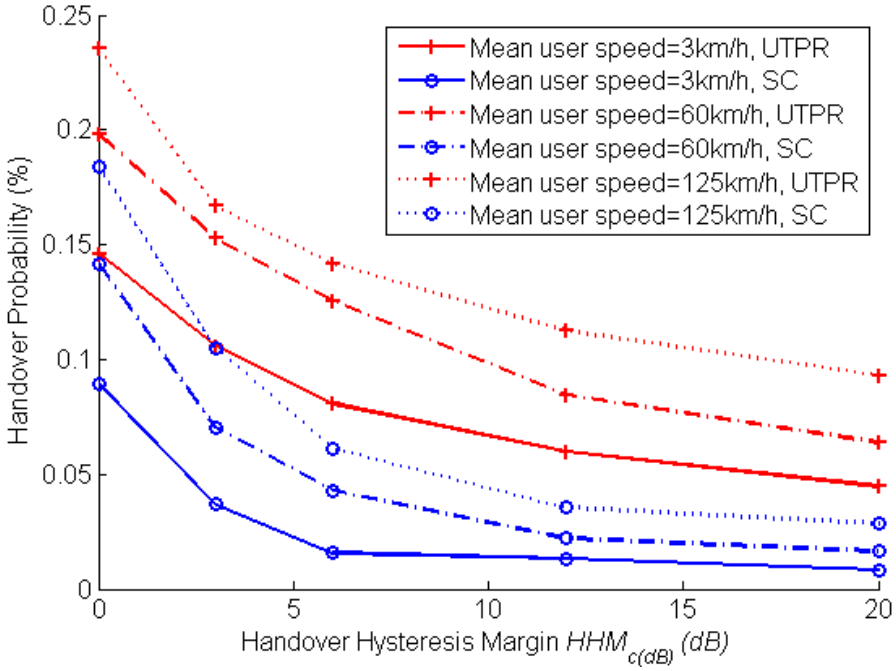

Figure 26: Handover probability versus the mobility HHM

Figure 26 plots the HO probability for varying mobility HHM, i.e, $HHM_{c,(dB)}$ parameter in (4.4), and (4.13). The results are derived for $d_{FB} = 0.05$, $r_{fc} = 0.2$, and three different mean user speeds, i.e., 3, 60 and 125 km/h. It can be seen

that although the employment of the proposed UTPR policy greatly lowers the UE power consumption owing to transmit power (Figure 24), and the network-wide RF interference (Figure 25), an increased HO probability is observed compared to the SC policy (Figure 26). This negative impact originates from a) the proposed policy's tendency to extend the femtocell utilization time, which results in increased sensitiveness on user mobility, and b) the fact that the proposed policy takes into account the RF interference at the cell sites, which is in general object to more variations compared to the RS power transmissions and the channel gain (SC policy). Figure 26 also shows that an increased $HHM_{c,(dB)}$ value can lower the HO probability for the UTPR policy, at comparable levels with the SC policy.

An increased $HHM_{c,(dB)}$ value, however, also comes with reduced potential to lower the UE power transmissions for the proposed HO policy (Figure 27). Nevertheless, the UTPR policy still results in significantly lower UE transmit power, varying from 3 to 8 dB for the scenario under consideration, depending on the mean user speed and the adopted $HHM_{c,(dB)}$ value. Note that the proposed policy lowers the UE transmit power even in high user speeds, where the femtocell tier is not utilized, owing to the proposed policy's capability to take into account the RF interference level at the macrocell sites. This positive impact follows from the random femtocell deployment pattern, which results in divergent RF interference to the LTE-Advanced macrocells.

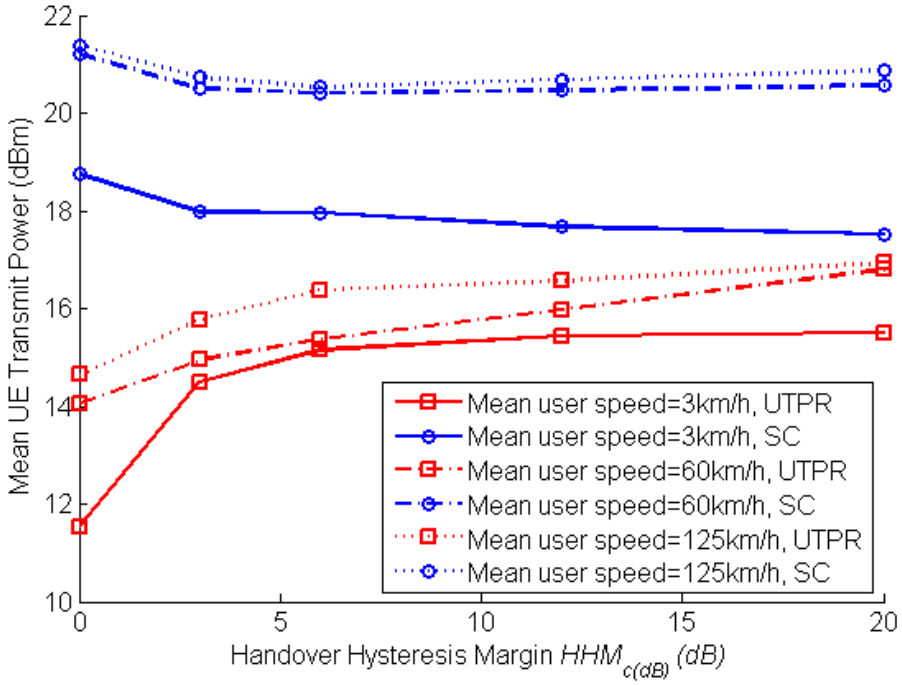

Figure 27: Mean UE transmit power versus the HHM

Summarizing, even though employing the proposed policy necessitates increased network signaling between cells, numerical results demonstrate greatly lower network-wide RF interference, and reduced UE power consumption owing to transmit power, compared to the strongest cell HO policy. The impact of using an increased HHM for mobility mitigation has also been investigated, both in terms of HO probability, and power saving potential.

4.4 The Proposed Handover Decision Algorithm

In this section, we extend the functionality of the proposed UTPR policy of the previous section and describe an advanced handover decision algorithm, which is

based on the employment of interference-aware and energy-efficient HO decision making. The key motivation for extending the proposed policy, is to additionally mitigate the negative impact of user mobility by additionally avoiding HOs to cells that can compromise wireless connectivity. Section 4.4.1 describes a methodology for sustaining wireless connectivity, while Section 4.4.2 describes a HO decision criterion for identifying the cell requiring the minimum UE transmit power. These procedures are integrated to the proposed algorithm in Section 4.4.3.

4.4.1 Sustained wireless connectivity

Let $\overline{P}_{max}^{x,T}$ denote the maximum allowed mean transmit power for node x, which corresponds either to the maximum transmit power of the target cell, or the UE power class, or a maximum transmit power constraint adapted with respect to interference mitigation criteria, e.g., as in [105]. Using Eq. (4.4) under the assumption of a symmetric channel gain, the mean UL channel gain between user u and cell c can be estimated as follows:

$$\overline{h}_{u\to c}^{T} \cong \overline{h}_{c\to u}^{T} = \frac{RSRP_{c\to u}^{T}}{P_{c,RS}^{T}} \qquad (4.16)$$

Let $\overline{h}_{c\to u,min}^{T}$ denote the minimum required channel gain for sustaining wireless connectivity between user u and cell c. Taking into account the minimum required RSRP value for sustaining wireless connectivity ($RSRP_{min}^{u}$), and the maximum allowed mean transmit power for user u and cell c, i.e., $\overline{P}_{max}^{u,T}$ and $\overline{P}_{max}^{c,T}$, respectively, the $\overline{h}_{c\to u,min}^{T}$ parameter can be estimated as follows:

$$\overline{h}_{c\to u,min}^{T} = \frac{RSRP_{min}^{u}}{\min\left(\overline{P}_{max}^{u,T}, \overline{P}_{max}^{c,T}\right)} \qquad (4.17)$$

Using Eq. (4.16) and (4.17) for the HO decision time horizon $T = TTT$ and under the condition for sustaining wireless connectivity $\overline{h}_{u\to c}^{TTT} > \overline{h}_{c\to u,min}^{TTT}$, the candidate cell set is limited as follows:

$$\boldsymbol{M_u} := \left\{ c \middle| RSRP_{c\to u,(dB)}^{TTT} > RSRP_{min,(dB)}^{u} + P_{c,RS,(dB)}^{TTT} - \min\left(\overline{P}_{max}^{u,TTT}, \overline{P}_{max}^{c,TTT}\right), and\ \mathrm{c} \in \boldsymbol{L_u} \right\} \qquad (4.18)$$

4.4.2 HO decision criterion for reduced mean UE transmit power

Having identified the candidate cell set that guarantees sustained wireless connectivity, this section describes a novel methodology for estimating the tagged user's mean UE transmit power on a per candidate cell basis, with respect to the prescribed mean SINR target and standard LTE-A measurements. The incorporation of the prescribed SINR target provisions for the supported QoS, while the utilization of standard LTE-A measurements provides an accurate estimation on the required mean UE transmit power. In the following, it is assumed that the tagged user u receives service from cell s, which has consistent measurements describing the status of every candidate cell $\mathrm{c} \in \boldsymbol{M_u}$ over the time interval $T = TTT$.

By taking into account the RIP measurement definition in [16], it follows that:

$$\overline{I}_{c}^{T} = \left(\sum_{c' \in \boldsymbol{C_n} - \{c\}} \overline{P}_{c'}^{T} \cdot \overline{h}_{c'\to c}^{T} + \sum_{u' \in \boldsymbol{U_n}} \overline{P}_{u'}^{T} \cdot \overline{h}_{u'\to c}^{T} + \left(\overline{\sigma}_{c}^{T}\right)^{2} \right) \qquad (4.19)$$

By using Eq. (4.2), (4.5), and (4.19), it can be readily shown that the mean UE transmit power for the current serving cell s can be estimated by (4.20).

$$\overline{P}_u^T = \frac{\overline{\gamma}_{target}^u \cdot P_{s,RS}^T \cdot \overline{I}_s^T}{RSRP_{s\to u}^T} \quad (4.20)$$

Under the same viewpoint, the mean UE transmit power for a candidate cell $c \in \boldsymbol{M_u}$ can be estimated as follows:

$$\overline{P}_{u\to c}^T = \begin{cases} \frac{\overline{\gamma}_{target}^u \cdot P_{c,RS}^T \cdot \left(\overline{I}_c^T - \overline{P}_u^T \cdot \overline{h}_{u\to c}^T\right)}{RSRP_{c\to u}^T}, & if\ c,s \in \boldsymbol{C_n} \\ \frac{\overline{\gamma}_{target}^u \cdot P_{c,RS}^T \cdot \overline{I}_c^T}{RSRP_{c\to u}^T}, & otherwise \end{cases} \quad (4.21)$$

where the condition $c,s \in \boldsymbol{C_n}$ is introduced to include the interference caused by the ongoing user link with cell s, i.e., $\overline{P}_u^T \cdot \overline{h}_{u\to s}^T$, if cells c and s operate in the same band. Let us now focus on the HO decision at the serving cell. A HO to the candidate cell $c \in \boldsymbol{M_u}$ is expected to lower the mean UE transmit power if the condition $\overline{P}_{u\to s}^{TTT} > \overline{P}_{u\to c}^{TTT}$ is met. By using (4.21) and taking the values in dB, it can be readily shown that this condition can be rearranged as follows:

$$RSRP_{c\to u,(dB)}^{TTT} > RSRP_{s\to u,(dB)}^{TTT} + HHM_{c,(dB)} \quad (4.22)$$

where the parameter $HHM_{c,(dB)}$ is adapted according to Eq. (4.23).

$$HHM_{c,(dB)} = \begin{cases} 10\log \frac{P_{c,RS}^{TTT} \cdot \left(\overline{I}_c^{TTT} - \frac{\overline{\gamma}_{target}^u \cdot P_{s,RS}^{TTT} \cdot \overline{I}_s^{TTT}}{RSRP_{s\to u}^{TTT}} \cdot \frac{RSRP_{c\to u}^{TTT}}{P_{c,RS}^{TTT}}\right)}{P_{s,RS}^{TTT} \cdot \overline{I}_s^{TTT}} & c,s \in \boldsymbol{C_n} \\ 10\log \frac{P_{c,RS}^{TTT} \cdot \overline{I}_c^{TTT}}{P_{s,RS}^{TTT} \cdot \overline{I}_s^{TTT}} & otherwise \end{cases} \quad (4.23)$$

Eq. (4.23) can be used as a HO decision criterion for lowering the mean UE transmit power in the two-tier LTE-A network. The latter is achieved by introducing the adaptive HHM in (4.23) in the standard HO decision procedure as follows:

$$\arg\max_{c\in \boldsymbol{M_u}} RSRP_{c\to u,(dB)}^{TTT} := \left\{c \middle|\ RSRP_{c\to u,(dB)}^{TTT} > RSRP_{s\to u,(dB)}^{TTT} + HHM_{c,(dB)}\right\} \quad (4.24)$$

Note that the aforementioned policy corresponds to the proposed UTPR policy of the previous section.

4.4.3 The Proposed HO Decision Algorithm

The proposed HO decision algorithm integrates the methodology for sustained wireless connectivity, and the HO decision criterion for reduced mean UE transmit power. To further reduce the HO failure probability, the proposed algorithm takes into account the resource availability on the candidate LTE-A cells, while to cope with critical LTE-A events, the decision time horizon of the proposed algorithm can be limited to a prescribed time duration, denoted by T_{max}. Finally, to deal with potential network signaling delay during the HO context acquisition procedure, the proposed algorithm handles the candidate cell list as a queue structure, which allows prioritized evaluation of the candidate cells with known status. Note that the required HO decision context consists of a) the operating frequency and bandwidth of the candidate cells, b) their current capacity value [28][30], c) the

signal quality measurements in Table 13, and d) the maximum allowed mean transmit power for user u and the candidate cells.

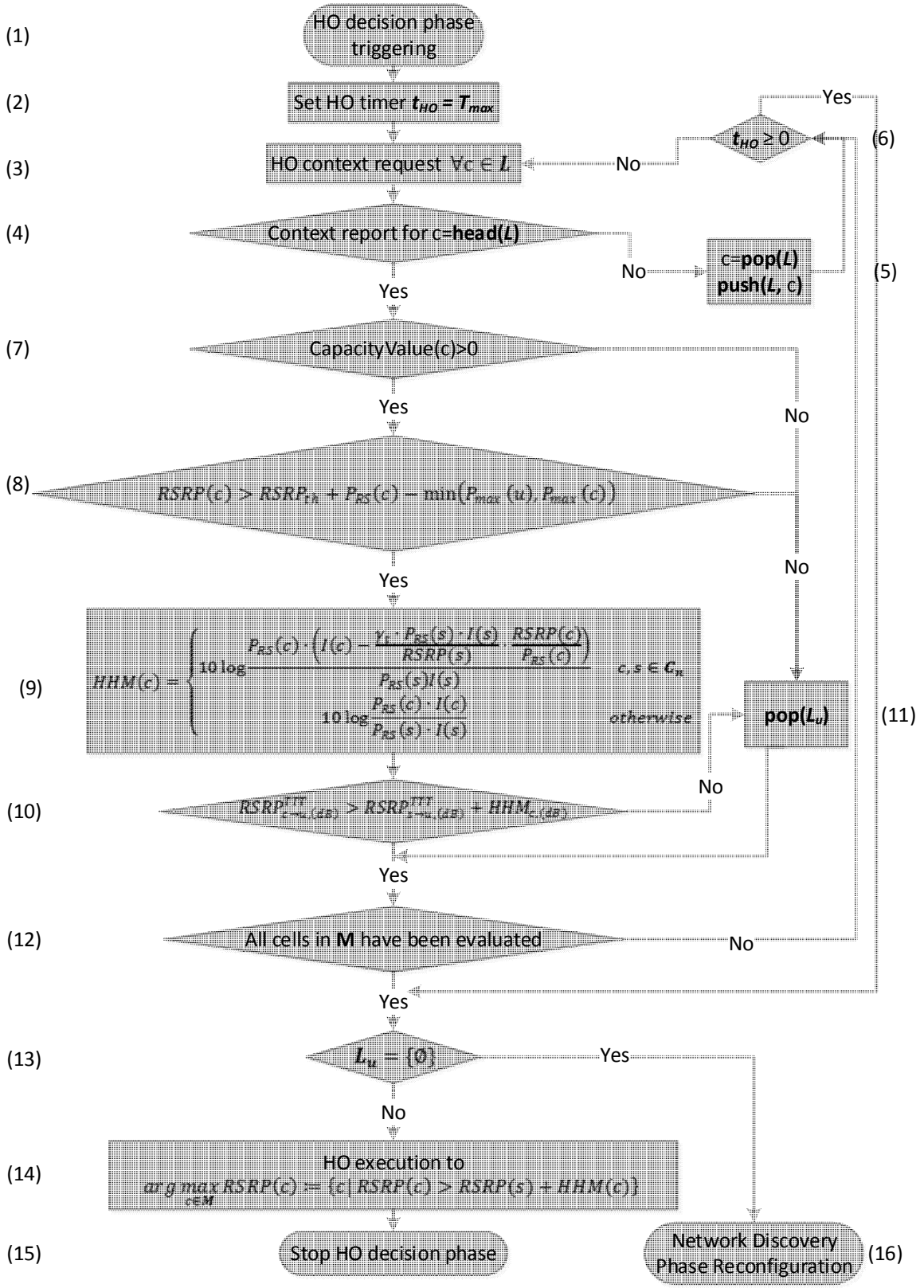

Figure 28: The proposed HO decision algorithm for the two-tier LTE-Advanced network

The proposed HO decision algorithm for the LTE-A network is illustrated in Figure 28. Upon HO decision triggering (step 1), the proposed algorithm initializes a HO decision countdown timer, denoted by t_{HO}, to the prescribed HO decision time

horizon T_{max} (step 2). This timer is assumed to be adapted with respect to critical LTE-A events, such as the ones described in [32].

In step 3, the proposed algorithm initiates a HO context acquisition request to derive the HO context describing the candidate cells' status. The network signaling procedure for performing this step is thoroughly investigated in Section 5. In step 4, the proposed algorithm handles the candidate cell set $\boldsymbol{L_u}$ as a queue structure and examines whether the required HO context for the queue head is reported to the serving cell, or not. If not, the proposed algorithm postpones the evaluation of the queue head in $\boldsymbol{L_u}$ (step 5), i.e., the queue head is moved to the end of the queue, and evaluates whether the HO decision countdown timer has expired (step 6). On the other hand, if the HO context is available to the serving cell, the proposed algorithm evaluates whether the residual capacity of the candidate cell c can support the tagged user (step 7). If not, the candidate cell c is removed from the queue structure $\boldsymbol{L_u}$ (step 11), and the evaluation procedure continues. If the residual capacity of cell c enables the support of the tagged user, the proposed algorithm evaluates whether the candidate cell c can sustain wireless connectivity (step 8). Note that this step employs the methodology for sustained wireless connectivity in section 4.4.1 with the addition of a HHM, denoted by $HHM_{c,(dB)}^{MM}$, which is introduced to further lower the HO probability for medium to high speed users. The impact of the $HHM_{c,(dB)}^{MM}$ parameter on the performance of the algorithm is investigated in section 4.5.

Once again, if the conditions for sustained wireless connectivity are not met, the proposed algorithm removes the candidate cell c from the queue (step 11), and proceeds with the evaluation procedure. If the condition in step (8) is met, however, the adaptive HHM for reduced UE transmit power is calculated in step (9). Accordingly, the HO decision criterion for reduced interference and energy consumption is employed (step 10), where a negative assessment leads to the removal of the candidate cell from the candidate cell set (step 11). If the HO decision criterion is met, the proposed algorithm checks whether all the candidate cells have been evaluated (step 12), and if not, the HO countdown timer is examined (step 6) and the loop in steps 3 to 12 is revisited. The proposed algorithm terminates this loop either when all the candidate cells have been evaluated (step 12), or when the HO countdown timer has expired (step 6). If at least one of these two stopping conditions is met, the proposed algorithm evaluates whether there exist candidate cells that meet the previous criteria (step 13). If such cells exist, the proposed algorithm initiates a HO to the candidate cell with the minimum required mean UE transmit power (step 14), and terminates the HO decision phase (step 15). In the opposite case, the proposed algorithm initiates a network discovery phase reconfiguration (step 16).

4.5 Handover Signaling Considerations

This section presents the feasible HO execution scenarios for the two-tier LTE-A network and describes two different network signaling approaches for employing the proposed algorithm, depending on whether the required HO context is reported and maintained in a network entity, or not. The first signaling approach, referred to as the reactive approach, is based on acquiring the HO context on demand to the candidate cells. The second signaling approach, referred to as the proactive approach, is based on acquiring the HO context on demand to the network entity which is responsible for maintaining and disseminating this context to the LTE-A cells. This HO context management entity can be either an LTE-A

core network entity, e.g., the MME, or a peripheral entity such as the ANDSF [20]. Without loss of generality, in the following it is assumed that the MME plays the role of the HO context management entity for the proactive approach.

Different from LTE Rel. 8/9, the LTE-A standard supports direct communication between the HeNBs through the standard X2 interface [27][28]. X2-based HO execution between HeNBs, however, is allowed only if no access control at the MME is needed, i.e., either when the HO is performed between closed/hybrid access HeNBs with the same CSG ID, or when the target HeNB supports open access. Even though the X2 interface is supported both between eNBs and between HeNBs, the LTE-A standard does not provision for direct X2-based communication between eNBs and HeNBs, due to the increased complexity required [59]. As a consequence, the HO execution between a) eNBs and HeNBs, or b) closed/hybrid HeNBs with different CSG IDs, or c) open access HeNBs, can only be employed through the MME and the standard S1-interface [29][30]. Table 8 summarizes the feasible HO execution scenarios for the two-tier LTE-A network and indicates the interface under use, depending on whether access control is required on the target cell, or not. Note that access control does not apply in the HO execution scenarios 1 and 2, i.e., when the target cell is an eNB, and that the serving cell in the HO scenario 3 can be either an eNB, or HeNB. The proposed HO decision algorithm applies to all the HO execution scenarios in Table 8, which can also be visually validated in Figure 10. To this end, the remainder of this section discusses the signaling procedures required for employing it, under both the reactive and the proactive HO context acquisition approaches.

Table 8: HO execution scenarios in the two-tier LTE-A network

HO Scenario	Serving Cell	Target Cell	Access Control	HO Type	HO Execution Interface
1	eNB	eNB	Does not apply	Regular E-UTRAN	X2
2	HeNB	eNB	Does not apply	Outbound from HeNB	S1
3	(H)eNB	HeNB	Yes	Inbound to HeNB	S1
4	eNB	HeNB	No	Inbound to HeNB	S1
5	HeNB	HeNB	No	Inbound to HeNB	X2 / S1

Figure 29:Reactive HO context acquisition approach for the HO execution scenario 1 illustrates the signaling procedure for the HO scenario 1 under the reactive HO context acquisition approach. Steps 0 – 2 correspond to the cell search and measurement phase at the UE. The HO decision algorithm is triggered in step 3, where the serving eNB signals a HO context request towards the candidate eNB through the X2-interface (step 4). Upon reception of the HO context report (step 5), the serving eNB reaches to a HO decision (step 6), and initiates the standard HO execution procedure (steps 7 – 21) [18]. Different from the reactive approach, the proactive approach (Figure 30) includes a periodic MME-configured HO context acquisition phase (steps 1 – 2) prior to the HO

decision phase (steps 7 – 9). The HO context request/report signals in steps 7 – 8 are initiated towards the MME through the S1 interface, rather than the target eNB through the X2 interface. Note that both the network discovery and the HO execution phases, i.e., steps 3 – 5 and steps 10 – 24, respectively, follow the standard signaling procedure as in the reactive approach (Figure 29). Both the reactive and proactive signaling approaches for the HO execution scenario 2, i.e., HO from a HeNB to an eNB, are similar to the ones followed in Fig. 3 and 4, respectively, and they are omitted due to space limitations. The key difference between the HO execution scenarios 1 and 2 is that the signaling procedure between the serving HeNB and the target eNB is performed through the MME and the S1 interface, i.e., steps 4, 5, 7, 9, and 11 in Figure 29, and steps 10, 12, 14 in Figure 30, given that the LTE-A standard does not support X2-based communication between HeNBs and eNBs.

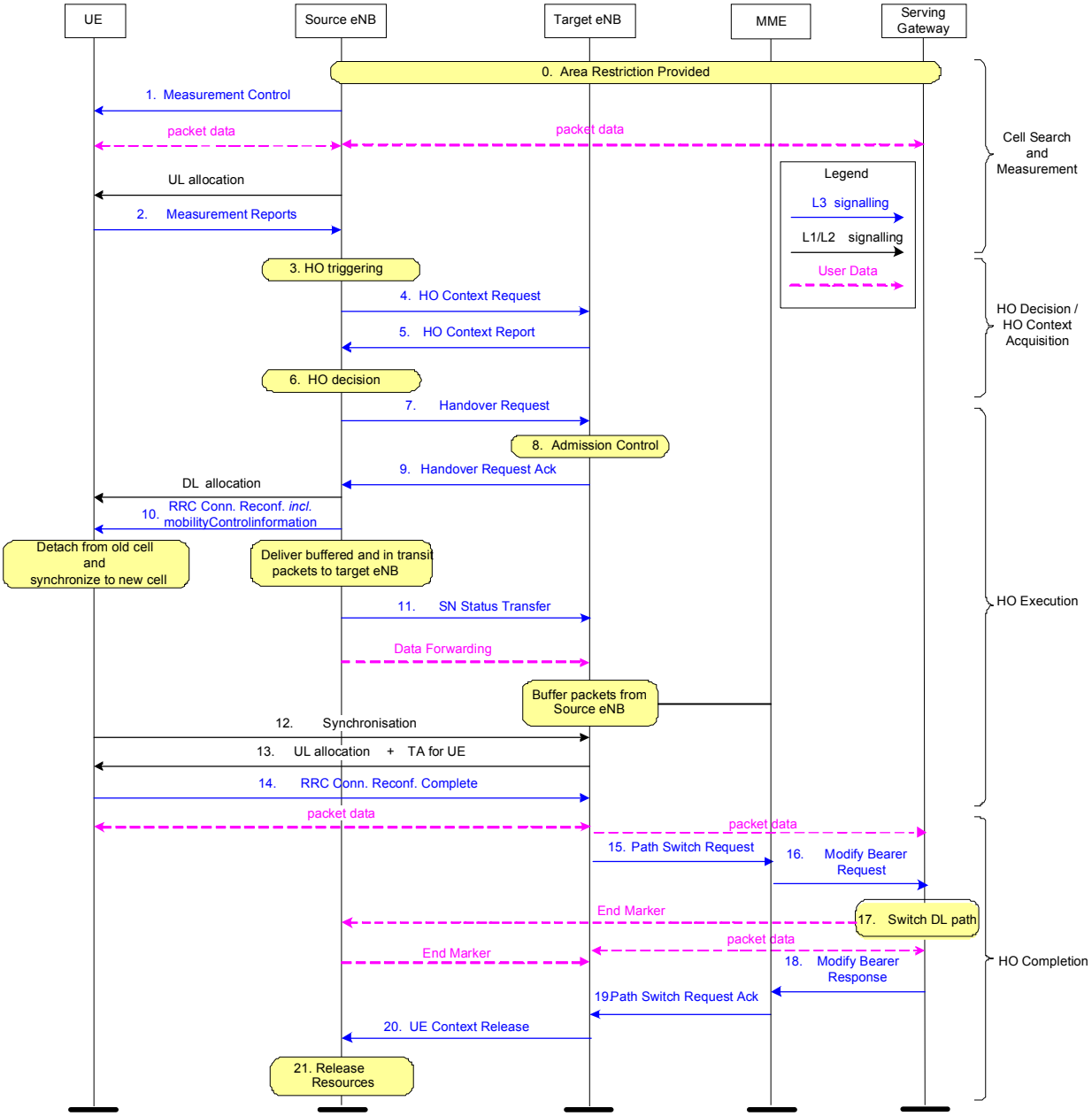

Figure 29:Reactive HO context acquisition approach for the HO execution scenario 1

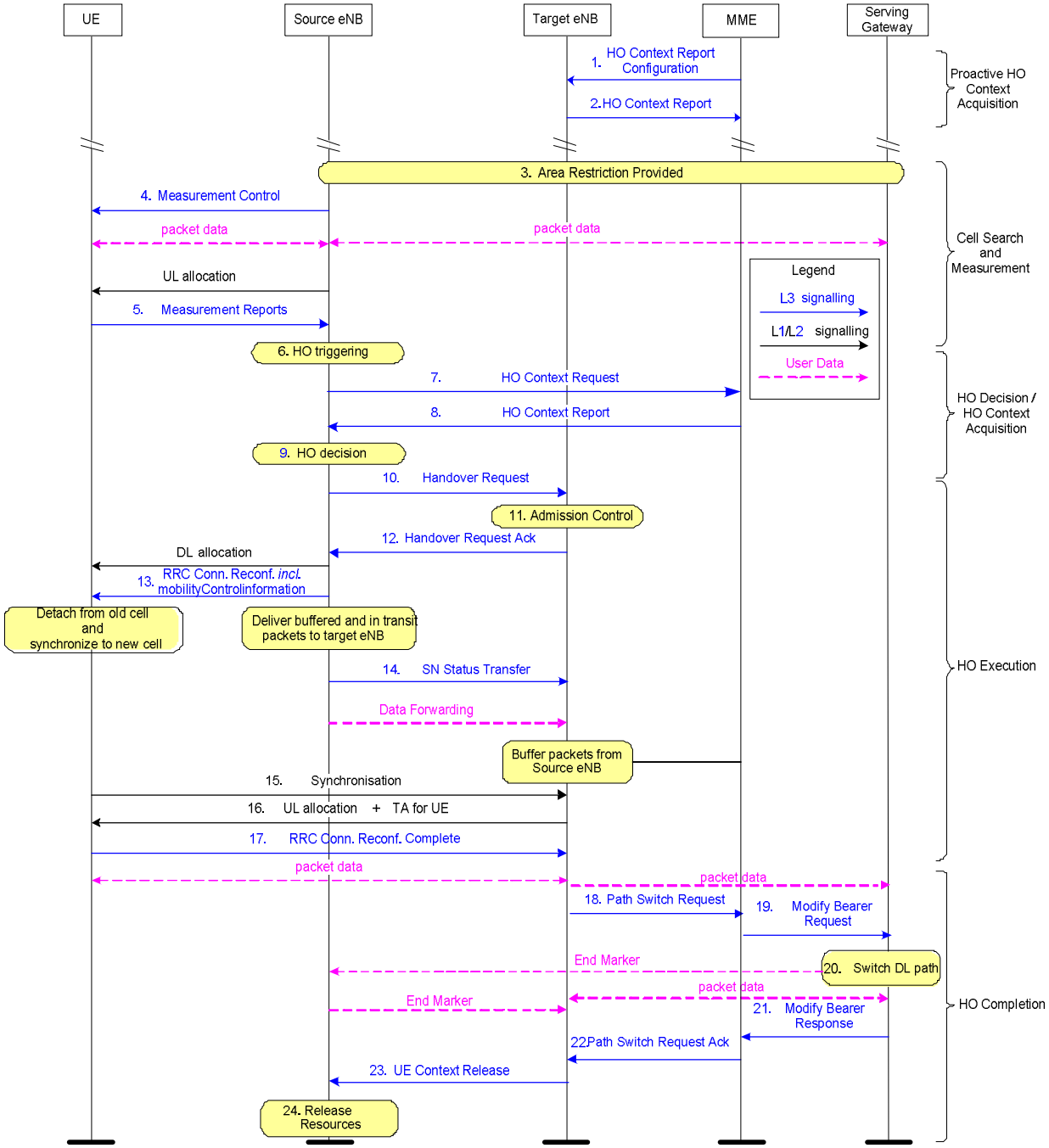

Figure 30: Proactive HO context acquisition approach for the HO execution scenario 1

Let us now focus on the HO signaling procedure for supporting inbound mobility towards a HeNB. Figure 31 illustrates the reactive HO signaling procedure for the HO execution scenario 3, i.e., eNB-to-HeNB, or HeNB-to-HeNB with access control. Note that the deployment of the HeNB Gateway is optional [18].

The cell search and measurement phase is performed in steps 1 – 7, and consists of the proximity indication (steps 1 – 2), measurement derivation (step 3 – 4), and cell identification (steps 5 – 7) phases [18]. Upon HO decision triggering (step 8), the serving (H)eNB initiates a HO context request towards the target HeNB through the S1 interface (steps 9 – 11), i.e., via the MME and the HeNB-GW. The target HeNB reports the required HO context (steps 12 – 14), and the HO decision algorithm terminates in step (15). Note that when the serving cell is a HeNB, the HO context request/report signals can be exchanged through the X2

interface. The HO procedure is completed in steps 16 – 24, where the standard HO execution phase takes place through the S1 interface. It should be noted that the HO execution phase is performed through the S1 interface regardless the type of the serving eNB, i.e., eNB or HeNB, given that MME-based access control is required for the HO execution scenario 3 (step 17). The key difference between the reactive and the proactive HO context acquisition approaches in the HO execution scenario 3, i.e., Figure 31 and Figure 32, respectively, is that in the proactive one the serving eNB acquires the HO context on demand to the MME (steps 13 – 14), which configures the target HeNB to report the HO context on a periodic basis (steps 1 – 4).

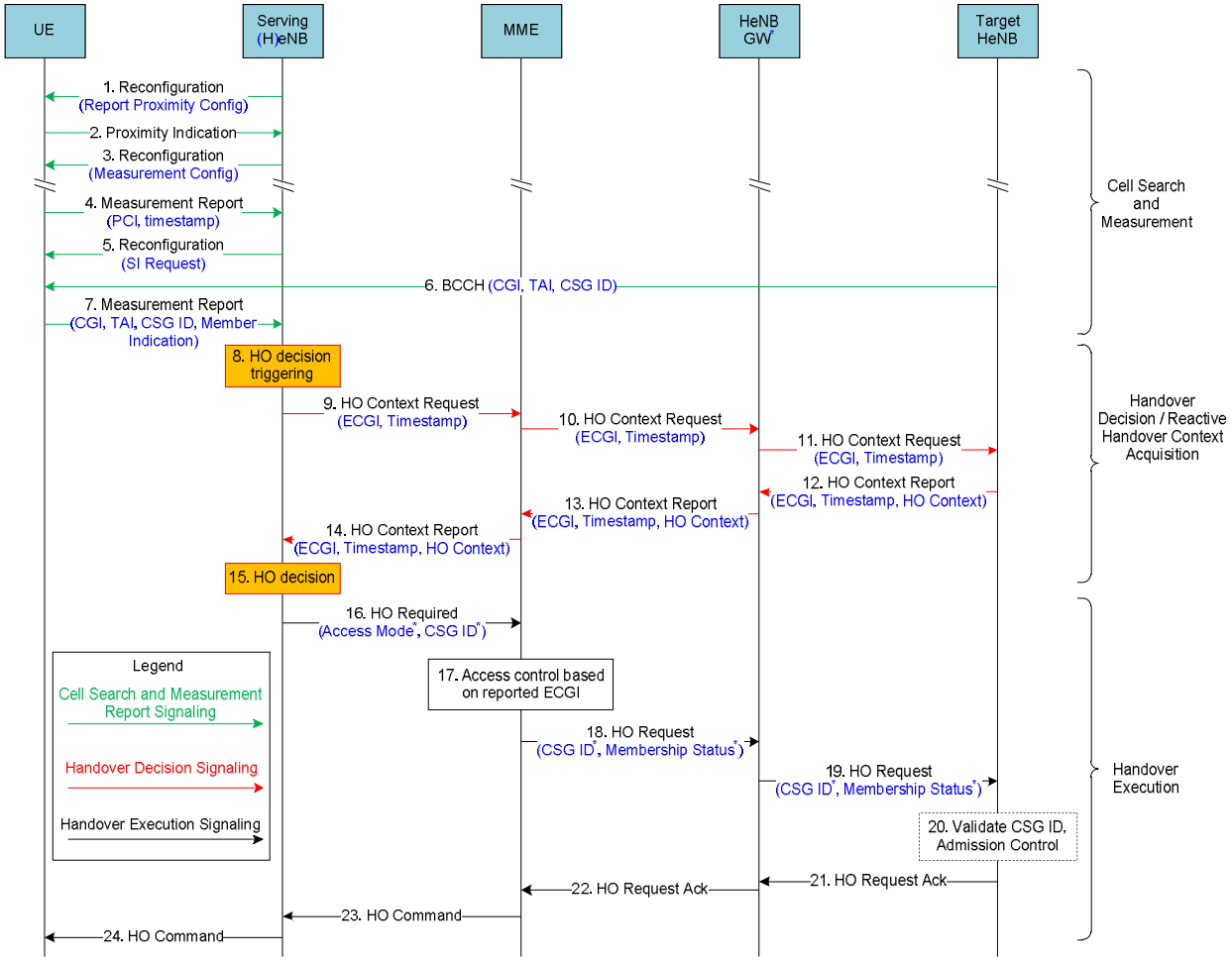

Figure 31: Reactive HO context acquisition approach for the HO execution scenario 3

Both the reactive and the proactive signaling approaches for the HO execution scenario 4 are similar to the ones depicted in Figure 31 and Figure 32, respectively, with the difference that the MME-based access control step is omitted (step 17). The same implies for the HO execution scenario 5, where in addition, the serving and the target HeNB can utilize the standard X2 interface to perform both the HO execution phase (steps 16 – 23 in Figure 31 and Figure 32), and the HO context acquisition phase for the reactive signaling approach (steps 9 – 14 in Figure 31).

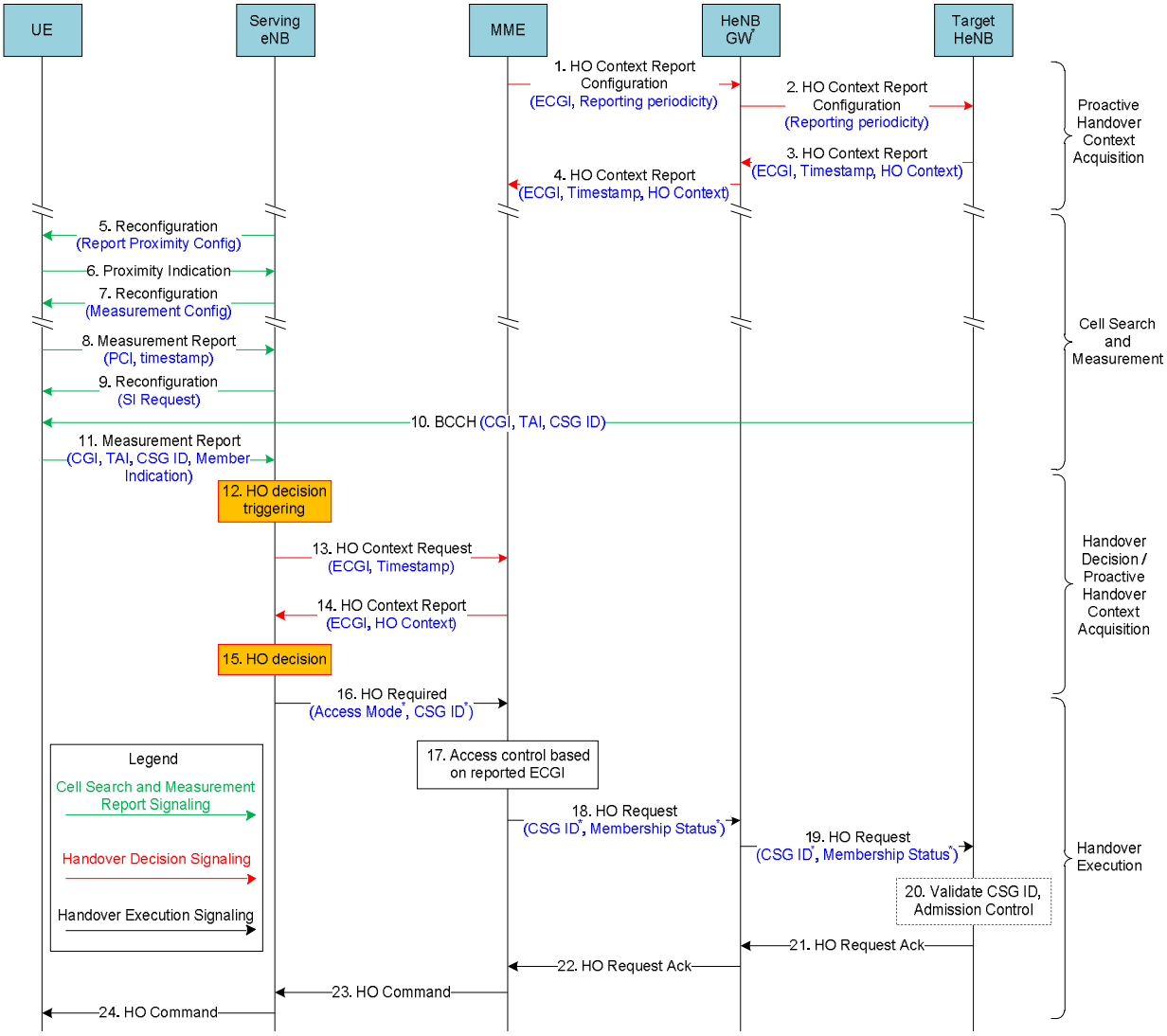

Figure 32: Proactive HO context acquisition approach for the HO execution scenario 3

Let us now focus on how the HO context request/report signals can be performed. The LTE-A standard describes a wide set of signals for the S1 and the X2 interfaces which, however, are not provisioned to transfer the entire HO decision context required for employing the proposed algorithm. Nevertheless, the HO context acquisition signaling can be performed either a) by using the private message mechanism for non-standard use described in [28] for the X2 interface, and in [30] for the S1 interface, or b) by introducing a new message type in future amendments of the LTE-A standard, to include the entire HO decision context required. The use of the private mechanism for non-standard use is already part of the LTE-A standard, and thus, the proposed HO decision algorithm can be employed with a simple software update at the eNBs, HeNBs, and the MME. On the other hand, the addition of a new message type and Information Element (IE) containing the required HO context, will enhance the functionality of the LTE-A system towards more sophisticated mobility and interference management support.

Referring to the differences of the reactive and proactive HO context acquisition approaches, the reactive approach is expected to lower the HO context request/report signaling commuted through the LTE-A CN, especially when an X2 interface is established between the serving and the target cells. On the other

hand, the proactive approach is expected to minimize the signaling overhead towards the LTE-A cells, as it eliminates the occurrence of multiple HO context report/ request signals for the same HO context. More frequent yet deterministic signaling overhead is expected for the proactive approach where the HO context signaling periodicity is configured by the MME, compared to the reactive approach, where the consequential signaling overhead is highly correlated to the occurrence rate of the HO events. Nevertheless, the proactive approach necessitates enhanced HO context management functionality at the LTE-A CN, in contrast with the reactive approach where no additional functionality enhancements are required.

4.6 Numerical Results

This section includes extensive system-level simulation results to demonstrate the performance of the proposed MM approach. Section 4.6.1summarizes the adopted simulation model and parameters, whereas Section 4.6.2 presents selected numerical results.

4.6.1 Simulation Model and Parameters

This section investigates the performance of the proposed mobility management approach, under both HO context acquisition procedures, based on an extended version of the system-level evaluation methodology described in [123]. A hexagonal LTE-A network is considered with a main cluster composed of 7 eNBs, where each eNB consists of 3 sectors. The wrap-around technique is used to extend the LTE-A network, by copying the main cluster symmetrically on each of the 6 sides. A set of blocks of apartments, referred to as femtoblocks, are uniformly dropped within the main cluster area with respect to the femtoblock deployment density parameter, denoted by d_{FB}, which indicates the percentage of the main cluster area covered with femtoblocks. Femtoblocks are modeled according to the dual stripe model for dense urban environments in [123], where each femtoblock consists of two stripes of apartments separated by a 10 m wide street and each stripe has two rows of 5 apartments of size 10x10m. The deployment of femtocells within each femtoblock is based on the femtocell deployment ratio parameter, denoted by r_{fc}, which indicates the percentage of femtoblock apartments with a femtocell installed. Femtocell stations and users are uniformly dropped inside the apartments, where each femtocell station initially serves one user. Each macrocell sector initially serves ten users, which are uniformly distributed within it. The LTE-A users are members of up to one CSG, where three CSG IDs are used in the network. The remainder simulation parameters are summarized in Table III.

Note that a higher d_{FB} corresponds to a denser femtoblock layout within the main LTE-A cluster, while a higher r_{fc} to a denser femtocell deployment within the femtoblocks. As a result, although a higher d_{FB} or r_{fc} parameter results in denser femtocell deployment layout, a higher r_{fc} leads to comparably denser femtocell deployment within small areas, i.e., femtoblock. It should also be noted that a higher d_{FB} or r_{fc} parameter results in the introduction of additional UEs in the network, provided that each femtocell is assumed to initially serve one user. The performance of the proposed approach is evaluated under both the HO context acquisition approaches, where the reactive version of the algorithm is referred to as Prop-R and the proactive as Prop-P3s. Different performance is attained for

the two different versions of the proposed algorithm, given that the HO context update for the Prop-P3s algorithm is performed once every 3 seconds.

The Prop-R and Prop-P3s are compared against the SC HO decision algorithm, referred to as the SC algorithm, and the algorithm in [59], referred to as the Zhang11 algorithm.

Table 9: System-level simulation model and parameters

Network layout		
Macrocell layout	7 clusters, 7 sites per cluster, 3 sectors per site, freq. reuse 1	
Macrocell inter-site distance	500 m	
Initial number of UEs per macrocell sector	10 UEs	
Macrocell UE distribution	Uniform within each sector	
Femtoblock layout	Dual stripe model for dense urban environments [123]	
Femtoblock distribution in the main LTE-A cluster	Uniform	
Femtocell station and UE distribution within an apartment	Uniform	
Initial number of UEs per femtocell station	1 UE	
Maximum number of supported UE per femtocell	4 UEs	
System operating parameters		
Parameter	**Macrocell**	**Femtocell**
Carrier frequency	2000 MHz	Uniformly picked from the set {1990, 2000, 2010} MHz
Channel bandwidth	10 MHz	10 MHz
Maximum Tx Power	$\overline{P}_{max}^{c,T} = 46$ dBm	$\overline{P}_{max}^{c,T} = 20$ dBm
Antenna gain	14 dBi	0 dBi
Noise figure	5 dB	8 dB
Shadowing standard deviation	8 dB	4 dB
RS transmit power (DL RS Tx)	Normally distributed with a mean value of 23 dBm and standard deviation 3dB	Uniformly distributed within the [0,20] dBm interval
CSG ID distribution	Does not apply	Uniform within {1, 2, 3}
Link-to-system mapping	Effective SINR mapping (ESM) [123]	
Path Loss Models		
Path loss	Models for urban deployment in [123]	
Interior / Exterior wall penetration loss (indoor UEs)	5 / 15 dB	
UE parameters		

UE power class	$\overline{P}_{max}^{u,T} = 23$ dBm		
UE antenna gain	0 dBi		
Mean UL SINR target	$\overline{\gamma}_{target}^{u} = 3$ dB		
CSG ID distribution	Uniformly picked from {1, 2, 3}		
Traffic model	Full buffer similar to [123]		
Mobility model [13]	User speed	$v_t = N(\bar{v}, s_u)$ m/s	
		Mean user speed	$\bar{v} = 3$ km/h
		User speed standard deviation	$s_u = 1$ km/h
	User direction	$\varphi_t = N\left(\varphi_{t-1}, 2\pi - \varphi_{t-1}\tan\left(\frac{\sqrt{v_t}}{2}\right)\Delta t\right)$	
	where Δt is the time period between two updates of the model, and $N(a, b)$ the Gaussian distribution of mean a and standard deviation b		
Other simulation parameters			
Overall simulation time			200 sec
Simulation time unit			$\Delta t = 1$ sec
HO context updating periodicity for the Prop-P3s algorithm			3 sec

4.6.2 System-level Simulation Results

Figure 33 illustrates the performance of the algorithms in terms of mean UE transmit power for varying femtoblock deployment density d_{FB}. Two different femtocell deployment ratios r_{fc} are used to investigate the algorithms' performance under both sparse and dense femtocell deployments per femtoblock, i.e., $r_{fc} = 0.1$ and $r_{fc} = 0.5$, respectively.

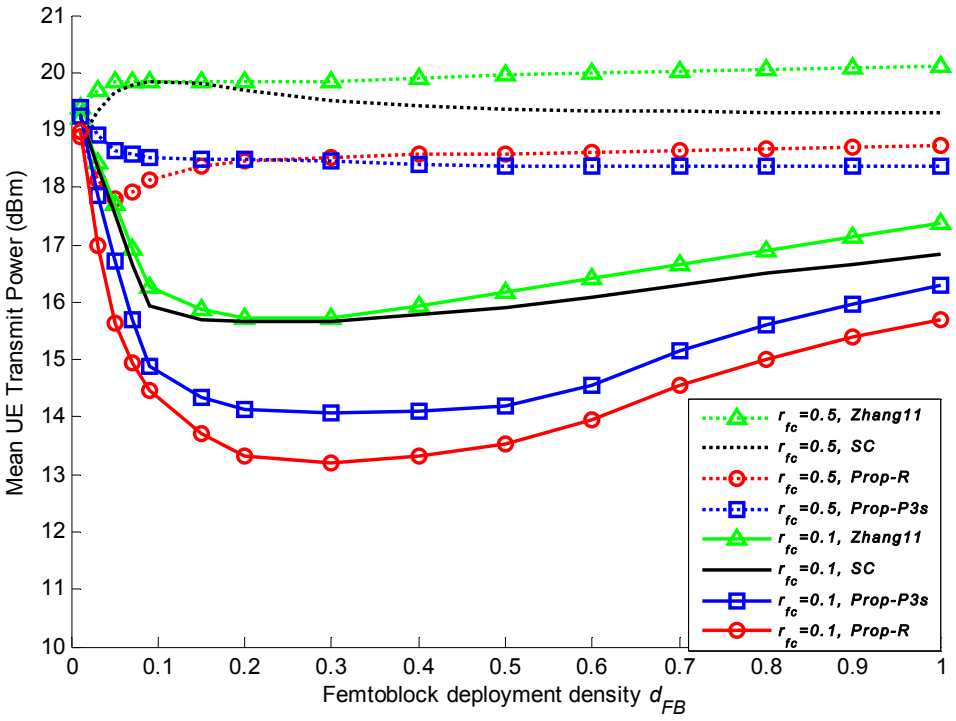

Figure 33: Mean UE transmit power vs. the femtoblock deployment density

For $r_{fc} = 0.1$, the mean UE transmit power lowers for all algorithms as the d_{FB} increases, owing to the shorter transmit – receive range of the sparsely deployed femtocell infrastructure. Above a certain d_{FB}, however, higher mean UE transmit power is required to sustain the mean UL SINR target $\overline{\gamma}^{u}_{target}$ for all algorithms, due to the comparably shorter inter-site distance between the HeNBs which rapidly raises the interference at the cell sites (Figure 34). Depending on the femtoblock deployment density d_{FB}, the Prop-R algorithm is shown to lower the mean UE transmit power from 0.5 to 2.6dB compared to the SC and the Zhang11 algorithms, i.e., 11% to 45% gain. Improved performance is attained by the Prop-P3s algorithm as well, where the respective gain is shown to reach up to 1.7 dB, i.e., 33%. Higher mean UE transmit power is required for all algorithms in denser femtocell deployments per femtoblock ($r_{fc} = 0.5$), where comparably shorter mean inter-site distance characterizes the femtocell layout even under low femtoblock deployment densities ($d_{FB} < 0.1$). Different from the competing algorithms, the Prop-R and Prop-P3s algorithms improve their performance for low d_{FB} values, while increased yet almost constant transmit power is observed for all algorithms in medium to high d_{FB} values. Once again, both versions of the proposed algorithm are shown to require up to 2dB lower UE transmit power compared to the competing algorithms, i.e., 37% gain, as they account for the actual interference level at the cell sites and the channel gain between the UEs and the (H)eNBs.

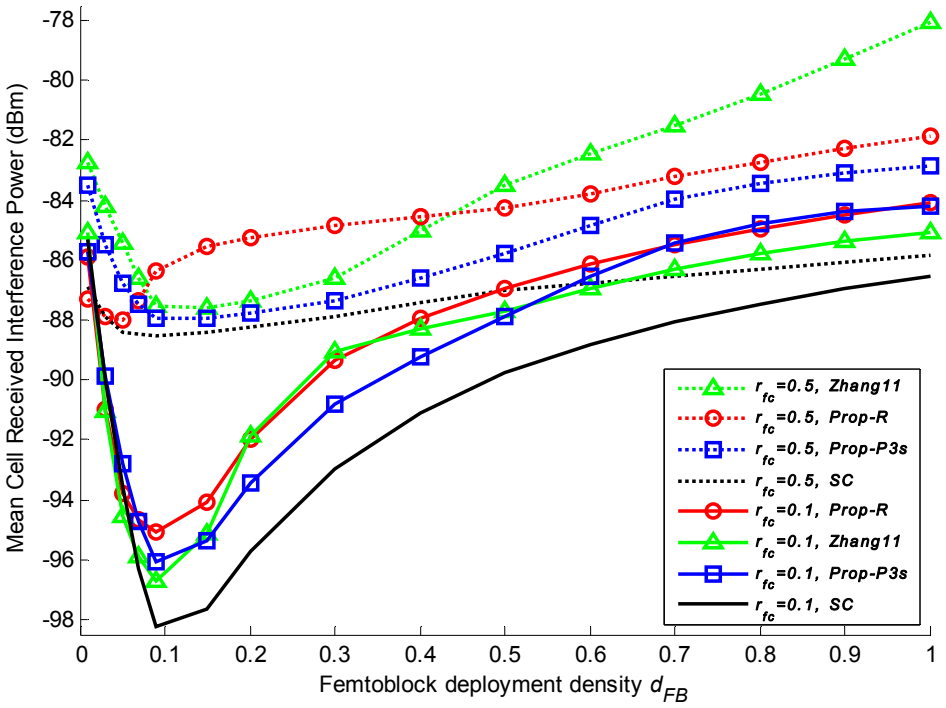

Figure 34: Mean cell received interference power vs. the femtoblock deployment density

Figure 34 depicts the performance of the algorithms in terms of mean received interference power at the cell sites, for varying d_{FB} and two r_{fc} values. As expected, a denser femtocell deployment per femtoblock ($r_{fc} = 0.5$) raises the interference at the cell sites for all algorithms, owing the short inter-site distance between the HeNBs. For $r_{fc} = 0.1$ on the other hand, even though a sparser femtoblock layout reduces the mean interference at the cell sites ($d_{FB} \leq 0.1$), above a d_{FB} value the mean interference level rapidly increases for all algorithms. The SC algorithm attains lower interference compared to the femtocell-specific algorithms, while compared to the Prop-R and the Zhang11 algorithms, improved performance is shown for the Prop-P3s algorithm as well. Interestingly, even though the Prop-R algorithm greatly lowers the mean UE transmit power compared to the other algorithms (Figure 33), it simultaneously results in higher cell interference under the same network layouts (Figure 34). This result follows from the comparably enhanced femtocell utilization attained by the Prop-R algorithm, which substantially raises the number of femtocell users compared to the competing algorithms (Table 10).

Table 10: Number of femtocell users / total number of users within the main LTE-A cluster

d_{FB}	Number of femtocell users / total number of users							
	$r_{fc} = 0.1$				$r_{fc} = 0.5$			
	SC	Zhang11	Prop-P3s	Prop-R	SC	Zhang11	Prop-P3s	Prop-R
0,01	2,5/211	3/211	8/211	8/211	7,5/218	7,5/218	10,5/218	10/218
0,05	7,5/215	7/215	22/215	29/215	14/242	14/242	27,5/242	29/242
0,1	17,5/224	16,5/224	42/224	52,5/224	19,5/271	17/271	36,5/271	53,5/271
0,25	27/239	29/239	66,5/239	75,5/239	39,5/359	55,5/359	62/359	74/359
0,5	45,5/269	56,5/269	88/269	105/269	77,5/500	99/500	107/500	129,5/500
0,75	52/303	69,5/303	109,5/303	128,5/303	115,5/641	142,5/641	158/641	193,5/641
1	60,5/337	82,5/337	136/337	159/337	153,5/782	186/782	209/782	257,5/782

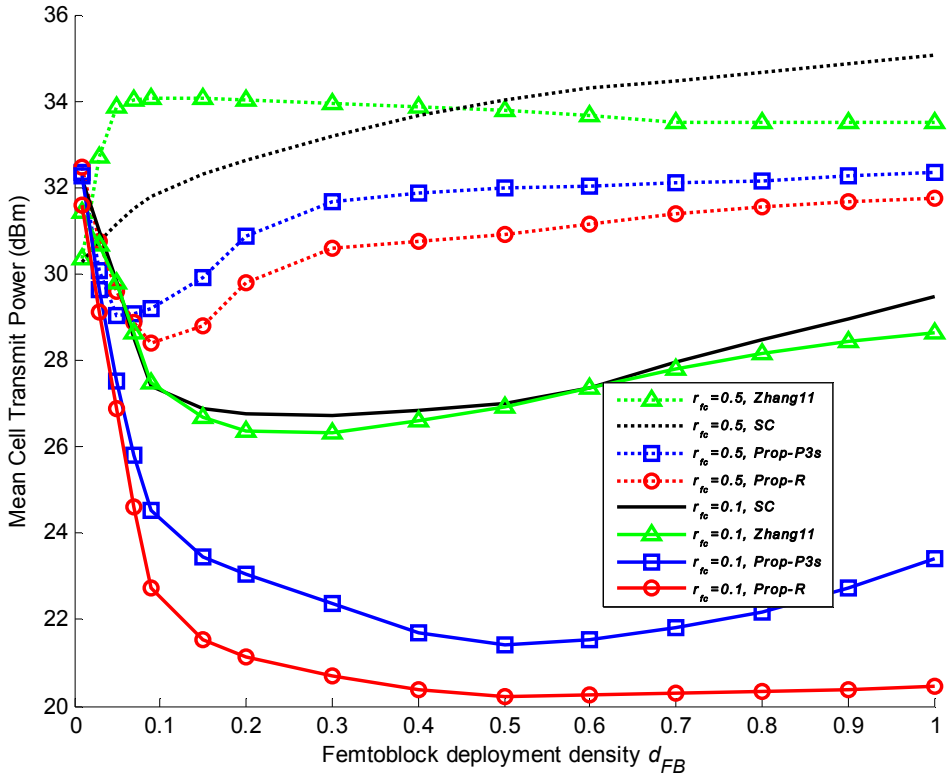

Figure 35: Mean cell transmit power vs. the femtoblock deployment density

Figure 35 depicts the mean cell transmit power performance of all algorithms, for varying d_{FB} and two different r_{fc} values. Note that for dense femtocell deployment per femtoblock ($r_{fc} = 0.5$) and low d_{FB} values, the Zhang11 algorithm increases the mean cell transmit power as it prioritizes femtocell access regardless the interference and propagation conditions at the UEs and the femtocell sites. For higher d_{FB} values, however, the performance of the algorithm improves due to the shorter femtocell inter-site distance. The Prop-R and Prop-P3s algorithms are shown to substantially lower the mean cell transmit power compared to the SC and Zhang11 algorithms, with the higher gains attained for sparse femtocell deployment ratios ($r_{fc} = 0.1$) and medium to high femtoblock deployment densities, i.e., up to 9 dB gain for the Prop-R and 6dB for the Prop-P3s algorithm.

The greatly lower mean cell transmit power attained by both the Prop-R and Prop-P3s algorithms, results in significantly reduced interference at the UEs as well (Figure 36). Noticeably, the performance of the Prop-R and Prop-P3s algorithms under dense femtocell deployment per femtoblock is better even compared to the one of the competing algorithms in sparse femtocell deployments per femtoblock. For $r_{fc} = 0.1$ the SC and Zhang11 algorithms show similar performance, whereas the Prop-R and Prop-P3s algorithms are shown to lower the mean UE interference by up to 10 and 8dB, respectively. Significantly lower mean UE interference is shown for the Prop-R and Prop-P3s algorithms under $r_{fc} = 0.5$ as well, with the higher gains attained under low to medium femtoblock deployment densities, i.e., $0.05 < d_{FB} < 0.3$. Note that the UE interference mitigation plays a key role for realizing the femtocell communication paradigm, given that the employment of interference management and self-optimization is typically performed at the LTE-A network rather than the UE side.

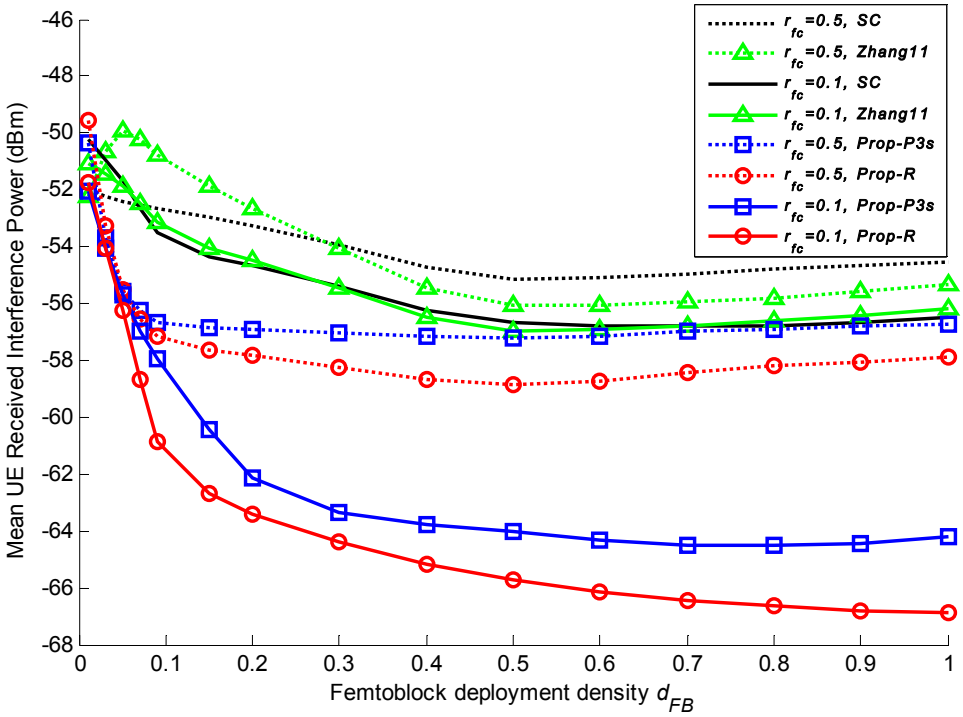

Figure 36: Mean UE received interference power vs. the femtoblock deployment density

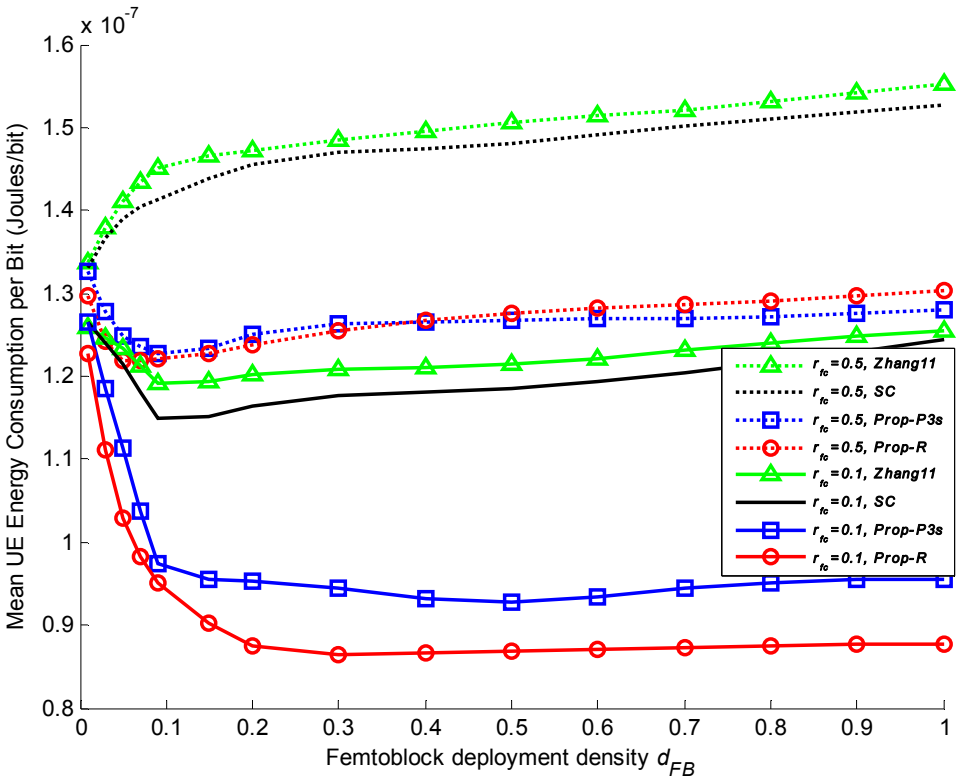

Figure 37: Mean UE energy consumption per bit vs. the femtoblock deployment density

Figure 37 illustrates the performance of the algorithms in terms of mean UE energy consumption per bit, owing to transmit power. For dense femtocell deployment per femtoblock ($r_{fc} = 0.5$), as the d_{FB} increases constantly increasing UE energy expenditure per bit is required for the SC and Zhang11 algorithms to sustain the mean UL SINR target $\overline{\gamma}^{u}_{target}$. On the other hand, improved performance is achieved for the Prop-R and Prop-P3s algorithms as the d_{FB} increases, where for $d_{FB} > 0.1$ rising yet comparably lower energy consumption per bit is required as well, compared to the competing algorithms. For sparse femtocell deployments per femtoblock ($r_{fc} = 0.1$), reduced energy expenditure overhead per bit is observed for all algorithms. Both versions of the proposed algorithm, however, attain substantially enhanced UE energy expenditure per bit compared to the competing algorithms, even for very low femtoblock deployment densities ($d_{FB} \geq 0.05$). Noticeably, the performance of all algorithms remains roughly unaffected above a certain d_{FB} value, i.e., $d_{FB} > 0.3$. Apart from enhanced UE energy consumption per bit, both versions of the proposed algorithm are shown resourcefully utilize the enhanced capacity potential offered by the femtocell infrastructure as well (Figure 38).

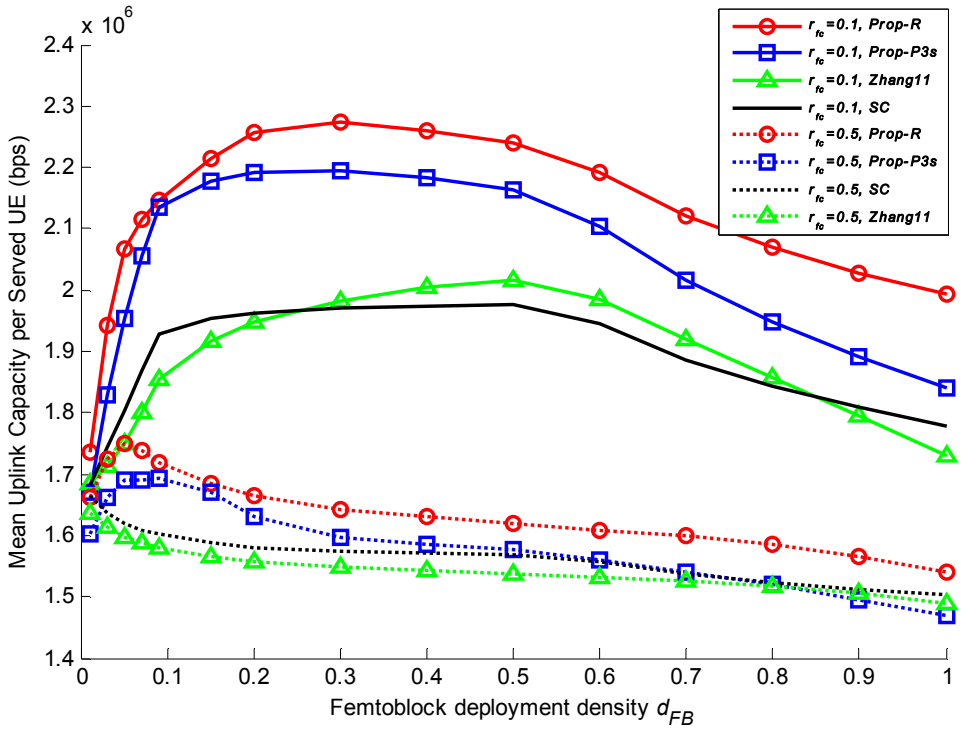

Figure 38: Mean uplink capacity per served user vs. the femtoblock deployment density

Compared to the SC and Zhang11 algorithms, which attain a similar behavior, the Prop-R algorithm is shown to enhance the mean UL capacity per served UE by up to 16% for $r_{fc} = 0.1$, and up to 9% for $r_{fc} = 0.5$. Lower yet comparable UL capacity gains are shown for the Prop-P3s algorithm as well, with the higher gains attained under low to medium femtoblock deployment densities. Even though a higher r_{fc} improves the overall network capacity, it simultaneously degrades the UL capacity per served UE for all algorithms (Figure 38), owing to the comparably higher interference level at the cell sites (Figure 34). Similar performance degradation is observed for higher d_{FB} values as well, where above a certain d_{FB} value the UL capacity per served UE degrades rather than improves depending on the HO decision algorithm and the r_{fc} value.

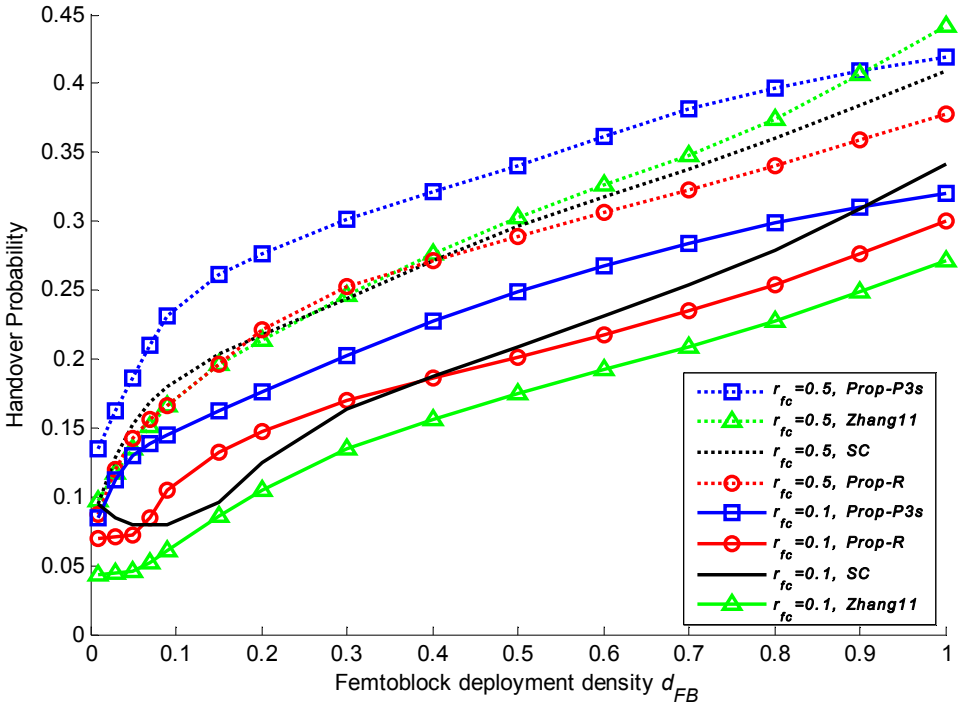

Figure 39: Handover probability vs. the femtoblock deployment density

Figure 39 depicts the HO probability performance for all algorithms for varying d_{FB} parameter. As expected, a higher HO probability is observed for all algorithms as the d_{FB} increases. The same implies for denser femtocell deployment per femtoblock ($r_{fc} = 0.5$), where a comparably lower mean inter-site distance characterizes the femtocell deployment layout. For $r_{fc} = 0.1$ the Zhang11 algorithm is shown to sustain the lowest HO probability, whereas the Prop-R algorithm attains an improved performance compared to the SC algorithm under very low and medium to high d_{FB}, i.e., for $d_{FB} < 0.1$ and $d_{FB} \geq 0.4$, respectively. On the other hand, the Prop-P3s algorithm results in the highest HO probability for both sparse and dense femtocell deployment ratios, while for $r_{fc} = 0.5$, even though the SC, Zhang11, and Prop-R algorithms show similar performance under low to medium deployment densities ($d_{FB} < 0.4$), in medium to high femtoblock deployment densities the Prop-R algorithm attains the lowest HO probability ($d_{FB} \geq 0.4$). As will be shown in the following, the HO probability of the Prop-R and Prop-P3s algorithms can be greatly lowered by using a higher $HHM_{c,(dB)}^{MM}$ value.

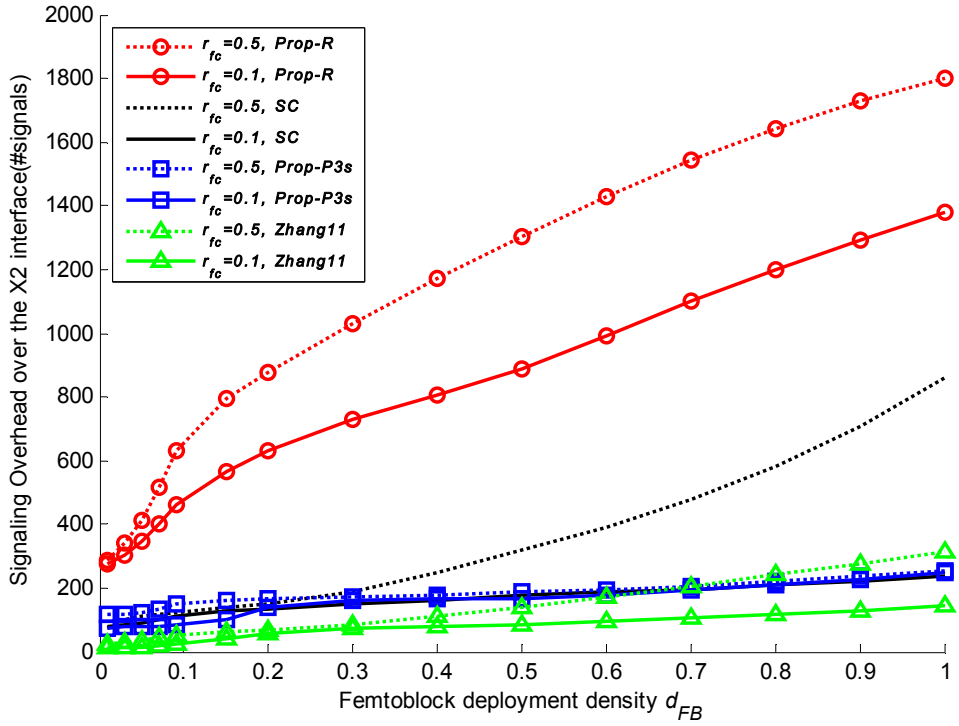

Figure 40: Signaling overhead over the X2 interface vs. the femtoblock deployment density

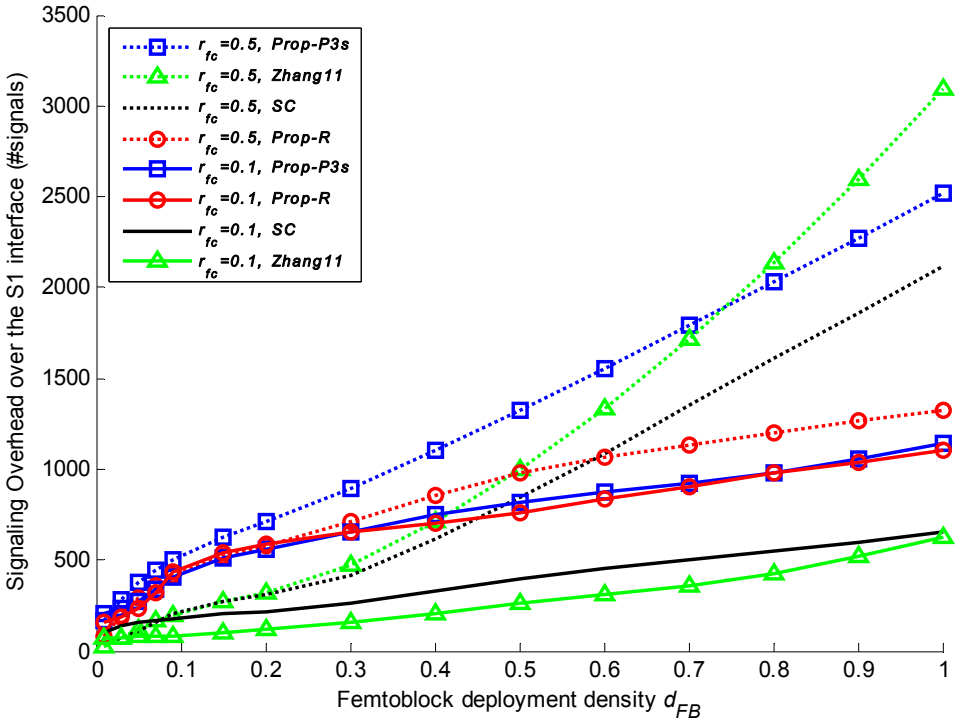

Figure 41: Signaling overhead over the S1 interface vs. the femtoblock deployment density

Figure 40 and Figure 41, depict the network-wide X2 and S1 signaling overhead per second, respectively, for all algorithms. Note that the depicted overhead includes both the HO execution and the HO context acquisition signaling (where necessary). In terms of X2 signaling (Figure 40), a higher femtoblock deployment density or femtocell deployment ratio enlarges the X2 signaling overhead for all algorithms due to the denser network layout. Higher X2 signaling requirements are shown for Prop-R algorithm, under both sparse and dense femtocell deployments per femtoblock, owing to the HO context acquisition procedure on a

per candidate cell basis. Enlarged X2 signaling overhead is also observed for the SC algorithm for $r_{fc} = 0.5$, whereas the performance of the Prop-P3s algorithm is shown to remain almost unaffected due to the MME-based HO context acquisition procedure over the S1 interface.

Different from the X2 signaling, the S1 signaling performance for all algorithms is shown to be strongly affected by the femtocell deployment ratio (Figure 41). For $r_{fc} = 0.1$ the performance of all algorithms grows almost linearly with respect to the d_{FB}. However, both versions of the proposed algorithm necessitate higher S1 signaling overhead due to the employment of the HO context acquisition. For $r_{fc} = 0.5$, a rapidly growing S1 signaling overhead is observed for the SC and the Zhang11 algorithms, whereas under medium to high d_{FB} the Prop-R algorithm is shown to require the lowest S1 signaling overhead, owing to the increased utilization of the X2 interface (Figure 40). On the other hand, the Prop-P3s algorithm is shown to require the highest signaling overhead compared to the other algorithms, which however grows roughly linearly with respect the d_{FB} parameter. Note that the S1 signaling overhead for the Prop-P3s algorithm can be mitigated by using a lower HO context acquisition periodicity at the MME. Reduced S1 signaling is also attained for both the Prop-R and Prop-P3s algorithms if a higher $HHM^{MM}_{c,(dB)}$ is used, given that the X2 and S1 signaling strongly depend on the HO probability.

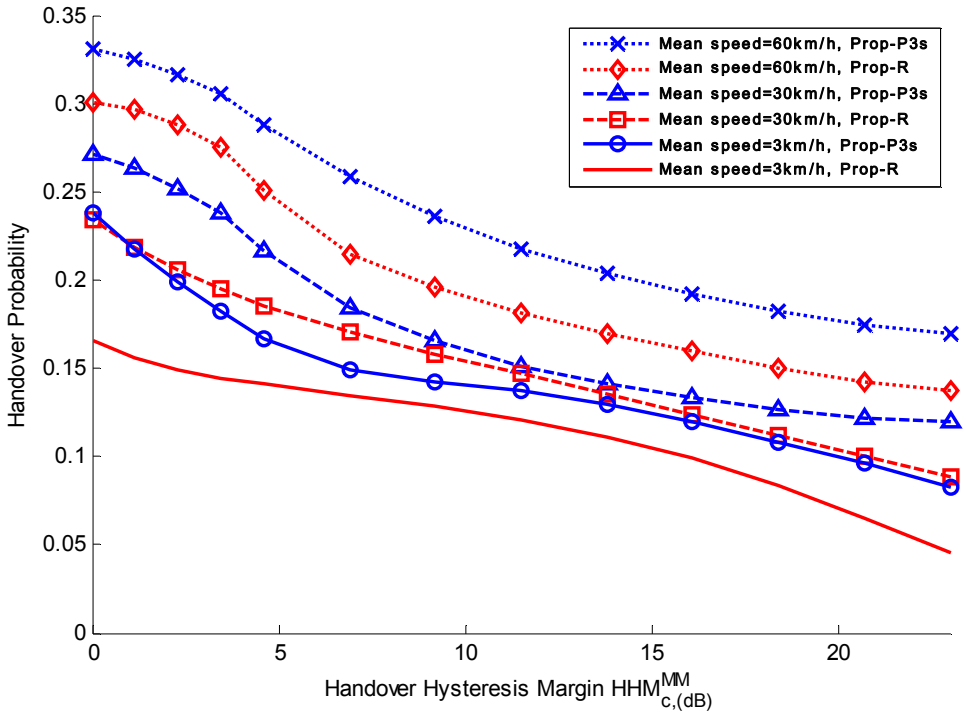

Figure 42: Handover probability vs. the Handover Hysteresis Margin $HHM^{MM}_{c,(dB)}$

Focusing on the Prop-R and Prop-P3s algorithms, Figure 42 and Figure 43 depict the HO probability and mean UE transmit power performance, respectively, for increasing $HHM^{MM}_{c,(dB)}$ parameter and various mean user speeds. These results are derived for $d_{FB} = 0.2$ and $r_{fc} = 0.3$. As expected, a higher user speed increases the HO probability for both versions of the proposed algorithm. Nevertheless, a higher $HHM^{MM}_{c,(dB)}$ value can be used to lower the HO probability depending on the mean user speed and the optimization requirements (Figure 42). The $HHM^{MM}_{c,(dB)}$ parameter also affects the remainder performance measures,

where the impact of varying $HHM_{c,(dB)}^{MM}$ on the mean UE transmit power is indicatively depicted in Figure 43. Interestingly, as the $HHM_{c,(dB)}$ increases, the mean UE transmit power lowers for both versions of the proposed algorithm (Figure 43). Depending on the mean user speed and the HO context acquisition approach, however, there exists a $HHM_{c,(dB)}^{MM}$ value above which a degraded performance is observed. Similar results were derived for the remainder performance measures as well, indicating that the $HHM_{c,(dB)}^{MM}$ can be used to optimize the proposed algorithm with respect to a particular performance measure/target.

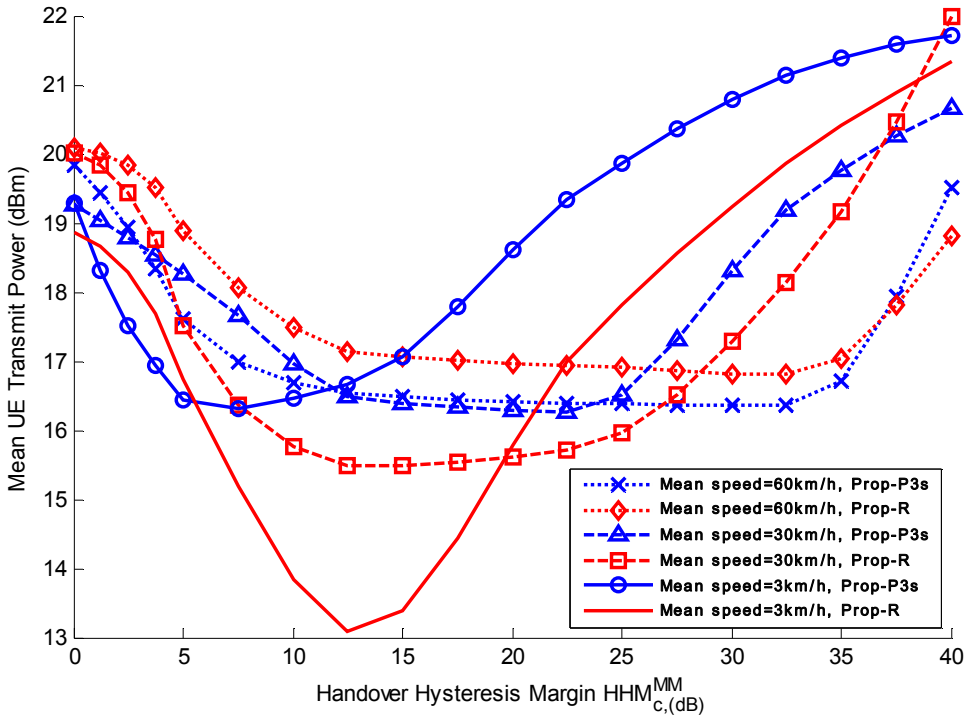

Figure 43: Mean UE transmit power vs. the Handover Hysteresis Margin $HHM_{c,(dB)}^{MM}$

4.7 Key Contributions and Conclusions

The random femtocell deployment may result in degraded SINR performance, increased outage probability, and enlarged network signaling, if the interference-agnostic strongest cell policy is employed during the HO decision phase. In this work, we have introduced a novel HO decision policy for reducing the UE power transmissions in the two-tier LTE-A network, while attaining a prescribed SINR target for the users. This policy is fundamentally different from the strongest cell HO policy, as it takes into account the RS power transmissions and the RF interference at the LTE-A cell sites. The proposed policy is compatible with LTE-A, as it is employed by adapting the HHM with respect to the user's mean SINR target and standard link quality measurements describing the status of the candidate LTE cells. A novel HO decision algorithm has also been proposed that jointly considers the impact of user mobility, interference, and power consumption. A detailed analysis has been provided with regards to the network signaling procedure for employing it in LTE-A system, and two different signaling approaches have been described, depending on whether a network entity maintains and disseminates the required HO decision context, or not. Extensive system-level simulation results have shown that compared to existing approaches, the proposed algorithm greatly reduces the mean UE and cell

transmit power, lowers the mean UE energy expenditure per bit and UE interference, and enhances the system capacity, at the cost of moderate increase of network signaling. To the best of our knowledge, this work is the first to propose the utilization of standard measurements on the radio status of the cellular base stations as means of employing energy-efficient handover decision in the macrocell – femtocell network. The detailed discussion on the required network signaling, along with the extensive system-level simulations using the Small Cell Forum evaluation methodology, are two important features of our work, towards validating its performance and deploying it in real-life systems.

5. NETWORK-ASSISTED ENERGY-EFFICIENT VERTICAL HANDOVER FOR HETEROGENEOUS WIRELESS NETWORKS

To address the challenging issues of energy-efficiency and seamless connectivity in heterogeneous networks, 3GPP and IEEE have recently incorporated several architectural and functional enhancements to the baseline operation of their standards for cellular and wireless local area network access, respectively. Based on the 3GPP ANDSF and the advanced measurement capabilities provided by the IEEE 802.11-2012 and the 3GPP LTE-A Standards, we propose an ANDSF-assisted energy-efficient vertical handover decision algorithm for the heterogeneous IEEE 802.11-2012 / LTE-A network. The proposed algorithm enables a multi-mode mobile terminal to select and associate with the network point of attachment that minimizes its average overall power consumption and guarantees a minimum supported quality of service for its ongoing connections. System-level simulation is used to evaluate the performance of the proposed algorithm and compare it to that of other competing solutions.

The remainder of the section is organized as follows. Section 5.1 describes the adopted system model and presents our power consumption model. In section 5.2, we propose a novel methodology for estimating the power consumption over the LTE-Advanced or the IEEE 802.11-2012 interface by using standard radio measurements. Based on the proposed power consumption estimation methods, we propose an energy-efficient policy for inter-system mobility between the two systems, and an energy-efficient intra-system mobility policy for identifying the point of attachment (PoA) that minimizes the UE power consumption. In section 5.3, we combine the two energy-efficient policies into a single ANDSF-assisted energy efficient vertical handover decision algorithm that aims at minimizing the overall UE power consumption given a prescribed SINR target for both systems. A comprehensive system-level simulation study is used in Section 5.4 to evaluate the performance of the proposed algorithm and compare it against that of other existing solutions. Finally, Section 5.5 summarizes the key contributions of this section and contains our conclusions.

5.1 System Model

A heterogeneous network is considered, consisting of a set of LTE-A cells, denoted by $\boldsymbol{C}$, a set of IEEE 802.11-2012 APs, denoted by $\boldsymbol{W}$, and a set of MMTs supporting both the LTE-A and IEEE 802.11-2012 radio interfaces, denoted by $\boldsymbol{U}$. Depending on the particular characteristics of the ongoing services, each MMT $u \in \boldsymbol{U}$ is assumed to have a known mean SINR target γ_l for service reception in the LTE-A network, and a known mean SINR target γ_w for service reception in the WLAN network. If not switched-off, the LTE-A and WLAN interfaces of the MMT can be in one of the communication states in $\boldsymbol{S} \coloneqq \{T, R, I\}$, where T refers to the transmit, R to the receive, and I to the idle state.

The ANDSF module assists the VHO decision at the MMTs by providing network discovery information (set of candidate PoAs) and an inter-system mobility policy. To achieve this, the ANDSF is assumed to be aware of the following context: a) the power consumption for both RATs on a per interface state basis [131][132], b) the probability of being in state $s \in \boldsymbol{S}$ for both RATs [133][134], c) the interference at the PoA sites and the transmit power on the pilot/reference signals (standard LTE-A and WLAN measurement capabilities [2][16]), and d) the received signal power on the pilot/reference signals at the MMTs on a per candidate PoA basis [2][16]. In Table 11, we summarize the paper notation for the key system

parameters and the LTE-A/WLAN measurements (see section 1.2 for the LTE-A and IEEE 802.11-2012 parameters).

Table 11: System model parameters and standard measurements

System Model Parameters	Notation
Mean Transmit Power of node x (PoA or user)	$t(x)$
Mean Noise Power in node x (PoA or user)	$\sigma(x)^2$
Mean Channel Gain from node x to node y (PoA or users)	$h(x,y)$
Maximum Allowed Transmit Power of node x (PoA or user)	$T_M(x)$
LTE-A Parameters [16]	
RSRP measurement for cell c	$RSRP(c)$
RIP measurement in cell c	$I(c)$
DL RS Tx measurement in cell c	$T_{RS}(c)$
Interface Power Consumption in state $s \in \boldsymbol{S}$	$P_l(s)$
Probability of being in state $s \in \boldsymbol{S}$	$q_l(s)$
IEEE 802.11-2012 Parameters [2]	
RCPI measurement for AP w	$RCPI(w)$
ANPI measurement in user u	$ANPI(u)$
ANPI measurement in AP w	$ANPI(w)$
TPU measurement in AP w	$T_{TPU}(w)$
Interface Power Consumption in state $s \in \boldsymbol{S}$	$P_w(s)$
Probability of being in state $s \in \boldsymbol{S}$	$q_w(s)$

5.1.1 Power Consumption Estimation Model

Given that the overall power consumption of an interface depends on the power consumption per interface state and the probability of being in each interface state [133], the overall average power consumption of the LTE-A interface is modeled as follows:

$$P_{LTE-A} = \sum_{s \in \boldsymbol{S}} q_l(s) \cdot P_l(s) \quad (5.1)$$

The probabilities of being in each interface state depend on the service type and the RAT under use, while they can be assumed to be fixed and known. A detailed analysis for their computation is included in [133][134]. The same applies for the power consumption in the Receive and Idle states, which are also assumed to be fixed and known. Some proper values for can be found in [131]. In this paper we refine the computation of the power consumption in the Transmit state by including both the baseline power consumption of the interface and the mean transmit power of the user, denoted by $P_l(T)$ and $t(c)$, respectively. Accordingly, the expected power consumption of the LTE-A interface is computed as in (5.2).

$$P_{LTE-A} = \sum_{s \in \{R,I\}} q_l(s) \cdot P_l(s) + q_l(T) \cdot \big(P_l(T) + t(c)\big) \quad (5.2)$$

Following a similar approach for the WLAN interface, we compute the overall average power consumption of the WLAN interface as follows:

$$P_{WLAN} = \sum_{s\in\{R,I\}} q_w(s) \cdot P_w(s) + q_w(T) \cdot \big(P_w(T) + t(w)\big) \quad (5.3)$$

where the probabilities $q_w(s)$ and the parameters $P_w(s)$ $\forall s \in \boldsymbol{S}$ are all assumed to be fixed, known and computed in a similar manner with [133] and [131], respectively.

Even though the parameters $q_l(s)$, $q_w(s)$, $P_l(s)$, $P_w(s)$ can be assumed fixed and known for every interface state, the mean transmit power of the LTE-A and WLAN interfaces varies according to the mean SINR target, the channel gain between the MMT and the cell and the current cell status [113], e.g., interference. Different from existing approaches, in this paper we account for the impact of the varying transmit power in the interface on the overall power consumption of the MMT ((5.2) and (5.3)), and propose a novel approach for estimating the mean transmit power of the LTE-A and WLAN interfaces.

5.2 Power Consumption Estimation and Energy-efficient Policies

This section describes a compatible methodology for estimating the average overall MMT power consumption over the LTE-Advanced (section 5.2.1) and the IEEE 802.11-2012 systems (section 5.2.2), and presents two novel inter-system and intra-system mobility policies for the heterogeneous WLAN / LTE-A network in sections 5.2.3 and 5.2.4, respectively.

5.2.1 Power Consumption Estimation for LTE-Advanced

Let $\boldsymbol{U_c}$ denote the set of all interfering LTE-A users operating in the same frequency band with cell c. The mean uplink SINR between user u and cell c is given as follows:

$$\gamma(c) = \frac{t(u)\cdot h(u,c)}{\sum_{u'\in \boldsymbol{U_c}} t(u')\cdot h(u',c) + \sigma(c)^2} \quad (5.4)$$

where the numerator corresponds to the signal strength from user u in cell c and the denominator to the interference caused by all interfering users plus the noise power in cell c. Given the prescribed mean SINR target γ_t, the mean transmit power of user u in cell c can be computed as in Eq. (5.5).

$$t(u) = \frac{\gamma_l \cdot \left(\sum_{u'\in \boldsymbol{U_c}} t(u')\cdot h(u',c) + \sigma(c)^2\right)}{h(u,c)} \quad (5.5)$$

Following a similar approach with [113], it can be shown that the mean transmit power in Eq. (5.5) can be estimated based on standard LTE-A measurements as follows:

$$t(u) = \gamma_l \cdot \frac{T_{RS}(c)}{RSRP(c)} \cdot I(c) \quad (5.6)$$

where the ratio $\frac{P_{RS}(c)}{RSRP(c)}$ is used to assess the multiplicative inverse of the path loss between user u and cell c [113], i.e., the ratio $\frac{1}{h(u,c)}$. Note that all measurements in Eq. (5.6) are assumed to be averaged within the operating bandwidth of the target cell over the time interval Time to Trigger (TTT).

5.2.2 Power Consumption Estimation for IEEE 802.11-2012

Under the same viewpoint, the expected transmit power of user u in a target WLAN AP can be also estimated by using standard WLAN measurements as follows:

$$t(w) = \gamma_w \cdot \frac{T_{TPU}(w)}{(RCPI(w) - ANPI(u))} \cdot ANPI(w) \quad (5.7)$$

where the ratio $\frac{T_{TPU}(w)}{(RCPI(w) - ANPI(w))}$ is used to estimate the multiplicative inverse of the path loss between user u and AP w. In the denominator of Eq. (5.7) we subtract the $ANPI(w)$ value from the $RCPI(w)$ provided that, by definition, the $RCPI(w)$ measurement includes the received signal power from all nearby cells [2] (including the serving cell). By combining Eq. (5.6) with Eq. (5.2) and Eq. (5.7) with Eq. (5.3), we can readily estimate the average overall power consumption for the LTE-A and WLAN interfaces, respectively, based on standard measurements and fixed parameters.

5.2.3 Energy-Efficient Inter-System Mobility Policy

The inter-system mobility policy, provided by the ANDSF, is used at the MMT to decide which of the available RATs to utilize. The inter-system mobility policy is provided in terms of rules, which are applicable under certain validity conditions[8][17][19]. In this section, we present an energy-efficient inter-system mobility policy for minimizing the average overall MMT power consumption. The proposed policy is built in the ANDSF based on a) fixed parameters, i.e., power consumption per state, probability of being in each interface state and mean SINR targets of the user, and b) standard LTE-A and WLAN measurements provided by the heterogeneous PoAs. The resulting set of rules is subsequently commuted to the MMT to select the least power consuming available RAT. The inter-system mobility decision in the heterogeneous WLAN / LTE-A network can be broken down into two scenarios: the MMT is connected to the LTE-A system and decides whether it should switch to the WLAN interface, and vice versa.

Let us now focus on the first scenario, where a tagged MMT $u \in \boldsymbol{U}$ receives service from the LTE-A cell $c \in \boldsymbol{C}$. Let $\boldsymbol{L}_w \subseteq \boldsymbol{W}$ denote the candidate set of WLAN PoAs provided by the ANDSF. Then, the utilization of the WLAN interface is more preferable in terms of average overall MMT power consumption if the following condition is satisfied:

$$P_{WLAN}(w) < P_{LTE-A}(c), \text{ for at least one } w \in \boldsymbol{L}_w \quad (5.8)$$

where the notation $P_{WLAN}(w)$ corresponds to the average overall power consumption on service reception from the AP w. By substituting (5.2), (5.3), (5.6) and (5.7) in (5.8), we can readily show that (5.8) results in the following condition:

$$RCPI(w) - ANPI(u) > A(c,w) \text{ for at least one } w \in \boldsymbol{L}_w \quad (5.9)$$

where the decision threshold $A(u,c,w)$ is given in (5.10).

$$A(c,w) = \frac{q_w(T) \cdot \gamma_w \cdot T_{TPU}(w) \cdot ANPI(w)}{\sum_{s \in \boldsymbol{S}} q_l(s) \cdot P_l(s) + q_l(T) \cdot \gamma_l \cdot \frac{T_{RS}(c)}{RSRP(c)} \cdot I(c) - \sum_{s \in \boldsymbol{S}} q_w(s) \cdot P_w(s)} \quad (5.10)$$

Following a similar approach for the second scenario, where the tagged MMT receives service from the WLAN AP $w \in \boldsymbol{W}$, and letting $\boldsymbol{L_c} \subseteq \boldsymbol{C}$ denote the set of candidate LTE-A cells, provided by the ANDSF, we can show that the utilization

of the LTE-A interface is more preferable in terms of average overall power consumption at the MMT, if the following condition is satisfied:

$$RSRP(c) > A(w,c) \text{ , for at least one } c \in \boldsymbol{L_c} \quad (5.11)$$

where the decision threshold $A(w,c)$ is given in (5.12).

$$A(w,c) = \frac{q_l(T)\cdot\gamma_l\cdot T_{RS}(c)\cdot I(c)}{\sum_{s\in \boldsymbol{S}} q_w(s)\cdot P_w(s) + q_w(T)\cdot\gamma_w\cdot\frac{T_{TPU}(w)}{(RCPI(w)-ANPI(w))}\cdot ANPI(w) - \sum_{s\in \boldsymbol{S}} q_l(s)\cdot P_l(s)} \quad (5.12)$$

Note that the parameters in (5.10) and (5.12) include a) standard LTE-A and WLAN PoA measurements, i.e., $T_{RS}(c)$, $I(c)$, $T_{TPU}(w)$ and $ANPI(w)$, which can be commuted to the ANDSF by using existing network signaling procedures, b) fixed and known values for the characteristics of the user's services, i.e., $q_l(s)$, $q_w(s)$, and SINR target , i.e., γ_l and γ_w, which can be provided by the serving PoA, and c) fixed and known values for the MMT power consumption per state, i.e., $P_l(s)$ and $P_w(s)$, which can be stored at the MMT and commuted to the ANDSF by using the push mode [18][19][20]. On the other hand, the left sides of (5.9) and (5.11) include standard MMT measurements, i.e., $RSRP(c)$, $RCPI(w)$ and $ANPI(u)$, which can be performed locally at the MMT and readily utilized for VHO decision. Based on the aforementioned observation, we propose the following energy-efficient inter-system mobility policy:

Energy-Efficient Inter-System Mobility Policy

Rule 1: (LTE-A to IEEE 802.11-2012)

if the serving PoA is of LTE-A type

if $RCPI(w) - ANPI(u) > A(c,w)$ for at least one $w \in \boldsymbol{L_w}$

Switch on the IEEE 802.11-2012 interface

Associate with $w \in \boldsymbol{L_w}$

Switch off the LTE-A interface

endif

endif

Rule 2: (IEEE 802.11-2012 to LTE-A)

if the serving PoA is of IEEE 802.11-2012 type

if $RSRP(c) > A(w,c)$ for at least one $c \in \boldsymbol{L_c}$

Switch-on the LTE-A interface

Associate with $c \in \boldsymbol{L_c}$

Switch-off the IEEE 802.11-2012 interface

endif

endif

Notably, the proposed policy can be deployed in a backwards-compatible manner at the MMT by conducting standard measurements locally and by acquiring the thresholds $A(c,w)$ and $A(w,c)$ on-demand to the ANDSF.

5.2.4 Energy-Efficient Intra-System Mobility Policy

Even though the selection of the least power consuming RAT can be based on the proposed policy in Section III.B, the selection of the least power consuming PoA of the same RAT type remains an open issue, i.e., intra-system mobility. In this section, we present an energy-efficient intra-system mobility policy which utilizes a) standard measurements performed locally at the MMT, and b) the decision thresholds in (5.10) and (5.12), provided by the ANDSF. We identify two different intra-system mobility decision scenarios: the intra-LTE-A and the intra-WLAN decision scenarios.

Let us focus on the intra-LTE-A scenario, where the tagged MMT $u \in \boldsymbol{U}$ receives service from the LTE-A cell $s \in \boldsymbol{C}$ and investigates the possibility of handing over to a LTE-A cell in the candidate set $\boldsymbol{L_c}$, provided by the ANDSF. A handover from cell $s \in \boldsymbol{C}$ to a cell $c \in \boldsymbol{L_c}$ will reduce the average overall MMT power if the following condition applies:

$$P_{LTE-A}(c) < P_{LTE-A}(s) \qquad (5.13)$$

By using (5.2) and (5.6), it can be shown that the condition in (5.13) is equivalent with the one in (5.14).

$$RSRP(c) > RSRP(s) \cdot \frac{T_{RS}(c) \cdot I(c)}{T_{RS}(s) \cdot I(s)} \qquad (5.14)$$

Taking into account that the ratio $\frac{T_{RS}(c) \cdot I(c)}{T_{RS}(s) \cdot I(s)}$ is equal to $\frac{A(w,c)}{A(w,s)}$ (the denominators in the decision thresholds are equal) and by extending (5.14) to the multi-cell decision scenario, we can readily show that the selection of the least power consuming LTE-A cell can be based on the following criterion:

$$\arg\max_{c \in \boldsymbol{L_c}} RSRP(c) := \left\{ c \mid RSRP(c) > RSRP(s) \cdot \frac{A(w,c)}{A(w,s)} \right\} \qquad (5.15)$$

where the decision thresholds $A(w,c)$ and $A(w,s)$ are taken with respect to a random WLAN PoA $w \in \boldsymbol{L_w}$.

Following a similar approach for the intra-WLAN scenario and letting v denote the serving WLAN AP, we can readily show that the selection of the least power consuming AP can be based on the following criterion:

$$\arg\max_{w \in \boldsymbol{L_w}} \big(RCPI(w) - ANPI(w)\big) := \Big\{ w \mid \big(RCPI(w) - ANPI(w)\big) > \big(RCPI(v) - ANPIv \cdot A(c,w) A(c,v) \qquad (5.16)$$

Interestingly, the set of parameters that allow the MMT to deploy the proposed energy-efficient inter-system mobility policy, also enable it to select the least power consuming PoA of the same RAT (energy-efficient intra-system mobility).

5.3 The Proposed Vertical Handover Decision Algorithm

In this section, we integrate the energy-efficient inter-system and intra-system mobility policies presented in the previous two subsections, respectively, into a single ANDSF-assisted energy-efficient VHO decision algorithm: the ARCHON algorithm. The ARCHON algorithm utilizes local MMT measurements and ANDSF information to select the least power consuming PoA in the heterogeneous network under all feasible VHO decision scenarios, i.e., WLAN to LTE-A, LTE-A to WLAN, intra-LTE-A and intra-WLAN. Let s denote the serving PoA when the

MMT is connected to the LTE-A system, and v when it is connected to the WLAN system. Then, the proposed algorithm is summarized as follows:

ARCHON Algorithm

1. VHO decision triggering
2. ANDSF request for candidate PoA $\boldsymbol{L_c}$ and $\boldsymbol{L_w}$
3. Standard measurements on the PoA sets $\boldsymbol{L_c}$ and $\boldsymbol{L_w}$
4. **if** the serving PoA is of LTE-A type
5. $w = rand(\boldsymbol{L_w})$
6. ANDSF request for $A(w,c)$ $\forall c \in \boldsymbol{L_c}$
7. $c = \arg\max_{c \in \boldsymbol{L_c}} RSRP(c) = \left\{c |\ RSRP(c) > RSRP(s) \cdot \frac{A(w,c)}{A(w,s)}\right\}$
8. ANDSF request for $A(c,w)$ $\forall w \in \boldsymbol{L_w}$
9. **if** $RCPI(w) - ANPI(u) > A(c,w)$ for one $w \in \boldsymbol{L_w}$
10. Switch on the IEEE 802.11-2012 interface
11. Associate with $w \in \boldsymbol{L_w}$ satisfying Eq. (5.16)
12. Switch off the LTE-A interface
13. **else if** $c \neq s$
14. Associate with the LTE-A PoA c
15. **endif**
16. **else if** the serving PoA is of IEEE 802.11-2012
17. $c = rand(\boldsymbol{L_c})$
18. ANDSF request for $A(c,w)$ $\forall w \in \boldsymbol{L_w}$
19. $w = \arg\max_{w \in \boldsymbol{L_w}} \big(RCPI(w) - ANPI(w)\big) = \big\{w | \big(RCPI(w) - ANPI(w)\big) > RCPIv - ANPIv \cdot A(c,w) A(c,v)$
20. ANDSF request for $A(w,c)$ $\forall c \in \boldsymbol{L_c}$
21. **if** $RSRP(c) > A(w,c)$ for at least one $c \in \boldsymbol{L_c}$
22. Switch on the LTE-A interface
23. Associate with $c \in \boldsymbol{L_c}$ satisfying Eq. (5.15)
24. Switch off the IEEE 802.11-2012 interface
25. **else if** $w \neq v$
26. Associate with the IEEE 802.11-2012 PoA w
27. **endif**
28. **endif**

Upon VHO decision triggering (step 1), the MMT requests for network discovery information from the ANDSF (step 2) and performs standard measurements to assess the radio status of the candidate PoAs (step 3). If the serving PoA is a LTE-A cell (step 4), the MMT randomly selects a candidate WLAN AP (step 5), requests from the ANDSF the inter-system mobility policy for the selected AP

(step 6) and deploys the proposed intra-system mobility criterion in Eq. (15) to identify the least power consuming LTE-A cell c (step 7). In the following, the MMT requests the ANDSF inter-system policy for the least power consuming LTE-A cell (step 8) and deploys the proposed energy-efficient inter-system mobility policy (steps 9-12). If all candidate WLAN APs result in higher power consumption compared to that of the LTE-A cell c, the MMT initiates a handover request towards cell c and the algorithm terminates (steps 13-15). A similar approach is followed when the serving PoA is a WLAN AP (steps 16-28).

5.4 Numerical Results

This section includes selected numerical results to evaluate the performance of the proposed VHO decision algorithm in the integrated LTE-Advanced – WLAN network. In section 5.4.1 we describe the developed system-level simulations model and the key parameters governing its operation. In section 5.4.2, we present comprehensive simulation results on the performance of the proposed VHO decision algorithm and compare it against a) a VHO algorithm that always prioritizes WLAN over LTE-Advanced macrocell access, referred to as the *baseline WLAN* algorithm in the following, and b) a VHO algorithm that always prioritizes LTE-Advanced over WLAN macrocell access, referred to as the *baseline LTE-Advanced algorithm* in the following.

5.4.1 Simulation Model and Parameters

A conventional hexagonal LTE-Advanced network is considered, including a main LTE-Advanced cluster composed of 7 LTE-Advanced cells, where each LTE-Advanced cell consists of 3 hexagonal sectors. The wrap-around technique is used to extend the LTE-Advanced network, by copying the main LTE-Advanced cluster symmetrically on each of the 6 sides. A set of blocks of apartments, referred to as *WLANblocks*, are uniformly dropped within the main LTE-Advanced cluster according to a scenario-related parameter d_{WB} indicating the WLAN block deployment density within the main LTE-Advanced cluster. The WLAN blocks are modeled in accordance with the dual stripe model for dense urban environments in [123], shown in Figure 44.

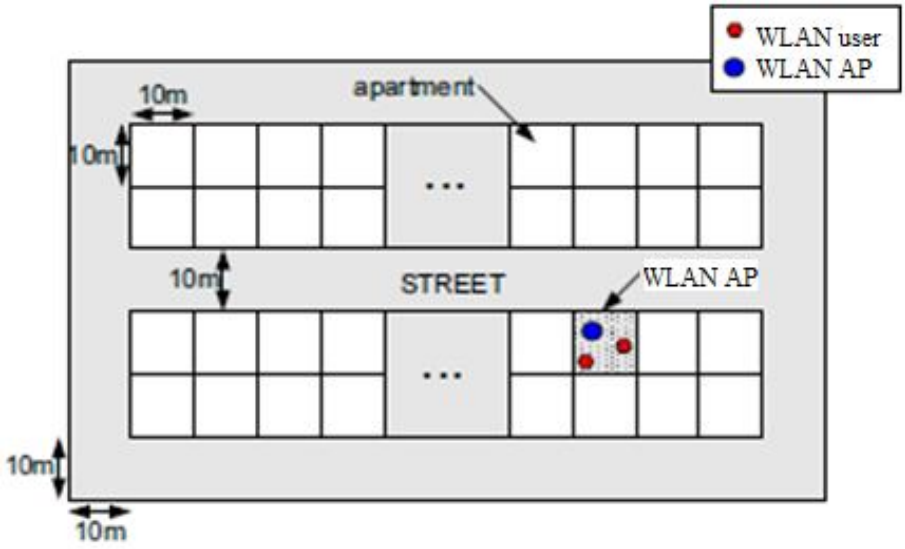

Figure 44: Dual-stripe WLAN block model for dense urban environments

According to it, each WLAN block consists of two stripes of apartments separated by a 10 m wide street while each stripe has two rows of $A = 5$ apartments of size

10×10 m. The WLAN APs are deployed with respect to a WLAN deployment ratio parameter $r_{wc} = 0.2$, indicating the probability of deploying a WLAN inside an apartment. Each WLAN AP is initially considered to provide service to one associated user. Both the WLAN APs and the associated users are uniformly dropped inside the apartment. Ten macrocell users are uniformly distributed within each LTE-Advanced sector, while both the WLAN APs and the LTE-Advanced users may freely move within the LTE-Advanced cluster area in accordance with the mobility model summarized in Table 12. Unless differently stated, the user mobility model is characterized by an average user speed $\bar{v} = 3$ km/h and a standard speed deviation $s_u = 1$ km/h.

The LTE-Advanced cells utilize a 10MHz bandwidth and operate in one of the bands centered in 1990, 2000, and 2010 MHz. The LTE-Advanced cell inter-site distance is set to 500m, while the WLAN APs are assumed to utilize one of the 1, 6, 11, and 14 ISM bands. The adopted Modulation and Coding Schemes (MCS) are in accordance with [135] for both systems, while the Exponential Effective SINR Mapping method is used to obtain the effective SINR per RB and the consequential MMT throughput [123]. The minimum required SINR per MMT is set to $\overline{\gamma}_t = 2.88$ dB for both systems, while the communications are carried out in full buffer in accordance to the traffic model parameters shown in Table III. The shadowing standard deviation for the LTE-Advanced and the WLAN systems are both assumed 8 dB, and the LTE-Advanced and WLAN noise figures are set to 5 and 8 dB in that order. The LTE-Advanced downlink RS power transmissions are normally distributed with a mean value of 23 dBm and a standard deviation of 3dB, whereas the respective WLAN beacon transmissions are normally distributed with a mean value of 23 dBm and a standard deviation of 3dB. The power class of the LTE-Advanced radio access interface is set to 23dBm, while the power class for the WLAN interface is set to 20 dBm. The maximum transmission powers for the LTE-Advanced and WLAN PoAs are set to 43 and 23dBm, respectively. The remainder simulations parameters, along with the aforementioned ones, are summarized in Table 12. Note that the power consumption values for the LTE-Advanced and WLAN interfaces are taken from [131] and [132], respectively.

Table 12: System-level simulation parameters

Network layout		
Macrocell layout	7 clusters, 7 sites per cluster, 3 sectors per site, freq. reuse 1	
Macrocell inter-site distance	500 m	
Initial number of UEs per macrocell sector	10 UEs	
Macrocell UE distribution	Uniform within each sector	
WLAN block layout	Dual stripe model for dense urban environments [123]	
WLAN block distribution in the main LTE-Advanced cluster	Uniform	
WLAN AP and UE distribution within an apartment	Uniform	
Initial number of UEs per WLAN AP	1 UE	
System operating parameters		
Parameter	**Macrocell**	**WLAN**

Carrier frequency	Uniformly picked from the set {1990, 2000, 2010} MHz		Uniformly picked from the set { 2412, 2437, 2462, 2484 } MHz (bands 1,6, 11,14)
Channel bandwidth	10 MHz		22 MHz
Maximum Tx Power	$\overline{P}_{max}^{c,T} = 46$ dBm		$\overline{P}_{max}^{c,T} = 20$ dBm
Antenna gain	14 dBi		5 dBi
Noise figure	5 dB		8 dB
Shadowing standard deviation	8 dB		8 dB
Transmit power on the pilot signals	Normally distributed with a mean value of 23 dBm and standard deviation 3dB		Normally distributed with a mean value of 20 dBm and standard deviation 5dB
Maximum Number of Users	50		20
Link-to-system mapping	Effective SINR mapping (ESM) [123]		
Path Loss Models			
Path loss	Models for urban deployment in [123]		
Interior / Exterior wall penetration loss (indoor UEs)	5 / 15 dB		
UE parameters			
UE power class	LTE: 23 dBm, WLAN: 20 dBm		
UE antenna gain	LTE: 0 dBi, WLAN: 0 dBi		
Mean UL SINR target	LTE: $\gamma_t^{LTE} = 2.88$ dB, WLAN: $\gamma_t^{WLAN} = 2.88$ dB		
Traffic model WLAN	Full buffer similar to [123], $p_{WLAN}(T) = 0.4$, $p_{WLAN}(I) = 0.3$. and $p_{WLAN}(R) = 0.3$		
Traffic model LTE	Full buffer similar to [123], $p_{LTE}(T) = 0.4$, $p_{LTE}(I) = 0.3$. and $p_{LTE}(R) = 0.3$		
Power Consumption parameters WLAN	$P_{B,WLAN} = 924\,mW$, $P_{WLAN}(R) = 594\,mW$, $P_{WLAN}(I) = 80\,mW$		
Power Consumption parameters LTE	$P_{B,LTE} = 1550\,mW$, $P_{LTE}(R) = 1420\,mW$, $P_{LTE}(I) = 160\,mW$		
Mobility model [71]	User speed	$v_t = N(\bar{v}, s_u)$ m/s	
		Mean user speed	$\bar{v} = 3$ km/h
		User speed standard deviation	$s_u = 1$ km/h
	User direction	$\varphi_t = N\left(\varphi_{t-1}, 2\pi - \varphi_{t-1}\tan\left(\frac{\sqrt{v_t}}{2}\right)\Delta t\right)$	
	where Δt is the time period between two updates of the model, and $N(a,b)$ the Gaussian distribution of mean a and standard deviation b		
Other simulation parameters			
Overall simulation time	200 sec		
Simulation time unit	$\Delta t = 1$ sec		

Fig. 7 demonstrates a random snapshot for the network topology used in our system-level simulator. The proposed algorithm has been compared against a) a

VHO algorithm that always prioritizes WLAN over LTE-Advanced macrocell access, referred to as the baseline WLAN algorithm in the following, and b) a VHO algorithm that always prioritizes LTE-Advanced over WLAN macrocell access, referred to as the baseline LTE-Advanced algorithm in the following.

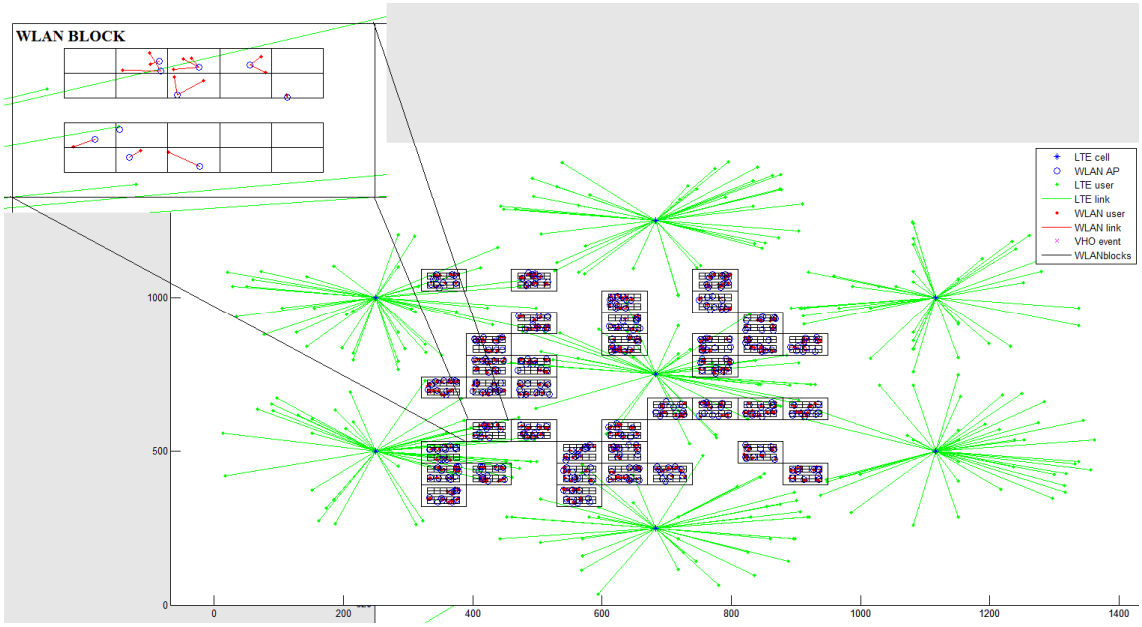

Figure 45: Snapshot of the dynamic system level simulator

The performance of the algorithms has been investigated for various performance measures for increasing WLANblock density d_{WB} and fixed WLAN deployment ratio per WLANblock equal to $r_{wc} = 0.2$, i.e., 20% of the apartments are equipped with a WLAN AP. The performance measures under investigation include the number of users per RAT type, MMT power consumption, mean MMT energy consumption per bit, mean MMT transmit power, mean cell received interference power, mean uplink capacity per user, mean PoA transmit power, signaling rate for the two RAT systems, and HO/VHO/NS probability. Unless differently stated, the performance of the algorithms is averaged over both the LTE-Advanced and WLAN interfaces or PoAs.

5.4.2 System-level Simulation Results

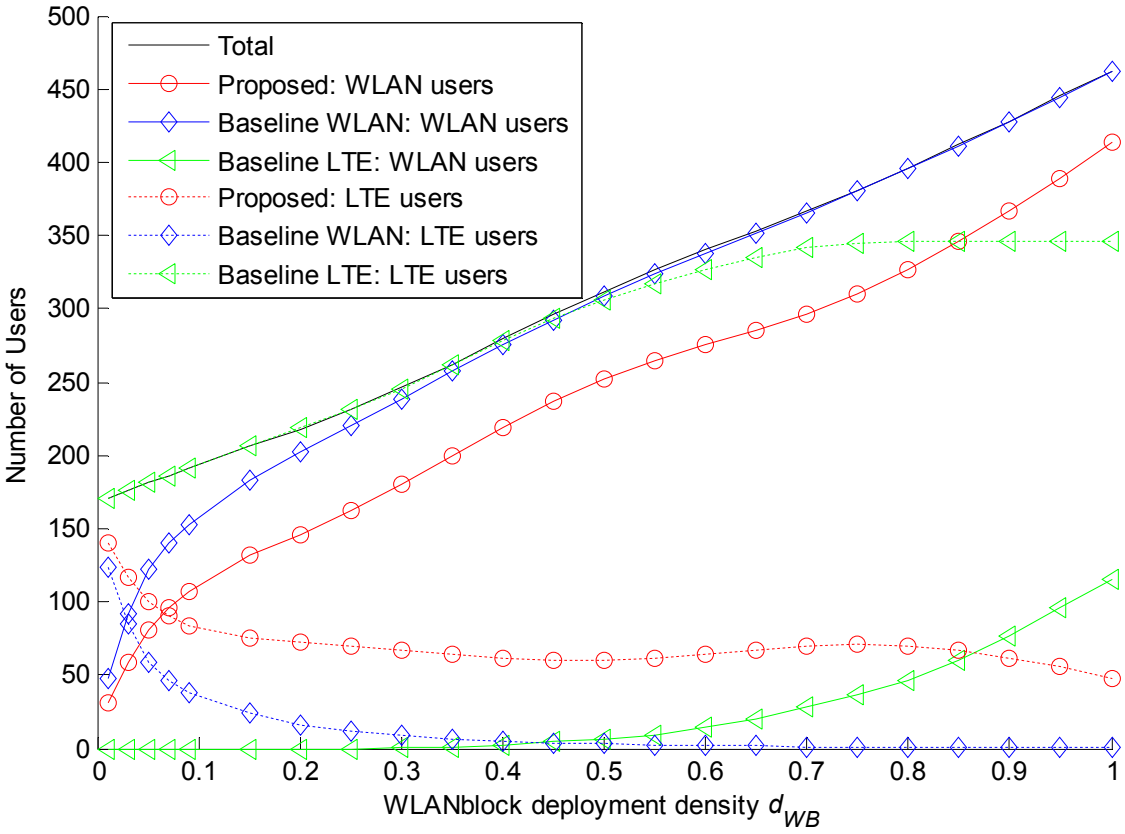

Figure 46: Number of Users versus the WLANblock deployment density

Figure 46 demonstrates the average number of users per RAT type for all algorithms and increasing WLANblock deployment density d_{WB}. Note that the total number of users in the system (black line) increases linearly for increasing WLANblock deployment density d_{WB}, provided that the introduction of additional WLANblocks not only increases the WLAN AP deployment density but also the number of users in the system (one additional user is introduced for each additional WLAN AP). As expected, all users are served by the LTE-Advanced system for the baseline LTE-Advanced VHO algorithm (dotted green line) until the maximum LTE-Advanced capacity on the cells is reached, i.e., for $d_{WB} = 0.6$ the number of users is close to 350, where the remainder users are required to connect to the WLAN system (compact green line). In contrast, the number of WLAN users increases rapidly for the baseline WLAN VHO algorithm (dotted blue line) as the density of WLANblocks increases in the system, until all users are finally served by the WLAN system. Interestingly, the proposed algorithm is capable of balancing the number of users between the LTE-Advanced and WLAN systems. However, this is achieved without sacrificing the energy saving opportunities provided by the WLAN system which, in the average, is more energy-efficient compared to the LTE-Advanced one. As seen in Figure 46, the proposed VHO algorithm sustains a roughly fixed number of LTE-Advanced users which, in particular, are in such a range from the LTE-Advanced macrocells that can result in lower power consumption compared to the one provided of the WLAN system. Summarizing, the proposed algorithm is capable of balancing the user load between the two heterogeneous systems, while attaining the lower power consumption for the MMTs (Figure 47).

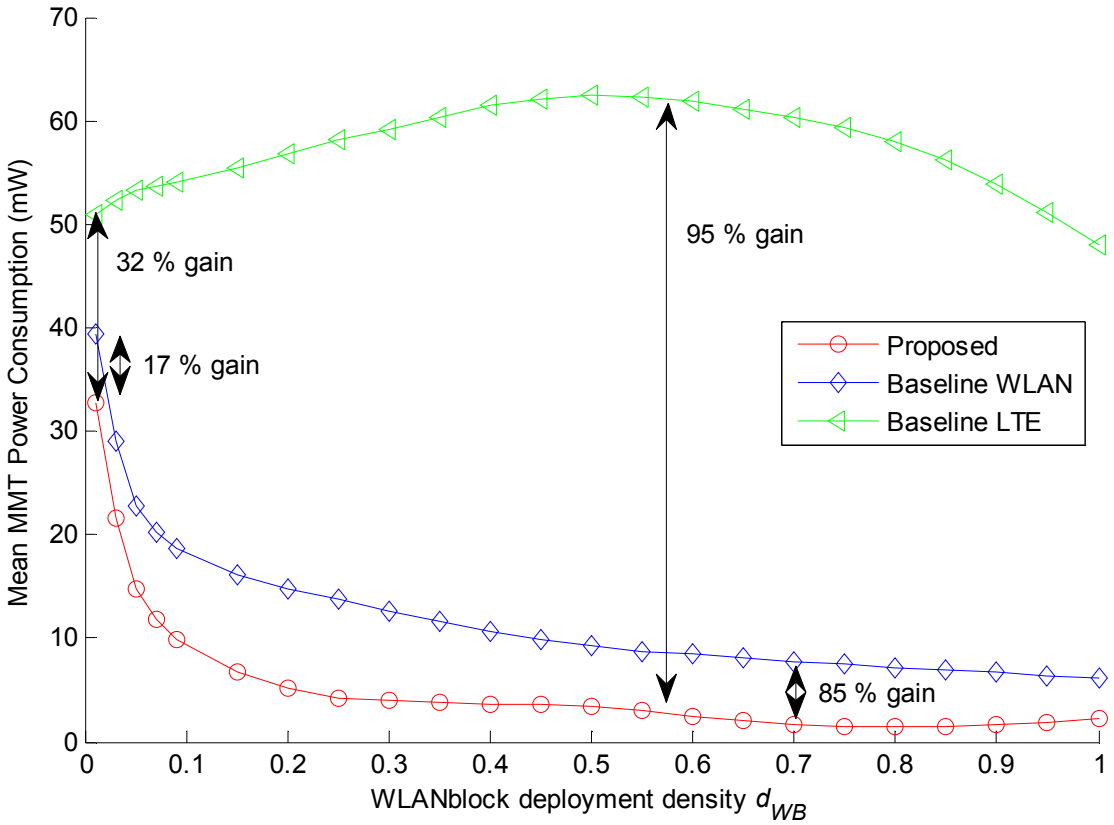

Figure 47: Mean MMT Power Consumption versus the WLANblock deployment density

Figure 47 demonstrates the mean MMT power consumption for all algorithms and for increasing WLANblock deployment density within the main LTE-Advanced cluster. As expected, prioritized access to the LTE-Advanced system results in higher power consumption for the MMTs compared to both the baseline WLAN and proposed VHO decision algorithms. On the other hand, utilizing the WLAN infrastructure is shown to reduce the MMT power consumption compared to the baseline LTE-Advanced algorithm, mainly owing to the shorter range nature of communications. The proposed algorithm is shown to reduce the MMT power consumption by up to 95% compared to the prioritized LTE-Advanced access scenario (baseline LTE-Advanced algorithm), with the higher gains attained in medium to high WLAN deployment densities, i.e., close to $0.4 < d_{WB} < 0.7$. In addition, the proposed algorithm is shown to greatly reduce the power consumption of the MMTs compared to the prioritized WLAN based algorithm (baseline WLAN) as well, providing power consumption gains that vary between 17% and 85%. On the average, the proposed algorithm reduces the power consumption of the MMTs compared to the baseline LTE-Advanced system by approximately 82%, whereas it also reduces the MMT power consumption compared to the baseline WLAN system by 73% compared to the baseline WLAN algorithm as well.

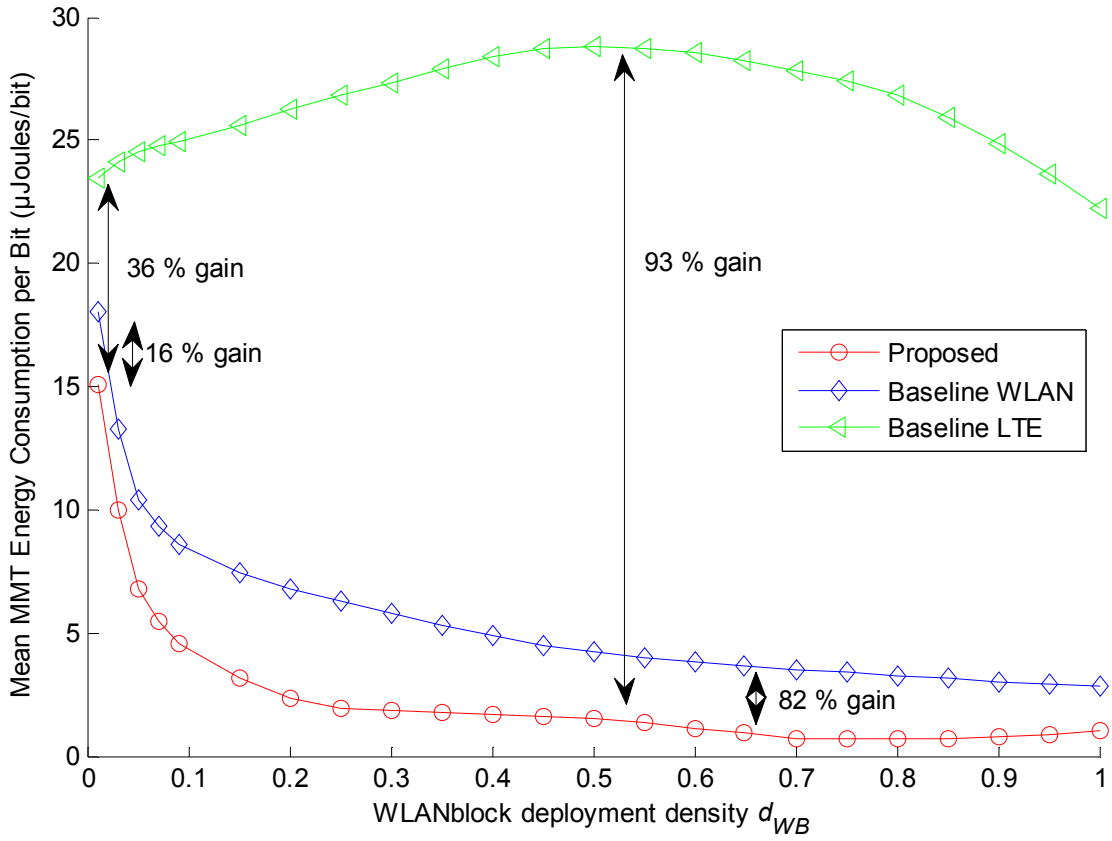

Figure 48: Mean MMT Energy Consumption per bit versus the WLANblock deployment density

The positive impact of the enhanced power consumption, attained by the proposed VHO algorithm, is also evident in terms of mean energy consumption per bit (joules/bit) (Figure 48). As shown in Figure 48, the proposed algorithm reduces the mean energy consumption per bit for the MMTs by up to 93% compared to the baseline LTE-Advanced VHO algorithm and up to 82% compared to the baseline WLAN algorithm. Interestingly, the proposed VHO algorithm cuts down to half the mean MMT energy consumption per bit compared to the other two competing algorithms, even when the WLAN deployment density is relatively low, i.e., $d_{WB} = 0.1$.

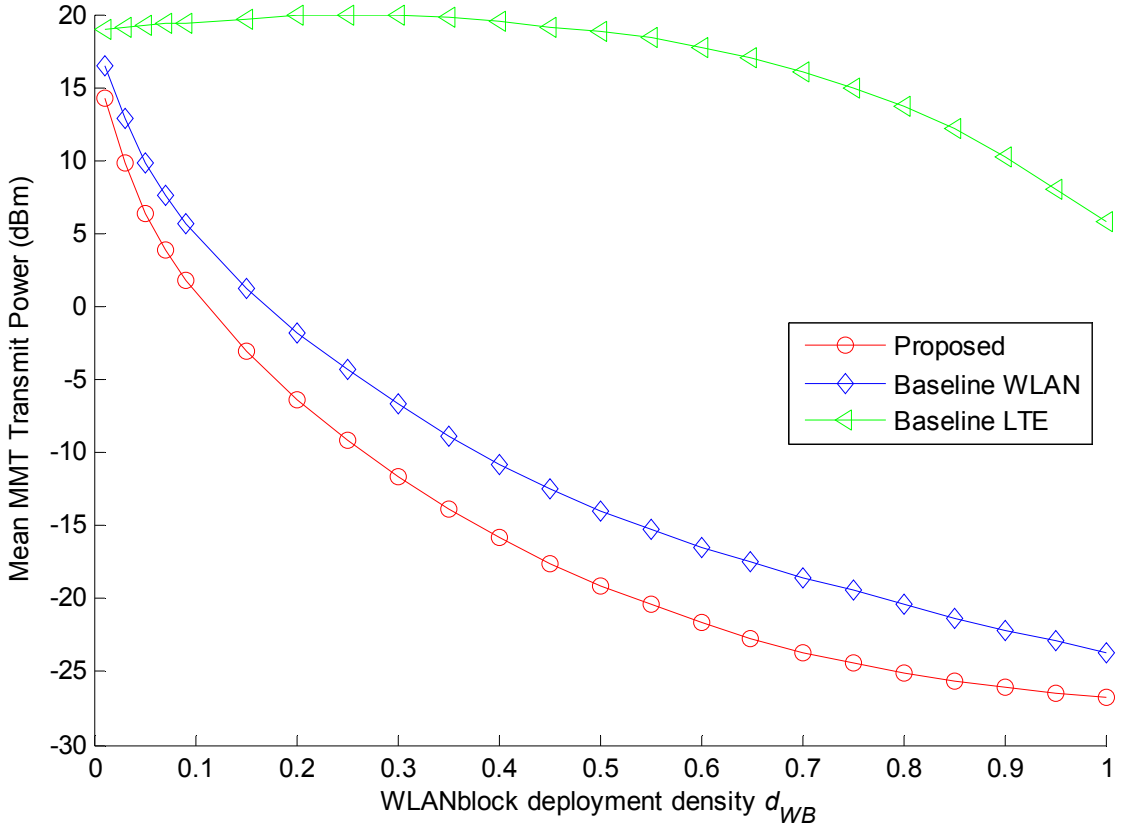

Figure 49: Mean MMT Transmit Power versus the WLANblock deployment density

Figure 49 demonstrates the mean MMT transmit power for all algorithms and increasing WLANblock deployment density. Figure 49 reveals that the reduced power consumption of the proposed algorithm not only originates from taking into account the actual power consumption per interface state, for the various RATs, but it is also a direct outcome of the algorithm's capability to account for the expected mean transmit power of the MMTs on the target PoAs. Interestingly, even though the proposed algorithm balances the number of users between the two different systems (Figure 46) it is capable of lowering the mean MMT transmit power compared to the baseline WLAN algorithm (Figure 49). In more detail, even though prioritizing WLAN access is expected to greatly reduce the mean transmit power for the MMTs, owing to the shorter transmit-receive range, this is not true in practice where a high utilization of the unlicensed ISM bands (high spectrum reusability) takes place leading to increased interference in the WLAN AP sites. Compared to the baseline WLAN algorithm, the proposed VHO algorithm reduces the required transmit power for the MMTs almost twofold, owing to the fact that it accounts for the interference at the PoA sites as well as the actual channel gain between the user and the target PoA ((5.18), (5.19), (5.26), and (5,28)). The same implies for the comparison between the proposed and the baseline LTE-Advanced algorithm.

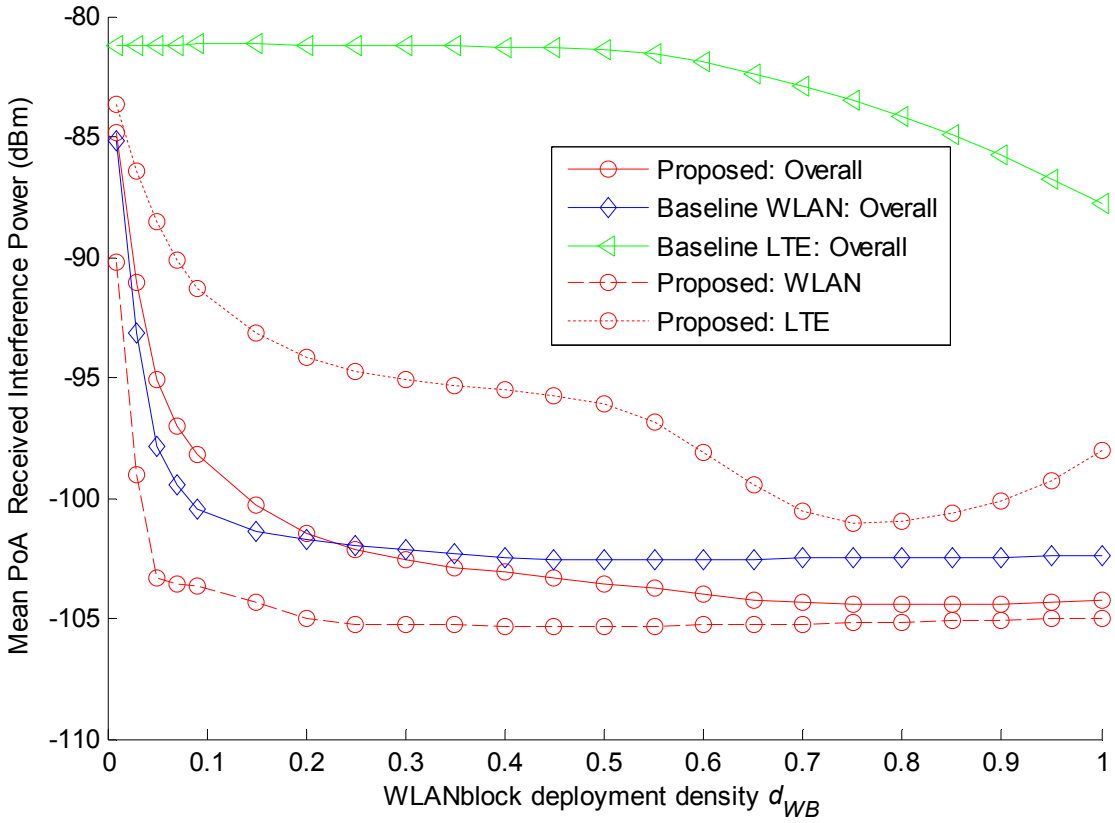

Figure 50: Mean PoA Received Interference Power versus the WLANblock deployment density

As expected, the positive impact of the reduced MMT transmit power, attained by the proposed VHO algorithm, is also depicted in terms of mean received interference power at the PoA sites (Figure 50). The baseline LTE-Advanced algorithm is shown to result in the highest interference at the PoA sites, on the average, owing to the severe underutilization of the WLAN infrastructure (Figure 46) which does not allow for the decongestion of the LTE-Advanced system. Nevertheless, when the maximum user capacity is reached for the LTE-Advanced system (Figure 46 for $d_W > 0.6$), the WLAN infrastructure is utilized and the mean PoA interference is ultimately being reduced. Figure 50 also shows that even though the proposed algorithm utilizes the LTE-Advanced infrastructure, the mean received interference performance at the PoAs is similar or even improved compared to the baseline WLAN algorithm. More importantly, the proposed algorithm is shown to greatly reduce the interference at the WLAN APs (dotted red line) in medium to high WLAN deployment densities, compared to the baseline WLAN algorithm (compact blue line), by up to 5 dBs, an improvement which is higher than a threefold decrease.

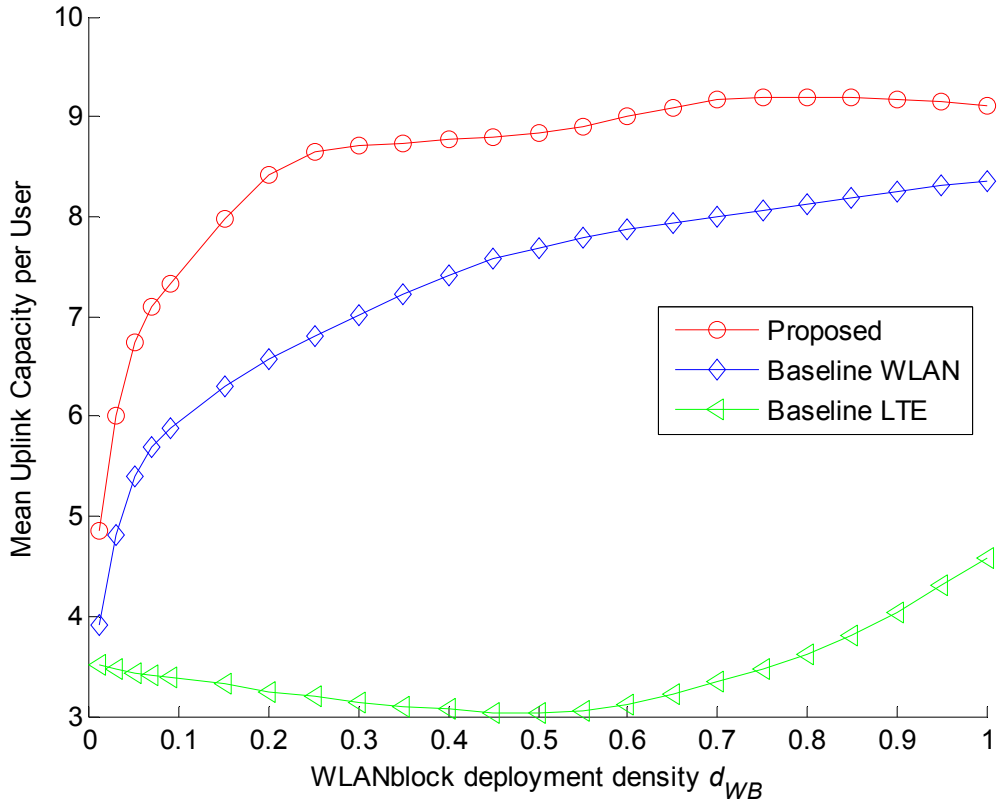

Figure 51: Mean Uplink Capacity per User versus the WLANblock deployment density

The smart utilization of both the LTE-Advanced and WLAN systems, both in terms of balancing the number of users in the two systems (Figure 46) and in terms of lowering the interference at the PoA sites (Figure 51), enables the proposed VHO algorithm to attain a significantly increased mean uplink capacity for the MMTs as well, compared to both the baseline WLAN and the baseline LTE-Advanced algorithms. Note that the mean uplink capacity per user corresponds to the uplink capacity that a user can attain if it fully utilizes the available bandwidth to its serving cell without using a specific mean SINR threshold. As expected, the baseline WLAN algorithm attains an improved mean uplink capacity per user compared to the baseline LTE-Advanced algorithm, which tends to attain a roughly fixed performance for $d_W > 0.5$. Note that the performance of the baseline LTE-Advanced algorithm improves above this value, given that the utilization of the WLAN infrastructure increases (Figure 46).

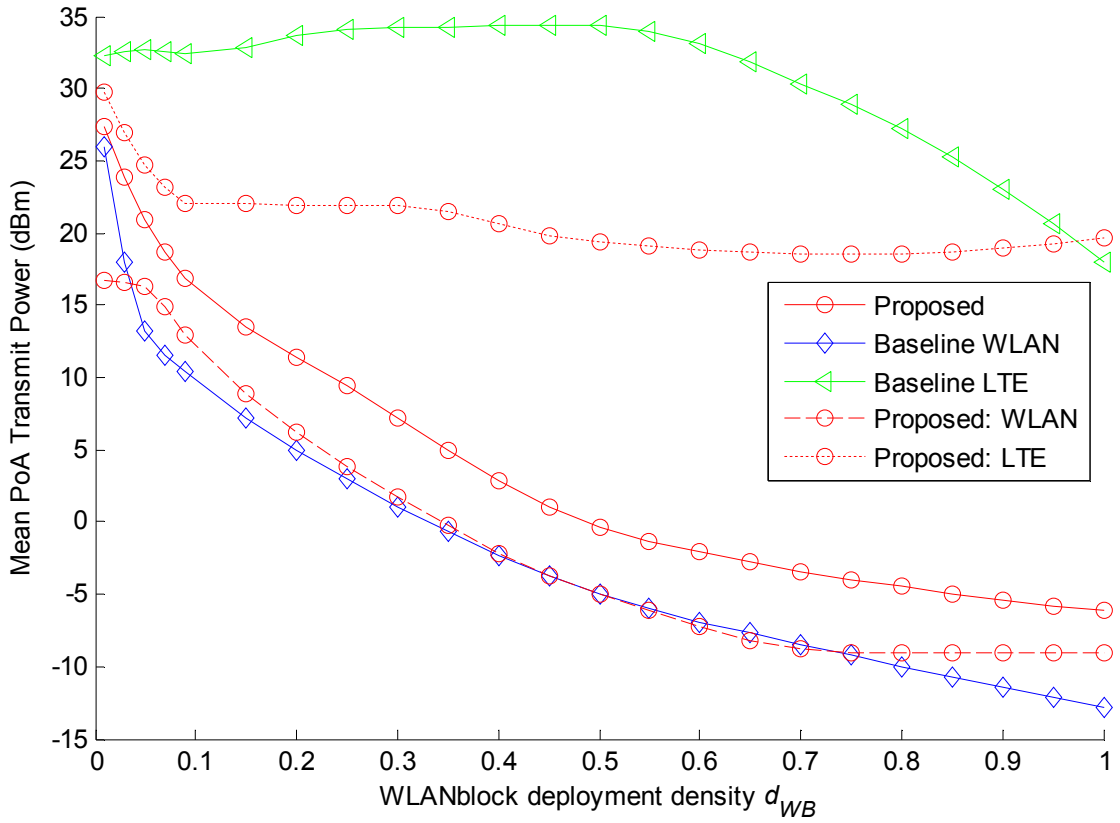

Figure 52: Mean PoA Transmit Power versus the WLANblock deployment density

Figure 52 demonstrates the mean PoA transmit power for all algorithms and increasing WLANblock deployment density. As expected, the baseline LTE-Advanced algorithm results in the highest transmit power at the PoA given that it is based on prioritizing the utilization of the marcocell infrastructure. On the other hand, the baseline WLAN algorithm is shown to result in the lower PoA transmit power owing to the highest possible utilization of the short-range nature of WLAN access. Referring to the performance of the proposed algorithm, three key observations are important to note. At first, the proposed algorithm requires increased PoA transmit power on the average (compact red line) compared to the baseline WLAN (compact blue line), owing to the higher utilization of the LTE-Advanced infrastructure. Nevertheless, if we focus on the WLAN infrastructure only, the proposed algorithm achieves comparable performance with the baseline WLAN algorithm (dashed red line), while if we focus only on the LTE-Advanced infrastructure, the proposed algorithm requires significantly reduced PoA transmit power compared to the baseline LTE-Advanced algorithm as well.

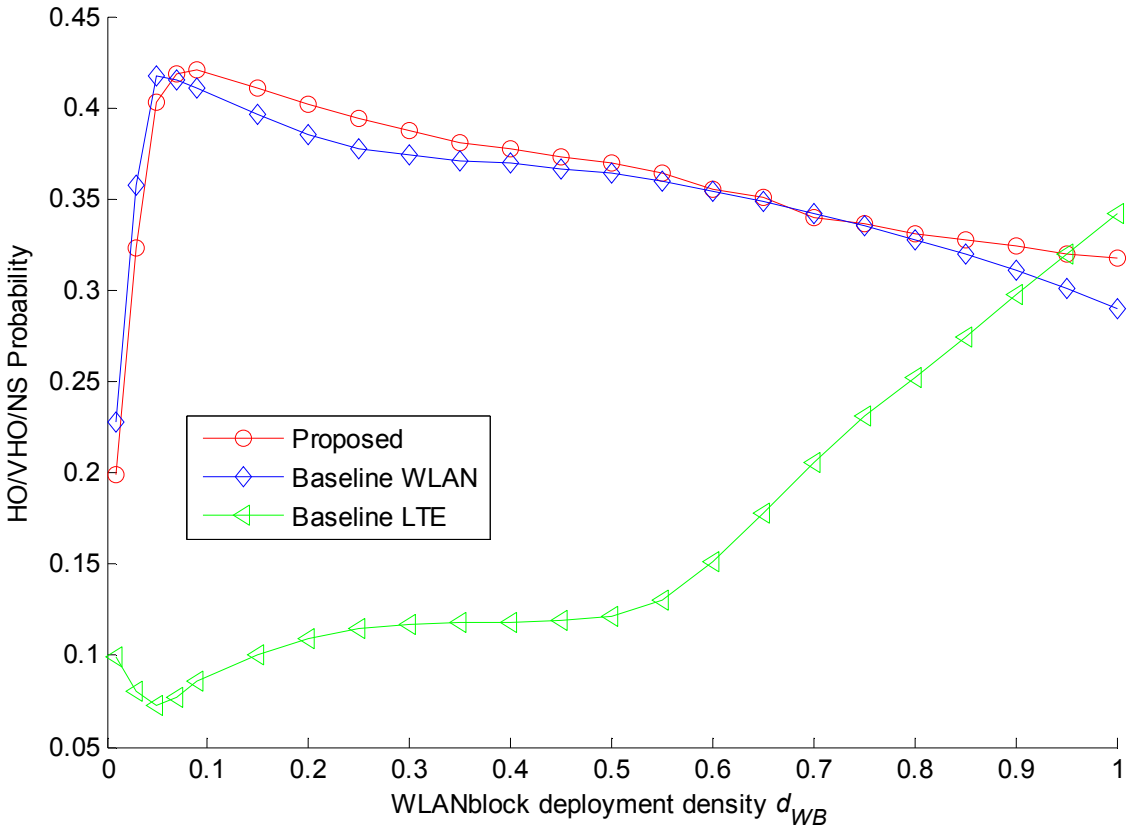

Figure 53: (V)HO probability versus the WLANblock deployment density

Figure 53 illustrates the summation of the HO probability in the LTE-Advanced network, the VHO probability between the LTE-Advanced – WLAN systems, and the number of network selection events in the WLAN systems, for all algorithms and varying WLANblock deployment density. As expected, until the LTE-Advanced system reaches its maximum capacity ($\sim d_W = 0.6$) the baseline LTE-Advanced algorithm results in significantly lower HO/VHO/NS probability compared to both the proposed and the WLAN system, owing to the longer transmit – receive range between the MMT and the PoA. However, upon this threshold the number of VHO and NS events increases rapidly for the baseline LTE-Advanced algorithm which ultimately reaches that of the other two competing schemes ($d_W = 0.9$). On the other hand, Figure 53 demonstrates that the proposed and the baseline WLAN VHO algorithms show similar performance in terms of VHO probability. As a consequence, even though the deployment of the proposed algorithm results in multiple benefits for the MMT and the integrated LTE-Advanced – WLAN system, it simultaneously results in similar HO/VHO/NS probability performance with the widely adopted approach to prioritize WLAN over LTE-Advanced access (baseline WLAN algorithm).

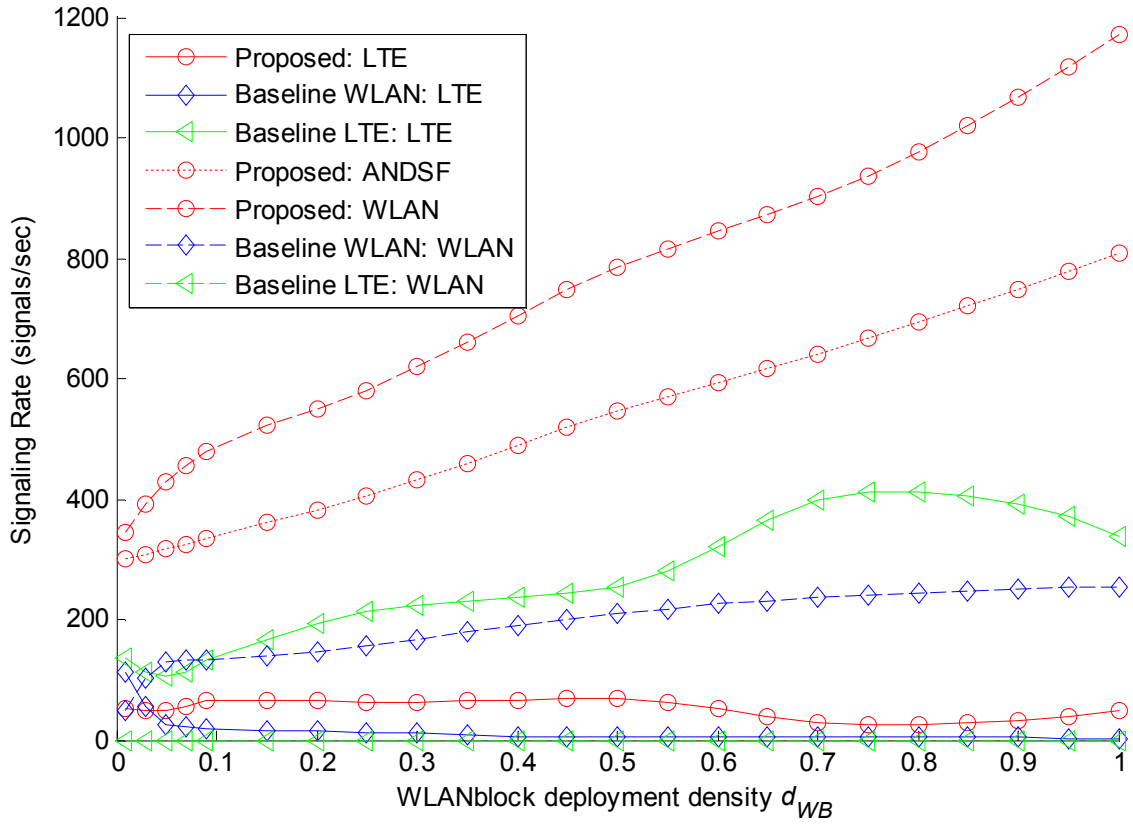

Figure 54: Signaling Rate versus the WLANblock deployment density

Figure 54 concludes our system-level simulation analysis by depicting the signaling rate, i.e., number of signals in the system per second, passing through the LTE-Advanced and the WLAN systems as well as the ANDSF module for the VHO algorithms under scope. Note that the ANDSF signaling only applies to the proposed algorithm, which uses the concept of inter-system mobility policy to attain backwards compatibility with the LTE-Advanced and WLAN systems. As expected, the baseline LTE-Advanced algorithm results in the highest signaling rate among the LTE-Advanced system as it avoids the utilization of the WLAN infrastructure. On the other hand, the LTE-Advanced network signaling requirements for the baseline WLAN algorithm reduces rapidly and is practically diminished provided that the vast majority of users in the system prioritize WLAN access. Interestingly, the deployment of the proposed algorithm significantly reduces the LTE-Advanced network signaling compared to the baseline LTE-Advanced algorithm, however, it also significantly increases the WLAN network signaling owing to its requirement for signal quality measurement exchange between the wireless stations and the MMT. Nevertheless, the required signaling load is increasing linearly for increasing WLANblock deployment density, allowing the system level engineer to anticipate for the signaling requirements for deploying the proposed algorithm.

5.5 Summary of Results and Conclusions

In this section we have proposed ARCHON: an ANDSF-assisted energy-efficient VHO decision algorithm for the heterogeneous IEEE 802.11-2012 / LTE-A network. ARCHON utilizes recent enhancements to the 3GPP and IEEE Standards, including the deployment of the ANDSF and the provision for enhanced radio measurement capabilities at the heterogeneous PoAs. System-level simulations have shown that even though the deployment of ARCHON asks

for increased ANDSF and WLAN network signaling, it enables efficient load balancing between the heterogeneous RATs, reduced MMT energy consumption per bit and enhanced uplink capacity per user. In more detail, system-level simulations have shown that:

- Compared to the prioritized LTE-Advanced or WLAN base algorithms, the proposed algorithm is shown to balance the number of users between the two heterogeneous systems.

- Compared to the prioritized LTE-Advanced or WLAN base algorithms, the proposed algorithm is shown to reduce the mean MMT power consumption by approximately 82% and 73%, respectively.

- The proposed algorithm reduces the mean MMT power consumption by up to 93% compared to the baseline LTE-Advanced VHO algorithm and up to 82% compared to the baseline WLAN VHO algorithm.

- The reduced power consumption of the proposed algorithm originates from the facts that a) it takes into account for the actual power consumption per interface state for the various RATs, and b) it also significantly reduces the mean transmit power of the MMTs on the target PoAs.

- The positive impact of the reduced MMT transmit power attained by the proposed VHO algorithm, is also depicted in terms of mean received interference power at the PoA sites.

- The smart utilization of both the LTE-Advanced and WLAN systems, both in terms of balancing the number of users in the two systems and in terms of lowering the interference at the PoA sites, enables the proposed VHO algorithm to attain a significantly increased mean uplink capacity for the MMTs as well, compared to both the baseline WLAN and the baseline LTE-Advanced algorithms.

- If we focus on the WLAN infrastructure only, the proposed algorithm achieves comparable performance with the baseline WLAN algorithm, while if we focus only on the LTE-Advanced infrastructure, the proposed algorithm requires significantly reduced PoA transmit power compared to the baseline LTE-Advanced algorithm as well.

- The proposed and the baseline WLAN VHO algorithms show similar performance in terms of (V)HO probability.

- The aforementioned gains of the proposed algorithm are attained at the cost of an higher yet linearly increasing ANDSF and WLAN signaling rate with respect to the WLAN deployment density in the network.

Future plans include performance analysis and detailed specification of the required network signaling procedure.

6. MOBILITY MANAGEMENT FOR FEMTOCELLS IN LTE-ADVANCED: KEY ASPECTS, SURVEY OF HANDOVER DECISION ALGORITHMS AND SIMULATION STUDY

Mobility Management in the presence of femtocells, is one of the most challenging issues for wireless networking nowadays, owing to the dense network layout, the short cell radii and the potentially unplanned deployment. The key challenges of MM support for femtocells are posed during the phases of a) cell identification, b) access control, c) cell search, d) cell selection/reselection, e) HO decision, and f) HO execution. Cell identification is cumbersome due to the unplanned and dense reuse of the same PCI within small areas, a.k.a. the PCI confusion problem [134]. On the other hand, given that the use of femtocells is subject to access control, MM is further complicated in three aspects: a) the mobile terminals should be aware of the femtocells they can access, b) the femtocell stations should enable the identification of the access type they support, and c) the membership status of the mobile terminals should be validated by a trusted network entity prior to accessing the femtocells. Cell search should also be reassessed in the context of femtocells, given that the dense yet unplanned deployment dictates the use of autonomous rather than network-controlled cell search procedures, whereas the short cell radii may unpredictably augment the required energy consumption and delay overhead. Cell selection/reselection is another critical issue in large-scale deployments of femtocells, where the tracking area size has a major impact on the user equipment battery lifetime and the network signaling load. More sophisticated HO decision algorithms are also required, in the presence of femtocells, to mitigate the negative impact of user mobility and cross-tier interference on the QoE and SINR performance at the UEs. Attaining a low service interruption probability for medium to high speed users is another challenging issue for the HO decision phase. Certain network architectural and procedural enhancements are also required to lower the delay and signaling overhead of the HO execution to/from femtocells.

The remainder of this section is organized as follows. Section 6.1 summarizes the main HO decision criteria used in the two-tier macrocell-femtocell LTE-A network, surveys and classifies current state-of-the-art HO decision algorithms, while section 6.2 discusses some recent trends for femtocell-specific performance evaluation and modeling. In section 6.3, we provide a detailed qualitative comparison of existing approaches, whereas in section 6.4 we present exhaustive system-level simulations on their performance by using the system-level evaluation methodology of the Small Cell Forum. In section 6.5, we summarize lessons learned from the design of handover decision algorithms for femtocells. Finally, in section 6.6 we highlight the key contributions of our work and draw our conclusions.

6.1 Survey of Handover Decision Algorithms for Femtocells

This section surveys and classifies current state-of-the-art HO decision algorithms for the two-tier macrocell-femtocell network. section 6.1.1 summarizes the main HO decision criteria in the current literature and section 6.1.2 presents a classification of existing HO decision algorithms for the referenced network. Finally, section 6.1.3 includes a detailed overview of selected HO decision algorithms for each class.

6.1.1 Handover Decision Criteria

Current literature includes various HO decision criteria and parameters for the two-tier macrocell-femtocell network. Below, we describe the most widely used.

Received Signal Strength (RSS) refers to the received power on the reference or pilot signals transmitted by a specific cell. The RSS is the main decision parameter in wireless networks and is used as an equivalent of the path loss between the UE and the target cells. Given that a) the RSS equals to the product of the RS transmit power and the path loss, and b) different RS transmit powers are radiated between the macrocell and femtocell stations [66][71], it follows that the RSS is a biased parameter for HO decision making in the presence of femtocells. To deal with this issue, existing RSS-based algorithms prioritize femtocell over macrocell access and incorporate other femtocell-specific criteria as well [52]-[56]. The use of a suitable RSS sampling duration and rate is another critical issue in the presence of femtocells, where non line of sight (NLOS) propagation conditions and fast variations characterize the radio environment. In the context of LTE-A, the RSS corresponds to the RSRP measurement (section 1.2), which is performed at the UE by using specific sampling rules [16] [50][136].

Received interference power (RIP) refers to the total received power from cells or users in proximity. When performed at the UE, the RIP measurement is usually referred to as the Received Signal Strength Indicator (RSSI). It is important to note that, different from other RATs, the RSS parameter in LTE-A corresponds to the received power in the RS of a specific cell, whereas the RSSI parameter corresponds to the received power from all interfering cells in proximity. Given that the RIP measurement strongly depends on the physical location of the measuring entity, the RSSI at the UE and the RIP at the target cell can be quite different. Even though the incorporation of the RIP at the target cells enhances the HO decision outcome, it also dictates the use of more complicated signaling procedures at the serving cell [71]. In LTE-A, the RIP measurement is a standard capability for both the UE and the (H)eNBs [16].

Received Signal Quality (RSQ) refers to the ratio of the RSS from a target cell to the total RIP at the UE. The RSQ is frequently used to estimate the SINR performance upon service reception from a target cell [67]-[70]. In the context of LTE-A, the RSQ corresponds to the RSRQ measurement performed at the UE (section 1.2) [16].

UE speed is a widely used parameter for enhancing inbound mobility to femtocells and reducing the number of unnecessary HOs for medium to high speed users [59][60]. Combined with information for the UE mobility pattern, the use of this parameter may significantly enhance the HO decision phase in the presence of femtocells [57]. Nevertheless, assessing the UE speed comes at the cost of increased monetary, energy consumption, or network signaling overhead.

Energy-efficiency is a critical issue for IMT-Advanced mobile devices, which are required to support multifarious user applications and a plethora of radio capabilities, e.g., carrier aggregation, multi-antenna and multi-interface transmissions. Some of the key energy-efficiency parameters in current literature are the UE battery power [60], the mean UE transmit power [66], and the UE power consumption [71].

Path loss includes the impact of various signal attenuation factors caused by the wireless medium and the ambient radio environment, e.g., propagation, absorption and diffraction losses. In contrast with the RSS parameter, which

strongly depends on the actual RS transmit power of the target cell, path loss is an unbiased measure of the actual propagation conditions between the UE and the target cell. Current literature includes various HO decision algorithms that account for the path loss parameter [63][66][71]. Nevertheless, accurately estimating the path loss parameter is a challenging issue [71].

RS transmit power corresponds to the cell transmit power on the RS. Existing algorithms use this parameter to assess the path loss between the UE and the target cell [66]. The RS transmit power measurement is a standard (H)eNB capability in LTE-A [16].

Traffic type is another widely used parameter for enhancing inbound mobility to femtocells [58][60], [63]-[65]. Existing classifications of the UE traffic-type mainly include: a) real time or non-real time traffic [58][60][64][65], and b) voice/video or data traffic [63].

Available bandwidth is a measure of the resource availability in the target cell. This parameter is used to minimize the HO failure probability due to admission control. Other bandwidth-related parameters include the cell load [64] and the cell capacity [62]. The number of camped or served UEs is another load indication measure [62]. Bandwidth-related criteria are typically used for performing preliminary admission control prior to HO execution.

UE residence time within the cell refers to the duration that a tagged UE is expected to remain within the coverage of a cell. This parameter is used in combination with other speed-related parameters to minimize the number of unnecessary HOs [57].

UE membership status is a unique feature of femtocell access. Existing HO decision algorithms account for the UE membership status to minimize the HO failure probability [65].

6.1.2 Classification of Handover Decision Algorithms for Femtocells

Even though HO decision making in the two-tier macrocell-femtocell network is a relatively new research area, current literature includes a noteworthy number of proposed algorithms [52]-[71]. The vast majority of algorithms use a mix of parameters to reach the final decision. Based on the primary HO decision criterion used, this section presents a classification of these algorithms into the following five groups: a) received signal strength based, b) speed based, c) cost-function based, d) interference-aware, and e) energy-efficient. The classification of the existing HO algorithms is driven by a) the analysis and the key ideas that motivated the algorithmic design in the original manuscripts, and b) the key parameter that affects the final decision outcome according to the sequence of the algorithm and the presented numerical results. The use the primary HO decision criterion as a classification criterion allows for an easy comparison between existing algorithms and a better understanding of their fundamental operation.

Received signal strength based algorithms: The algorithms in this class are based on using RSS criteria [52]-[57]. There exist various approaches on how to use the RSS during the HO decision phase, mainly including a) RSS comparison of the serving and the target cells (relative RSS) either directly or with hysteresis margin, b) RSS comparison of the serving or the target cell with absolute thresholds (absolute RSS), or c) combination of these approaches. Although the

RSS is an integral part of HO decision algorithms, in this class we include algorithms where the decision outcome is strongly affected by the RSS status.

Speed based algorithms: The algorithms in this class use the UE speed as the primary HO decision criterion [58]-[61]. The HO decision is taken by comparing the UE speed to absolute thresholds which, in most of the cases, are arbitrarily picked. Speed based algorithms incorporate other HO decision criteria as well, mainly including the RSS of the serving and the target cells, the UE traffic type, the available bandwidth on the target cells and the UE membership status.

Cost-function based algorithms: The algorithms in this class integrate a wide range of HO decision parameters within a single cost-function [62]-[65], e.g., battery lifetime, traffic type, cell load, RSS and speed. The HO decision is reached by comparing the outcome of the cost-function for the serving and the candidate cells. Existing approaches integrate the HO decision parameters into a multi-parameter function [62][63], or use a weighted summation [64][65].

Interference-aware algorithms: The algorithms in this class account for the impact of interference at the UEs or the cell sites [66]-[70]. The main decision parameters in this class include a) RSQ measurements, b) the RIP at the cell sites, c) the RS transmit powers of the cells, and d) interference constraints at the cells. RSQ-based algorithms typically compare the RSQ of the serving and the target cells, or allow inbound mobility to femtocells whenever the RSQ of a nearby femtocell is higher than a RSQ threshold. On the other hand, algorithms that account for the RS transmit power, interference level, or interference constraints at the cells, improve the SINR performance. However, the incorporation of these parameters dictates the use of more complicated network signaling procedures [71].

Energy-efficient algorithms: The algorithms in this class aim at utilizing the energy saving potential offered by the low-power operation of femtocells [71]. Energy-efficient algorithms use as a primary HO decision criterion the UE battery power, the expected UE energy consumption, or the mean UE transmit power. Given that the energy consumption strongly depends on the interference at the network nodes, these algorithms are closely related to the interference-aware algorithms [66] [137].

Figure 55 illustrates the assignment of selected HO decision algorithms into the five classes proposed in this paper. Note that the vast majority of these algorithms utilize parameters that span over the five classes. To this end, we choose to classify existing HO decision algorithms depending on the primary HO decision criterion used.

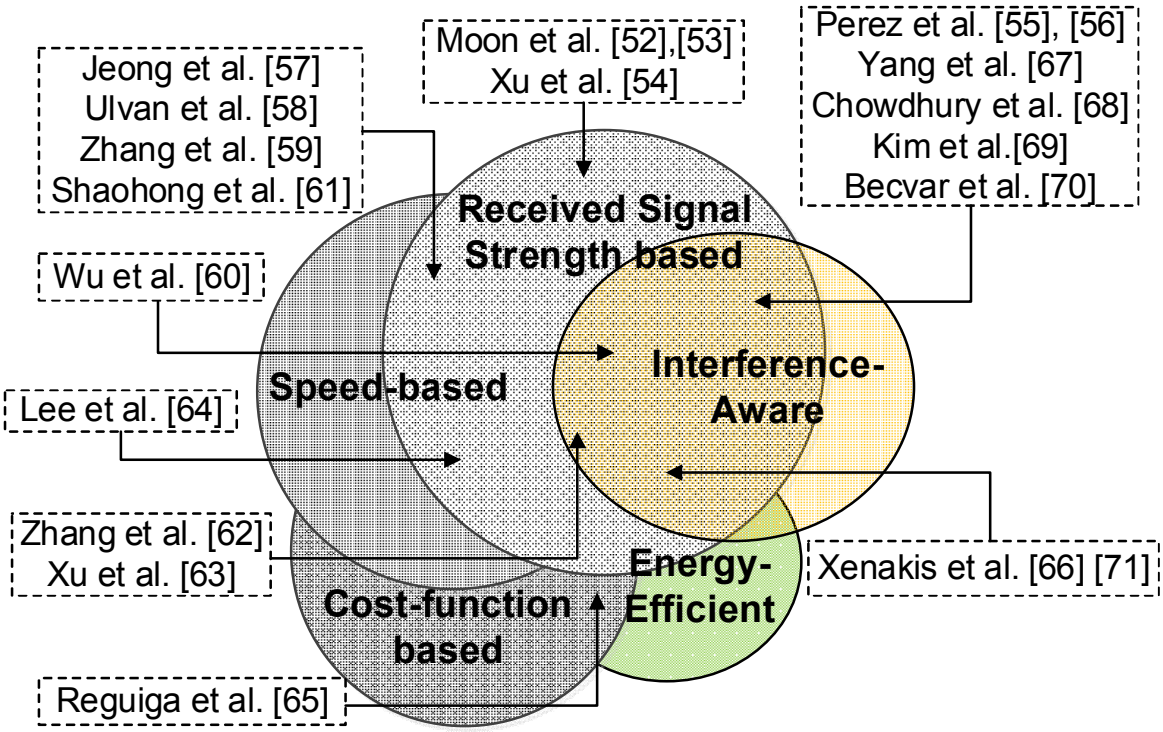

Figure 55: Classification of selected HO algorithms for the two-tier macrocell-femtocell network

6.1.3 Handover Decision Algorithms

Current state-of-the-art algorithms for HO decision for femtocells use divergent system assumptions, different notation, a plethora of decision parameters, and various methodologies for describing their fundamental operation. As a result, a holistic and easy-to-comprehend methodology is needed for readily comparing existing HO algorithms. Towards this direction, in this subsection we provide a detailed overview of selected HO decision algorithms for the two-tier macrocell femtocell network. The selected algorithms are among the most representative ones in each class. The discussion for each algorithm is accompanied with a) a brief summary of its key features, b) a detailed flowchart describing its fundamental operation and c) an overview of its main advantages and disadvantages. To ease the reader, we adapt the presentation of each algorithm in the context of the LTE-A system and use a common notation for the main HO decision parameters (Table 13).

Table 13: Notation for the main HO decision parameters

LTE-A band set	$\boldsymbol{N} \coloneqq \{1, \dots, N\}$
Set of cells operating in band n	$\boldsymbol{C_n}$
Set of active users connected to a cell in $\boldsymbol{C_n}$.	$\boldsymbol{U_n}$
Prescribed mean SINR target for attaining the required QoS	$\overline{\gamma}_t$
Minimum required RSRP value for sustaining wireless connectivity with the network	R_{min}
Set of candidate and accessible LTE-A cells for a tagged user	$\boldsymbol{L}$
Transmit power of node x	$\overline{P}[x]$
Mean noise power in node x	$\overline{\sigma}[x]^2$

Mean channel gain from node x to node y	$\overline{h}[x,y]$
UL SINR between user $u \in \boldsymbol{U_n}$ and cell $s \in \boldsymbol{C_n}$ for the tagged time interval T	$\overline{\gamma}[s]$
Mean transmit power of user u on a candidate cell $c \in \boldsymbol{L}$	$\overline{P}_c[u]$

6.1.3.1 Received Signal Strength Based

The vast majority of RSS based algorithms use a HO Hysteresis Margin (HHM) to compare the RSS of the serving and target cells, with the aim to lower the HO probability and minimize the ping-pong effect. In the following, we discuss three representatives of the RSS based class.

a. Received Signal Strength based HO Algorithm for Inbound Mobility in Hierarchical Macrocell-Femtocell Networks

The algorithm in [52] applies to the single-macrocell single-femtocell HO decision scenario where the UE enters the coverage of a femtocell. The main idea of the proposed algorithm is to combine the RSS of the macrocell and the femtocell stations in order to compensate the uneven RS power transmissions between them. To mitigate fast variation of the RSS, the algorithm applies an exponential window function to the RSS measurements of the macrocell and the femtocell stations as follows:

$$\bar{s}_m(k) = w(k) * RSRP(m,k) \text{ and } \bar{s}_f(k) = w(k) * RSRP(f,k) \qquad (6.1)$$

where $RSRP(m,k)$ and $RSRP(f,k)$ denote the RSS of the macrocell and the femtocell at time k, respectively, and $w(k)$ the exponential window function. The filtered RSS parameters of the macrocell and the femtocell stations, denoted by $\bar{s}_m(k)$ and $\bar{s}_f(k)$, respectively, are integrated into a RSS-based decision parameter as follows:

$$s_{pro}^{\alpha}(k) = \bar{s}_f(k) + \alpha \cdot \bar{s}_m(k) \qquad (6.2)$$

where $\alpha \in [0,1]$ denotes a factor introduced to compensate the uneven RS transmit powers of the macrocell and the femtocell stations.

Figure 56 depicts the proposed algorithm in [52]. The algorithm enables inbound mobility to the femtocell station if a) the filtered RSS of the femtocell exceeds over a minimum required RSRP threshold $RSRP_{th,f}$ and the combination parameter $s_{pro}^{\alpha}(k)$ exceeds over the filtered RSS of the macrocell plus the HHM $HHM(c)$, or if b) the filtered RSS of the femtocell falls below the $RSRP_{th,f}$ threshold yet it exceeds over the filtered RSS of the macrocell plus the HHM. The details of the window function and the optimal selection of the α parameter are thoroughly discussed in [52][53].

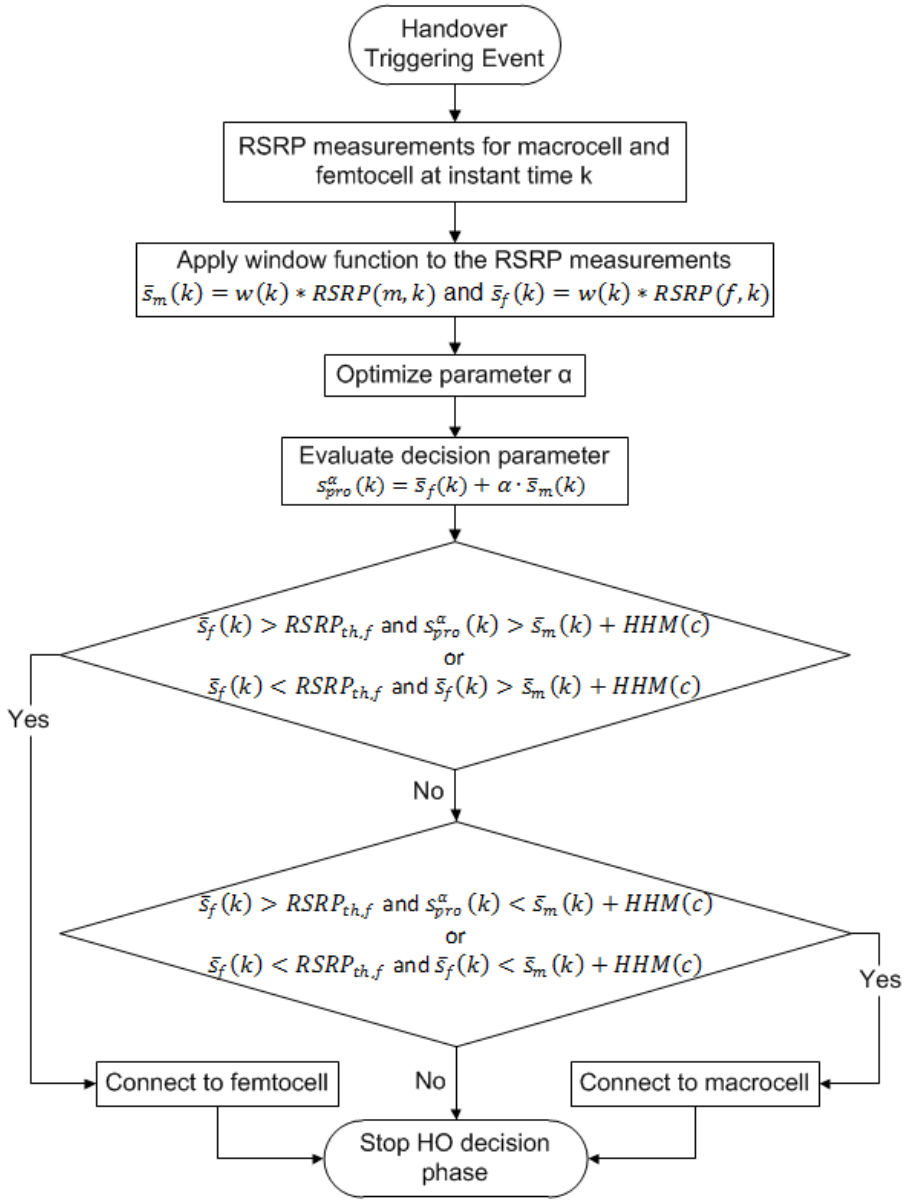

Figure 56: Moon et al. HO algorithm [52][53]

Among the advantages of the proposed algorithm is that a) it accounts for the uneven RS transmit powers between the macrocell and the femtocell stations, b) it includes an optimization methodology for the α parameter, and c) its performance is validated through analytical results and under various performance measures. Nevertheless, the system model assumes a single-macrocell single-femtocell network layout and uses a methodology similar to the one in [138]. In addition, the interference and throughput performance of the algorithm is not thoroughly discussed. Optimizing the α parameter in real-life deployments can also be very challenging.

b. Received Signal Strength and Path Loss based HO algorithm for Inbound Mobility in Hierarchical Macrocell-Femtocell Networks

The HO decision algorithm in [54] incorporates RSS and path loss based parameters to support inbound mobility to femtocells. Similar to the proposals in[52][53], the proposed algorithm considers the single-macrocell single-femtocell network layout and applies a window function $w(k)$ on the RSRP measurements of the macrocell and the femtocell stations. Inbound mobility to the femtocell station is allowed only if a) the filtered RSRP measurement of the femtocell

exceeds over a minimum threshold, denoted by $RSRP_{th,f}$, b) the filtered RSRP status of the femtocell exceeds over the filtered RSRP status of the macrocell plus the HHM, and c) the path loss between the UE and the macrocell is greater than the one observed between the UE and the femtocell. Figure 57 illustrates the flowchart version of the algorithm in [54].

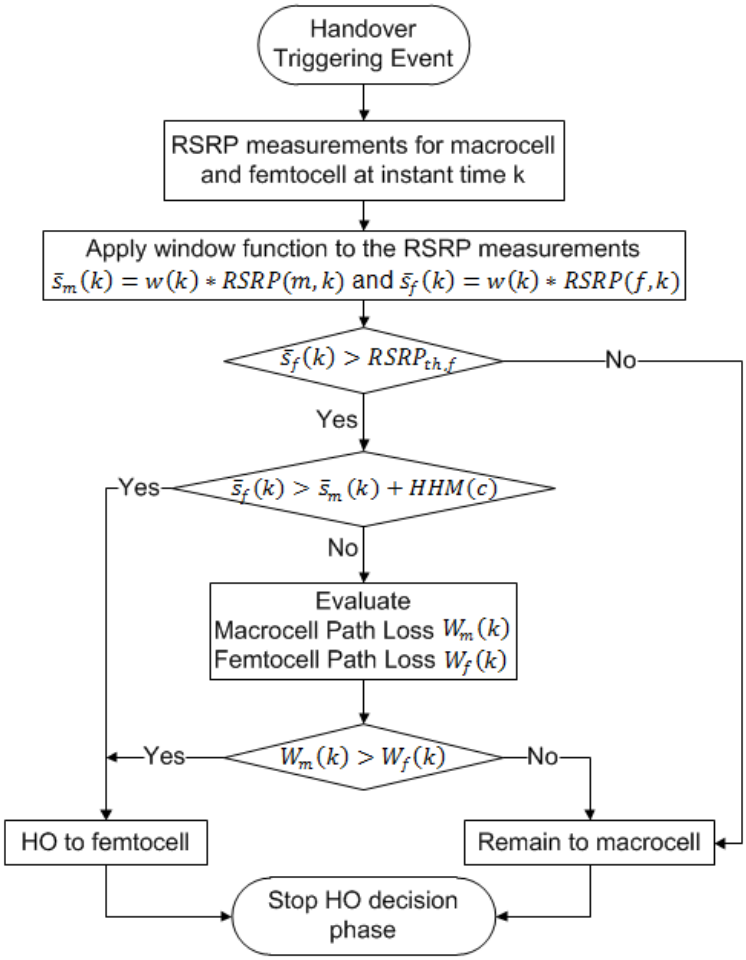

Figure 57: Xu et al. RSS based HO algorithm [54]

One of the strong aspects of the algorithm is the incorporation of the actual path loss between the UE and the candidate cells. However, the signaling procedure for acquiring the RS transmit power of the stations and assessing the path loss is not thoroughly discussed. On the other hand, even though the performance of the proposed algorithm is validated by a performance analysis, the use of the single-macrocell single-femtocell system model questions the real-life deployment of the algorithm. Provided that the path loss of the cells can be subject to fast variations, the proposed algorithm may also be vulnerable to the ping-pong effect.

c. Intracell HO Algorithm for Interference and HO Mitigation in Two-Tier Macrocell-Femtocell Networks

Founded on the concept of intracell HO (IHO), the authors in [55][56] propose a HO decision algorithm that jointly handles interference mitigation and HO decision in the presence of femtocells. The IHO is a special case of HO where the serving and the target cell is the same cell, i.e., the UE is relocated to a new channel in its current serving cell. The proposed algorithm applies to the scenario where the UE is served by a macrocell and is interfered by multiple femtocells. The main idea of the proposed algorithm is to perform an IHO to the macrocell or cast an IHO to all interfering femtocells, whenever a non-subscribed macrocell UE suffers from

cross-tier interference. Figure 58 depicts a flowchart version of the proposed algorithm. Note that the parameter ΔQ_{IHO} is an IHO hysteresis margin and that parameter r is used to access the list of interfering femtocells, denoted by Θ_k, sequentially.

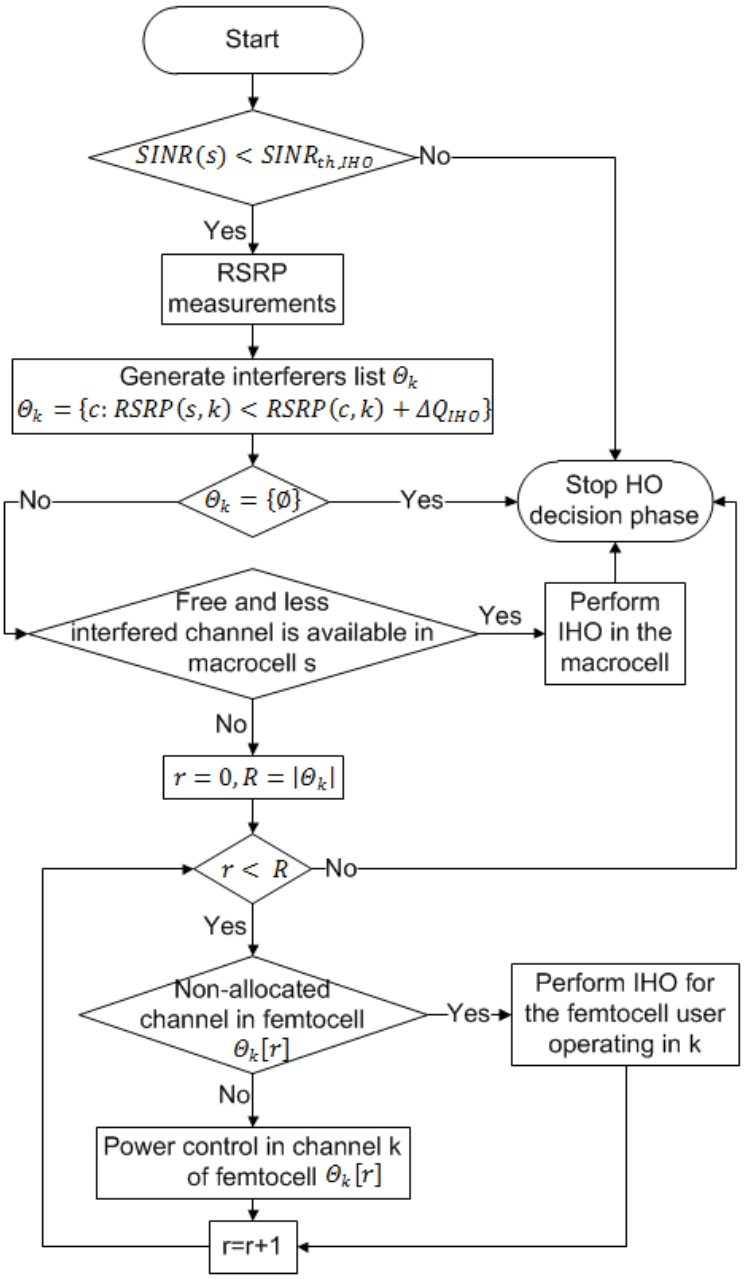

Figure 58: Perez et al. IHO algorithm [55][56]

The IHO decision process is triggered whenever the SINR status of the user falls below a prescribed threshold $SINR_{th,IHO}$. Upon IHO decision triggering, the serving macrocell configures the UE to measure the RSS of nearby femtocells. Based on the reported measurements, the macrocell uses a relative RSS with hysteresis margin procedure to construct the list of interfering femtocells. If the serving macrocell identifies a less interfered channel within its operating bandwidth, it reallocates the user to it and the IHO algorithm terminates. In the opposite case, the serving macrocell sends an IHO command to all the interfering femtocells. Accordingly, the interfering femtocells either assign a new channel to the interfering femtocell users (IHO), or perform power control in the interfered channel.

Among the strong aspects of the algorithm is that it accounts for the received interference power from nearby cells and that it applies to the single-macrocell multiple-femtocell HO decision scenario. The use of extensive system-level simulations for assessing the HO probability, interference, and throughput performance of the algorithm is another strong aspect of the proposal in [55]. Nevertheless, relocating the interfering femtocell users to other channels may unpredictably raise the interference in nearby femtocells or users, and cause fluctuations in the network performance. On the other hand, even though the coordination between the macrocell and the femtocells lowers the HO probability and reduces the interference at the UEs, it also augments the signaling and delay overhead of the HO decision phase.

6.1.3.2 Speed Based

The algorithms of this class typically compare the UE speed with absolute speed thresholds to lower the HO probability for medium to high speed users. Note that the vast majority of speed-based algorithms incorporate other HO decision parameters as well, mainly including the RSS, traffic-type and available bandwidth on the target cell. In the following, we discuss three representative speed based HO decision algorithms.

a. *Speed and Traffic-type based HO Algorithm for the Macrocell-Femtocell Network*

The algorithm in [58] consists of two different HO decision strategies: the proactive and the reactive. In the proactive strategy, a HO is initiated before the RSS of the serving cell reaches an absolute HO hysteresis threshold. To achieve this, the algorithm estimates the residual time prior to the HO execution. In the reactive strategy, the HO execution is initiated when the minimum required RSS is (almost) reached. The proactive strategy aims at minimizing the packet loss and the delay of the HO decision, whereas the reactive strategy aims at lowering the number of unnecessary HOs. The proposed algorithm applies to the multiple-macrocell multiple-femtocell HO decision scenario. Figure 59 illustrates the fundamental operation of the proposed algorithm.

When the UE speed is higher than 10km/h, the proposed algorithm avoids inbound mobility to femtocells and performs normal RSS-based HO decision. On the other hand, if the UE speed varies between 5 km/h and 10 km/h the proposed algorithm uses mobility prediction and employs the proactive strategy for real-time traffic or the reactive strategy for non real-time traffic. A similar approach is followed when the UE speed is lower than 5 km/h; however, without using mobility prediction. The mobility prediction scheme is discussed in [139].

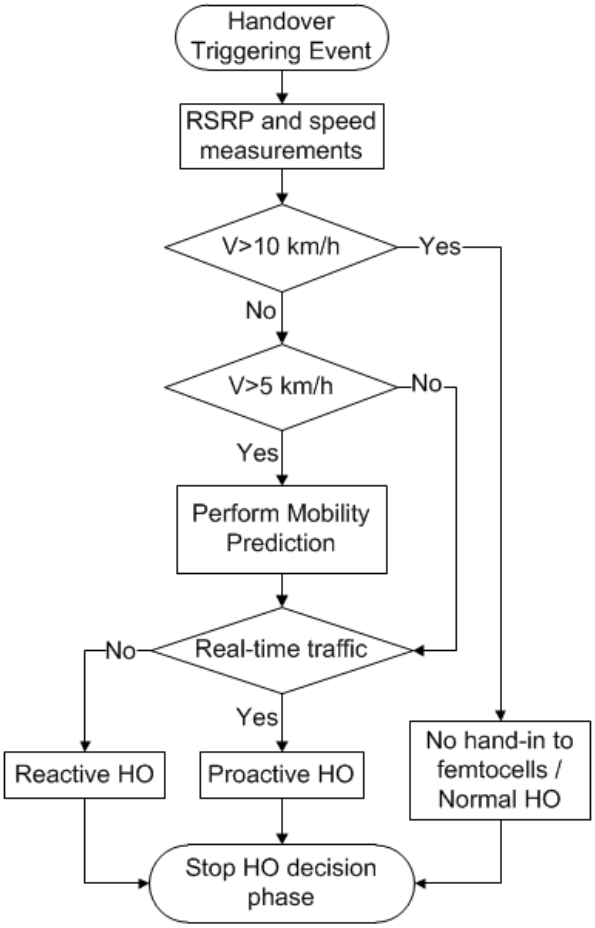

Figure 59: Ulvan et al. HO algorithm [58]

The use of mobility prediction in combination with the UE speed is a strong feature of the algorithm in [58], which is expected to lower the HO probability for medium to high speed users. An improved QoE is also expected for the proposed algorithm, owing to the use of different HO decision strategies depending on the traffic-type. Nevertheless, the motivation for using the specific speed thresholds and the mobility prediction scheme should be discussed in more detail. The impact of the reactive HO decision strategy on the interference and throughput performance of nearby cells should be thoroughly investigated as well.

b. Low-complexity HO Algorithm for the Macrocell-Femtocell LTE-Advanced Network

The authors in [59] propose a low-complexity HO decision algorithm for the macrocell-femtocell LTE-A network. A signaling cost evaluation model accompanies the algorithm based on the work in [109]. The proposed algorithm applies to the single-macrocell single-femtocell HO decision scenario and consists of handing over to the femtocell station whenever a) the RSRP status of the femtocell exceeds over the RSRP status of the macrocell plus a HHM and b) the UE speed is lower than a prescribed speed threshold. The proposed algorithm is depicted in Figure 60.

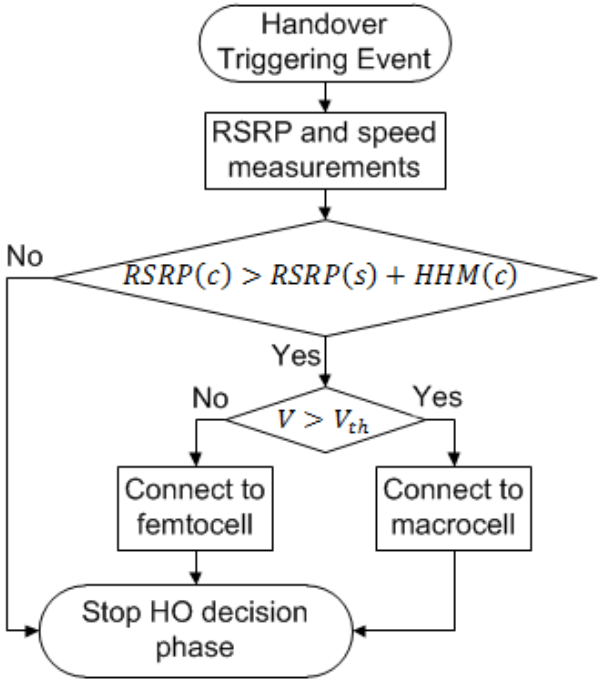

Figure 60: Zhang et al. speed based HO algorithm [59]

Among the advantages of the algorithm in [59] is that it attains backwards compatibility with the LTE-A system and its signaling performance is validated by a performance analysis. The algorithm is also expected to lower the HO probability for medium to high speed users compared to SC-based HO decision algorithms. Nevertheless, the selection of an appropriate speed threshold is not thoroughly investigated and further numerical results are required to validate the performance of the algorithm in terms of interference, throughput and UE energy consumption.

c. HO Algorithm for the LTE-Advanced Network with Hybrid Femtocells

The algorithm in [60] incorporates a wide range of parameters to reach the HO decision, mainly including the RSS of the serving and the target cells, the UE speed, the interference level at target femtocells, the bandwidth availability on the target cell, the UE membership status and the traffic type. The algorithm can be used to a) remain in the current serving cell, b) handover to the macrocell, or c) handover to a hybrid femtocell. The algorithm is illustrated in Figure 61.

If the serving cell is a HeNB, the proposed algorithm performs a HO to the macrocell only if a) the UE speed exceeds over a prescribed speed threshold $V_{t,1}$ and the macrocell can support the bandwidth requirements of the UE, or b) the RSRP status of the serving HeNB decreases and the macrocell can support the bandwidth requirements of the UE. If the serving cell is not a HeNB and the UE is not member of the CSG supported by the target femtocell, a HO is performed only if a) the interference level at the hybrid femtocell is greater than a prescribed threshold I_{th}, b) the UE speed is lower than a prescribed threshold $V_{t,2}$, and c) the target femtocell can support the bandwidth requirements of the UE. On the other hand, if the UE belongs to the CSG of the target femtocell, the algorithm performs an inbound HO by using a) absolute RSS and relative RSS with hysteresis margin, b) UE speed, c) traffic-type, and d) bandwidth-related criteria.

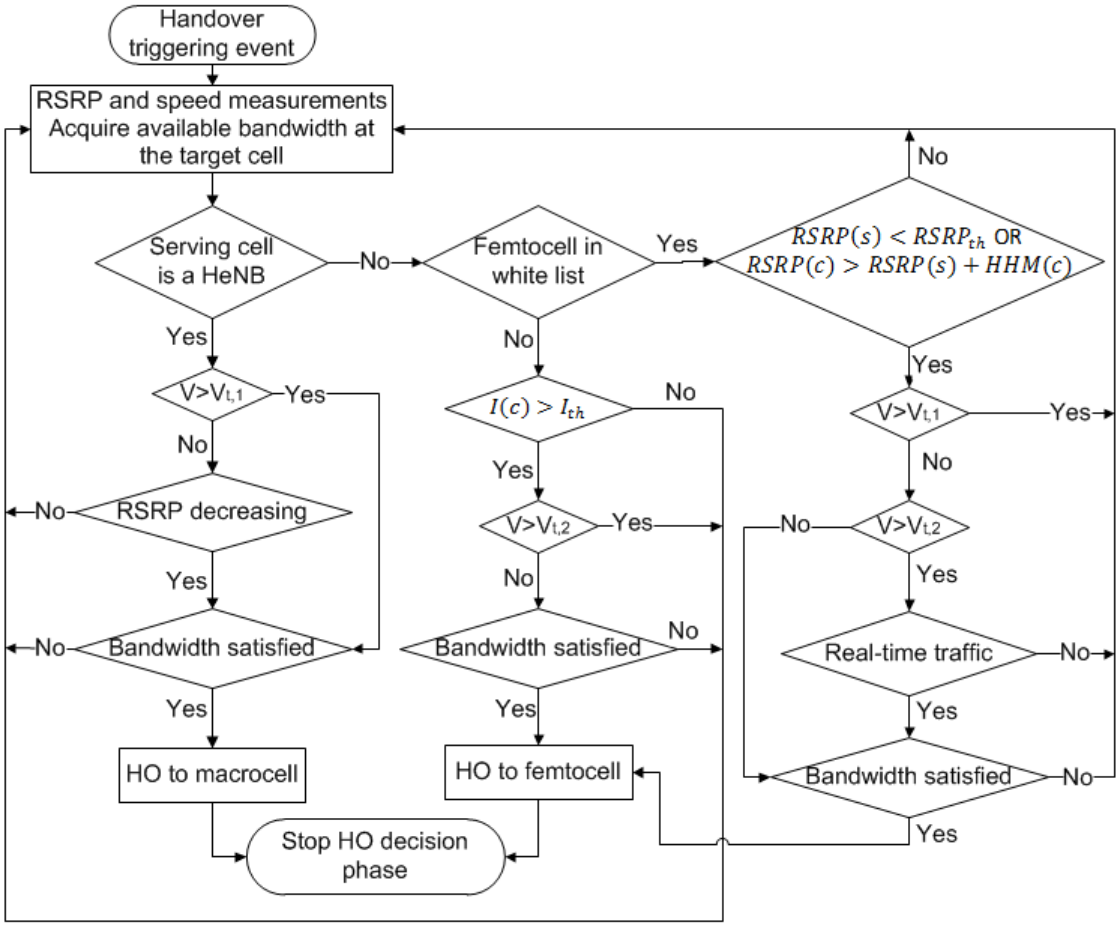

Figure 61: Wu et al. HO algorithm [60]

The algorithm in [60] accounts for a wide range of HO decision criteria, which are expected to minimize the HO failure probability. However, the required signaling and delay overhead for commuting these parameters to the serving cell should be further investigated. The speed and interference thresholds should be specified, whereas system-level simulation results are also required to validate the performance of the algorithm. The HO decision for CSG cells can be further improved by taking into account the operating frequency of the UE and the femtocell, i.e., validate whether the UE and the femtocell operate in the same band.

6.1.3.3 Cost-function Based

This class includes algorithms that integrate a wide range of HO decision parameters within a single cost-function. The outcome of the cost-function is subsequently used as the primary HO decision criterion. Even though the use of cost-functions enables more sophisticated HO decision making, the weights related to the cost-function should be carefully adapted as well. The signaling overhead for assessing the parameters should also be investigated. The remainder of this section discusses three representative algorithms of this class.

a. Cost-function based HO Algorithm for the Macrocell-Femtocell Network

A cost-function based algorithm is proposed in [62] aiming to enhance inbound mobility to femtocells. The algorithm applies to the single-macrocell single-femtocell scenario, where the UE is connected to a macrocell and enters the coverage of a femtocell. The cost-function can be based on either the RSRP or the RSRQ status of the macrocell and femtocell stations. To ease the reader, we indicate the serving macrocell with m and the target femtocell with f. For a cell

$c \in \{m, f\}$, the cost-function is denoted by $M(c)$ and is given as follows:

$$M(c) = \frac{M_0(c) \cdot C_{max}(c) \cdot G(c)}{\log(e \cdot k(c) + U(c))} \quad (6.3)$$

where $M_0(c)$ denotes the RSRP or RSRQ status of cell c, $C_{max}(c)$ the capacity of cell c, $G(c)$ a factor used to adjust the value of the cost-function, $k(c)$ a factor adapted with respect to the type of cell c, and $U(c)$ the number of UEs camped on cell c.

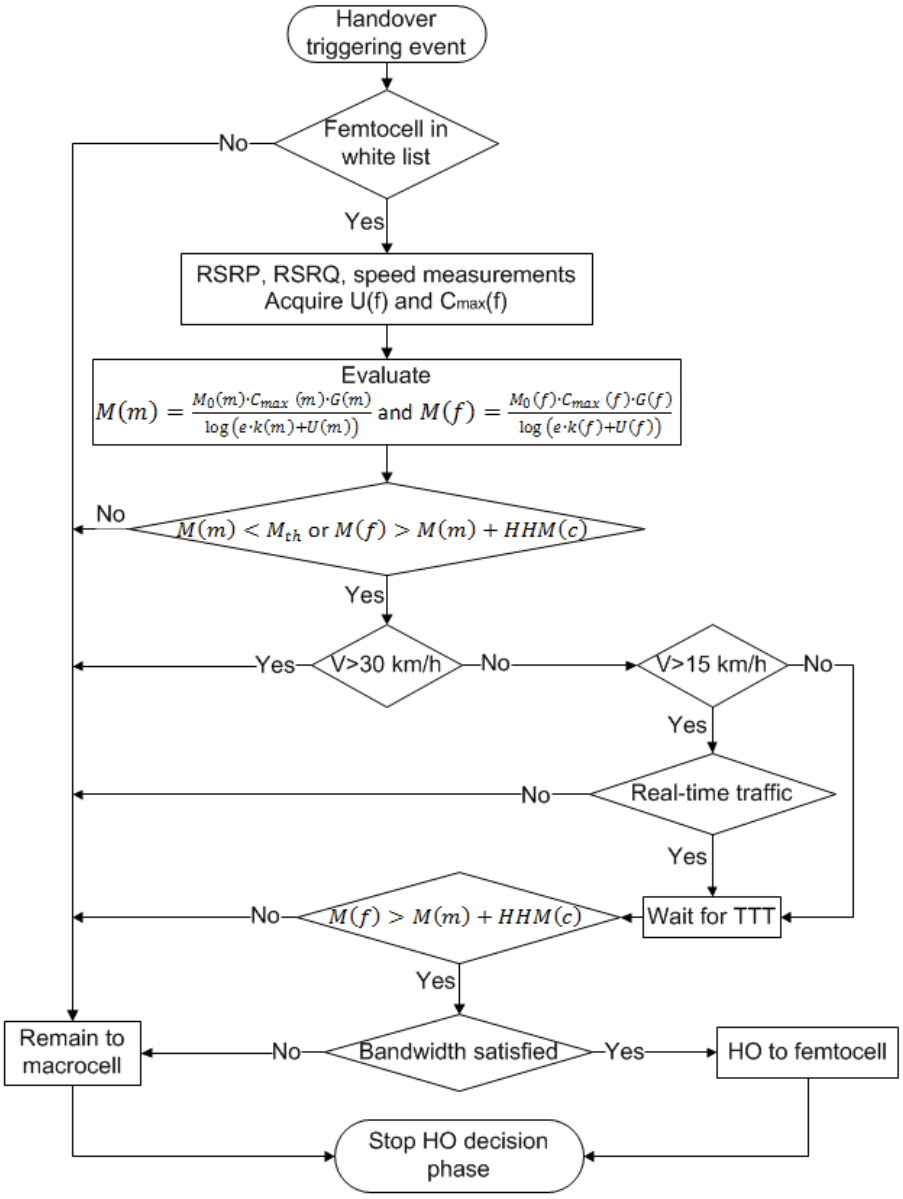

Figure 62: Zhang et al. cost-function based HO algorithm [62]

The proposed algorithm is illustrated in Figure 62. Firstly, the algorithm validates the UE membership status on the target femtocell. The HO decision parameter set is subsequently acquired and the cost-functions for the serving macrocell and the target femtocell are evaluated. The HO decision phase continues either if the cost-function outcome for the serving macrocell is lower than a prescribed threshold, denoted by M_{th}, or if the cost-function outcome for the target femtocell is greater than the one of the serving macrocell plus a HHM. If the UE moves faster than 30 km/h the algorithm avoids inbound mobility to the

target femtocell. In the opposite case, the algorithm continues either if a) the UE speed is lower than 15 km/h or b) the UE speed is between 15 km/h and 30 km/h and the user connection is of real-time. In both cases, the proposed algorithm waits for a time interval equal to TTT and evaluates whether the cost-function outcome for the femtocell is greater than the one of the macrocell plus a HHM. If so, the bandwidth availability on the femtocell is validated and a HO is initiated.

The proposed algorithm accounts for the bandwidth availability and the UE speed to lower the HO failure probability due to admission control and mitigate the number of unnecessary HOs for medium to high speed users, respectively. The integration of the number of camped UEs within the cost-function enables load balancing between the macrocell and the femtocell tiers as well. However, even though the $G(c)$ and $k(c)$ parameters majorly affect the decision outcome, a methodology for optimizing their values is not provided. Moreover, the motivation for using the specific speed thresholds is not discussed, whereas the signaling and delay overhead for acquiring the number of camped UEs and the available bandwidth of the target cell need to be further examined.

b. User State and Signal Quality based HO Algorithm for Hierarchical Cell Networks

The authors in [63] describe a cost-function based algorithm that applies to the single-macrocell single-femtocell scenario, where the UE receives service from a macrocell and enters the coverage of a femtocell. The algorithm uses a simple cost-function, which integrates the traffic-type and the UE speed. Two traffic types are considered: voice/video and data. To ease the reader, we indicate the serving macrocell with m and the target femtocell with f.

The proposed algorithm is depicted in Figure 63. Upon HO decision triggering, the proposed algorithm acquires the RSQ of the target cells, assesses the UE speed and examines the traffic-type of the user connection. The algorithm subsequently compares the RSQ of the macrocell and femtocell stations. Note that we replace the SINR comparison of the original manuscript with the RSRQ comparison, given that the SINR of the target femtocell can be only evaluated upon service reception. The algorithm subsequently compares the UE speed with an absolute speed threshold and classifies the traffic-type of the user to calculate the speed and traffic-type costs, denoted by $f(V)$ and $f(q)$, respectively. These costs are integrated in the cost-function, denoted by R_{ms}, which is ultimately used to reach to the HO decision.

The proposed algorithm integrates the UE speed and traffic-type within a simple cost-function. The use of these parameters is expected to lower the HO probability for medium to high speed users and enhance the QoE of the mobile users. However, even though the incorporation of the RSQ parameters aims at improving the SINR performance at the UEs, the absence of a HHM during the relative RSQ comparison may unpredictably raise the HO probability due to fast variations of the wireless medium. The performance of the proposed algorithm should also be compared to other non-RSQ based algorithms and evaluated in terms of interference, throughput and energy consumption at the UEs.

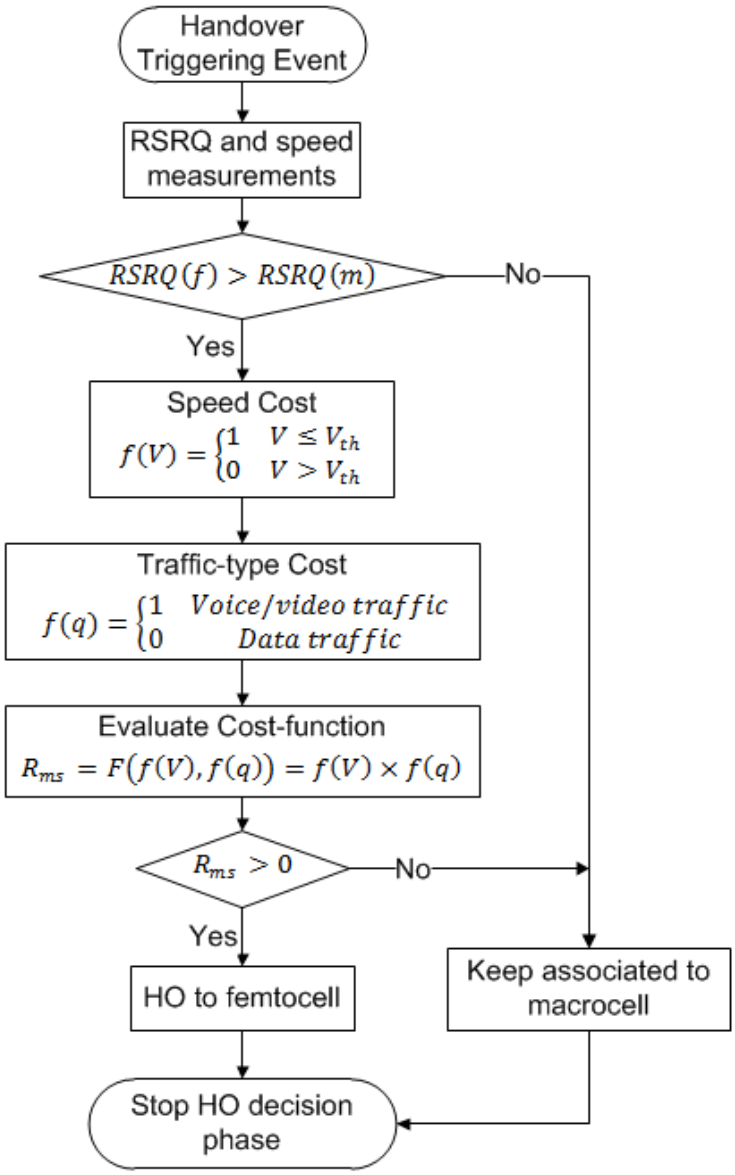

Figure 63: Xu et al cost-function based HO algorithm [63]

c. Cost-Based Adaptive HO Hysteresis Algorithm to Minimize the Handover Failure Rate

The proposal in [64] is a representative cost-function based algorithm that readily applies to the two-tier macrocell-femtocell network. The cost-function consists of a weighted summation of parameters related to the UE speed, cell load, and number of user connections. The cost-function outcome is integrated in a standard RSS-based procedure as an adaptive HHM. The algorithm uses individual cost-functions for the cell load, the UE speed, and the number of UE connections, denoted by N_l, N_v, and N_s, respectively. The corresponding weights are denoted by w_l, w_v, and w_s, respectively, whereas the cost-function by $f_{l,v,s}$.

The proposed algorithm is depicted in Figure 64. Upon HO decision triggering, the algorithm calculates a) the number of real-time and non real-time connections of the tagged UE, denoted by N_{RT} and N_{nonRT}, respectively, b) the UE speed, and c) the cell load of the current serving and the candidate cells, denoted by $L(s)$ and $L(c)$, respectively. The algorithm subsequently evaluates the cost-functions for the cell load, the UE speed and the number of user connections. The outcome

is integrated within the cost-function $f_{l,v,s}$. Note that the UE speed is normalized to the maximum speed among the UEs, while the $L(s)$ and $L(c)$ parameters are expressed as the ratio of the occupied bandwidth to the total bandwidth of the cell. The result of the cost-function is multiplied with an adjustment parameter, denoted by α, and is incorporated in a standard RSS-based procedure as an additional HHM.

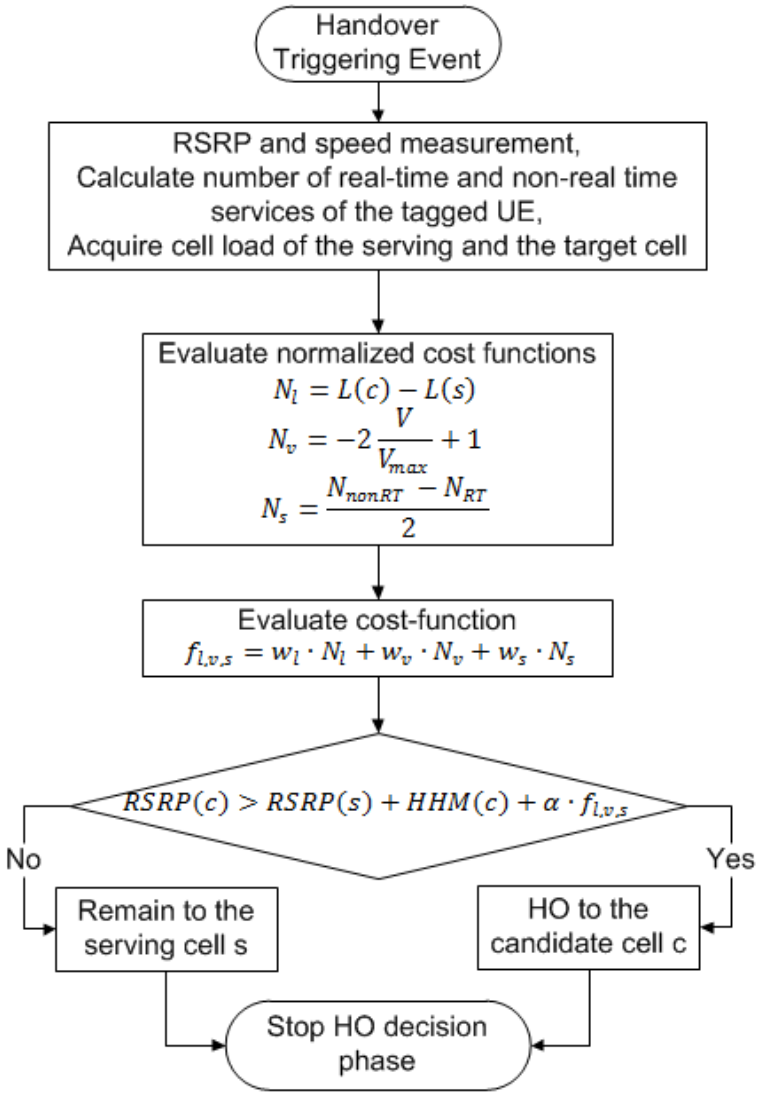

Figure 64: Lee et al. HO algorithm [64]

Among the strong features of the proposed algorithm is the use of the adaptive HHM, which can be readily integrated in the standard RSS-based HO decision. The incorporation of the load difference between the serving and the target cell is also expected to balance the load distribution among the cells and increase the bandwidth availability for the UEs. A reduced HO probability is expected for medium to high speed users as well, given that the algorithm accounts for the UE speed. However, the proposed algorithm lacks of a methodology for optimizing the cost-function weights. On the other hand, even though the proposed algorithm is shown to attain a lower HO failure rate compared to other competing algorithms, further numerical results are required to evaluate its performance in terms of HO probability, load distribution and throughput. Increased signaling is also required to commute the load occupation of the target cells to the serving cell.

6.1.3.4 Interference-aware

Interference-aware HO decision making is a key enabler for shifting to the femtocell communication paradigm. In this class we include algorithms that account for the co-tier and cross-tier interference by using parameters such as the interference level at the cell sites [66] or the RSQ at the UEs [67]-[70]. In the following, we discuss three representative algorithms of the interference-aware class.

a. Handover Decision Policy for Reducing Power Transmissions in the Two-Tier Network

The proposed HO decision policy in [66] aims at reducing the UE power transmissions in the two-tier macrocell-femtocell LTE-Advanced network. To achieve this, the policy estimates the mean UE transmit power on a per candidate cell basis based on a) a prescribed mean SINR target and b) standard UE and E-UTRAN measurements. The estimation outcome is used for handing over to the candidate cell that minimizes the mean UE transmit power. The proposed policy applies to the multiple-macrocell multiple-femtocell HO decision scenario, while it is integrated in the standard RSS-based procedure by utilizing an adaptive HHM. The adaptive HHM is used to transform the relative RSS comparison with HHM to a relative mean UE transmit power comparison with HHM. Note that a fixed HHM is used as well, to mitigate the negative impact of user mobility and reduce the ping-pong effect.

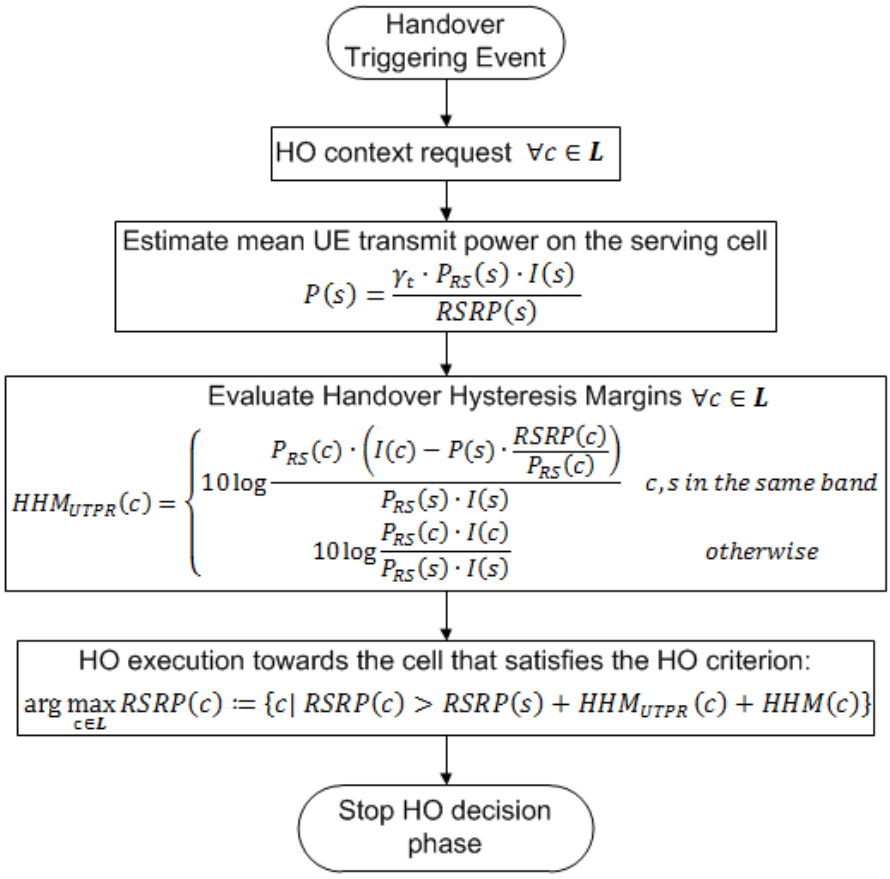

Figure 65: Xenakis et al. interference-aware HO policy [66]

The proposed policy is depicted in Figure 65. Upon HO decision triggering, the serving cell signals a HO context request to the candidate cells in order to acquire a) the RIP at the cell site, b) the downlink RS transmit power, and c) the operating band of the cell. The mean UE transmit power of the serving cell policy is

subsequently estimated by using a) the RSRP measurement, b) the parameters for the candidate cell status and b) the prescribed mean SINR target. Depending on the operating band of the candidate cell, the adaptive HHM is evaluated on per candidate cell basis and a HO is initiated to the candidate cell that minimizes the mean UE transmit power.

The proposed policy is compatible with the LTE-A system as it utilizes standard UE and E-UTRAN measurements to adapt the HHM. The performance of the policy is assessed by using the widely accepted evaluation methodology of the Small Cell Forum [123]. The incorporation of the actual RS transmit power and RIP of the candidate cell is another strong feature of the proposed policy, which is shown to a) reduce the mean UE and cell transmit power, and b) lower the interference level at the UE and (H)eNBs sites. However, the signaling procedure for commuting the HO decision parameters to the serving cell is only briefly discussed by the authors. On the other hand, even though simulation results demonstrate the impact of the fixed HHM on the performance of the algorithm, a more detailed HHM selection methodology is required to optimize the performance of the proposed policy.

b. Signal Quality based Handover Algorithm for the Macrocell-Femtocell LTE-Advanced Network

A RSQ-based algorithm is proposed in [67] aiming to mitigate the number of unnecessary HOs in the presence of femtocells. The proposed algorithm applies to the scenario where the UE is served by a macrocell and enters the coverage of a femtocell. The fundamental operation of the algorithm is similar to the one of the algorithms in [68][69]. The HO decision is reached by taking into account the RSRP, RSRQ and available bandwidth parameters. This algorithm accounts for the impact of the interference by using the RSQ measurements provided by the UE. The proposed algorithm is presented in Figure 66.

The algorithm continuously monitors the RSRP and RSRQ of the target femtocell if at least one of the following conditions apply: a) the RSRP of the femtocell is lower than a prescribed RSRP threshold, denoted by $RSRP_{th,2}$, b) the RSRP of the femtocell does not exceed the $RSRP_{th,2}$ threshold for over a prescribed time interval T, or c) the RSRQ of the femtocell is lower than a prescribed RSRQ threshold, denoted by $RSRQ_{th,2}$. On the other hand, the algorithm handovers to the femtocell if a) the RSRP of the serving macrocell is lower than a prescribed RSRP threshold, denoted by $RSRP_{th,1}$, b) the RSRQ of the femtocell is greater than the one of the macrocell and c) the femtocell can support the bandwidth requirements of the UE. A handover to the femtocell is also initiated when a) none of the conditions for continuous RSRP and RSRQ monitoring are in effect, b) the RSRQ of the femtocell is greater than the one of the serving macrocell and c) the bandwidth requirements of the UE are satisfied. Note that the outcome of the HO decision is the same either if the condition for a higher RSRQ for the femtocell is satisfied or if the RSRQ of the target femtocell is greater than the absolute threshold $RSRQ_{th,2}$.

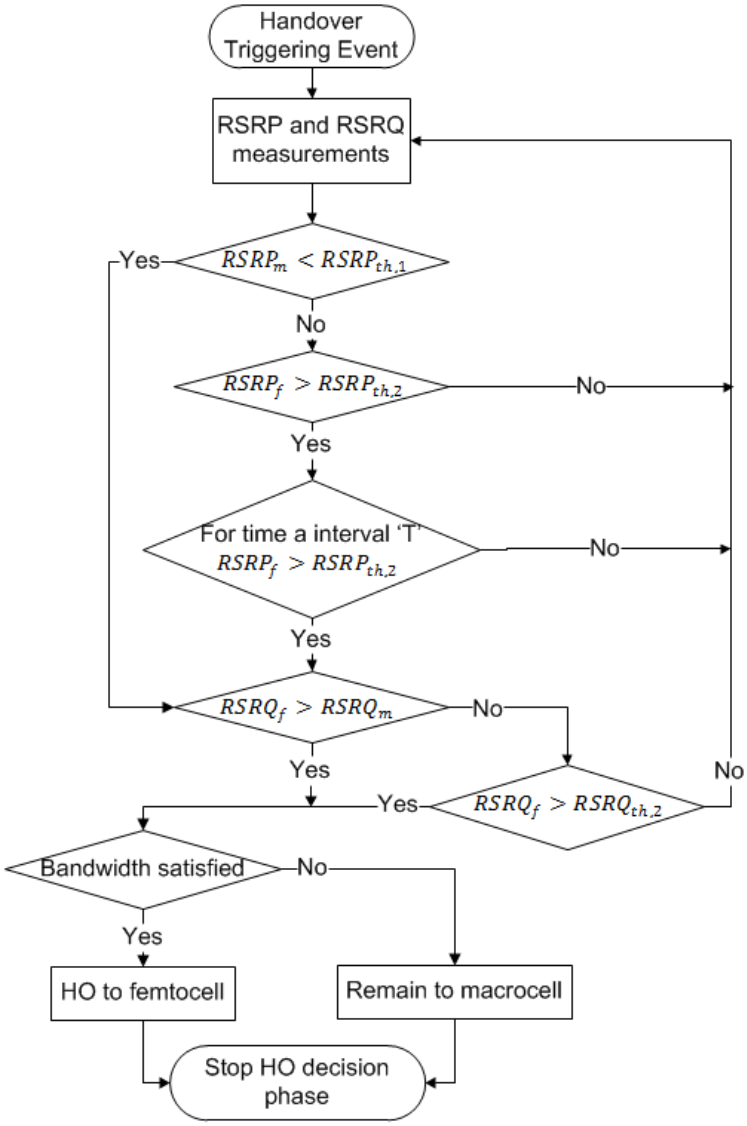

Figure 66: Yang et al. HO algorithm [67]

Among the strong features of the proposed algorithm is the use of preliminary admission control prior to the HO execution, which is expected to eliminate the HO failure probability due to admission control. The incorporation of the RSQ measurements is another strong feature of the algorithm, which is expected to enhance the SINR performance at the UEs. However, the absence of a HHM during the relative RSQ comparison may unpredictably raise the HO probability in the presence of deep channel fading. A more detailed methodology is required to select the RSRP and RSRQ thresholds, while the QoS maintenance and UE energy consumption overhead for continuously monitoring the RSRQ and RSRP should also be examined.

c. Adaptive Hysteresis Margin HO Algorithm in Femtocell Networks

An adaptive HHM approach is presented in [70] to lower the number of unnecessary HOs in the two-tier macrocell-femtocell network. The authors highlight that the interference level at the UEs majorly affects the shape of the femtocell service area, which should be reassessed in the context of the RSQ at the UEs. The proposed algorithm compares the RSQ status of the serving and the target cells by using an adaptive HHM. The HHM is adapted with respect to the RSQ at the UE and the estimated path loss. The algorithm applies to the scenario where the UE is served from a macrocell and enters the proximity of a

femtocell.

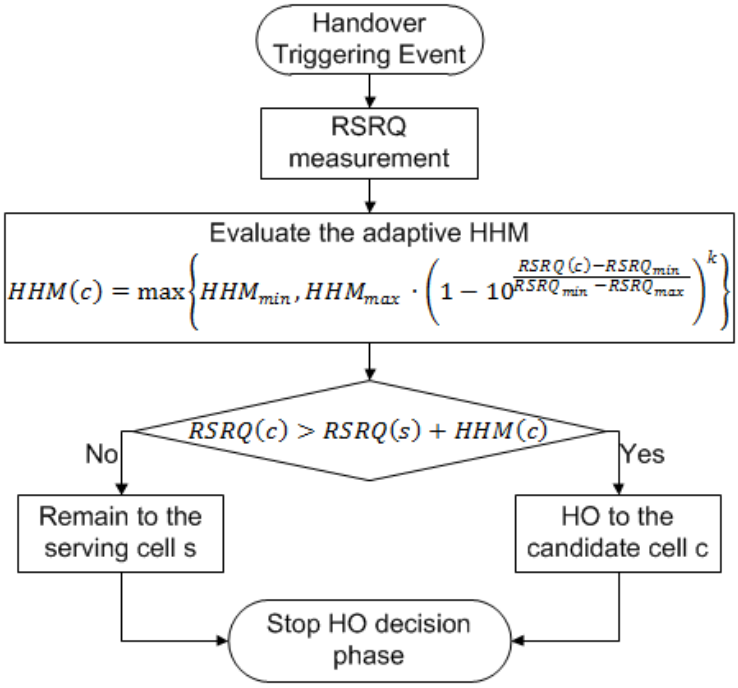

Figure 67: Becvar et al. HO algorithm [70]

The flowchart version of the proposed algorithm is depicted in Figure 67. Upon HO decision triggering, the UE performs RSRQ measurements to evaluate the RSQ status of the macrocell and femtocell stations. The HHM is subsequently adapted as follows:

$$HHM_c = \max\left\{HHM_{min}, HHM_{max} \cdot \left(1 - 10^{\frac{RSRQ(c)-RSRQ_{min}}{RSRQ_{min}-RSRQ_{max}}}\right)^{k}\right\} \quad (6.4)$$

where HHM_{min} denotes a minimum HHM value, HHM_{max} a maximum HHM value, k the path loss exponent between the UE and the cell, $RSRQ_{min}$ the minimum required RSRQ threshold for sustaining service continuity with the network, and $RSRQ_{max}$ an algorithm-related parameter. A HO to the femtocell is initiated when the RSRQ of the target femtocell is greater than the RSRQ of the serving macrocell plus the adaptive HHM.

Among the strong features of the proposed algorithm is the use of distance estimation based on the RSQ reported by the UEs. The proposed algorithm also requires minimum interventions to the standard (H)eNB functionality as it can be employed by adapting the HHM. The performance of the algorithm is validated by using the evaluation methodology in [123], while various system-level simulation results are derived as well. Nevertheless, the selection of an appropriate path loss exponent can be very challenging in real-life deployment scenarios, if we consider the NLOS conditions and the fast variations of the wireless medium. Even though the authors provide guidelines on how to calculate the $RSRQ_{max}$ value, a more detailed methodology is required to optimize this parameter in real-time. More extensive simulation results are also required to investigate the impact of the proposed RSQ-based algorithm on the interference and energy consumption of nearby cells. The performance of the proposed algorithm should be compared against other non RSQ-based algorithms as well.

6.1.3.5 Energy-efficient

The utilization of femtocells can greatly enhance the energy saving potential for both the UE and network sides [23]. In this class we include algorithms that use the energy-efficiency as the primary HO decision criterion. In the following, we present the HO decision algorithm in [71], which is the only algorithm that falls in this class, to the best of our knowledge.

a. Energy-Centric HO Algorithm for the Integrated Macrocell-Femtocell Network

An energy-centric HO decision algorithm is presented in [71] aiming to utilize the energy saving potential provided by the low-power operation of femtocells. The proposed algorithm accounts for a wide range of parameters, referred to as HO context, mainly including: a) the RS transmit power of the target cells, b) the RIP at the target cell sites, c) the operating frequency, d) the bandwidth availability, e) the UE membership status, f) the UE power class, and g) the interference limitation at the target cells. The signaling procedure for acquiring the decision parameters is thoroughly investigated, while an adaptive HHM is used to integrate the proposed energy-efficient criterion into the standard RSS based decision phase.

The proposed algorithm is depicted in Figure 68. Upon HO decision triggering, the algorithm sets a countdown HO decision timer, denoted by t_{HO}, to the value of T_{max}, which is adapted with respect to LTE-A critical events described in [136]. A HO context request is subsequently signaled to the target cells and a queue structure, denoted by A, is used to handle random HO context acquisition delay. To achieve this, the algorithm moves at the end of the queue cells for which the HO context report is not received, i.e., it postpones their evaluation. If the HO context is available, the algorithm validates the UE membership status and the bandwidth availability on the target cell. The adaptive HHM and the mean UE transmit power for the target cell denoted by HHM_{UPCM} and $P_{UL}(c)$, respectively, are subsequently evaluated. The algorithm verifies whether the mean UE transmit power on the target cell is higher than the interference limitation at the target cell or the UE power class, denoted by P_{UL}^{c} and P_{max}^{u}, respectively. If not, the proposed algorithm uses a relative RSS comparison by using a fixed HHM and the adaptive HHM. The algorithm removes from the queue target cells that fail to satisfy the UE power consumption minimization (UPCM) criterion. The proposed algorithm terminates the loop either when all the candidate cells have been evaluated or when the countdown timer expires. In the absence of candidate cells with preferential UE power consumption, the algorithm reconfigures the cell search and measurement phase. In the opposite case, a HO is initiated towards the cell that minimizes the mean UE power consumption. The calculation of the HHM_{UPCM} and $P_{UL}(c)$ parameters are discussed thoroughly discussed in [71].

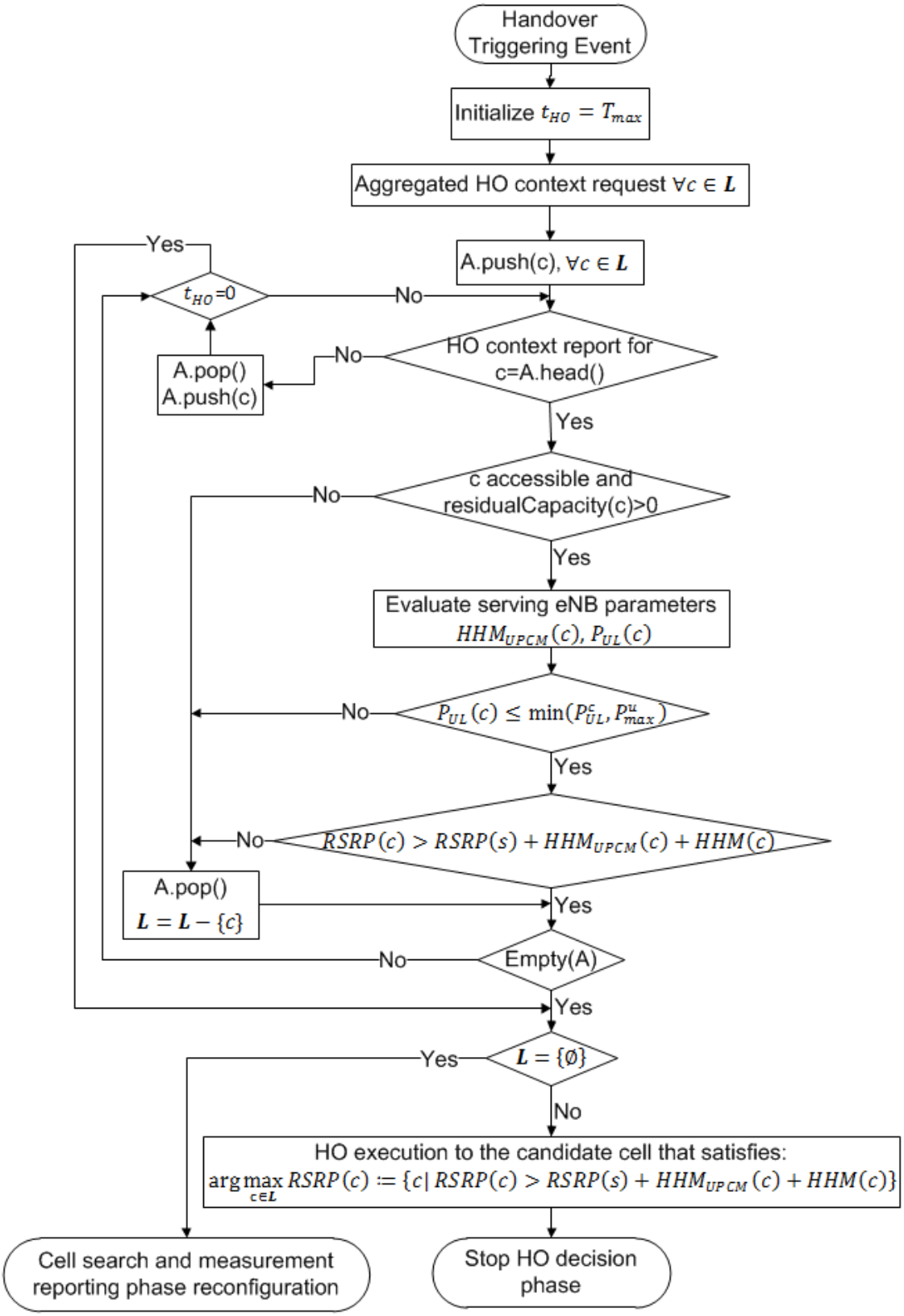

Figure 68: Xenakis et al. energy-efficient HO algorithm [71]

The proposed algorithm utilizes the femtocell energy saving potential, incorporates the actual RS transmit power, accounts for the interference level at the cell sites, and performs preliminary admission control prior to the HO execution. The use of the evaluation methodology of the Small Cell Forum and the performance comparison against two competing algorithms are two more strong features of the proposed algorithm in [71]. The detailed discussion of the

required network signaling procedure also enables backwards compatible employment with the LTE-A system. However, even though the impact of the fixed HHM parameter is investigated through system-level simulations, a more detailed HHM selection methodology is required to optimize the performance of the algorithm. More extensive system-level simulations are also required to assess the signaling requirements of the algorithm.

6.2 Performance Evaluation and Modeling Issues

Most of the existing HO decision algorithms for femtocells are accompanied with numerical results to demonstrate their performance under various measures, such as the number of unnecessary HO events, HO probability, HO failure probability, user throughput and signaling cost. The evaluation is either based on simulations [56]-[58], [61], [63][64], [66]-[71] or on analytical modeling [52]-[54], [59]. In the following, we discuss some recent trends for performance evaluation and modeling in the area of femtocell-specific MM.

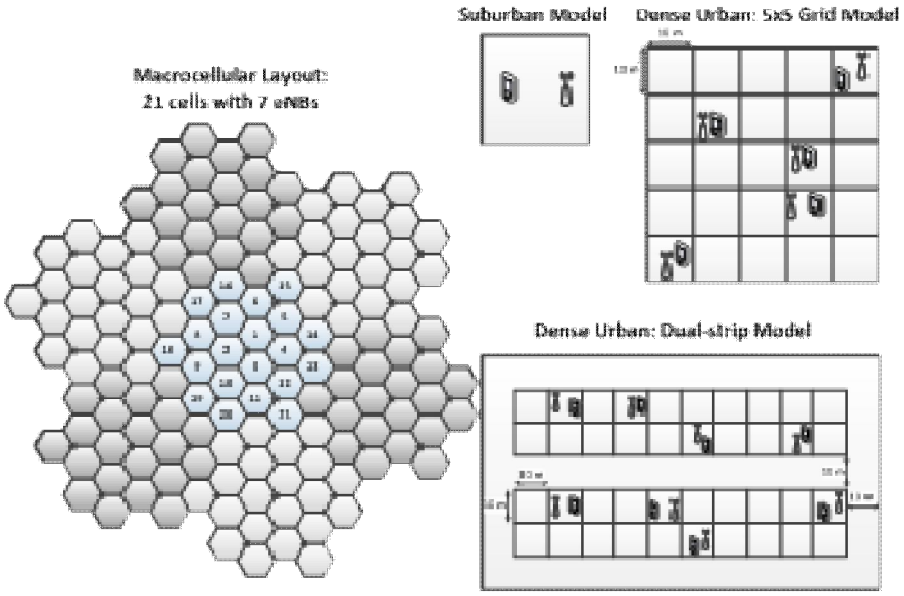

Figure 69: Network layout and femtocell deployment models [123]

In 2010, the Small Cell Forum - formerly known as the Femto Forum - has published an evaluation methodology for system-level simulations in OFDMA-based femtocell networks [123]. Even though this methodology aimed to study the interference risks from OFDMA-based femtocell deployments and recommend efficient interference mitigation techniques, it can be readily used to evaluate the performance of novel MM solutions, such as the HO decision. The evaluation methodology considers a hexagonal macrocellular layout that consists of a main cluster area including either 57 cells with 19 eNBs or 21 cells with 7 eNBs. Each macrocell includes 3 sectors, whereas the wrap-around technique is used to extend the network by copying the main cluster symmetrically on each of the 6 sides. Macrocell users are uniformly dropped within the macrocell coverage while, based on the desired femtocell deployment density, a set of femtocell apartments are dropped within the network following a uniform distribution. The evaluation methodology can be adapted to simulate both suburban and dense urban deployments. In the suburban deployment, the apartments are modeled as two-dimensional rectangular houses. In the dense urban deployment, the femtocell apartments can be modeled according to either the 5x5 grid or the dual-stripe models. In the 5x5 grid model, a single floor with 25 apartments is

considered, placed next to each other on a 5x5 grid. In the dual-stripe model, each block consists of two stripes of 2 by N femtocell apartments, where both stripes are surrounded and separated by a street with 10m width. Note that more than one floor per block can be deployed in this model. In both the 5x5 grid and dual-stripe models, the femtocell density within the femtocell blocks is adapted according to the deployment ratio parameter, which indicates the percentage of apartments with a femtocell. The femtocell stations and UEs are uniformly dropped inside the apartments. Figure 69 depicts the macrocellular layout of 7 clusters with 21 cells (7 eNBs) as well as some illustrative examples for all the aforementioned femtocell deployment models.

Depending on the femtocell deployment model, different path loss models are described in [123]. Other system-level simulation parameters and models are suggested as well, mainly including a) the baseline parameters for the macrocell and femtocell operation, e.g., inter-site distance, UE power class, and antenna gain, b) the baseline shadowing and fast-fading models, c) three alternative link-to-system mapping approaches: the Exponential Effective SINR Mapping (EESM), the per-subcarrier mapping and the Attenuated and Truncated Shannon Bound (ATSB) model, c) the baseline scheduling and power control operation of the cells, d) two alternative traffic models: the full buffer and the bursty traffic model (fixed packet size with exponential distribution for the packet inter-arrival times), and e) some low-complexity interference modeling techniques. A key feature of the evaluation methodology is the use of the Monte-Carlo random sampling technique, which considers many independent instances of the network in the time domain. For each instant, the simulated scenario uses a set of random variables for the positions of the users, the required channels and the ongoing services.

The evaluation methodology of the Small Cell Forum is an important tool for evaluating the performance of novel MM solutions, based on system-level simulations, under realistic and heterogeneous femtocell deployment scenarios. Nevertheless, analytical modeling also plays a key role in deriving useful insights and providing concrete mathematical results for the performance of the proposed MM solutions. Current literature for HO decision in the presence of femtocells, includes only a few works that use mathematical modeling to evaluate the performance of the proposed algorithms [52]-[54], [59]. The authors in [52]-[54] calculate the macrocell / femtocell assignment and HO probabilities for the proposed algorithms. However, the presented results are derived under the assumption of a single-macrocell single-femtocell network layout and the HO scenario with inbound mobility to the femtocell. Similar assumptions are made in [59], where the HO probability and signaling performance of the proposed algorithm are evaluated assuming two distinct mobility states for the users: the low (walking speed or stationary) and the high (e.g., driving a car). The analytical results are derived assuming known distributions for the camping and holding times of the users when located within the femtocell coverage.

It follows that existing modeling approaches for HO decision in the presence of femtocells are typically based on simple network layouts and do not capture the impact of the dense yet random femtocell deployment on the interference, outage and HO probability performance. On the other hand, there is a growing literature for modeling large-scale wireless networks with randomly distributed nodes based on the use of stochastic geometry (SG) [140]. SG has been widely used to calculate spatial averages that capture the key dependencies of the network performance, e.g., the interference, spectral efficiency, and transmission capacity,

as a function of a relatively small number of system parameters [141]-[143]. SG provides a natural way of defining and computing macroscopic properties of large networks by averaging over all potential geometrical patterns for the nodes. The most basic object studied in SG is the Point Process (PP), which can be visualized as a random collection of points in space. A PP can be a) *simple* or not, if the multiplicity of a point is at most one, b) *stationary* or not, if the law of the PP is invariant by translation, c) *isotropic* or not, if the law of the PP is invariant to rotation, and d) *marked* or not, where the marks assign labels to the points of the process, which are typically independent of the PP as well as independent and identically distributed (i.i.d). The Poisson PP (PPP) is the most commonly used PP in SG, as it offers the highest level of analytical tractability [143]. Some of the key properties of a PPP include the: a) *superposition*, where the superposition of two or more independent PPPs is again a PPP, b) *independent thinning*, the PP obtained by randomly and independently removing a point from the initial PPP is still a PPP, and c) *displacement theorem*, where the PP obtained by displacing a point x independently of everything else, according to some Markov kernel that defines the distribution of the displaced position of the point x, yields another PPP.

Current literature includes various results for the performance of Poisson networks, mainly with regards to the interference, outage probability, transmission capacity, and spectral efficiency of distributed wireless networks [141]-[143]. Recently, the fundamental theorems and results of SG are used to evaluate the performance of multi-tier cellular networks, given that the PPP is a good approximation of the spatial distribution of small cells [1], [144]-[146]. However, in most of the cases, static network topologies and fixed UL transmit power are assumed to analyze the performance of multi-tier cellular networks. Both these assumptions complicate the derivation of deep insights for the performance of novel MM solutions, such as the HO decision. To this end, novel SG-based modeling approaches are required to capture the impact of user mobility [147] and the divergent UL transmit powers among the mobile terminals [145], on the performance of the proposed femtocell-specific MM solutions.

6.3 Comparative Summary of HO Decision Algorithms – A Qualitative Comparison

Current state-of-the-art algorithms for HO decision making in the presence of femtocells use divergent system assumptions, simulation setups, and performance measures, which make a comprehensive performance comparison between them difficult. Nevertheless, this section presents a comparative summary of existing algorithms based on the main HO decision parameters used (Table 14), as well as the a) HO decision scenario under consideration, b) the performance evaluation methodology and results, and c) their key features (Table 15).

Table 14: Comparative summary of selected HO decision algorithms – Decision parameters

Algorithms / HO parameters	RSS-based				Speed-based				Cost-function based				Interference-Aware					E. E.
	Moon et. al [52][53]	Xu et al. [54]	Perez et al. [55][56]	Jeong et al. [57]	Ulvan et al.[58]	Zhang et al. [59]	Wu et al. [60]	Shaohong et al. [61]	Zhang et al. [62]	Xu et al.[63]	Lee et al. [64]	Reguiga et al. [65][65]	Xenakis et al. [66]	Yang et al. [67]	Chowdhury et al. [68]	Kim et al. [69]	Becvar et al. [70]	Xenakis et al. [71]
RSS related																		
RSS	v	v	v	v	v	v	v	v	v		v		v	v	v	v		v
Minimum required RSS for service continuation	v				v			v										
Path loss		v											v				v	
RS transmit power		v											v					v
Window function on the RSS	v	v																
Handover Hysteresis Margin related																		
HHM	v	v				v			v		v		v				v	
Interference related																		
RSQ									v	v				v	v	v	v	
Minimum required RSQ for service continuation																		
Received interference power at the cell sites													v					v
Interference constraints on the target cell(s)							v											v
Speed related																		
UE speed				v	v	v	v	v	v	v	v							
UE residence time in the cell				v														
UE mobility pattern				v														
Bandwidth related																		
Available bandwidth / Cell load							v		v		v	v		v	v	v		v
Cell capacity									v									
Number of camped UEs on the target cell									v									
Number of UE connections per traffic-type											v							
Cell type									v									
Traffic related																		
Traffic-type					v		v			v	v							
Mean SINR target of the UE													v					v
Bit Error Rate (BER)												v						
Current SINR at the serving cell			v															
Energy-efficiency related																		
UE power class																		v
UE battery power												v						
Mean UE transmit power													v					v
Other																		
UE membership status							v					v				v		v
UE priorities												v						

As expected, in the literature, the RSS is a common basis for HO decision making (Table 14). The UE speed is broadly used to anticipate the negative impact of user mobility, whereas the available bandwidth and the traffic-type are also utilized to lower the HO failure probability due to the lack of resources and mitigate service interruption for delay-sensitive services, respectively.

Table 15: Comparative summary of selected HO decision algorithms – Key features

Points of Comparison \ Algorithms	RSS-based				Speed-based				Cost-function based				Interference-Aware					E. E.
	Moon et. al [52][53]	Xu et al. [54]	Perez et al. [55][56]	Jeong et al. [57]	Ulvan et al.[58]	Zhang et al. [59]	Wu et al. [60]	Shaohong et al. [61]	Zhang et al. [62]	Xu et al.[63]	Lee et al. [64]	Reguiga et al. [65][65]	Xenakis et al. [66]	Yang et al. [67]	Chowdhury et al. [68]	Kim et al. [69]	Becvar et al. [70]	Xenakis et al. [71]
HO DECISION SCENARIO																		
Single-macrocell single-femtocell for inbound HO to femtocell		v		v					v	v				v	v	v	v	
Single-macrocell single-femtocell	v					v	v					v						
Single-macrocell multiple-femtocell			v					v										
Multiple-macrocell multiple-femtocell					v						v		v					v
PERFORMANCE EVALUATION RESULTS																		
Analytical (A) / Simulation (S) results	A	A	S	S	S	A	x	S	x	S	S	x	S	S	S	S	S	S
HO probability	v	v				v		v					v				v	v
HO failure probability			v								v							
Assignment probability to femtocell	v	v																
Assignment probability to macrocell	v	v																
Number of HOs	v	v	v		v					v				v	v	v		
Number of unnecessary HOs				v										v				
Unnecessary HO probability															v	v		
Impact of the HHM			v										v				v	v
Throughput			v					v									v	
Signaling overhead						v												
Transmit power													v					v
Received interference power													v					v
Energy consumption per bit																		v
Power consumption																		v
Uses the evaluation methodology in [123]													v				v	v
Includes a comparison with other algorithms	v	v		v		v		v					v	v	v	v		v

KEY FEATURES																	
Accounts for the uneven RS transmit powers	v	v						v					v				v	v
Accounts for the impact of interference by using the RSRQ/SINR status			v						v	v		v		v	v	v	v	
Accounts for the impact of interference by using the RIP at the cell sites													v					v
Accounts for potential IF limitations at the cells							v											v
Jointly performs interference mitigation and HO			v				v						v					v
Performs preliminary admission control							v		v			v		v	v	v		v
Enables load balancing									v		v	v						
Uses a HHM to lower the HO probability and minimize the ping-pong effect	v	v	v				v		v		v		v				v	v
Requires the assessment of the UE speed					v	v	v	v	v	v	v	v						
Uses mobility prediction for HO mitigation				v	v													
Accounts for the UE service requirements/ characteristics			v		v		v		v	v	v	v	v					v
Requires interventions to the standard network functionality or architecture			v	v														
Requires increased signaling/processing overhead		v	v	v			v		v		v		v					v
The signaling procedure for supporting the algorithm is described, e.g., parameter acquisition																		v
Algorithm-related parameters are fully specified	v	v		v								v	v					v
Accounts for the UE energy-efficiency												v	v					v

v: Yes A: Analytical results S: Simulation results

As depicted in Table 15, RSS-based algorithms are in general of low-complexity and easier to validate through performance analysis. Minimum network interventions are required for supporting them, unless more sophisticated capabilities are deployed, e.g., interference mitigation [55][56] or mobility prediction [57]. Nevertheless, RSS-based algorithms are generally interference-agnostic, as they do not account for the impact of interference on SINR, throughput and energy consumption performance. Speed-based algorithms aim at reducing the HO probability and mitigate the number of unnecessary HOs for medium to high speed users. To achieve this, the algorithms compare the UE speed to absolute thresholds and incorporate additional decision parameters as well. However, even though the speed thresholds greatly affect the outcome of the HO decision, their values are, in most of the cases, arbitrarily chosen. On the other hand, the monetary, signaling and energy consumption overhead for assessing and commuting the UE speed to the serving cell is not incorporated, whereas the impact of the algorithms on the interference and throughput performance is not assessed.

Cost-function based algorithms incorporate a wide set of parameters to reach a HO decision. The integration of bandwidth-related parameters often enables the deployment of preliminary admission control or load balancing. Nevertheless, the vast majority of existing approaches do not provide a detailed methodology for calculating the optimal weights or adjustment factors of the cost-function. On the other hand, the performance of the algorithms is typically evaluated by fixing the weights and adjustment factors of the cost-function. Interference-aware algorithms are expected to improve the SINR performance and allow for interference handling at a macroscopic level. However, the relative RSQ comparison of cells is required to incorporate a HHM for lowering the HO probability and reducing the ping-pong effect. On the other hand, the incorporation of the RIP at the cell sites or the RS transmit power dictates the deployment of more complicated signaling procedures. Energy-efficient algorithms reduce the energy expenditure, improve the SINR performance and enhance the QoE of the users. Nevertheless, they also increase the signaling and processing overhead to keep track or estimate the energy-efficiency at the network nodes.

From Table V, it can be seen that the HO decision scenario under scope can also be used as a criterion for classifying the existing HO decision algorithms for femtocells. As a result, existing algorithms can be classified into one of the following four classes as well: a) single-macrocell single-femtocell for inbound HO to femtocell [54][57][62][63] [67]-[70] b) single-macrocell single-femtocell [52][53][59][60][65], c) single-macrocell multiple-femtocell [55][56][61], and d) multiple-macrocell multiple-femtocell [58][64][66][71].

6.4 Simulation Study on the Performance of HO Decision Algorithms – A Quantitative Comparison

In this section, we assess the performance of the proposed algorithm and one representative algorithm from each HO decision class. The emphasis is given both on revealing the strong and weak aspects for each HO decision approach, as well as on algorithm performance comparisons. The HO algorithms under scope are the ones in [52],[59],[70], [66] and [62], which will be referred to as RSS-based, speed-based, interference-aware, energy-efficient, and cost-function, respectively. The system-level simulations are conducted according to the Small Cell Forum evaluation methodology [16]. Given that the simulation model and parameters are in line with [16] (pp. 107-110), below, we only briefly discuss some key features of the simulation setup.

We consider a hexagonal LTE-A network with a main cluster composed of seven macrocells. The network is extended by using the wrap-around technique, while a certain number of blocks with apartments, referred to as *femtoblocks*, are uniformly dropped within the LTE-A network area in accordance with the femtoblock deployment density parameter, denoted by d_{FB}. This parameter adjusts the percentage of the network area covered with femtoblocks and takes values in [0, 1]. Each femtoblock consists of two stripes of apartments, each having 2x10 apartments of 10mx10m size (dual stripe model [4]). In between and around the stripes, we consider a street with 10m width, leading to an overall block size of 120m x 70m. Femtocell stations and users are uniformly dropped within the apartments, where each femtocell initially serves one associated user. Each apartment is equipped with a femtocell with probability 0.2. All femtocells support one Closed Subscriber Group, i.e., closed access only, where three CSG are considered for the entire network. All LTE-A users are members of up to one

CSG. Each macrocell initially serves thirty users (ten users per sector), which are uniformly dropped within it. Aiming to guarantee a minimum QoS, all algorithms are evaluated using the same mean SINR target 3dB (fixed user throughput). User mobility is modeled in accordance with [71]. Note that apart from increasing the femtocell density in the network, a higher d_{FB} also increases the number of users in the system, i.e., one additional user per femtocell.

Table 16: Femtocell utilization

Algorithm	Number of femtocell users / Total number of users						
	$d_{FB} = 0.01$	$d_{FB} = 0.05$	$d_{FB} = 0.1$	$d_{FB} = 0.25$	$d_{FB} = 0.5$	$d_{FB} = 0.75$	$d_{FB} = 1$
Proposed	11/171	22/181	33/194	58/231	100/312	112/381	135/462
Cost-function based	11/171	18/181	32/194	54/231	88/312	95/381	95/462
Energy-Centric	11/171	22/181	30/194	47/231	67/312	81/381	100/462
RSS-based	3/171	8/181	14/194	30/231	68/312	70/381	79/462
Speed-based	3/171	7/181	11/194	23/231	66/312	74/381	86/462
Interference-aware	3/171	5/181	10/194	20/231	49/312	50/381	68/462

Table 16 depicts a concrete measure of femtocell utilization: the number of users associated with a femtocell. Note that the proposed algorithm considerably increases femtocell utilization compared to the other algorithms, as it accounts for the actual interference and path loss between the UE and the neighbor cells. Increased femtocell utilization is also observed for the cost-function based algorithm, which uses an enriched set of parameters to allow inbound mobility to femtocells. High femtocell utilization is shown for the energy-centric algorithm as well, as it tends to utilize the energy saving potential of femtocells. On the other hand, the speed-based algorithm reduces femtocell utilization due to the use of speed thresholds, whereas low utilization is also observed for the interference-aware algorithm, which limits inbound mobility to femtocells to mitigate cross-tier interference.

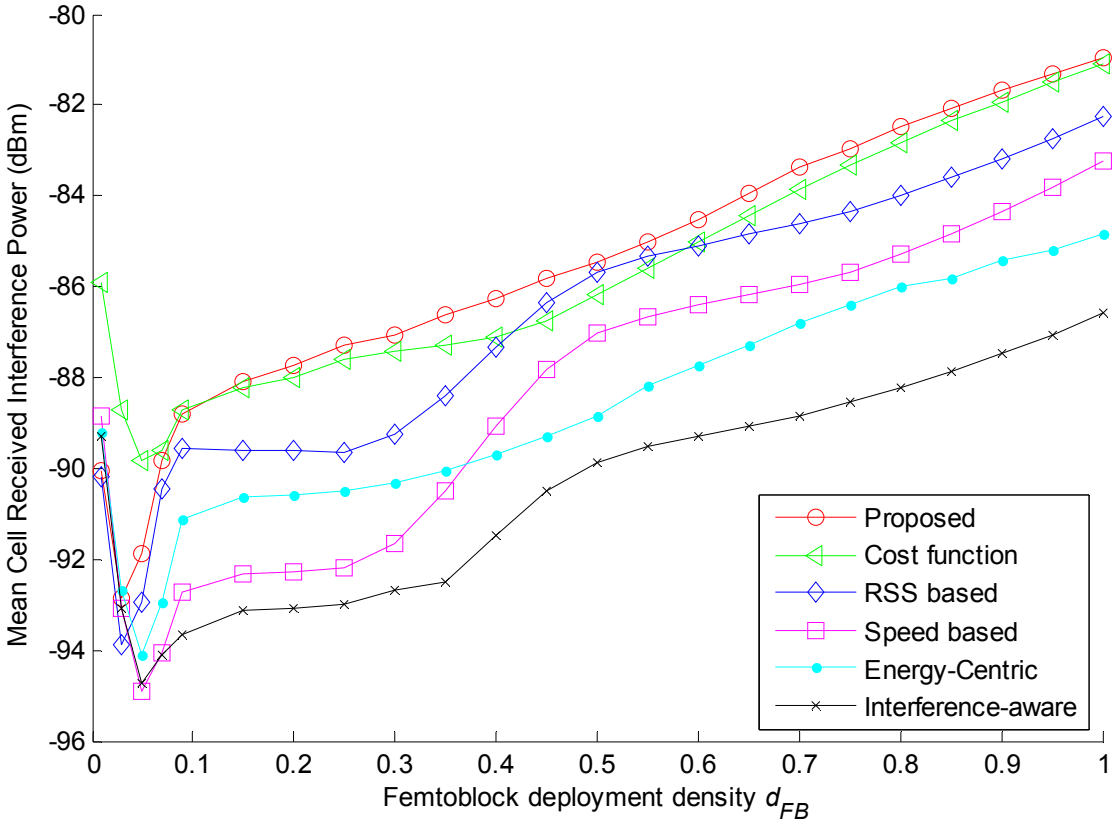

Figure 70: Mean Received Interference Power at the cells (eNBs and HeNBs)

We now demonstrate the mean received interference power at the cells (Figure 70), including both eNBs and HeNBs, and the UEs (Figure 71) versus the femtoblock density d_{FB}. Interestingly, even though the proposed algorithm increases the interference at the cells (Figure 70), it offers a considerable reduction of the UE interference at the same time (Figure 71). The former property follows from the high offloading gain towards the small cells, which increases the number of uplink interferers operating within the small cell tier. On the other hand, the former property follows from the high utilization of small cells, which reduces the mean inter-site distance between the devices and the serving base station. The cost-function based algorithm increases the cell interference as well. However, at the same time, it results in medium to high UE interference for the same reasons. Similar, yet slightly worse, performance is observed for the RSS-based algorithm, whereas the speed-based and energy-centric algorithms show roughly the same performance. In contrast, the interference-aware algorithm attains the lowest cell interference and the highest interference at the UEs, which is quite the opposite behavior compared to the proposed one.

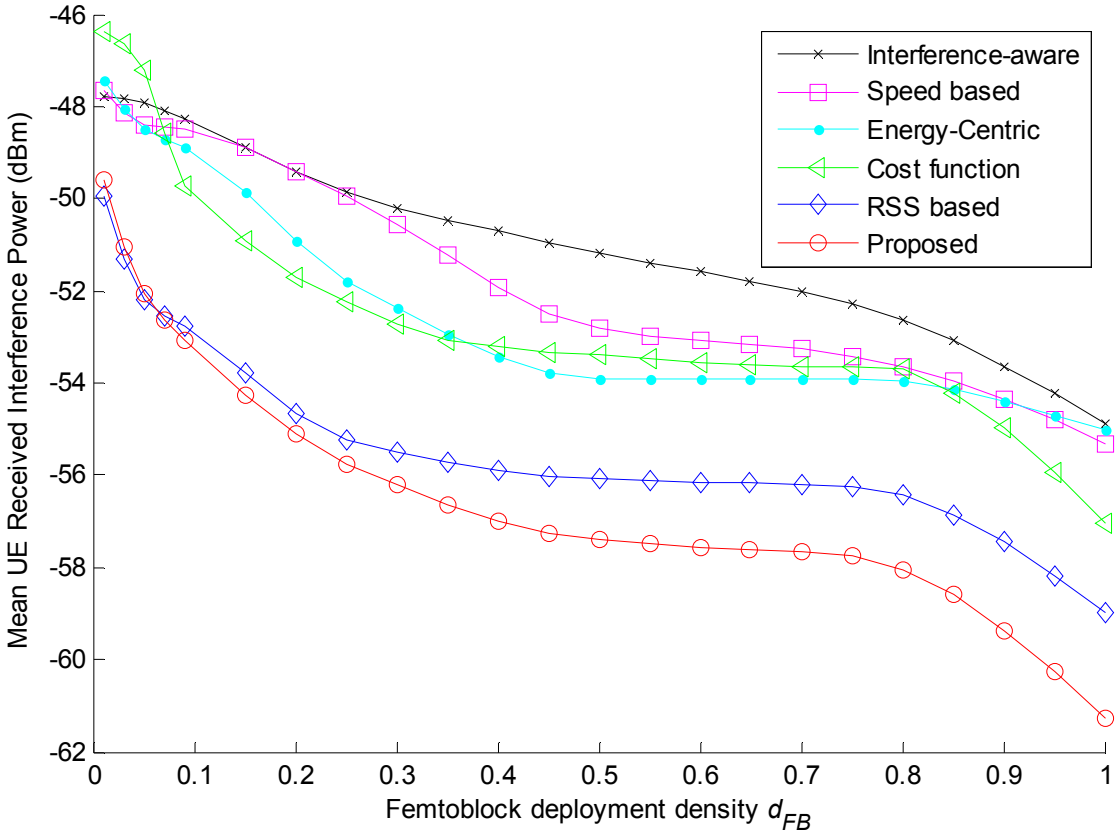

Figure 71: Mean Received Interference Power at the UEs

The results in Figure 70 and Figure 71 reveal an important performance trade-off for the LTE-A small cell network. Even though HO algorithms with high small cell utilization increase the interference at the cells, they simultaneously result in considerable interference mitigation at the UEs and increased offloading gain for the macrocell tier. Thus, apart from interference and load handling at the LTE-A cells, small cell specific HO decision can also complement the interference management in the downlink direction.

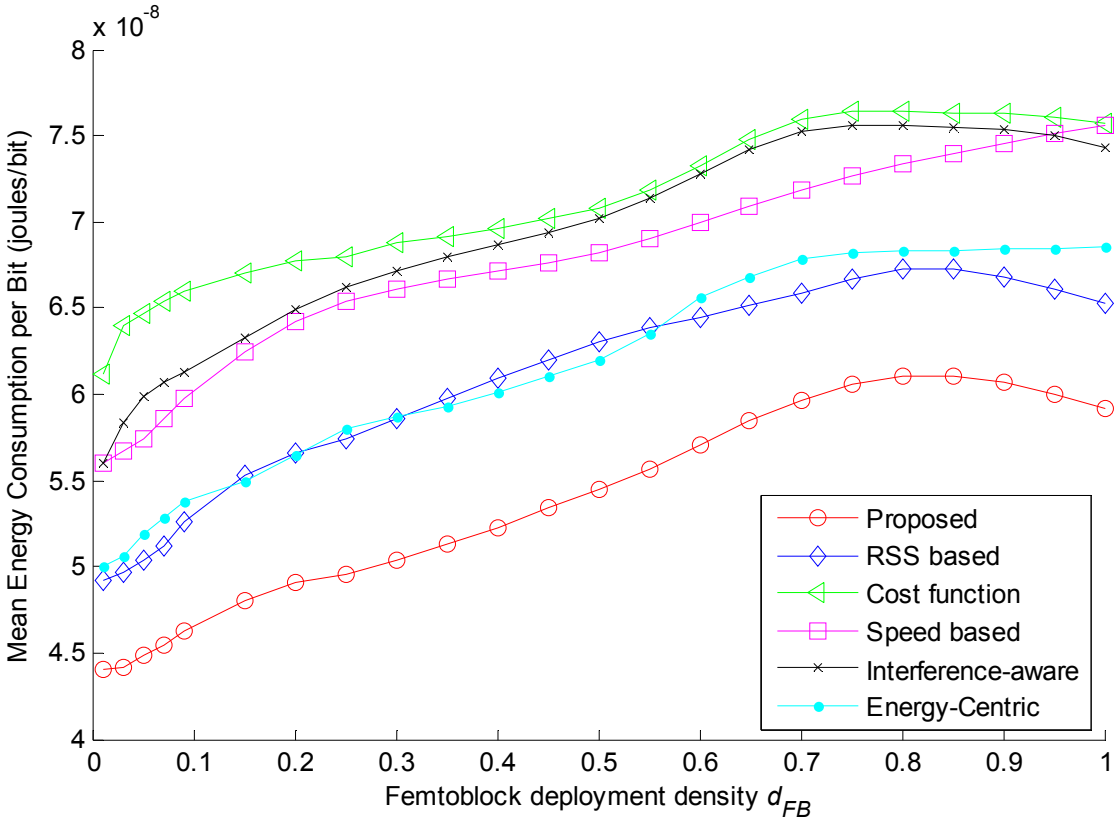

Figure 72: Mean UE Energy Consumption per Bit (Joules / bit)

Figure 72 illustrates the mean energy consumption per bit at the user, owing to transmit power, for all algorithms. Although the cost-function algorithm results in high femtocell utilization (Table 16), it simultaneously requires the highest UE energy expenditure per bit (Figure 72). This result reveals that even though prioritizing femtocell over macrocell access enhances femtocell utilization, the smart selection of a target femtocell plays a key role for sustaining low cross-tier interference (Figure 70), and utilizing the energy saving opportunities offered by the femtocells (Figure 72). As expected, the speed-based and the interference-aware algorithms show relatively high energy consumption per bit compared to other algorithms, mainly due to the high macrocell utilization (Table 16). Interestingly, the energy-centric and RSS-based algorithms demonstrate roughly similar performance, whereas the proposed algorithm reduces the energy expenditure per bit by 10% to 29% compared to all algorithms, depending on the femtocell deployment density. This performance improvement follows from the proposed algorithm's tendency to drastically increase the utilization of small cells, which in turn reduces the (average) distance between the UEs and their respective serving cells.

From Figure 72, it follows that even though a higher femtocell utilization increases the mean cell interference in the system (Figure 70), comparably lower energy expenditure per bit can be achieved if the actual cell interference and path loss between the UE and the target cells are taken into account. This is one of the key design differences between the proposed and the cost-function based algorithms.

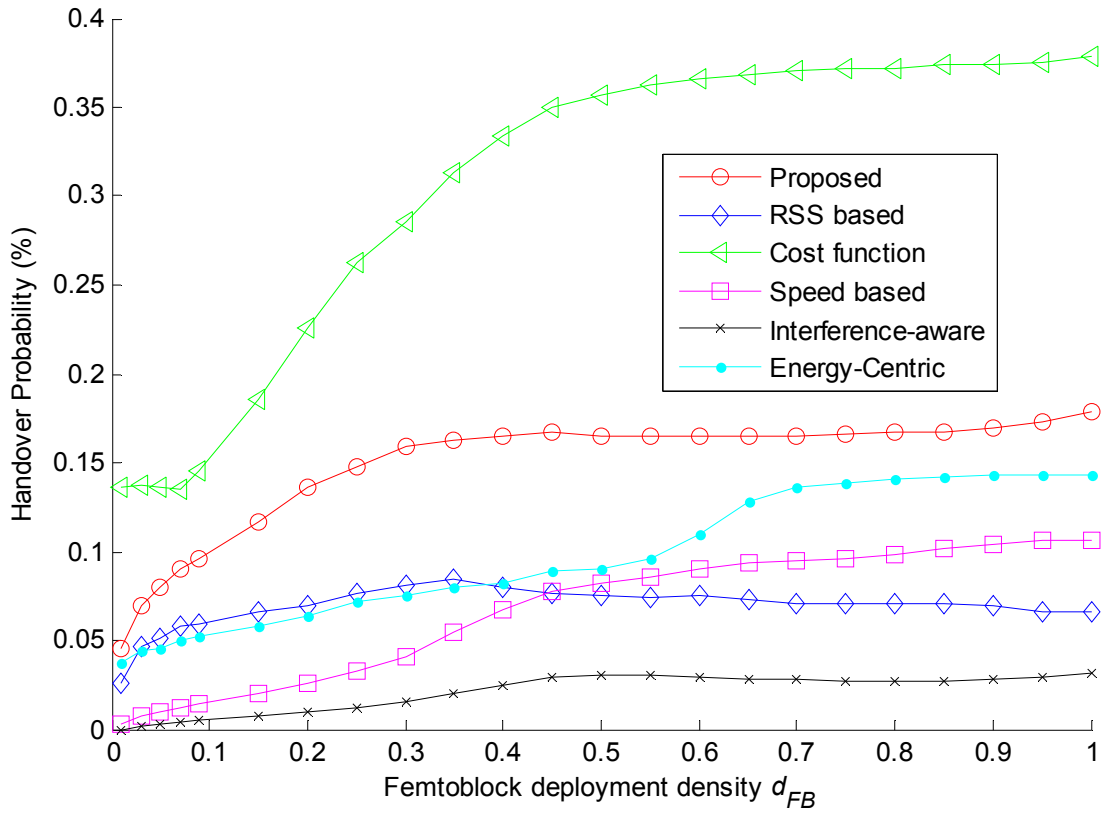

Figure 73: Average HO probability (%)

As expected, the HO probability strongly depends on the actual utilization of femtocells, given that HO algorithms that increase the femtocell utilization also result in higher HO probability (Figure 73). Note that even though the proposed algorithm achieves the highest femtocell utilization, it attains significantly lower HO probability compared to the cost-function algorithm. Moreover, the RSS-based algorithm shows roughly constant HO probability for increasing femtocell density, whereas the HO probability for the speed-based and energy-centric algorithms is proportional to the femtocell deployment density. As expected, the interference-aware algorithm attains the lowest HO probability, owing to the increased macrocell utilization.

In Table 17: Performance comparison for $\boldsymbol{d_{FB} = 0.5}$, we summarize and compare the performance of all HO algorithms for $d_{FB} = 0.5$ under different performance measures. Note that the results refer to mean values while the signaling rate refers to the number of signals per second exchanged within both the core and the access network. The RSS-based algorithm achieves a relatively medium small cell utilization, energy consumption and interference performance, while it sustains low HO probability and signaling rate as well. On the other hand, even though enhanced small cell utilization is shown for the cost-function algorithm, the results indicate that the cost-function weights should be carefully selected to improve its uplink capacity, interference, and HO probability/signaling performance. The incorporation of user mobility criteria enables the speed-based algorithms to significantly reduce the cell interference and attain very low HO probability / signaling. However, further enhancements are required to lower the interference at the UEs and improve their energy-efficiency. Interference-aware algorithms greatly reduce the cell interference and keep the HO probability / signaling low. However, they result in poor utilization of the low power operation of small cells, leading to enlarged energy consumption and interference at the

user terminals. The energy-centric algorithm substantially enhances the mean uplink capacity and reduces the energy expenditure for both the cells and the UEs. Nevertheless, the use of higher HHM should be considered to further reduce the HO probability / signaling required for monitoring the UE energy consumption.

Table 17: Performance comparison for $d_{FB} = 0.5$

Algorithm / Measure	Proposed	RSS-based	Cost-function based	Speed-based	Interference-aware	E. E.
Small Cell Utilization	Very High (32%)	Medium (22%)	High (28%)	Medium (21%)	Low (16%)	Medium (22%)
Mean UL Capacity	High (14.5 Mbps)	High (14 Mbps)	Low (12.6 Mbps)	Medium (13.7 Mbps)	Medium (13.5 Mbps)	High (15 Mbps)
Mean Energy Consumption per bit	Very Low (54 nJ/b)	Medium (63 nJ/b)	Very High (71 nJ/b)	Medium (68 nJ/b)	High (70 nJ/b)	Medium (63 nJ/b)
Mean UE transmit power	Very Low (17dBm)	Low (18dBm)	Very High (19.5dBm)	Medium (18.5dBm)	High (19dBm)	Very Low (17dBm)
Mean Cell Transmit Power	Very Low (29 dBm)	Low (32 dBm)	Medium (33dBm)	Medium (33dBm)	High (34 dBm)	Low (32dBm)
Mean UE Received Interference	Very Low (-58dBm)	Low (-56dBm)	Medium (-54dBm)	High (-53dBm)	High (-51dBm)	Medium (-54dBm)
Mean Cell Interference	High (-85dBm)	Medium (-87dBm)	High (-86dBm)	Medium (-87dBm)	Very Low (-91dBm)	Low (-89dBm)
HO probability	High (0.15)	Medium (0.08)	Very High (0.35)	Low (0.07)	Very Low (0.04)	Medium (0.09)
HO failure probability	Very Low (0.001)	Very Low (0.001)	Very High (0.3)	Low (0.05)	Very Low (0.003)	Low (0.03)
S1 signaling rate	High (1200/sec)	Low (420/sec)	Very High (3250/sec)	Very Low (70/sec)	Very Low (130/sec)	Medium (620/sec)
X2 signaling rate	High (1020/sec)	Medium (460/sec)	Very High (2100/sec)	Low (310/sec)	Very Low (140/sec)	Medium (540/sec)

Based on the results in Table 17 we can conclude that compared to all other algorithms under scope, the proposed algorithm attains superior performance in terms of energy expenditure per bit, uplink capacity, cell and UE transmit power, and mean UE interference. These performance improvements follow from the exchange and utilization of the LTE-A measurements, which allow for an accurate estimation of the actual cell interference and path loss between the UE and the target cells. Nevertheless, even though the utilization of measurements from other cells enables this robust performance, i.e., increased small cell utilization combined with smart selection of cells, it is also the origin for increased cell interference and HO probability/signaling.

6.5 Lessons Learned and Future Research Directions

We now discuss lessons learned from the design of HO decision algorithms for femtocells. RSS-based algorithms are in general of low-complexity and easier to validate through performance analysis. Minimum network interventions are also required to support them, unless more sophisticated capabilities are deployed, e.g., mobility prediction. However, this kind of algorithms are in general

interference-agnostic and do not consider the impact of interference on the SINR, throughput, or energy consumption performance. On the other hand, speed-based algorithms reduce the HO probability and mitigate the number of unnecessary HOs for medium to high speed users. However, in most of the cases, existing algorithms compare the user speed with arbitrarily chosen thresholds, which are not the outcome of simulation or analysis. Another weak aspect of existing speed-based algorithms is that they do not consider the monetary, signaling, or energy consumption overhead, required for evaluating the UE speed and its transfer to the serving cell.

Interference-aware algorithms improve the SINR and allow for interference handling at a macroscopic level. However, algorithms that are based on relative RSQ comparisons are required to optimize their HHM both to lower the HO probability and reduce the ping-pong effect. On the other hand, the incorporation of the RIP at the cell sites, or the RS transmit power, dictates the deployment of more complex signaling procedures, which are typically outside the scope of the respective works. Energy-efficient algorithms reduce the energy expenditure and typically improve the SINR performance in the uplink. However, they also increase the signaling and processing overhead to keep track and evaluate the energy-efficiency at the cellular nodes. Cost-function based algorithms incorporate a wide set of parameters to reach a HO decision. The integration of bandwidth-related parameters often enables preliminary admission control or load balancing. Nevertheless, cost-function based algorithms typically do not provide a detailed methodology for calculating the optimal weights or adjustment factors of the cost-function, which, however, may have a major impact on the final decision outcome. In Table 18, we summarize the strong and weak aspects of the aforementioned algorithmic classes.

Table 18: Comparison of HO decision classes

<table>
<tr><th></th><th>RSS-based</th><th>Speed-based</th><th>Interference-aware</th><th>Energy-efficient</th><th>Cost-function based</th></tr>
<tr><td rowspan="3">Strong aspects</td><td>(+) Low-complexity</td><td>(+) Reduce HO probability</td><td>(+) Enhance SINR performance</td><td>(+) Reduce energy expenditure</td><td>(+) Enable preliminary admission control</td></tr>
<tr><td>(+) Easier to analyze</td><td>(+) Mitigate unnecessary HOs for medium to high speed users</td><td rowspan="2">(+) Enable interference handling</td><td rowspan="2">(+) Improve SINR performance in the uplink</td><td rowspan="2">(+) Load balancing</td></tr>
<tr><td colspan="2">(+)Minimum network interventions</td></tr>
<tr><td rowspan="3">Weak aspects</td><td>(-) Interference-agnostic</td><td>(-) Arbitrary speed thresholds</td><td>(-) Require HHM optimization</td><td>(-) Increase complexity</td><td>(-) Require optimization of the weights and adjustment factors</td></tr>
<tr><td rowspan="2">(-) Do not account for SINR, interference and energy energy-efficiency</td><td rowspan="2">(-) Increase monetary and signaling cost for estimating the UE speed</td><td>(-) Increase complexity</td><td colspan="2" rowspan="2">(-) Increase network signaling</td></tr>
<tr><td>(-) Increase network signaling</td></tr>
</table>

Based on the previous discussion, we identify four key design principles for robust HO decision algorithmic design in small cell networks: a) focus on the multiple-macrocell multiple-small cell HO scenario, b) be compatible with the

cellular system, c) optimize decision-related parameters, and d) use widely-accepted evaluation methodologies.

Most existing algorithms consider a single-macrocell single-small cell HO decision scenario, e.g., [52][53][59][60][65]. Nevertheless, existing reports foresee that the number of small cells will surpass that of deployed macrocells by up to six times within the next few years [148], transforming the operator-planned network of medium to large radii cells to a multi-tier network with numerous user-deployed small sized stations. In such an environment, the robust support of inter-cell mobility asks for HO algorithms that are optimized to operate under the multiple-macrocell multiple-small cell HO scenario.

Referring to the issue of compatibility, existing solutions incorporate a rich set of parameters to improve the cell HO performance. However, only a few describe the additional network functionality and signaling procedures required to support them. Specifying in detail all necessary architectural and functional enhancements is critical, as it guarantees the smooth integration of the proposed solution and provides stimulus for further research, innovation, and standardization.

Another critical issue is the optimization of all parameters involved in the HO decision. The use of a HHM during the RSS / RSQ comparison plays a key role in handling the fast variations of the wireless medium and mitigating the ping-pong effect. This effect is even more prominent in the presence of small cells due to the overlapping cell coverage. Combined with speed-based parameters, the utilization of a HHM can significantly reduce the HO probability, especially for medium to high speed users. However, optimizing the HHM is cumbersome and should be based on robustly handling the (negative) impact of user mobility while, at the same time, making the most out of the short transmit-receive range.

Since the evaluation of a HO decision algorithm is integral part of its design, validating the performance of the proposed algorithms using realistic system assumptions and simulation setups is also important. Even though some of the existing proposals conduct mathematical analysis, the assumption of simplistic network layouts raises questions about their scalability in real-life systems. Besides, recent trends for performance evaluation of multi-tier networks, such as the Small Cell Forum evaluation methodology or stochastic geometry [142], should be integral part of future proposals for HO decision in a small cell network.

6.6 Key Contributions and Conclusions

The smooth integration of femtocells into the macro-cellular network dictates architectural and procedural enhancements that go beyond the standard cellular operation. Aiming to launch the design of novel femtocell-specific MM proposals for real-life systems, in this section we have overviewed the open MM issues and solutions in the two-tier macrocell – femtocell LTE-A system. Cell identification dictates the deployment of more sophisticated procedures to uniquely and swiftly identifying the femtocell infrastructure, whereas the distributed selection of PCIs is of critical importance for accommodating with the random yet dense femtocell deployment. Founded on the concepts of cognitive and cooperative networking, the design of UE-based autonomous cell search algorithms and the development of femtocell-specific DRX and packet scheduling algorithms will also play a key role for maintaining the energy consumption and QoS maintenance overheads within acceptable levels in the LTE-A system. The design of femtocell-specific selection / reselection strategies, in combination with the optimized formation of

tracking areas, will have a great impact on the efficiency of the idle-state mobility procedure in the presence of femtocells as well, whereas more sophisticated signaling procedures should be proposed to integrate femtocell-specific processes, such as autonomous cell search and access control, into the standard HO execution phase.

Motivated by the challenges and the current state-of-the-art for HO decision making in the presence of femtocells, in this section we also have surveyed and classified existing algorithms for the two-tier macrocell – femtocell network, based on the primary decision criterion used. By utilizing a common notation for the main HO decision parameters and adapting the presentation in the context of the LTE-A system, we have discussed the main advantages and disadvantages of the most representative algorithms per class. The key performance evaluation and modeling issues for femtocell-specific MM have been thoroughly discussed, with the emphasis given in overviewing the Small Cell Forum evaluation methodology for system-level simulations and discussing the emerging trend of using Stochastic Geometry for femtocell-specific mathematical modeling. A comparative summary of existing algorithms has also been provided, focusing on the main decision parameters, system model assumptions, performance evaluation results, and key features of the algorithms. It was found that the vast majority of existing algorithms applies to the single-macrocell single-femtocell HO decision scenario, although the need to address the multiple-macrocell multiple-femtocell HO decision scenario is currently of core importance. The detailed specification of the additional network functionality and signaling for supporting the HO decision algorithms has been shown to constitute an integral prerequisite for attaining backwards compatibility with prominent cellular standards, such as the LTE-A system. The incorporation of a HHM has been identified as a powerful tool in anticipating the fast variations of the wireless medium and mitigating the ping-pong effect. However, an optimized HHM selection is also required to handle the impact of user mobility without sacrificing the femtocell utilization opportunities. The use of realistic system model assumptions, system-level simulation setups, and performance comparisons with other competing algorithms, are three more key enablers for ensuring the real-life deployment of the proposed algorithms.

Using the Small Cell Forum evaluation methodology, we have validated our views on lessons learned for HO decision in the presence of small cells, and have revealed the key advantages and main weaknesses of existing design approaches. The simulation study has shown that the utilization of standard LTE-A measurements allows the proposed algorithm to double the macrocell offloading gain, enhance the uplink capacity (around 0.5 Mbps per user) and reduce the interference at the UEs (up to 7 dB). On the other hand, the intense utilization of the small cell infrastructure combined with the exchange of the standard LTE-A measurements have been shown to increase the cell interference (up to 8 dB) and the HO probability / signaling requirements. Our results highlight the need for small cell specific interference mitigation and novel cell HO protocols tailored to the specific characteristics of the small cell network.

In summary, MM in the two-tier macrocell-femtocell network is challenging in many aspects and poses a number of open issues that are yet to be solved. The detailed discussion on the key aspects and research challenges of MM in the LTE-A system is expected to launch the design of femtocell-specific MM solutions, whereas the comprehensive survey and comparative summary of

existing HO decision algorithms will provide a concrete basis for future design of HO decision making in the two-tier macrocell-femtocell network.

7. CONCLUSIONS, SUMMARY OF CONTRIBUTIONS, AND FUTURE WORK

The nowadays heterogeneous wireless network (HWN) is a collection of ubiquitous wireless networking elements (WNEs) that support diverse functional capabilities and networking purposes. In such a heterogeneous networking environment, localization and mobility management will play a key role for the seamless support of emerging applications that span from the direct exchange of localized traffic between homogeneous WNEs (peer-to-peer communications) to the unsupervised navigation of battery-operated robotic nodes using spatial information from the ubiquitous HWN infrastructure. Since most of the existing wireless networking technologies enable the direct (or indirect) estimation of the distances and angles between their WNEs, as well as the assessment of their current radio status, e.g. interference level, the integration and utilization of information on the radio status and spatial distribution of the heterogeneous WNEs is a natural solution for robustly handling the challenging issues of localization between not necessarily homogeneous WNEs and the mobility management of moving WNEs throughout the heterogeneous wireless networking infrastructure. In this work, we have moved well beyond state-of-the-art in four key research areas: i) localization and peer-discovery between non-homogeneous WNEs, ii) network-assisted device-to-device (D2D) discovery in cellular networks, iii) energy-efficient handover (HO) decision in the macrocell – femtocell network, and iv) network-assisted vertical handover decision (VHO) for the integrated cellular and WLAN heterogeneous wireless network.

In the area of localization and peer-to-peer discovery in HWNs, we have proposed the integration of spatial information on the distances and angles between the heterogeneous WNEs as means of enhancing the performance of localization and peer-discovery between not necessarily homogeneous WNEs. Among others, we have derived closed-form expressions for the conditional probability density function (pdf) and complementary cumulative distribution function (ccdf) of the relative distance between two heterogeneous WNEs, given partial (or full) knowledge of the spatial relations between their upper-tier parent WNEs. In the sequel, we have used the pdf expressions to describe the statistical behavior of localization between distant and not necessarily homogeneous WNEs, and used the ccdf expressions to analyze the performance of location-aware peer discovery between heterogeneous WNEs given partial (or full) knowledge of the spatial relations between their upper-tier WNEs. Optimal strategies for the deployment of WNEs, as means of maximizing the probability of successful discovery between two WNEs of interest, have also been presented, and useful guidelines for the design of localization and peer discovery in the nowadays HWN have been drawn. To the best of our knowledge, this is the first work to consider this disruptive localization and peer-to-peer discovery paradigm with and analyze its performance using mathematical analysis. Future work in the area includes the exploitation of the derived expressions to analyze the performance of emerging issues for peer-to-peer discovery in HWN, including the derivation of optimal strategies and performance bounds for the unsupervised navigation of communication-enabled robotic nodes, and the design of innovative mechanisms for the emerging paradigm of physical layer security.

In the area of network-assisted D2D discovery in cellular networks, we have derived closed-form expressions for the conditional pdf and ccdf of the distance between two tagged D2D peers, given various combinations of location

information parameters including at least the inter-site distance or the neighboring degree of their associated cellular base stations. In the sequel, we have used the derived expression to quantify how different levels of spatial knowledge affect the performance of D2D discovery probability and identified conditions under which the deployment of additional cellular base stations can be used to optimize the performance of D2D discovery. Useful design guidelines for network-assisted D2D discovery have also been provided, launching the design of more efficient D2D discovery mechanisms in the future 5G network. To the best of our knowledge, our work the first to address the challenging issue of network-assisted D2D discovery in random spatial networks and analyze its performance using mathematical analysis. Future work in the area includes the exploitation of the derived expressions to analyze the performance of emerging issues for D2D communications in cellular networks, including the design of more efficient formation of tracking areas in D2D-enabled cellular networks and the derivation of optimal strategies and performance bounds for SINR-based D2D discovery.

In the area of handover decision for the macrocell – femtocell network, our contributions are three-fold. Firstly, we have shown that the handover decision phase is a powerful tool for handling cross-tier interference in the two-tier macrocell-femtocell network and revealed that the exploitation of standard cellular measurements can play a key role in minimizing the energy consumption of the mobile terminals by employing energy-efficient handover decisions. Secondly, we have proposed an energy-efficient handover decision algorithm for the two-tier macrocell – femtocell network, thoroughly discussed all signaling procedures required to support it in the LTE-A system, and demonstrated that compared to existing algorithms, the proposed algorithm greatly reduces the mean UE and cell transmit power, lowers the mean UE energy expenditure per bit and UE interference, and enhances the system capacity, at the cost of moderate increase of network signaling. Thirdly, we have successfully identified a notable list of open issues related to MM support in the presence of femtocells, surveyed and classified current state-of-the-art in HO decision making for femtocells, provided qualitative and quantitative comparisons of their performance by using the widely-accepted evaluation methodology of the Small Cell Forum, and summarized lessons learned from the design of handover decision algorithms for the LTE-A femtocell network. The latter contributions are expected to provide a concrete basis for future algorithmic design in the area by the research community.

In the area of vertical handover decision for the integrated cellular and WLAN heterogeneous wireless network, we have proposed an energy-efficient VHO decision algorithm that utilizes recent enhancements to the 3GPP and IEEE Standards, such as the deployment of the ANDSF and the provision for enhanced radio measurement capabilities at the base stations and the access points. To the best of our knowledge, this is the first work to focus on the employment of energy-efficient vertical handover decision in the LTE-A – IEEE 802.11-2012 systems, and to demonstrate that the exploitation of their exciting new capabilities can be the cornerstone for reducing the energy consumption at the multi-mode mobile terminals by employing energy-efficient vertical handover decisions. Extensive system-level simulations on the performance of the proposed algorithm, the ARCHON algorithm, have shown that even though the deployment of ARCHON asks for increased ANDSF and WLAN network signaling, it enables efficient load balancing between the heterogeneous RATs, reduced MMT energy consumption per bit and enhanced uplink capacity per user. Future work in the area includes performance analysis of the proposed algorithm using stochastic geometry.

TERMINOLOGY

Ξενόγλωσσος όρος	**Ελληνικός Όρος**
Reliability	Αξιοπιστία
Editor	Επιμελητής
Recommendations	Υποδείξεις

ACRONYMS

3GPP	3rd Generation Partnership Project
4G	Fourth Generation
5G	Fifth Generation
ANPI	Average Noise Power Indicator
AoA	Angle of Arrival
AP	Access Point
ARCHON	Andsf-assisted eneRgy-effiCient vertical Handover decision
ATSB	Attenuated and Truncated Shannon Bound
BCCH	Broadcast Control Channel
BS	Base Station
CCDF	Complementary Cumulative Distribution Function
CGI	Cell Global Identifier
CN	Core Network
CoMP	Coordinated Multipoint
CSG	Closed Subscribers Group
D2D	Device-to-Device
DL	Downlink
DRX	Discontinuous Reception
ECGI	E-UTRAN cell global identifier
EE	Energy Efficient
EESM	Exponential Effective SINR Mapping
eNB	E-UTRAN Node B
EPC	Evolved Packet Core
ESM	Effective SINR mapping
E-UTRAN	Evolved Universal Terrestrial Radio Access Network
FDD	Frequency Division Duplexing
HARQ	Hybrid Automatic Repeat request
HeNB	Home eNB
HeNB GW	HeNB gateway
HHM	Handover Hysteresis Margin
HO	Handover
HWN	Heterogeneous Wireless Network
IE	Information Element

IHO	Intracell Handover
IMT	International Mobile Telecommunications
ITU	International Telecommunication Union
LIS	Location Information Server
LTE-A	Long Term Evolution – Advanced
MAC	Medium Access Control
MCS	Modulation and Coding Schemes
MIMO	Multiple Input Multiple Output
MM	Mobility Management
MME	Mobility Management Entity
MMT	Multi-mode Mobile Terminal
MTP	Max Transmit Power
MUD	Multi-User Detection
NCL	Neighbor Cell List
NLOS	Non Line Of Sight
OAM	Operation, Administration, and Maintenance
P2P	Peer-to-Peer
PCI	Physical Cell Identifier
PDF	Probability Density Function
P-GW	Packet Data Network Gateway
PHY	Physical
PLMN	Public Land Mobile Network
PoA	Point of Attachment
PP	Point Process
PPP	Poisson Point Process
QoE	Quality of Experience
QoS	Quality of Service
RAT	Radio Access Technology
RAT	Radio Access Technologies
RB	Resource Block
RCPI	Received Channel Power Indicator
RF	Radio Frequency
RIP	Received interference power
RRM	Radio Resource Measurement

RS	Reference Signals
RSNI	Received Signal to Noise Indicator
RSQ	Received Signal Quality
RSRP	Reference Symbol Received Power
RSRQ	Reference Symbol Received Quality
RSS	Received Signal Strength
RSSI	Received Signal Strength Indicator
RV	Random Variable
S1AP	S1 Application Protocol
SC	Strongest Cell
SG	Stochastic Geometry
S-GW	Serving Gateway
SIB	System Information Block
SINR	Signal to Interference plus Noise Ratio
STA	Station
TA	Tracking Area
TD	Timing Difference
ToA	Time of Arrival
TPU	Transmit Power Used
TS	Technical Specification
TTT	Time To Trigger
UE	User Equipment
UL	Uplink
UMTS	Universal Mobile Telecommunications System
UPCM	UE Power Consumption Minimization
UTPR	UE Transmit Power Reduction
UTRA	UMTS Terrestrial Radio Access
UWB	Ultra Wide-Band
VHO	Vertical Handover
Wi-Fi	Wireless-Fidelity
WiMAX	Worldwide Interoperability for Microwave Access
WLAN	Wireless Local Area Network
WNE	Wireless Networking Element
X2AP	X2 application protocol

APPENDIX I

I.A Proof of Theorem 2.1

Let $T_{i,x}$ and $T_{i,y}$ denote the x and y-axis components (projections), respectively, of the *relative* distance between the tier-i and tier-$(i-1)$ parent WNEs of the target peer as shown in Figure 11 ($i \leq m_t$). In addition, let $S_{j,x}$ and $S_{j,y}$ denote the respective x and y-axis components of the *relative* distance between the tier-j and tier-$(j-1)$ parent WNEs of the source peer ($j \leq m_s$). Then, the distance Z between the two peers is given by (Figure 11: Localization and (location-aware) peer discovery using spatial information from heterogeneous WNEs):

$$Z = \sqrt{\left(D + \sum_{j=1}^{m_s} S_{j,x} + R_{s,x} - \sum_{i=1}^{m_t} T_{i,x} - R_{t,x}\right)^2 + \left(\sum_{i=1}^{m_t} T_{i,y} + R_{t,y} - \sum_{j=1}^{m_s} S_{j,y} - R_{s,y}\right)^2}. \quad (2.17)$$

For $i \in \mathcal{L}_t$, where $\mathcal{L}_t$ is the set of parent WNEs of the target peer for which the relative polar coordinates are known, the x and y-axis components of the relative distance T_i between the tier-i and the tier-$(i-1)$ parent WNEs of the target peer can be readily computed by

$$T_{i,x} = T_i \cos\theta_i \text{and} T_{i,y} = T_i \sin\theta_i, \text{for} i \in \mathcal{L}_t. \quad (2.18)$$

In a similar manner, for $j \in \mathcal{L}_s$, where $\mathcal{L}_s$ is the set of parent WNEs of the source peer for which the relative polar coordinates are known, the x and y-axis components of the relative distance S_j between the tier-j and the tier-$(j-1)$ parent WNEs of the source peer are given by

$$S_{j,x} = S_j \cos\phi_j \text{and} S_{j,y} = S_j \sin\phi_j, \text{for} j \in \mathcal{L}_s \quad (2.19)$$

If the relative polar coordinates (R_t, ξ_t) of the target peer are known to the LIS, then the x and y-axis components of the distance R_t between the target peer and its associated WNE are given by $R_{t,x} = R_t \cos\xi_t$ and $R_{t,y} = R_t \sin\xi_t$, respectively. On the other hand, if the relative polar coordinates (R_s, ξ_s) of the source peer are known, then the x and y-axis components of the distance R_s between the source peer and its associated WNE are given by $R_{s,x} = R_s \cos\xi_s$ and $R_{s,y} = R_s \sin\xi_s$, respectively. Let us now define two RVs Q_x and Q_y as follows:

$$Q_x = D + \sum_{j\in\mathcal{L}_s} S_j \cos\phi_j + \sum_{j\in\bar{\mathcal{L}}_s} S_{j,x} + R_{s,x} - \sum_{i\in\mathcal{L}_t} T_i \cos\theta_i + \sum_{i\in\bar{\mathcal{L}}_t} T_{i,x} - R_{t,x} \quad (2.20)$$

$$Q_y = \sum_{i\in\mathcal{L}_t} T_i \sin\theta_i + \sum_{i\in\bar{\mathcal{L}}_t} T_{i,y} + R_{t,y} - \sum_{j\in\mathcal{L}_s} S_j \sin\phi_j - \sum_{j\in\bar{\mathcal{L}}_s} S_{j,y} - R_{s,y}. \quad (2.21)$$

By combining (2.17)-(2.21) it can be readily shown that $Z = \sqrt{Q_x^2 + Q_y^2}$. Let us assume that the relative polar coordinates of the source and target WNEs are not known to the LIS. By taking a closer look to (2.20) it can be seen that the RV Q_x is composed by i) a sum of fixed and known parameters, i.e. the sum $\left(D + \sum_{j\in\mathcal{L}_s} S_j \cos\phi_j - \sum_{i\in\mathcal{L}_t} T_i \cos\theta_i\right)$, and ii) a sum of unknown RVs, i.e. the sum $\left(\sum_{j\in\bar{\mathcal{L}}_s} S_{j,x} + R_{s,x} - \sum_{i\in\bar{\mathcal{L}}_t} T_{i,x} - R_{t,x}\right)$. From Lemma 2.1, the x component of the relative distances T_i and S_j, i.e. the RVs $T_{i,x}$ and $S_{j,x}$, are normally distributed with variance σ_i^2 and σ_j^2, respectively. Under the assumption of independence of the x and y distance components between the source/target WNEs and their associated WNEs, it can be proved that the RVs $R_{s,x}$ and $R_{t,x}$ are normally distributed with variance σ_s^2 and σ_t^2, respectively.

On the other hand, the RVs $T_{i,x}$, $S_{j,x}$, $R_{s,x}$ and $R_{t,x}$ are mutually independent. The independence follows by construction, since i) all tier-m clusters are i.i.d. and independent of the parent tier-*(m-1)* PP Φ_{m-1}, and ii) the locations of the two peers are mutually independent and independent from the locations of other WNEs. Now, since the RV Q_x is composed by a fixed sum and a sum of mutually independent and normally distributed RVs (2.20), it can be proved that it is normally distributed with mean $\eta_x = \left(D + \sum_{j\in\mathcal{L}_s} S_j \cos\phi_j - \sum_{i\in\mathcal{L}_t} T_i \cos\theta_i\right)$ and variance $\sigma^2 = \left(\sum_{j\in\bar{\mathcal{L}}_s} \sigma_j^2 + \sigma_s^2 + \sum_{i\in\bar{\mathcal{L}}_t} \sigma_i^2 + \sigma_t^2\right)$, i.e. $Q_x \sim \mathcal{N}(\eta_x, \sigma^2)$.

By following a similar approach, it can be shown that Q_y is normally distributed with mean $\eta_y = \left(\sum_{i\in\mathcal{L}_t} T_i \sin\theta_i - \sum_{j\in\mathcal{L}_s} S_j \sin\phi_j\right)$ and variance σ^2. Furthermore, Q_y and Q_x are independent, since all RVs that constitute Q_y (y-axis components) are independent of the ones that constitute Q_x (x-axis components). The independence follows by Lemma 2.1 and by using the facts that i) the x and y components of the relative distance between the source/target peers and their associated WNEs are independent, ii) all tier-m clusters are i.i.d. and independent of the parent tier-*(m-1)* PP Φ_{m-1} , and iii) the locations of the two peers are mutually independent and independent of the locations of other WNEs. Since the RVs $Q_x \sim \mathcal{N}(\eta_x, \sigma^2)$ and $Q_y \sim \mathcal{N}(\eta_y, \sigma^2)$ are independent, their joint distribution is given by

$$f_{Q_x,Q_y}(x,y) = \frac{1}{2\pi\sigma^2} e^{-\frac{(x-\eta_x)^2+(y-\eta_y)^2}{2\sigma^2}}. \qquad (2.22)$$

Now, let ΔA_z denote the region of the plane such that $z < \sqrt{x^2+y^2} < z + \mathrm{d}z$. Then, the region ΔA_z is a circular ring with inner radius z and thickness $\mathrm{d}z$ [124]. By working in polar coordinates, i.e. $x = z\cos\xi$, $y = z\sin\xi$, and $\mathrm{d}x\mathrm{d}y = z\mathrm{d}z\mathrm{d}\xi$, we get

$$f_{Z|D}(z)\mathrm{d}z = \int_{\Delta A_z} f_{Q_x,Q_y}(x,y)\mathrm{d}x\mathrm{d}y \qquad (2.23)$$

$$= \frac{1}{2\pi\sigma^2}\int_0^{2\pi} e^{-\frac{(z\cos\xi-\eta_x)^2+(z\sin\xi-\eta_y)^2}{2\sigma^2}} z\mathrm{d}z\mathrm{d}\xi. \qquad (2.24)$$

By eliminating $\mathrm{d}z$ from both sides in (2.24) and solving the integral, we finally reach to (2.3). We now derive the conditional ccdf $\bar{F}_{Z|D}(z)$ as follows:

$$\bar{F}_{Z|D}(z) = \int_z^\infty f_{Z|D}(x)\mathrm{d}x \qquad (2.25)$$

$$= \int_z^\infty \frac{x}{\sigma^2} e^{-\frac{\eta_x^2+\eta_y^2+x^2}{2\sigma^2}} I_0\left[\frac{x\sqrt{\eta_x^2+\eta_y^2}}{\sigma^2}\right]\mathrm{d}x \qquad (2.26)$$

$$= \int_{\frac{z}{\sigma}}^\infty q e^{-\frac{q^2+\left(\frac{\sqrt{\eta_x^2+\eta_y^2}}{\sigma}\right)^2}{2}} I_0\left[q\frac{\sqrt{\eta_x^2+\eta_y^2}}{\sigma}\right]\mathrm{d}q \qquad (2.27)$$

$$= Q_1\left[\frac{\sqrt{\eta_x^2+\eta_y^2}}{\sigma}, \frac{z}{\sigma}\right], \qquad (2.28)$$

where $Q_M[a,b]$ is the Marcum-Q function [149], (2.26) is derived by substituting (2.3), (2.27) by employing a change of variables $q = \frac{x}{\sigma}$, and (2.28) by the definition of the

Marcum-Q function, i.e. $Q_M[a,b]=\int_b^\infty x\left(\frac{x}{a}\right)^{M-1}e^{-\frac{x^2+a^2}{2}}I_{M-1}[ax]\mathrm{d}x$, where $I_{M-1}[x]$ is the modified Bessel function of the first kind and $(M-1)$-th order. Using a similar methodology, it can be shown that (2.3) (2.28) also apply when the LIS has additional knowledge of the relative polar coordinates of the source peer and/or the target peer. However, the parameters η_x, η_y, and σ^2 should be replaced as follows. If the relative polar coordinates (R_s,ξ_s) of the source peer are available, then

$$\eta_x=D+\sum_{j\in\mathcal{L}_s}S_j\cos\phi_j+R_s\cos\xi_s-\sum_{i\in\mathcal{L}_t}T_i\cos\theta_i, \quad (2.29)$$

$$\eta_y=\sum_{i\in\mathcal{L}_t}T_i\sin\theta_i-\sum_{j\in\mathcal{L}_s}S_j\sin\phi_j-R_s\sin\xi_s, \quad (2.30)$$

$$\sigma^2=\sum_{j\in\bar{\mathcal{L}}_s}\sigma_j^2+\sum_{i\in\bar{\mathcal{L}}_t}\sigma_i^2+\sigma_t^2. \quad (2.31)$$

If the relative polar coordinates (R_t,ξ_t) of the target peer are available, then

$$\eta_x=D+\sum_{j\in\mathcal{L}_s}S_j\cos\phi_j-\sum_{i\in\mathcal{L}_t}T_i\cos\theta_i-R_t\cos\xi_t, \quad (2.32)$$

$$\eta_y=\sum_{i\in\mathcal{L}_t}T_i\sin\theta_i+R_t\sin\xi_t-\sum_{j\in\mathcal{L}_s}S_j\sin\phi_j, \quad (2.33)$$

$$\sigma^2=\sum_{j\in\bar{\mathcal{L}}_s}\sigma_j^2+\sigma_s^2+\sum_{i\in\bar{\mathcal{L}}_t}\sigma_i^2. \quad (2.34)$$

If the relative polar coordinates of both the source and the target peers are available,

$$\eta_x=D+\sum_{j\in\mathcal{L}_s}S_j\cos\phi_j+R_s\cos\xi_s-\sum_{i\in\mathcal{L}_t}T_i\cos\theta_i-R_t\cos\xi_t, \quad (2.35)$$

$$\eta_y=\sum_{i\in\mathcal{L}_t}T_i\sin\theta_i+R_t\sin\xi_t-\sum_{j\in\mathcal{L}_s}S_j\sin\phi_j-R_s\sin\xi_s, \quad (2.36)$$

$$\sigma^2=\sum_{j\in\bar{\mathcal{L}}_s}\sigma_j^2+\sum_{i\in\bar{\mathcal{L}}_\mathrm{t}}\sigma_i^2. \quad (2.37)$$

I.B Proof of Theorem 2.2

Provided that $\mathcal{L}_s=\emptyset$ and $\mathcal{L}_t=\emptyset$, the parameters in (2.4)-(2.6) are given by $\eta_x=D$, $\eta_y=0$, and

$$\sigma=\sum_{j=1}^{m_s}\sigma_j^2+\sigma_s^2+\sum_{i=1}^{m_t}\sigma_i^2+\sigma_t^2. \quad (2.38)$$

Under this viewpoint, the conditional pdf $f_{Z|k}(z)$ is derived as follows (Remark 2.1).

$$f_{Z|k}(z)=\int_0^\infty P[Z|D=x]P[D=x|k]\mathrm{d}x \quad (2.39)$$

$$=\int_0^\infty\frac{z}{\sigma^2}e^{-\frac{x^2+z^2}{2\sigma^2}}I_0\left[\frac{zx}{\sigma^2}\right]\frac{2(\pi\lambda_B)^k}{\Gamma[k]}x^{2k-1}e^{-\pi\lambda_Bx^2}\mathrm{d}x \quad (2.40)$$

$$=\frac{2(\pi\lambda_B)^k}{\sigma^2\Gamma[n]}ze^{-\frac{z^2}{2\sigma^2}}\int_0^\infty x^{2n-1}e^{-\frac{(2\pi\lambda\sigma^2+1)x^2}{2\sigma^2}}I_0\left[\frac{zx}{\sigma^2}\right]\mathrm{d}x \quad (2.41)$$

$$=\frac{1}{\sigma^2}\left(\frac{2\pi\lambda\sigma^2}{2\pi\lambda\sigma^2+1}\right)^kze^{-\frac{\pi\lambda z^2}{2\pi\lambda\sigma^2+1}}L_{k-1}\left[-\frac{z^2}{2\sigma^2(2\pi\lambda\sigma^2+1)}\right] \quad (2.42)$$

where $L_n[z]$ is the Laguerre polynomial, (2.40) is derived by substituting (2.1) and (2.3), (2.41) by rearranging (2.40), and (2.42) by solving the integral using [[150],pp.303] and

elaborating with the result. We now turn our attention to the derivation of the respective ccdf $\bar{F}_{Z|k}(z)$.

$$\bar{F}_{Z|k}(z) = \int_{y=0}^{\infty} f_{D|k}(y)\bar{F}_{Z|D=y}(x)\mathrm{d}y \tag{43}$$

$$= \int_{y=0}^{\infty} \left(\frac{2(\pi\lambda)^k}{\Gamma[k]} y^{2k-1} e^{-\pi\lambda y^2}\right)\left(Q_1\left[\frac{y}{\sigma},\frac{z}{\sigma}\right]\right)\mathrm{d}y \tag{44}$$

$$= \frac{e^{-\frac{\pi\lambda z^2}{2\pi\lambda\sigma^2+1}}}{2\pi\lambda\sigma^2+1} \sum_{n=0}^{k-1} \varepsilon_n \left(\frac{2\pi\lambda\sigma^2}{2\pi\lambda\sigma^2+1}\right)^n L_n\left[-\frac{z^2}{2\sigma^2(2\pi\lambda\sigma^2+1)}\right], \tag{45}$$

where (2.43) follows from the law of total probability, (2.44) by substituting (2.28) and (2.1), and (2.45) by solving the integral using [149] for $\varepsilon_n = 1, \forall n < k-1$ and $\varepsilon_{k-1} = 2\pi\lambda\sigma^2 + 1$. The expressions in (2.10) and (2.11) are derived by plugging $\varepsilon_{k-1} = 2\pi\lambda\sigma^2 + 1$ in (2.42) and (2.45), respectively.

I.C Proof of Theorem 2.3

From Corollary 2.1, the distance Z is given by

$$z = g(D_n) \triangleq \sqrt{(D + Z_x)^2 + Z_y^2}, \tag{2.46}$$

where the parameters Z_x and Z_y are fixed and equal to (2.8) and (2.9), respectively. By taking a closer look to (2.46) it follows that the distance Z is always greater or equal to $|Z_y|$. Thus, $f_{Z|k,full} = 0$ for $Z < |Z_y|$. On the other hand, for $Z \geq |Z_y|$, the distance Z is a function of a single RV (the distance D) with known probability distribution (2.1). Therefore, for $z \geq |Z_y|$ the conditional pdf $f_{Z|k,full}$ can be derived as follows [[124], pp. 93]:

$$f_{Z|k,full}(z) = \frac{f_D(d_1)}{|g\prime(d_2)|} + \frac{f_D(d_2)}{|g\prime(d_2)|}, \tag{2.47}$$

where $d_1 = -Z_x - \sqrt{z^2 - Z_y^2}$ and $d_2 = -Z_x + \sqrt{z^2 - Z_y^2}$ are the real roots of (2.46), and $g'(d)$ is the derivative of $g(d)$ in (2.46). Substituting $g'(d) = \frac{d+Z_x}{z}$ in (2.47), yields (2.12). Note that the unit step function $U[x]$ is used to ensure that the distance D is strictly positive. The ccdf $\bar{F}_{Z|k,full}(z)$ for $z \geq Z_y$ is derived by substituting d_1 and d_2 in (2.12), and integrating with respect to z:

$$\bar{F}_{Z|k,full}(z) = \int_z^{\infty} \frac{2(\pi\lambda)^k}{\Gamma[k]} \frac{x}{\sqrt{x^2-Z_y^2}} \frac{\left(-Z_x-\sqrt{x^2-Z_y^2}\right)^{2k-1} U\left[\left(-Z_x-\sqrt{x^2-Z_y^2}\right)\right]}{e^{\pi\lambda\left(-Z_x-\sqrt{x^2-Z_y^2}\right)^2}}\mathrm{d}x$$
$$+ \int_z^{\infty} \frac{2(\pi\lambda)^n}{\Gamma[n]} \frac{y}{\sqrt{y^2-Z_y^2}} \frac{\left(-Z_x+\sqrt{y^2-Z_y^2}\right)^{2k-1} U\left[\left(-Z_x+\sqrt{y^2-Z_y^2}\right)\right]}{e^{\pi\lambda\left(-Z_x+\sqrt{y^2-Z_y^2}\right)^2}}\mathrm{d}y \tag{2.48}$$

$$= -\int_{-\infty}^{-Z_x-\sqrt{z^2-Z_y^2}} \frac{2(\pi\lambda)^k}{\Gamma[k]} \frac{v^{2k-1}U[v]}{e^{\pi\lambda v^2}}\mathrm{d}v + \int_{-Z_x+\sqrt{z^2-Z_y^2}}^{\infty} \frac{2(\pi\lambda)^k}{\Gamma[k]} \frac{g^{2k-1}U[g]}{e^{\pi\lambda g^2}}\mathrm{d}g, \tag{2.49}$$

where in (2.49) we have employed the change of variables $v = -Z_x - \sqrt{x^2 - Z_y^2}$ and $g = -Z_x + \sqrt{y^2 - Z_y^2}$. The ccdf in (2.13) is derived by solving the integrals in (2.49) and substituting $d_1 = -Z_x - \sqrt{z^2 - Z_y^2}$ and $d_2 = -Z_x + \sqrt{z^2 - Z_y^2}$.

I.D Proof of Theorem 4

By combining Lemma 2.3 and Theorem 2.1, it can be shown that the peer discovery probability $\mathcal{A}_D$ is given by $\mathcal{A}_D = 1 - Q_1\left[\frac{\sqrt{\eta_x^2+\eta_y^2}}{\sigma}, \frac{1}{\sigma}\left(\frac{c}{Z_{th}}\right)^{\frac{1}{a}}\right]$. Let us now define the ratio $\zeta = \sqrt{\eta_x^2+\eta_y^2}\left(\frac{c}{Z_{th}}\right)^{-\frac{1}{a}}$, which corresponds to the ratio of the arguments in the Marcum-Q function. By using the transform in [[151], (4.16)] for $\zeta < 1$, we re-write the probability $\mathcal{A}_D$ as follows:

$$\mathcal{A}_D = 1 - \frac{1}{2\pi}\int_{-\pi}^{\pi} \frac{(1+\zeta\sin\theta)e^{-\frac{\left(\frac{c}{Z_{th}}\right)^{\frac{2}{a}}}{2\sigma^2}(1+2\zeta\sin\theta+\zeta^2)}}{1+2\zeta\sin\theta+\zeta^2}\mathrm{d}\theta. \quad (2.50)$$

By plugging $\sigma^2 = \sigma_n^2 + \sigma_o^2$ in (2.50) and differentiating with respect to σ_o^2, we get:

$$\frac{\partial\mathcal{A}_D}{\partial\sigma_o^2} = -\frac{\left(\frac{c}{Z_{th}}\right)^{\frac{2}{a}}}{4\pi(\sigma_n^2+\sigma_o^2)^2}\int_{-\pi}^{\pi}(1+\zeta\sin\theta)e^{-\frac{\left(\frac{c}{Z_{th}}\right)^{\frac{2}{a}}}{2(\sigma_n^2+\sigma_o^2)}(1+2\zeta\sin\theta+\zeta^2)}\mathrm{d}\theta \quad (2.51)$$

$$= \frac{\left(\frac{c}{Z_{th}}\right)^{\frac{2}{a}}}{2(\sigma_n^2+\sigma_o^2)^2}e^{-\frac{\left(\frac{c}{Z_{th}}\right)^{\frac{2}{a}}}{2(\sigma_n^2+\sigma_o^2)}(1+z^2)}\left(\zeta I_1\left[\frac{\zeta\left(\frac{c}{Z_{th}}\right)^{\frac{2}{a}}}{\sigma_n^2+\sigma_o^2}\right] - I_0\left[\frac{\zeta\left(\frac{c}{Z_{th}}\right)^{\frac{2}{a}}}{\sigma_n^2+\sigma_o^2}\right]\right). \quad (2.52)$$

Since all parameters in (2.52) are positive real and by definition $I_0[x] > I_1[x]\ \forall x > 0$, the sign of (2.52) for $\zeta < 1$ is always negative. Therefore, the peer discovery probability $\mathcal{A}_D$ decreases with σ_o^2 when $\zeta < 1$. We now examine the monotonicity of $\mathcal{A}_D$ when $\zeta > 1$. For notational convenience, we use the parameter $q = \frac{1}{\zeta}$. By using the transform in [[151], (4.19)], the probability $\mathcal{A}_D$ can be re-written as follows:

$$\mathcal{A}_D = -\frac{1}{2\pi}\int_{-\pi}^{\pi} \frac{(q^2+q\sin\theta)e^{-\frac{\eta_x^2+\eta_y^2}{2(\sigma_n^2+\sigma_o^2)}(1+2q\sin\theta+q^2)}}{1+2q\sin\theta+q^2}\mathrm{d}\theta. \quad (2.53)$$

By following a similar methodology with the one used for (2.53), we reach to

$$\frac{\partial\mathcal{A}_D}{\partial\sigma_o^2} = \frac{q(\eta_x^2+\eta_y^2)}{2(\sigma_n^2+\sigma_o^2)^2}e^{-\frac{(1+q^2)(\eta_x^2+\eta_y^2)}{2(\sigma_n^2+\sigma_o^2)}}\left(I_1\left[\frac{q(\eta_x^2+\eta_y^2)}{\sigma_n^2+\sigma_o^2}\right] - qI_0\left[\frac{q(\eta_x^2+\eta_y^2)}{\sigma_n^2+\sigma_o^2}\right]\right). \quad (2.54)$$

Since all parameters in (2.54) are positive real, $I_0[x] > I_1[x]\ \forall x > 0$, and $q = \frac{1}{\zeta} < 1$, there exists an optimal variance parameter σ_o^{2*} for which the weighted difference of the

Bessel functions is equal to zero. The optimal σ_o^{2*} satisfies $\frac{\partial \mathcal{A}_D}{\partial \sigma_o^{2*}} = 0$, which is equivalent to (2.14). By employing the approximations $I_0[x] = \frac{e^x}{\sqrt{2\pi x}}\left(1 + \frac{1}{8x}\right)$ and $I_1[x] = \frac{e^x}{\sqrt{2\pi x}}\left(1 - \frac{3}{8x}\right)$ [152] in (2.14), we reach to (2.15).

APPENDIX II

II.A Proof of Theorem 3.1

Since the user and BS point processes are stationary and isotropic, we work in the Cartesian plane xy centered at the position of the associated BS of the D2D source and having as a positive x-axis the direction from the associated BS of the D2D source to the associated BS of the D2D target (Figure 17). Let X_s and X_t be the projections of the distances R_s and R_t on the x-axis, respectively, and Y_s and Y_t the respective projections in the y-axis. Note that $[X_s, Y_s]$ are the Cartesian coordinates of the D2D source in the xy plane, whereas the respective ones for the D2D target are $[D_k + X_t, Y_t]$. From Fig. 1, it follows that the distance Z between the D2D source and the D2D target is given by

$$Z = \sqrt{(D_k + X_t - X_s)^2 + (Y_t - Y_s)^2}. \quad (3.23)$$

We now define the auxiliary RVs: $Q_x = D + X_t - X_s$ and $Q_y = Y_t - Y_s$. The proof is based on the fact that the RVs Q_x and Q_y are independent normal RVs with different mean yet equal variance. To prove this, we will show that a) the RVs X_s and Y_s are independent normal RVs with zero mean and equal variance $b^2 = \frac{1}{2\pi\lambda_B}$, b) the RVs X_t and Y_t are independent normal RVs with zero mean and equal variance b^2, and c) the RVs X_s, Y_s, X_t, and Y_t, are mutually independent. Since the distance R_s between the D2D source and its associated BS is Rayleigh distributed with parameter b^2 (Lemma 3.1) and the angle θ_s is uniform in $(-\pi, \pi]$ and independent of the distance R_s (Assumption 3.1), by using a similar approach with the one in [[124], pp.146] it can be proved that the RVs $X_s = R_s\cos\theta_s$ and $Y_s = R_s\sin\theta_s$ are independent normal RVs with zero mean and equal variance: $X_s, Y_s \sim \mathcal{N}\left(0, \frac{1}{2\pi\lambda_B}\right)$. The same arguments can be used to show that the RVs $X_t = R_t\cos\theta_t$ and $Y_t = R_t\sin\theta_t$ are independent normal RVs with zero mean and equal variance b^2 as well.

Now, since the coordinates of the D2D source do not depend on the ones of the D2D target (Section II), it readily follows that Q_x equals to the difference of two independent normal RVs plus a fixed value $D_k = D$. Thus, Q_x is normally distributed with mean D and variance $2b^2 = \frac{1}{\pi\lambda_B}$: $Q_x \sim \mathcal{N}(D, \frac{1}{\pi\lambda_B})$. By following a similar approach, it can be shown that Q_y is a normal RV with zero mean and variance $2b^2$: $Q_y \sim \mathcal{N}(0, \frac{1}{\pi\lambda_B})$. In addition, Q_y is independent of Q_x, since the RV X_t, X_s, Y_t, and Y_s are shown to be mutually independent. As a consequence, the joint distribution of Q_x and Q_y is given by

$$f_{Q_x,Q_y}(x, y) = \frac{\lambda_B}{2} e^{-\frac{\pi\lambda_B}{2}\left((x-D)^2 + y^2\right)}. \quad (3.24)$$

Now, let ΔA_z denote the region of the plane such that $z < \sqrt{x^2 + y^2} < z + \mathrm{d}z$. Then, the region ΔA_z is a circular ring with inner radius z and thickness $\mathrm{d}z$. By working in polar coordinates, i.e. $x = z\cos\xi$, $y = z\sin\xi$, and $\mathrm{d}x\mathrm{d}y = z\mathrm{d}z\mathrm{d}\xi$, we get

$$f_{Z|D_k}(z)\mathrm{d}z = \int_{\Delta A_z} f_{Q_x,Q_y}(x, y)\mathrm{d}x\mathrm{d}y \quad (3.25)$$

$$= \frac{\lambda_B}{2}\int_0^{2\pi} e^{-\frac{\pi\lambda_B}{2}\left(z\cos\xi - D)^2 + (z\sin\xi)^2\right)} z\mathrm{d}z\mathrm{d}\xi. \quad (3.26)$$

Therefore,

$$f_{Z|D_k}(z) = \frac{\lambda_B z}{2} e^{-\frac{\pi\lambda_B}{2}\left(z^2 + D^2\right)} \int_0^{2\pi} e^{\pi\lambda_B z D\cos\xi}\mathrm{d}\xi \quad (3.27)$$

$$= \pi\lambda_B z e^{-\frac{\pi\lambda_B}{2}\left(z^2 + D^2\right)} I_0[\pi\lambda_B z D], \quad (3.28)$$

where (3.28) follows from the integral representation of the modified Bessel function of the first and zero-th order: $I_0[x] = \frac{1}{2\pi}\int_0^{2\pi} e^{x\cos\xi}\mathrm{d}\xi$. Having derived the conditional pdf $f_{Z|D_k}(z)$, we proceed with the derivation of the conditional ccdf $\bar{F}_{Z|D_k}(z)$ as follows:

$$\bar{F}_{Z|D_k}(z) = \int_z^{\infty} f_{Z|D_k}(x)\mathrm{d}x \quad (3.29)$$

$$= \int_z^{\infty} \pi\lambda_B x e^{-\frac{\pi\lambda_B}{2}(x^2+D^2)} I_0[\pi\lambda_B xD]\mathrm{d}x \quad (3.30)$$

$$= \int_{\sqrt{\pi\lambda_B}z}^{\infty} q e^{-\frac{q^2+\left(\sqrt{\pi\lambda_B}D\right)^2}{2}} I_0\left[q\left(\sqrt{\pi\lambda_B}D\right)\right]\mathrm{d}q \quad (3.31)$$

$$= Q_1\left[\sqrt{\pi\lambda_B}D, \sqrt{\pi\lambda_B}z\right], \quad (3.32)$$

where $Q_M[a,b] = \int_b^{\infty} x\left(\frac{x}{a}\right)^{M-1} e^{-\frac{x^2+a^2}{2}} I_{M-1}[ax]\mathrm{d}x$ is the Marcum-Q function, $I_{M-1}[x]$ the modified Bessel function of the first kind and $(M-1)$-th order, (3.30) is derived by substituting (3.28), (3.31) by employing a change of variables $q = \frac{x}{\sqrt{\pi\lambda_B}}$, and (3.32) by the definition of the Marcum-Q function.

II.B Proof of Theorem 3.2

Since the user and BS PP are stationary and isotropic (Section II), we work in the Cartesian plane $x'y'$ centered at the position of the associated BS of the D2D source and having as a positive x-axis the direction from the associated BS of the D2D source to the D2D target (Figure 17). Let (X'_s, Y'_s) be the Cartesian coordinates of the D2D source in the $x'y'$ plane. Given that the distance R_s between the user and its associated BS is Rayleigh distributed (Lemma 3.1) and Assumption 1 holds, the RVs X'_s and Y'_s are independent normal RVs with zero mean and equal variance $b^2 = \frac{1}{2\pi\lambda_B}$ [[124], pp. 146]: $X'_s, Y'_s \sim \mathcal{N}(0, b^2)$. From Fig. 1, the distance Z between the D2D source and the D2D target is given by $Z = \sqrt{(T_{k+1} - X'_s)^2 + {Y'_s}^2}$, where T_{k+1} is the distance between the D2D target and the associated BS of the D2D source. Since the parameters $D_k = D$, $R_t = T$ and $\theta_t = \rho$ are fixed, the distance T_{k+1} is a fixed parameter that can be readily estimated by using the law of cosines in the triangle $|R_t||D_k||T_{k+1}|$

$$T_{k+1} = \sqrt{D^2 + T^2 - 2DT\cos(\pi - \rho)}. \quad (3.33)$$

Let us now define the auxiliary RV $Q_x = T_{k+1} - X'_s$. Since T_{k+1} is fixed and $X'_s \sim \mathcal{N}(0, b^2)$ is normally distributed with zero mean and variance b^2, the RV Q_x is normally distributed with mean T_{k+1} and variance b^2. Moreover, given that X'_s is independent of Y'_s, it follows that Q_x is independent of Y'_s as well. Therefore, the joint distribution of Q_x and Y'_s is given by

$$f_{Q_x,Y'_s}(x,y) = \frac{1}{2\pi b^2} e^{-\frac{(x-T_{k+1})^2+y^2}{2b^2}}. \quad (3.34)$$

Now, provided that $Z = \sqrt{Q_x^2 + {Y'_s}^2}$, where the RVs $Y'_s \sim \mathcal{N}(0, b^2)$ and $Q_x \sim \mathcal{N}(T_{k+1}, b^2)$ are independent, it can be proved that the conditional pdf $f_{Z|D_k,R_t,\theta_t}(z)$ is given by

$$f_{Z|D_k,R_t,\theta_t}(z) = \frac{ze^{-\frac{z^2+T_{k+1}^2}{2b^2}}}{b^2} I_0\left[\frac{zT_{k+1}}{b^2}\right]. \quad (3.35)$$

The respective proof is similar to the one presented in Theorem 3.1 ((3.25) - (3.28). Accordingly, the conditional ccdf $\bar{F}_{Z|D_k,R_t,\theta_t}(z)$ is derived as follows:

$$\bar{F}_{Z|D_k,R_t,\theta_t}(z) = \int_z^{\infty} f_{z|D_k,R_t,\theta_t}(x)\mathrm{d}x \quad (3.36)$$

$$= \int_z^{\infty} \frac{xe^{-\frac{x^2+T_{k+1}^2}{2b^2}}}{b^2} I_0\left[\frac{xT_{k+1}}{\mathrm{b}^2}\right]\mathrm{d}x \quad (3.37)$$

$$= Q_1\left[\frac{T_{k+1}}{b}, \frac{z}{b}\right], \quad (3.38)$$

where (3.37) is derived by substituting (3.35), and (3.38) by employing the change of variables $q = \frac{x}{b}$ and the definition of Marcum-Q. The proof is completed by substituting (3.33) and $b = \frac{1}{\sqrt{2\pi\lambda_B}}$, in (3.35) and (3.38).

II.C Proof of Theorem 3.3

The conditional pdf $f_{Z|k}(z)$ and ccdf $\bar{F}_{Z|k}(z)$ can be derived by integrating the results in Theorem 3.1 with respect to the distance D_k given that the neighboring degree equals to $k = n$.

$$f_{Z|k}(z) = \int_0^{\infty} P[Z|D_k = x]P[D_k = x|k = n]\mathrm{d}x \quad (3.39)$$

$$= \int_0^{\infty} \pi\lambda_B z e^{-\frac{\pi\lambda_B}{2}(z^2+x^2)} I_0[\pi\lambda_B xz] \frac{2(\pi\lambda_B)^n}{\Gamma[n]} x^{2n-1} e^{-\pi\lambda_B x^2}\mathrm{d}x \quad (3.40)$$

$$= \frac{2(\pi\lambda_B)^{n+1}}{\Gamma[n]} z e^{-\frac{\pi\lambda_B z^2}{2}} \int_0^{\infty} x^{2n-1} e^{-\frac{3\pi\lambda_B x^2}{2}} I_0[\pi\lambda_B zx]\mathrm{d}x \quad (3.41)$$

$$= \pi\lambda_B \left(\frac{2}{3}\right)^n z e^{-\frac{\pi\lambda_B z^2}{2}} {}_1F_1\left[n, 1, \frac{\pi\lambda_B z^2}{6}\right], \quad (3.42)$$

where ${}_1F_1[n, 1, x]$ is the confluent Hypergeometric Function. (3.40) is derived by substituting (3.2) and (3.4), (3.41) by rearranging (3.40), and (3.42) by solving the integral [[150], pp.303]. By using the functional identities ${}_1F_1[n, 1, x] = e_1^x F_1[1 - n, 1, -x]$ and $L_n[x] =_1 F_1[-n, 1, x]$, where $L_n[z] = \sum_{m=0}^{n} {n \choose m} \frac{(-1)^m}{m!} x^m$ is the Laguerre polynomial, we reach to the pdf expression in (3.10). The conditional ccdf $\bar{F}_{Z|k}(z)$ is derived as

$$\bar{F}_{Z|k}(z) = \int_z^{\infty} f_{Z|k}(x)\mathrm{d}x \quad (3.43)$$

$$= \int_{x=z}^{\infty} \int_{y=0}^{\infty} f_{Z|D_k=y,k=n}(x) f_{D_k|k=n}(y)\mathrm{d}y\mathrm{d}x \quad (3.44)$$

$$= \int_{y=0}^{\infty} f_{D_k|k=n}(y) \int_{x=z}^{\infty} f_{Z|D_k=y}(x)\mathrm{d}x\mathrm{d}y \quad (3.45)$$

$$= \int_{y=0}^{\infty} \left(\frac{2(\pi\lambda_B)^n}{\Gamma[n]} y^{2n-1} e^{-\pi\lambda_B y^2}\right)\left(Q_1\left[\frac{y}{b}, \frac{z}{b}\right]\right)\mathrm{d}y \quad (3.46)$$

$$= \frac{1}{3} e^{-\frac{\pi\lambda_B z^2}{3}} \sum_{m=0}^{n-1} \varepsilon_m \left(\frac{2}{3}\right)^m L_m\left[-\frac{\pi\lambda_B z^2}{6}\right], \quad (3.47)$$

where (3.44) follows from the law of total probability, (3.45) by rearranging (3.44), (3.46) by substituting (3.32) and (3.2), and (3.47) by solving the integral using the result in [149] for $\varepsilon_m = 1, \forall m < n - 1$ and $\varepsilon_{n-1} = 3$.

II.D Proof of Theorem 3.4

By using Proposition 3.1, the distance Z is given by

$$Z = g(D_n) \triangleq \sqrt{(D_n + Q_x)^2 + Q_y^2}, \qquad (3.48)$$

where the fixed parameters $Q_x \triangleq R_t\cos\rho - R_s\cos\varphi$ and $\mathrm{Q}_y \triangleq R_t\sin\rho - R_s\sin\varphi$. From (3.48) it follows that the distance Z is at least equal to $|Q_y|$ and thus, $f_{Z|k,R_t,\theta_t,R_s,\theta_s} = 0$ for $Z < |Q_y|$. On the other hand, the RV Z is a function of only the distance D_n ((3.48)). Since the pdf of the RV D_n is known ((2)), the conditional pdf $f_{Z|k,R_t,\theta_t,R_s,\theta_s}$ for $z \geq |Q_y|$ can be derived by using [[124], pp. 93]:

$$f_{Z|k,R_t,\theta_t,R_s,\theta_s}(z) = \frac{f_{D_n}(d_1)}{|g'(d_2)|} + \frac{f_{D_n}(d_2)}{|g'(d_2)|}, \qquad (3.49)$$

where $d_1 = -Q_x - \sqrt{Z^2 - Q_y^2}$ and $d_2 = -Q_x + \sqrt{Z^2 - Q_y^2}$ are the real roots of (3.48) and $g'(d) = \frac{d+Q_x}{\sqrt{(d+Q_x)^2+Q_y^2}} = \frac{d+Q_x}{z}$ is the derivative of $g(d)$ in ((3.48). By substituting d_1, d_2 and $g'(d)$, we obtain

$$f_{Z|k,R_t,\theta_t,R_s,\theta_s}(z) = \sum_{m=1}^{2} \frac{2(\pi\lambda_B)^n z}{\Gamma[n]} \frac{d_m^{2n-1} e^{-\pi\lambda_B d_m^2} U[d_m]}{|d_m + Q_x|} \qquad (3.50)$$

$$= \sum_{m=1}^{2} \frac{2(\pi\lambda_B)^n}{\Gamma[n]} \frac{z}{\sqrt{z^2-Q_y^2}} \frac{\left(-Q_x + q_m\sqrt{z^2-Q_y^2}\right)^{2n-1} U\left[\left(-Q_x + q_m\sqrt{z^2-Q_y^2}\right)\right]}{e^{\pi\lambda_B\left(-Q_x + q_m\sqrt{z^2-Q_y^2}\right)^2}}, \qquad (3.51)$$

where in (3.50) we use the unit step function $U[x]$ to model the fact that the distance D_k can only take positive values while, for notational convenience, in (3.51) we use the parameter q_m, which takes the values $q_1 = 1$ and $q_2 = -1$. The ccdf $\bar{F}_{Z|k,R_t,\theta_t,R_s,\theta_s}(z)$ is defined only for $z \geq Q_y$ and is derived as

$$\bar{F}_{Z|k,R_t,\theta_t,R_s,\theta_s}(z) = \int_z^\infty f_{Z|k,R_t,\theta_t,R_s,\theta_s}(x)\mathrm{d}x \qquad (3.52)$$

$$= \int_z^\infty \frac{2(\pi\lambda_B)^n}{\Gamma[n]} \frac{x}{\sqrt{x^2-Q_y^2}} \frac{\left(-Q_x - \sqrt{x^2-Q_y^2}\right)^{2n-1} U\left[\left(-Q_x - \sqrt{x^2-Q_y^2}\right)\right]}{e^{\pi\lambda_B\left(-Q_x - \sqrt{x^2-Q_y^2}\right)^2}} \mathrm{d}x$$

$$+ \int_z^\infty \frac{2(\pi\lambda_B)^n}{\Gamma[n]} \frac{y}{\sqrt{y^2-Q_y^2}} \frac{\left(-Q_x + \sqrt{y^2-Q_y^2}\right)^{2n-1} U\left[\left(-Q_x + \sqrt{y^2-Q_y^2}\right)\right]}{e^{\pi\lambda_B\left(-Q_x + \sqrt{y^2-Q_y^2}\right)^2}} \mathrm{d}y \qquad (3.53)$$

$$= -\int_{-\infty}^{-Q_x - \sqrt{z^2-Q_y^2}} \frac{2(\pi\lambda_B)^n}{\Gamma[n]} \frac{v^{2n-1} U[v]}{e^{\pi\lambda_B v^2}} \mathrm{d}v + \int_{-Q_x + \sqrt{z^2-Q_y^2}}^{\infty} \frac{2(\pi\lambda_B)^n}{\Gamma[n]} \frac{g^{2n-1} U[g]}{e^{\pi\lambda_B g^2}} \mathrm{d}g, \qquad (3.54)$$

where (3.53) is derived by using (3.51), and (3.54) by employing the change of variables $v = -Q_x - \sqrt{x^2 - Q_y^2}$ and $g = -Q_x + \sqrt{y^2 - Q_y^2}$ in the respective integrals. The proof is completed by solving the integrals and plugging $d_1 = -Q_x - \sqrt{z^2 - Q_y^2}$ and $d_2 = -Q_x + \sqrt{z^2 - Q_y^2}$ in the final result.

II.E Proof of Theorem 3.5

By using Theorem 3.1 and (3.1), it follows that $\mathcal{A}_{D_k}$ is given by $\mathcal{A}_{D_k} = 1 - Q_1\left[\sqrt{\pi\lambda_B}D, \sqrt{\pi\lambda_B}\left(\frac{P_t}{P_r}\right)^{\frac{1}{a}}\right]$. Observe now that the ratio of the arguments in the Marcum-Q function is equal to $q = D\left(\frac{P_t}{P_r}\right)^{-\frac{1}{a}}$. By using the transform for the Marcum-Q function given in [[151], (4.16)] for $q < 1$, the D2D discovery probability $\mathcal{A}_{D_k}$ can be rewritten as follows:

$$\mathcal{A}_{D_k} = 1 - \frac{1}{2\pi}\int_{-\pi}^{\pi} \frac{(1+q\sin\theta)e^{-\frac{\pi\lambda}{2}\left(\frac{P_t}{P_r}\right)^{\frac{2}{a}}(1+2q\sin\theta+q^2)}}{1+2q\sin\theta+q^2}\mathrm{d}\theta. \quad (3.55)$$

Now, by differentiating with respect to λ_B we get:

$$\frac{\partial\mathcal{A}_{D_k}}{\partial\lambda_B} = \frac{\left(\frac{P_t}{P_r}\right)^{\frac{2}{a}}}{4}\int_{-\pi}^{\pi}(1+q\sin\theta)e^{-\frac{\pi\lambda}{2}\left(\frac{P_t}{P_r}\right)^{\frac{2}{a}}(1+2q\sin\theta+q^2)}\mathrm{d}\theta \quad (3.56)$$

$$= \frac{\pi\left(\frac{P_t}{P_r}\right)^{\frac{2}{a}}}{2e^{\frac{\pi\lambda}{2}\left(\frac{P_t}{P_r}\right)^{\frac{2}{a}}(1+q^2)}}\left(I_0\left[\pi\lambda_B\left(\frac{P_t}{P_r}\right)^{\frac{2}{a}}q\right] - qI_1\left[\pi\lambda_B\left(\frac{P_t}{P_r}\right)^{\frac{2}{a}}q\right]\right). \quad (3.57)$$

Since all parameters in Eq (3.57) are positive real numbers and by definition $I_0[x] > I_1[x]\ \forall x > 0$, for $q < 1$ the sign of Eq (3.57) is always positive. Hence, $\frac{\partial\mathcal{A}_{D_k}}{\partial\lambda_B} > 0$, which implies that for $q < 1$ the D2D discovery probability is monotonically increasing with respect to λ_B. Let us now examine the scenario where $q > 1$. By using [[151], (4.19)] for $\zeta = \frac{1}{q}$, we can rewrite $\mathcal{A}_{D_k}$ as follows:

$$\mathcal{A}_{D_k} = -\frac{1}{2\pi}\int_{-\pi}^{\pi} \frac{(\zeta^2+\zeta\sin\theta)e^{-\frac{\pi\lambda}{2}D^2(1+2\zeta\sin\theta+\zeta^2)}}{1+2\zeta\sin\theta+\zeta^2}\mathrm{d}\theta. \quad (3.58)$$

By differentiating with respect to λ_B we obtain

$$\frac{\partial\mathcal{A}_{D_k}}{\partial\lambda_B} = \frac{D^2}{4}\int_{-\pi}^{\pi}(\zeta^2+\zeta\sin\theta)e^{-\frac{\pi\lambda}{2}D^2(1+2\zeta\sin\theta+\zeta^2)}\mathrm{d}\theta \quad (3.59)$$

$$= \frac{\pi D^2}{2e^{\frac{\pi\lambda}{2}D^2(1+\zeta^2)}}(\zeta I_0[\pi\lambda_B D^2\zeta] - I_1[\pi\lambda_B D^2\zeta]). \quad (3.60)$$

Now, since all parameters in (3.60) are positive real numbers and the existence of an optimal point requires $\frac{\partial\mathcal{A}_{D_k}}{\partial\lambda_B} = 0$, from Eq (3.60) it readily follows that the optimal BS density λ_B^* satisfies

$$I_0\left[\frac{\pi\lambda_B^* D^2}{q}\right] - qI_1\left[\frac{\pi\lambda_B^* D^2}{q}\right] = 0. \quad (3.61)$$

If the (common) argument in the two modified Bessel functions in (3.61) is sufficiently large, typically higher than 2, then each Bessel function can be approximated as

$$I_0[x] = \frac{e^x}{\sqrt{2\pi x}}\left(1 + \frac{1}{8x}\left(1 + \frac{9}{2(8x)}(1+\cdots)\right)\right), \quad (3.62)$$

$$I_1[x] = \frac{e^x}{\sqrt{2\pi x}}\left(1 - \frac{3}{8x}\left(1 + \frac{5}{2(8x)}(1 + + \cdots)\right)\right). \quad (3.63)$$

Obviously, the more terms we use from (3.62) and (3.63), the more accurate the approximation. Assuming that $\frac{\pi\lambda_B^* D^2}{q}$ is sufficiently large, we use the first three terms of (3.62) and (3.63) to approximate the Bessel functions in (3.61). By substituting the approximations in (3.61) and elaborating with the result, we reach to the following quadric equation with respect to λ_B^*:

$$-128{\lambda_B^*}^2 D^4 \pi^2 (q-1) + 16\lambda_B^* D^2 \pi q(1+3q) + 3q^2(3+5q) = 0 \quad (3.64)$$

For $q > 1$ and $D > 0$, (3.64) has the unique solution given in (3.18).

REFERENCES

[1] H. S. Dhillon, R. K. Ganti, F. Baccelli, and J. G. Andrews, "Modeling and Analysis of -tier Downlink Heterogeneous Cellular Networks," IEEE J. Sel. Areas Commun., vol. 30, no. 3, pp. 550-560, Mar. 2012.

[2] IEEE Std 802.11-2012 (Revision of IEEE 802.11-2007), "Part 11: Wireless LAN Medium Access Control (MAC) and Physical Layer (PHY) Specifications", March 2012.

[3] IEEE Std 802.15.4 (Revision of IEEE Std 802.15.4-2006), "Part 15.4: Low-Rate Wireless Personal Area Networks (LR-WPANs)", June 2011.

[4] Y. Yan, Y. Qian, H. Sharif, and D. Tipper, "A Survey on Smart Grid Communication Infrastructures: Motivations, Requirements and Challenges", IEEE Comm. Surv. & Tut., vol. 15, no. 1, pp. 5-20, 1st Quarter 2013.

[5] X. Lin, J.G. Andrews, A. Ghosh, R. Ratasuk, "An overview of 3GPP device-to-device proximity services", IEEE Commun. Magazine, vol.52, no.4, pp.40-48, Apr. 2014.

[6] Y. Yan, Y. Mostofi, "Co-Optimization of Communication and Motion Planning of a Robotic Operation under Resource Constraints and in Fading Environments", IEEE Trans. on Wirel. Commun., vol.12, no.4, pp.1562-1572, April 2013.

[7] J. G. Andrews, S. Buzzi, W. Choi, S. Hanly, A. Lozano, A. Soong, J. C. Zhang, "What will 5G be?", invited paper, to appear, IEEE J. on Sel. Areas in Commun., July 2014.

[8] 3GPP, "Evolved Universal Terrestrial Radio Access (E-UTRA) and Evolved Universal Terrestrial Radio Access Network (E-UTRAN); Overall description", TS 36.300 V12.0.0, Jan. 2014.

[9] S. Parkvall, A. Furuskär, E. Dahlman, "Evolution of LTE toward IMT-advanced", IEEE Communications Magazine, vol.49, no.2, pp.84-91, Feb. 2011.

[10] A.Ghosh, R. Ratasuk, B. Mondal, N. Mangalvedhe, T. Thomas, "LTE-advanced: next-generation wireless broadband technology", IEEE Wireless Communications, vol.17, no.3, pp.10-22, June 2010.

[11] M. Iwamura, K. Etemad, Mo-Han Fong, R. Nory, R. Love, "Carrier aggregation framework in 3GPP LTE-advanced", IEEE Communications Magazine, vol.48, no.8, pp.60-67, Aug. 2010.

[12] Q. Li, G. Li, W. Lee, M. Lee, D. Mazzarese, B. Clerckx, Z. Li, "MIMO techniques in WiMAX and LTE: a feature overview", IEEE Communications Magazine, vol.48, no.5, pp.86-92, May 2010.

[13] K. Loa, C. Wu, S. Sheu, Y. Yuan, M. Chion, D. Huo, L. Xu, "IMT-advanced relay standards", IEEE Communications Magazine, vol.48, no.8, pp.40-48, Aug. 2010.

[14] G. Boudreau, J. Panicker, Ning Guo, Rui Chang, Neng Wang, S. Vrzic, "Interference coordination and cancellation for 4G networks", IEEE Comm., vol.47, no.4, pp.74-81, Apr. 2009.

[15] K. Zheng, B. Fan, J. Liu, Y. Lin, W. Wang, "Interference coordination for OFDM-based multihop LTE-advanced networks", IEEE Wireless Communications, vol.18, no.1, pp.54-63, Feb. 2011.

[16] 3GPP, "Physical layer - Measurements", TS 36.214 V11.1.0, Dec. 2012.

[17] W.Song, Jong-Moon Chung, Daeyoung Lee, Chaegwon Lim, Sungho Choi, Taesun Yeoum, "Improvements to seamless vertical handover between mobile WiMAX and 3GPP UTRAN through the evolved packet core," IEEE Comm. Mag., vol.47, no.4, pp.66-73, April, 2009.

[18] 3GPP, "Access to the 3GPP Evolved Packet Core (EPC) via non-3GPP access networks", TS 24.302 V10.4.0, June, 2011

[19] 3GPP, "Architecture enhancements for non-3GPP accesses", TS 24.402 V10.4.0, June, 2011

[20] 3GPP, "Access Network Discovery and Selection Function (ANDSF) Management Object (MO)", TS 24.312 V10.3.0, June, 2011.

[21] IEEE Std 802.11-2007 (Revision of IEEE Std 802.11-1999), "IEEE Standard for Information Technology-Telecommunications and Information Exchange Between Systems-Local and Metropolitan Area Networks-Specific Requirements - Part 11: Wireless LAN Medium Access Control (MAC) and Physical Layer (PHY) Specifications," June, 2007.

[22] IEEE Std 802.11k-2008, "IEEE Standard for Information Technology-Telecommunications and Information Exchange Between Systems-Local and Metropolitan Area Networks-Specific Requirements - Part 11: Wireless LAN Medium Access Control (MAC) and Physical Layer (PHY) Specifications, Amendment 1: Radio Resource measurement of Wireless LANs," June, 2008.

[23] J. G. Andrews, H. Claussen, M. Dohler, S. Rangan, M. C. Reed, "Femtocells: Past, Present, and Future", IEEE J. on Sel. Areas in Comm., vol.30, no.3, pp.497-508, Apr. 2012.

[24] T. Zahir, K.Arshad, A. Nakata, K. Moessner, "Interference Management in Femtocells", IEEE Comm. Surv. & Tut. vol., no.99, pp.1-19, 2012.

[25] N. Saquib, E. Hossain, L. B. Le, and D. I. Kim, "Interference management in OFDMA femtocell networks: Issues and approaches," IEEE Wirel. Comm., vol.19, no.3, pp.86-95, June 2012.

[26] 3GPP, “E-UTRA and E-UTRAN Overall Description”, TS 36.300 V10.7.0, Mar. 2012.

[27] 3GPP, “X2 general aspects and principles”, TS 36.420 V10.2.0, Sept. 2011.

[28] 3GPP, “X2 application protocol (X2AP)”, TS 36.423 V10.5.0, Mar. 2012.

[29] 3GPP, “S1 general aspects and principles”, TS 36.410 V10.2.0, Sept. 2011.

[30] 3GPP, “S1 application protocol (S1AP)”, TS 36.413 V10.5.0, Mar. 2012.
[31] H. Zhang, W. Zheng, X. Wen, C. Jiang, "Signalling Overhead Evaluation of HeNB Mobility Enhanced Schemes in 3GPP LTE-Advanced", 2011 IEEE 73rd Vehic. Techn. Conf. (VTC-Spring), pp.1-5, May 2011.
[32] 3GPP, “Radio Resource Control (RRC); Protocol specification”, TS 36.331 V10.5.0, Mar. 2012.
[33] A. Golaup, M. Mustapha, L.B. Patanapongpibul, "Femtocell access control strategy in UMTS and LTE", IEEE Comm., vol.47, no.9, pp.117-123, Sept. 2009.
[34] X. Zhang, D. Zhou, Z. Xiao, E. Liu, J. Zhang, A. A. Glasunov, "Dynamic Group PCI Assignment Scheme", The 7th Internat. Conf. on Wirel. and Mobile Comm., pp. 101-106, June 2011.
[35] Y. Liu, W. Li, H. Zhang, W. Lu, "Graph based automatic centralized PCI assignment in LTE", 2010 IEEE Symp. on Comp.s and Comm. (ISCC), vol., no., pp.919-921, June 2010.
[36] S. Kwon, N. Lee, "Virtual extension of cell IDs in a femtocell environment", 2011 IEEE Wirel. Comm. and Netw. Conf. (WCNC), vol., no., pp.428-433, Mar. 2011.
[37] Y. Liu, W. Li, H. Zhang, L. Yu, "Distributed PCI Assignment in LTE Based on Consultation Mechanism", 2010 6th Internat. Conf. on Wirel. Comm. Netw. and Mobile Comp. (WiCOM), vol., no., pp.1-4, 23-25 Sept. 2010.
[38] T. Wu, L. Rui, A. Xiong, S. Guo, "An Automation PCI Allocation Method for eNodeB and Home eNodeB Cell", 2010 6th Internat. Conf. on Wirel. Comm. Netw. and Mobile Comp. (WiCOM), vol., no., pp.1-4, 23-25 Sept. 2010.
[39] J. Lim, D. Hong, "Management of neighbor cell lists and physical cell identifiers in self-organizing heterogeneous networks", J. of Comm. and Networks, vol.13, no.4, pp.367-376, Aug. 2011.
[40] H. Kallin, J. Moe, "Method for automatically selecting a physical cell identity (PCI) of a long term evolution (LTE) radio cell", U.S. Patent, Pub. No. US 2010/0331025 A1, Dec. 2010.
[41] G. de la Roche, A. Valcarce, D. Lopez-Perez, Jie Zhang, "Access control mechanisms for femtocells", IEEE Comm., vol.48, no.1, pp.33-39, Jan. 2010.
[42] Y. Shen, T. Luo, M. Z. Win, "Neighboring Cell Search for LTE Systems", IEEE Trans. on Wirel. Comm., vol.11, no.3, pp.908-919, Mar. 2012.
[43] J. Lim, D. Hong, "Management of neighbor cell lists and physical cell identifiers in self-organizing heterogeneous networks", J. of Comm. and Nets., vol.13, no.4, pp.367-376, Aug. 2011.
[44] F. Meshkati, Y. Jiang, L. Grokop, S. Nagaraja, M. Yavuz, and S. Nanda, “Mobility and Femtocell Discovery in 3G UMTS Networks,” Qualcomm Whitepaper, Feb. 2010.
[45] F. Meshkati, Y. Jiang; L. Grokop, S. Nagaraja, M. Yavuz, and S. Nanda, "Mobility and Capacity Offload for 3G UMTS Femtocells", IEEE Global Telecom. Conf. (GLOBECOM) 2009, pp.1-7, Dec. 2009.
[46] H. Lee, Y. Lin, "A cache scheme for femtocell reselection", IEEE Comm. Letters, vol.14, no.1, pp.27-29, Jan. 2010
[47] L. Zhou, H. Xu, H. Tian, Y. Gao, L. Du, L. Chen, "Performance Analysis of Power Saving Mechanism with Adjustable DRX Cycles in 3GPP LTE", 2008 IEEE 68th Vehic. Techn. Conf. (VTC-Fall), vol., no., pp.1-5, Sept. 2008.
[48] C. Bontu, E. Illidge, "DRX mechanism for power saving in LTE", IEEE Comm., vol.47, no.6, pp.48-55, June 2009.
[49] J. Wigard, T. Kolding, L. Dalsgaard, C. Coletti, "On the User Performance of LTE UE Power Savings Schemes with Discontinuous Reception in LTE", 2009 IEEE Internat. Conf. on Comm. (ICC) Workshops, vol., no., pp.1-5, 14-18 June 2009.
[50] 3GPP, “Physical Channels and Modulation”, TS 36.211 V10.4.0, Dec. 2011.
[51] S. Sesia, I. Toufik, M. Baker, “LTE – The UMTS Long Term Evolution: From Theory to Practice”, John Wiley & Sons, ISBN: 978-0-470-69716-0, 2009.
[52] J. Moon, D. Cho, "Efficient handoff algorithm for inbound mobility in hierarchical macro/femto cell networks", IEEE Comm. Letters, vol.13, no.10, pp.755-757, Oct. 2009.
[53] J. Moon, D. Cho, "Novel Handoff Decision Algorithm in Hierarchical Macro/Femto-Cell Networks", IEEE Wirel. Comm. and Netw. Conf. (WCNC) 2010, pp.1-6, Apr. 2010.
[54] P. Xu, X. Fang, R. He, Z. Xiang, "An efficient handoff algorithm based on received signal strength and wireless transmission loss in hierarchical cell networks", Telecom. Sys. J., Elsevier, pp. 1-9, Sept. 2011.
[55] D. Lopez-Perez, A. Ladanyi, A. Juttner, Jie Zhang, "OFDMA Femtocells: Intracell Handover for Interference and Handover Mitigation in Two-Tier Networks", 2010 IEEE Wirel. Comm. and Netw. Conf. (WCNC), pp.1-6, Apr. 2010.
[56] D. Lopez-Perez, A. Valcarce, A. Ladanyi, G. de la Roche, J. Zhang, "Intracell handover for interference and handover mitigation in OFDMA two-tier macrocell-femtocell networks", EURASIP J. on Wirel. Comm. and Netw. - SI on femtocell networks, vol. 10, no. 1, Jan. 2010.
[57] B. Jeong, S. Shin, I. Jang, N. W. Sung, H. Yoon, "A Smart Handover Decision Algorithm Using Location Prediction for Hierarchical Macro/Femto-Cell Networks," 2011 IEEE Vehic. Techn. Conf. (VTC-Fall), pp.1-5, Sept. 2011.

[58] A. Ulvan, R. Bestak, M. Ulvan, "Handover Scenario and Procedure in LTE-based Femtocell Networks", The 4th Internat. Conf. on Mob. Ubiq. Comput., Syst., Serv. and Technolog., pp. 213-218, Oct. 2010.
[59] H. Zhang, W. Ma, W. Li, W. Zheng, X. Wen, C. Jiang, "Signalling Cost Evaluation of Handover Management Schemes in LTE-Advanced Femtocell", 2011 IEEE 73rd Vehic. Techn. Conf. (VTC Spring), pp.1-5, May 2011.
[60] S. Wu, S. Lo, "Handover Scheme in LTE-based Networks with Hybrid Access Mode Femtocells", J. of Convergence Inform. Techn., vol. 6, no. 7, pp. 68-78, July 2011.
[61] W. Shaohong, Z. Xin, Z. Ruiming, Y. Zhiwei, F. Yinglong, Y. Dacheng, "Handover Study Concerning Mobility in the Two-Hierarchy Network", IEEE 69th Vehic. Techn. Conf. (VTC), pp.1-5, Apr. 2009.
[62] H. Zhang, X. Wen, B. Wang, W. Zheng, Y. Sun, "A Novel Handover Mechanism Between Femtocell and Macrocell for LTE Based Networks", IEEE 2nd Internat. Conf. on Comm. Softw. and Nets. 2010 (ICCSN), pp.228-231, Feb. 2010.
[63] P. Xu, X. Fang, J. Yang, Y. Cui, "A User's State and SINR-Based Handoff Algorithm in Hierarchical Cell Networks", 2010 IEEE 6th Internat. Conf. on Wirel. Comm. Netw. and Mobile Comp. (WiCOM), pp.1-4, Sept. 2010.
[64] D. Lee, G. Gil, D. Kim, "A Cost-Based Adaptive Handover Hysteresis Scheme to Minimize the Handover Failure Rate in 3GPP LTE System", EURASIP J. on Wirel. Comm. and Netw., vol. 2010, no. 6, Feb. 2010.
[65] K. S. B. Reguiga, F. Mhiri, R. Bouallegue, "Handoff Management in Green Femtocell Network", Internat. J. of Comp. Apps., vol. 27, no. 4, pp. 1-7, Aug. 2011.
[66] D. Xenakis, N. Passas, and C. Verikoukis, "A Novel Handover Decision Policy for Reducing Power Transmissions in the two-tier LTE network", 2012 IEEE Internat. Comm. Conf. (ICC), pp.1352-1356, June 2012.
[67] G. Yang, X. Wang, X. Chen, "Handover control for LTE femtocell networks," 2011 IEEE Internat. Conf. on Electronics, Comm. and Control (ICECC), vol., no., pp.2670-2673, Sept. 2011.
[68] M. Z. Chowdhury, W. Ryu, E. Rhee, Y. M. Jang, "Handover between macrocell and femtocell for UMTS based networks," IEEE 11th Internat. Conf. on Advanced Comm. Techn. (ICACT) 2009, vol.01, no., pp.237-241, Feb. 2009.
[69] J. Kim, T. Lee, "Handover in UMTS networks with hybrid access femtocells," IEEE 12th Internat. Conf. on Advanced Comm. Techn. (ICACT) 2010, vol.1, no., pp.904-908, Feb. 2010.
[70] Z. Becvar, P.Mach, "Adaptive Hysteresis Margin for Handover in Femtocell Networks", IEEE 6th Internat. Conf. on Wirel. and Mobile Comm., pp.256-261, Sept. 2010.
[71] D. Xenakis, N. Passas, and C. Verikoukis, ""An Energy-Centric Handover Decision Algorithm for the Integrated LTE Macrocell - Femtocell Network Computer Communications", Comp.Comm., Elsevier, vol. 35, is. 14, pp. 1684-1694, Aug. 2012.
[72] A. Rath and S. S. Panwar, "Fast Handover in Cellular Networks with Femtocells," 2012 IEEE Internat. Comm. Conf. (ICC), June 2012.
[73] O. Tipmongkolsilp, S. Zaghloul, A. Jukan, "The Evolution of Cellular Backhaul Technologies: Current Issues and Future Trends", IEEE Comm. Surv. & Tut., vol.13, no.1, pp.97-113, First Quarter 2011.
[74] A. Attar, L. Haoming, V.C.M. Leung, "Green last mile: how fiber-connected massively distributed antenna systems can save energy", IEEE Wirel. Comm., vol.18, no.5, pp.66-74, Oct. 2011.
[75] N. Ghazisaidi, M. Maier, "Fiber-wireless (FiWi) access networks: Challenges and opportunities", IEEE Network, vol.25, no.1, pp.36-42, Feb. 2011.
[76] C. Lim, A. Nirmalathas, M. Bakaul, P. Gamage, K. Lee, Y. Yang, D.Novak, R. Waterhouse, "Fiber-Wirel. Networks and Subsystem Technologies", J. of Lightwave Techn., vol.28, no.4, pp.390-405, Feb. 2010.
[77] 3GPP, "Study on architecture enhancements to support Proximity Services (D2D)", TR 23.703 V1.1.0, Jan. 2014.
[78] D. Xenakis, N. Passas, L. Merakos, and C. Verikoukis, "Mobility Management for Femtocells in LTE-Advanced: Key Aspects and Survey of Handover Decision Algorithms", IEEE Comm. Surv. & Tut., vol. 16, no. 1, pp. 64-91, 2014.
[79] S. Marano, W. M. Gifford, H. Wymeersch, M. Z. Win, "NLOS identification and mitigation for localization based on UWB experimental data", IEEE J. Sel. Areas Commun., vol.28, no.7, pp.1026-1035, September 2010.
[80] T. Hazim, G. K. Karagiannidis, T.A. Tsiftsis, "Probability of early detection of ultra-wideband positioning sensor networks", IET Wireless Sensor Systems, vol.1, no.3, pp.123-128, September 2011.
[81] Y. Chen, M. Li, L. Shu, L. Wang, T.Q. Duong, "The scheme of mitigating the asymmetric links problem in wireless sensor networks", IEEE GLOBECOM Workshops, pp.272-276, Dec. 2010.
[82] B. Shim, J. W. Choi, I. Kang, "Towards the Performance of ML and the Complexity of MMSE: A Hybrid Approach for Multiuser Detection", IEEE Trans. on Wirel. Commun., vol.11, no.7, pp.2508-2519, July 2012.

[83] G. Giorgetti, S. K. S. Gupta, and G. Manes, "Understanding the limits of RF-based collaborative localization", IEEE/ACM Trans. on Networking, vol. 19, no. 6, pp. 1638–1651, 2011.
[84] G. Garcia, S. Muppirisetty, E. Schiller, H. Wymeersch, "On the Trade-off Between Accuracy and Delay in Cooperative UWB Localization: Performance Bounds and Scaling Laws", IEEE Trans. on Wirel. Commun., accepted, 2014.
[85] J. Ni, R. Srikant, X. Wu, "Coloring Spatial Point Processes With Applications to Peer Discovery in Large Wireless Networks", IEEE/ACM Trans. on Networking, vol.19, no.2, pp.575-588, April 2011.
[86] T. Kwon, J. Choi, "Spatial Performance Analysis and Design Principles for Wireless Peer Discovery", IEEE Trans. on Wirel. Commun., accepted, 2014.
[87] R. Verdone, F. Fabbri, C. Buratti, "Maximizing area throughput in clustered wireless sensor networks", IEEE J. Sel. Areas Commun., vol.28, no.7, pp.1200-1210, September 2010
[88] Y. Zhong and W. Zhang, "Multi-Channel Hybrid Access Femtocells: A Stochastic Geometric Analysis", IEEE Trans. on Commun., Vol. 61, No. 7, pp. 3016-3026, Jul. 2013.
[89] G. Alfano, M. Garetto, E. Leonardi, "Capacity scaling of wireless networks with inhomogeneous node density: upper bounds", IEEE J. Sel. Areas Commun., vol.27, no.7, pp.1147-1157, Sept. 2009.
[90] R. K. Ganti, M. Haenggi, "Interference and Outage in Clustered Wireless Ad Hoc Networks", IEEE Trans. on Inform. Theory, vol.55, no.9, pp.4067-4086, Sept. 2009.
[91] B. Kaufman, J. Lilleberg, and B. Aazhang, "Spectrum Sharing Scheme between Cellular Users and ad-hoc Device-to-Device Users", IEEE Trans. on Wirel. Comm., vol. 12, no. 3, pp. 1038–1049, Mar. 2013.
[92] S.-L. Chao, H.-Y. Lee, C.-C. Chou, and H.-Y. Wei, "Bio-Inspired Proximity Discovery and Synchronization for D2D Communications", IEEE Comm. Letters, vol. 17, no. 12, pp. 2300-2303, Dec. 2013.
[93] H.-S. Jo, Y. J. Sang, P. Xia, and J. G. Andrews, "Heterogeneous Cellular Networks with Flexible Cell Association: A Comprehensive Downlink SINR Analysis", IEEE Trans. on Wirel. Comm., vol. 11, no. 10, pp. 3484-3495, Oct. 2012.
[94] J. G. Andrews, F. Baccelli, and R. K. Ganti, "A Tractable Approach to Coverage and Rate in Cellular Networks", IEEE Trans. on Comm., vol. 59, no. 11, pp. 3122-3134, Nov. 2011.
[95] H. S. Dhillon, M. Kountouris, and J. G. Andrews, "Downlink MIMO HetNets: Modeling, Ordering Results and Performance Analysis," IEEE Trans. on Wirel. Comm., vol. 12, no. 10, pp. 5208-5222, Oct. 2013.
[96] M. Haenggi, "On Distances in Uniformly Random Networks", IEEE Trans. Inform. Theory, vol. 51, no. 10, pp. 3584-3586, Oct. 2005.
[97] X. Lin, R. Ratasuk, A. Ghosh, and J. G. Andrews, "Modeling, Analysis and Optimization of Multicast Device-to-Device Transmission", submitted to IEEE Trans. on Wirel. Comm., Sep. 2013.
[98] Q. Ye, M. Al-Shalash, C. Caramanis, and J. G. Andrews, "Resource Optimization in Device-to-Device Cellular Systems Using Time-Frequency Hopping", submitted to IEEE Trans. on Wirel. Comm., Sep. 2013.
[99] X. Lin, J. G. Andrews, and A. Ghosh, "Spectrum Sharing for Device-to-Device Communication in Cellular Networks", submitted to IEEE Trans on Wirel. Comm., May 2013.
[100] N. Lee, X. Lin, J. G. Andrews, and R. W. Heath Jr., "Power Control for D2D Underlaid Cellular Networks: Modeling, Algorithm and Analysis", submitted to IEEE J. Sel. Areas Commun., May 2013.
[101] M. Kim, H.W. Je, F.A. Tobagi, "Cross-Tier Interference Mitigation for Two-Tier OFDMA Femtocell Networks with Limited Macrocell Information", 2010 IEEE Global Telecommunications Conf. (GLOBECOM 2010), pp.1-5, Dec. 2010.
[102] D. Lopez-Perez, A. Valcarce, G. de la Roche, Jie Zhang, "OFDMA femtocells: A roadmap on interference avoidance", IEEE Communications Magazine, vol.47, no.9, pp.41-48, Sept. 2009.
[103] M. Yavuz, F. Meshkati, S. Nanda, A. Pokhariyal, N. Johnson, B. Raghothaman, A. Richardson, "Interference management and performance analysis of UMTS/HSPA+ femtocells", IEEE Communications Magazine, vol.47, no.9, pp.102-109, Sept. 2009.
[104] V. Chandrasekhar, J.G. Andrews, T. Muharemovic, Z. Shen, A. Gatherer, "Power control in two-tier femtocell networks", IEEE Trans. on Wireless Commun., vol.8, no.8, pp.4316-4328, Aug. 2009.
[105] H. Jo, C. Mun, J. Moon, J. Yook, "Interference mitigation using uplink power control for two-tier femtocell networks", IEEE Trans. on Wireless Commun., vol.8, no.10, pp.4906-4910, Oct. 2009.
[106] A. Galindo-Serrano, L. Giupponi, M. Dohler, "Cognition and Docition in OFDMA-Based Femtocell Networks", 2010 IEEE Global Telecommunications Conf. (GLOBECOM 2010), pp.1-6, Dec. 2010.
[107] S. Park, W. Seo, Y. Kim, S. Lim, D. Hong, "Beam Subset Selection Strategy for Interference Reduction in Two-Tier Femtocell Networks", IEEE Trans. on Wirel. Commun. vol.9, no.11, pp.3440-3449, Nov. 2010.
[108] J. Chang, Y. Li, S. Feng, H. Wang, C. Sun, P. Zhang, "A Fractional Soft Handover Scheme for 3GPP LTE-Advanced System", 2009 IEEE International Conf. on Comm. (ICC 2009), pp.1-5, June 2009.

[109] U. Narayanan, J. Xie, "Signaling Cost Analysis of Handoffs in a Mixed IPv4/IPv6 Mobile Environment", IEEE Global Telecommunications Conf. 2007 (GLOBECOM 2007), pp.1792-1796, Nov. 2007.
[110] S. Oh, H. Kim, B. Ryu, N. Park, "Inbound Mobility Management on LTE-Advanced Femtocell Topology Using X2 Interface", 2011 Proceed. of 20th Intern. Conf. on Comp. Comm. and Net., pp.1-5, Aug. 2011.
[111] M. Kassar, B. Kervella, G. Pujolle, "An overview of vertical handover decision strategies in heterogeneous wireless networks", Comp. Comm., Elsevier, vol. 31, no. 10, pp. 2607–2620, Jan. 2008.
[112] X. Yan, Y. A. Şekercioğlu, S. Narayanan, "A survey of vertical handover decision algorithms in Fourth Generation heterogeneous wireless networks", Comp. Networks, Elsevier, col. 54, no. 11, pp. 1848-1863, Aug. 2010.
[113] D. Xenakis, N. Passas, L. Merakos, and C. Verikoukis, "Energy-Efficient and Interference-Aware Handover Decision for the LTE-Advanced Femtocell Network", IEEE Intern. Commun. Conf. (ICC), June 2013.
[114] D. Xenakis, N. Passas, L. Merakos, and C. Verikoukis, "ARCHON: An ANDSF-Assisted Energy-Efficient Vertical Handover Decision Algorithm for the Heterogeneous IEEE 802.11/LTE-Advanced Network", IEEE International Communications Conference (IEEE ICC), June 2014..
[115] D. Xenakis, N. Passas, L. Di Gregorio, and C. Verikoukis, "A Context-Aware Vertical Handover Framework Towards Energy-Efficiency", The 73rd IEEE Veh. Tech. Conf. (VTC), May 2011.
[116] H. Kwak, P. Lee, Y. Kim, N. Saxena, and J. Shin, "Mobility Management Survey for Home-eNB Based 3GPP LTE Systems", J. of Inform. Process. Sys., Vol.4, No.4, Dec. 2008.
[117] Y. Li, A. Maeder, L. Fan, A. Nigam, J. Chou, "Overview of femtocell support in advanced WiMAX systems", IEEE Comm., vol.49, no.7, pp.122-130, July 2011.
[118] R. Y. Kim, I. Jung, X. Yang, C. Chou, "Advanced handover schemes in IMT-advanced systems [WiMAX/LTE Update]", IEEE Comm., vol.48, no.8, pp.78-85, Aug. 2010.
[119] S. K. Ray, K. Pawlikowski, H. Sirisena, "Handover in Mobile WiMAX Networks: The State of Art and Research Issues", IEEE Comm. Surv. & Tut., vol.12, no.3, pp.376-399, Third Quarter 2010.
[120] B. V. Quang, R. V. Prasad, I. Niemegeers, "A Survey on Handoffs — Lessons for 60 GHz Based Wirel. Systems", IEEE Comm. Surv. & Tut., vol.14, no.1, pp.64-86, First Quarter 2012.
[121] S. Fernandes, A. Karmouch, "Vertical Mobility Management Architectures in Wirel. Networks: A Comprehensive Survey and Future Directions," IEEE Comm. Surv. & Tut., vol.14, no.1, pp.45-63, First Quarter 2012.
[122] P. Makris, D. Skoutas, C.Skianis, "A Survey on Context-Aware Mobile and Wireless Networking: On Networking and Computing Environments' Integration," IEEE Comm. Surv. & Tut., vol., no.99, pp.1-25, 2012.
[123] Small Cell Forum, “Interference Management in OFDMA Femtocells”, Small Cell Forum, Mar. 2010.
[124] A. Papoulis, Probabilities, Random Variables and Stochastic Processes, 3rd ed., McGraw-Hill, 1991.
[125] R. Peng, M. L. Sichitiu, "Angle of Arrival Localization for Wireless Sensor Networks", IEEE Commun. Society on Sensor and Ad Hoc Commun. and Networks (SECON), pp.374,382, Sept. 2006.
[126] C. Wong, R. Klukas, G. Messier, "Using WLAN Infrastructure for Angle-of-Arrival Indoor User Location", IEEE Vehic. Tech. Conf. (VTC) Fall, Sept. 2008.
[127] G. Fodor, E. Dahlman, G. Mildh, S. Parkvall, N. Reider, G. Miklos, and Z. Turanyi, "Design Aspects of Network Assisted Device-to-Device Communications", IEEE Comm. Mag., vol. 50, no. 3, pp. 170-177, Mar. 2012.
[128] 3GPP, "Evolved Universal Terrestrial Radio Access (E-UTRA) - User Equipment (UE) Radio Transmission and Reception", TS 36.101 V12.2.0, Jan. 2014.
[129] Q. Ye, M. Al-Shalash, C. Caramanis, and J. G. Andrews, "Resource Optimization in Device-to-Device Cellular Systems Using Time-Frequency Hopping", submitted to IEEE Trans. on Wirel. Comm., Sep. 2013.
[130] D. Stoyan, W. Kendall, and J. Mecke, Stochastic Geometry and its Applications, 2nd ed., John Wiley and Sons, 1996.
[131] A. R. Jensen, M. Lauridsen, P. Mogensen, T. B. Sørensen, P. Jensrn, "LTE UE Power Consumption Model For System Level Energy and Performance Optimization", IEEE Vehicular Technology Conference (VTC Fall), 2012.
[132] P. Serrano, A. Garcia-Saavedra, M. Hollick, A. Banchs, "On the energy efficiency of IEEE 802.11 WLANs", 2010 European Wireless Conference (EW), pp.932-939, 12-15 April 2010.
[133] J.-S. Liu, C.-H. R. Lin, "ECTP: An Energy-Efficiency Label-Switching MAC Protocol for Infrastructure Wireless Networks," IEEE Transactions on Vehicular Technology, vol.56, no.3, pp.1399-1417, May 2007

[134] J. Zhang, G. de la Roche, “Femtocells : technologies and deployment”, John Wiley & Sons Ltd, ISBN 978-0-470-74298-3, 2010.
[135] Q. Liu, S. Zhou, and G. B. Giannakis, “Queuing with adaptive modulation and coding over wireless link: cross-layer analysis and design”, IEEE Trans. Wireless Commun., vol. 4, pp. 1142-1153, May 2005.
[136] 3GPP, “Requirements for support of radio resource management", TS 36.133 V10.6.0, Mar. 2012
[137] K. Zheng, Y. Wang, W. Wang, M. Dohler, J. Wang,"Energy-efficient wireless in-home: the need for interference-controlled femtocells", IEEE Wirel. Comm., vol.18, no.6, pp.36-44, Dec. 2011.
[138] K. I. Itoh, S. Watanabe, J.-S. Shih, T. Sato, "Performance of handoff algorithm based on distance and RSSI measurements", IEEE Trans. on Vehic. Techn., vol.51, no.6, pp. 1460- 1468, Nov 2002.
[139] A. Ulvan, M. Ulvan, and R. Bestak, ”The Enhancement of Handover Strategy by Mobility Prediction in Broadband Wirel. Access”, Netw. and Electronic Commerce Research Conf. (NAEC) 2009, TX: American Telecom. Sys. Mgmt. Assoc. Inc., pp. 266-276, 2009. ISBN 978-0-9820958-2-9.
[140] M. Haenggi, J.G. Andrews, F. Baccelli, O. Dousse, M. Franceschetti, "Stochastic geometry and random graphs for the analysis and design of wireless networks", IEEE J. on Sel. Areas in Comm., vol.27, no.7, pp.1029-1046, Sept. 2009.
[141] M. Haenggi and R. K. Ganti, “Interference in large wireless networks,” Found. Trends Netw., vol. 3, no. 2, pp. 127–248, 2008.
[142] F. Baccelli and B. Błaszczyszyn, “Stochastic Geometry and Wireless Networks”, Found. Trends Netw., Vol. 3: No 3-4, pp 249-449, 2009.
[143] S. Weber and J. Andrews, “Transmission capacity of wireless networks,” Found. Trends Netw., vol. 5, no. 2-3, pp. 109–281, 2012.
[144] Y. Kim, S. Lee, D. Hong, "Performance Analysis of Two-Tier Femtocell Networks with Outage Constraints," IEEE Trans. on Wirel. Comm., vol.9, no.9, pp.2695-2700, Sept. 2010.
[145] N. Chakchouk, B. Hamdaoui, "Uplink Performance Characterization and Analysis of Two-Tier Femtocell Networks", IEEE Trans. on Vehic. Techn., vol.61, no.9, pp.4057-4068, Nov. 2012.
[146] Z. Gong, M. Haenggi, "Mobility and Fading: Two Sides of the Same Coin2010 IEEE Global Telecom. Conf., pp.1-5, Dec. 2010.
[147] Z. Gong and M. Haenggi, “Interference and Outage in Mobile Random Networks: Expectation, Distribution, and Correlation”, IEEE Trans. on Mob. Comp., 2013, accepted.
[148] Informa Telecoms & Media, "Small Cell Market Status", Small Cell Forum, Feb. 2012.
[149] A. H. Nuttall, "Some integrals involving the function", IEEE Trans. on Inf. Theory, vol. 21, no. 1, pp. 95-96, Jan. 1975
[150] A. P. Prudnikov, Y. A. Brychkov, and O. I. Marichev, Integrals and Series: Special functions, vol. 2, CRC Press, 1986.
[151] M. K. Simon and M. S. Alouini, Digital Communication Over Fading Channels: A Unified Approach to Performance Analysis, New York: Wiley-Interscience, 2000.
[152] J. R. Culham, "Bessel Functions of the First and Second Kind", available online at: http://www.mhtlab.uwaterloo.ca/courses/me755/web_chap4.pdf.